

Smart cementitious composites
Development of multi-functional printable SHCC

Chaves Figueiredo, S.

DOI

[10.4233/uuid:d5a37f00-3123-461d-baf5-33314ee56930](https://doi.org/10.4233/uuid:d5a37f00-3123-461d-baf5-33314ee56930)

Publication date

2023

Document Version

Final published version

Citation (APA)

Chaves Figueiredo, S. (2023). *Smart cementitious composites: Development of multi-functional printable SHCC*. [Dissertation (TU Delft), Delft University of Technology]. <https://doi.org/10.4233/uuid:d5a37f00-3123-461d-baf5-33314ee56930>

Important note

To cite this publication, please use the final published version (if applicable).
Please check the document version above.

Copyright

Other than for strictly personal use, it is not permitted to download, forward or distribute the text or part of it, without the consent of the author(s) and/or copyright holder(s), unless the work is under an open content license such as Creative Commons.

Takedown policy

Please contact us and provide details if you believe this document breaches copyrights.
We will remove access to the work immediately and investigate your claim.

SMART CEMENTITIOUS COMPOSITES

DEVELOPMENT OF MULTI-FUNCTIONAL PRINTABLE SHCC

SMART CEMENTITIOUS COMPOSITES

DEVELOPMENT OF MULTI-FUNCTIONAL PRINTABLE SHCC

Proefschrift

ter verkrijging van de graad van doctor
aan de Technische Universiteit Delft,
op gezag van de Rector Magnificus prof.dr. ir. T.H.J.J. van der Hagen,
voorzitter van het College voor Promoties,
in het openbaar te verdedigen op maandag 6 november 2023 om 15:00 uur

door

Stefan CHAVES FIGUEIREDO

Master of Science in Civil Engineering,
Centro Federal de Educação Tecnológica de Minas Gerais, Belo Horizonte, Brazilië
geboren te Belo Horizonte - Minas Gerais, Brazilië.

Dit proefschrift is goedgekeurd door de

promotor: prof. dr. ir. E. Schlangen

promotor: dr. O. Çopuroğlu

Samenstelling promotiecommissie:

Rector Magnificus,
Prof. dr. ir. E. Schlangen,
Dr. O. Çopuroğlu,

Technische Universiteit Delft, voorzitter
Technische Universiteit Delft, promotor
Technische Universiteit Delft, promotor

Onafhankelijke leden:

Prof. dr. C. de Souza Rodrigues Federal Center for Technological Education
of Minas Gerais, Brazil

Dr. ir. F.P. Bos, Technical University of Munich, Germany

Prof. dr -ing. V. Mechtcherine Dresdem University of Technology, Germany

Prof. dr. H.M. Jonkers, Technische Universiteit Delft, The Netherlands

Prof. dr. ir. M.A.N. Hendriks, Technische Universiteit Delft, The Netherlands



Keywords: Additive manufacturing, 3D printing, strain hardening cementitious composites, autogenous self-healing, self-sensing

Printed by: Ipskamp Printing, The Netherlands

Cover design: Stefan Chaves Figueiredo, Bianca Fraga Silva and Yading Xu

Copyright © 2023 by Stefan Chaves Figueiredo

All rights reserved. No part of the material protected by this copyright notice may be reproduced or utilized in any form or by any means, electronic or mechanical, including photocopying, recording, or by any information storage and retrieval system, without written permission from the author.

ISBN 978-94-6366-762-3

An electronic version of this dissertation is available at
<http://repository.tudelft.nl/>.

What we know is a drop, what we don't know is an ocean.

Isaac Newton

ACKNOWLEDGMENTS

First of all I would like to thank Erik that back in 2014 accepted me to join the Microlab for a PhD. It was exactly what I was willing at that time, and fortunately he granted me this opportunity. Moreover, during the PhD journey you were an amazing supervisor delivering the best research environment that a student could ever thought about. Bos, you are a true leader bringing interesting discussions and a very creative environment to be explored.

Somebody else that had a very special role during my studies was Oğuzhan. You are a very smart person with whom I learned and will most probably continue to learn for the rest of my life. Your reaction speed to a problem and the volume of information that you know in different areas is fascinating! You open my eyes to several of my pitfalls and pointed to ways for me to learn something new to overcome those problems. I had the lectures with you during forensic engineering and the opportunity to follow you during the microscopy course. In both cases I could experience how much you take care of those courses and how much effort you put trying to reach your best every year. This search for perfection and your care in making your students understand the essence of the problem makes you an amazing teacher. Thank you very much for all your patience and transmitted knowledge.

During my very broad PhD studies I had also the chance to have some interesting discussions with dr. Wolfgang Gard. I must acknowledge the chance that I had to work with you and learn a little bit more about wood structures and its composition. Thank you for guiding me in the beginning of my PhD towards a fast track to acquire the needed knowledge for the project.

Widening even more the scope of the PhD I had the chance to be introduced to Freek Bos. The challenging project of enhance the ductility of printed materials was a very nice chance to meet you. Your "hands on" mentality is something very nice for the teamwork and says a lot about you the success of the TU Eindhoven 3d printing team. We had very nice discussions about the project and how to get the best out of the results that we obtained. Your questions and discussions were very important to improve the quality of my work and challenge me! Thank you very much for the opportunity given to me to join the TU Eindhoven 3D printing team during this challenging project during my PhD and also for my future. You know very well that working with fibres is something that I love, and working with these fibres where they are very much needed and probably will deliver results never before reached is something that sparks me!! Thank you!

What to say about a Brazilian which was "accidentally" born in under a dutch skin?! Maiko (or Maikinho) my friend, you are an amazing person! You are not only the technician with whom I worked a lot, you are somebody that look after all of us in the *Maikolab* making sure that everything was working well. When I say everything, I mean not only the equipment but also the people which works there!! My friend, thank you so much for letting me and Bianca to be a little part of the van Leuwens. Your friendship, to-

gether with Danielle, Nienke and Jari is something for us so important that made us feel comfortable and at home even across the Atlantic Ocean. Your summer barbecues, the passion that you put in all that you do, that new's years eve, our Eindhoven trips, and many other things that I will never have be able to acknowledge you enough. Thank you very much!!!!

I must also acknowledge all the help given during my PhD work to colleges John, Gerh, Arjan and Rhom Penners. Thank you very much for the very nice time that we had in the lab with you all giving your best for me to learn and achieve all the desired goals. Thank you very much!

A special thank you here goes also for my friend Tom (of misschien Tontje). Much more than a colleague you became a good friend! Thank you for all your help and patience in the Macrolab and for the amazing time in Serbia!!

I think that not even one thousand thanks would not be enough for the DEMO team. Cees, Paul, Rom, Martin and Giorgos thank you so much for all your attention with my problems. We had a very challenge start during my first one and a half year approximately, that I am very sure to say that I would never have succeed there without the intensive help of Kees. Thank you very much!!

You can never finish a long task without a help. And that was very much needed in my case. I must acknowledge the help given by Igor, Yashila, Kevin and Lars for the direct intensive help given during the development of yours bachelors thesis. I must also extend my gratitude to Claudia and Joost with whom I had the opportunity to learn and help during the development of their master thesis. For sure your works were a very important piece of a greater work that was this thesis. Besides that I must also thank you all for the patience that you all had during the time working with me. It was of great value for me being a part of your journey where I am sure that I learned much more than the knowledge that I had to offer you all. Thank you very much for teaching me in how to supervise, assist and trigger the curiosity on you all.

A very important part of this journey stated in Brazil with three very important persons in my learning life: Professors Conrado de Souza Rodrigues, Paulo Henrique Ribeiro Borges and Flávio de Andrade Silva. Conrado was the first to give me an opportunity to start to work with research back in the time of my bachelors. He trusted me a scientific initiation position that brought me into this amazing research world. He had the patience of guide me during the very beginning showing the scientific methods and how to perform a successful research. Further he supervised me during my bachelors and masters thesis where I could learn even more from that creative mind. I became fascinated to the fibre reinforced cementitious materials world and Conrado provided me the environment where I could experiment a lot during that time. Paulo came afterwards, with intriguing questions and very nice opportunity to work as teaching assistant with him, where I could sharpen my teaching skills and construction and building materials knowledge. Flávio, you were a crucial element for me to come to Delft. Though you I could contact somebody in the Microlab and express my wills to continue working in academia and dedicating myself in a PhD project in that lab. Your questions, criticism and your amazing knowledge in fibre reinforced materials were very important to give me so much sureness of the next step that I was about to give in going abroad to continue my studies. I am very much happy to have you three during my academic life.

Thank you!

As I said once before, you can never accomplish such a long task as a PhD without help. This help also came from the friends/colleges that I could find in the Microlab. Thank you so much for all the time that we have spent together. Without your questions, curiosity and kindness this journey would not have been so fun!!

Thank you for the very important task that you all have Nynke, Iris, Cláudia, Claire, Jaap and Jaqueline. Without your help organizing everything to make our working environment prepared for us to dedicate to the research and teaching activities.

The concrete nest!! Wow this people from this nest!!! So important for my life!! It seems that this office is composed by only four people sited in their chairs concentrated looking to their computers. Oh... such a mistake! This is a very united family where you can bring your research results and have a discussion, you can talk about your life problems and success, you can always bring the love of your life or also find him there, you can visit for a project and realize that this is the place where you dreamed to work or you can come and show how much better this place is with your jokes and sarcasm. Seriously Marija/Patrick, Cláudia/Fernando and Yading you are such a good friends that I cannot measure the importance of each of you in our life (mine and Bianca). You are true friends that are there for any type of problem or just for a good work related discussion. Thank you very much!!!

Love of my life, thank you! You are so important to me!! Thank you for joining me in this crazy adventure of a PhD. How to not remember that October 31st of 2014? That was Mari and André's wedding. On that same day you got the bouquet on their wedding and I got granted my PhD proposal among other challenges on that same day. Such a day!! I will never forget it! Since that day a lot changed: we got married, we moved to Delft... Your presence here by my side during this journey was absolutely important for its success. I really appreciate that you have accepted the challenge of moving abroad and face a new culture, new work, new life style because of my dream. I am sure that this challenge have also changed your perceptions about life, priorities and how much we can achieve if we decide to make an extra effort on everything. I am learning a lot living by your side!! Thank you for all your help and support! I love you!

Since I am defending my PhD thesis much latter than I expected, I can also add one extra paragraph just some weeks before the defence. This paragraph is dedicated to the newest part of the family who arrived 13 days ago and join me on my arms while I write this. Pietro, you are joining us in this adventure where I can only tell you that we will make sure that you will enjoy as much as we (me and you mother) are enjoying. You are the cutest little thing ever! Your joyful smiles give us an enormous strength to pursue the best for you. Every day, you are making us the happiest parents ever! We love you!

Even some thousands of kilometres far away, our family is very important supporting us. I must thanks the support that we (me and Bianca) have received from our families. Thank you very much for everything veio, veia (or also formally know as Vital and Nailê :)), Anamir, Elisabeth, Tia Pim, Dindinha, Rubens, Ranier, Dani, Luca, Naiara (Madaaaaaaaa!!!), Sávio and Marlon. I must also acknowledge the ones that saw this journey start but unfortunately could not see its end Dário and Maria. Thank you for all the support!!

I must also acknowledge the funding from Science Without Borders from the Na-

tional Council for Scientific and Technological Development of Brazil (CNPq) (201620/2014-6).

CONTENTS

Acknowledgments	vii
Summary	xv
Samenvatting	xix
1 Introduction	1
1.1 Introduction	2
1.2 Thesis outline	3
2 Smart constructions: An overview from the building phase to the durability surveillance	7
2.1 Introduction	8
2.2 Construction Management	8
2.3 Additive manufacturing	9
2.4 Service life assessment	12
2.5 Smart cementitious composites	12
2.5.1 Self-sensing	12
2.5.2 Self-healing	15
2.6 Conclusions	17
3 An approach to develop printable strain hardening cementitious composites	19
3.1 Introduction	20
3.2 Theoretical background	22
3.3 Experimental methods	24
3.3.1 Materials and sample preparation	24
3.3.2 Rheology measurements	25
3.3.3 Printing trials	29
3.3.4 Mechanical tests	30
3.4 Results	31
3.4.1 Rheology	31
3.4.2 Printing experiments	39
3.4.3 Mechanical properties	41
3.5 Conclusions	43
4 Mechanical behaviour of printed strain hardening cementitious composites	47
4.1 Introduction	48
4.2 Experimental methods	50
4.2.1 Materials and methods	50
4.2.2 Mechanical characterization	51
4.2.3 Air void content and fibre orientation assessment	54

4.3	Results	55
4.3.1	Compressive strength	55
4.3.2	Fracture toughness test	55
4.3.3	Four-point bending	57
4.3.4	Uni-axial tensile test	58
4.3.5	Tensile bond strength of interface	63
4.3.6	CT-scan	66
4.4	Conclusions.	67
5	Effect of viscosity modifier admixture on Portland cement paste hydration and microstructure	73
5.1	Introduction	74
5.2	Experimental methods	76
5.3	Results	79
5.3.1	Isothermal calorimetry test	80
5.3.2	Thermogravimetry analysis	81
5.3.3	X-ray diffraction	84
5.3.4	Fourier transform infrared spectroscopy	85
5.3.5	Qualitative and quantitative image analysis	86
5.3.6	Rheology properties	91
5.3.7	Mechanical properties	97
5.4	Conclusions.	99
6	Autogenous self-healing of cementitious materials: The influence of rheology modifiers and cellulose pulp	101
6.1	Introduction	102
6.2	Theoretical background.	102
6.2.1	Autogeneous self-healing	102
6.2.2	The use of natural fibres	103
6.3	Experimental methods	105
6.3.1	Materials and sample preparation	105
6.3.2	Fibre treatment	106
6.3.3	Isothermal calorimetry analysis	107
6.3.4	Accelerated ageing cycles	107
6.3.5	Self-healing cycles	108
6.3.6	Self-healing performance assessment	108
6.4	Results	112
6.4.1	Fibre treatment	112
6.4.2	Isothermal calorimetry analysis	113
6.4.3	Accelerated ageing cycles	115
6.4.4	Self-healing performance	117
6.5	Conclusions.	136

7 Piezoresistive properties of cementitious composites reinforced by PVA fibres	139
7.1 Introduction	140
7.2 Experimental	141
7.3 Results and Discussion	144
7.4 Conclusions.	148
8 Conclusion and suggestions for further research	149
8.1 Conclusions.	150
8.2 Suggestions for further research.	151
References	153
List of Publications	173

SUMMARY

Adding extra functionality to cementitious materials will enhance the capabilities of understanding the use of structures where they are used and at the same time increase its life span. The construction industry is one of the most important economic sectors in many countries. Therefore, efforts to improve its productivity can result in significant developments in the economy of a region. Higher productivity can be achieved for instance by means of process automation, by adding value to the product generated with an activity or via the extension of the use of a given asset.

The use of automation in the construction sector has been a challenge that many companies and researchers have dedicated time searching for improvements and understanding. The large complexity of the activities together with the big social impact of a durable solution are some of the challenges that impose difficulties on the implementation of new technologies in this sector.

The use of machinery to facilitate the movement of heavy products is largely adopted in the building industry. However, only lately the automation of complex activities gained space. The employment of extrusion-based additive manufacturing also largely called extrusion-based 3D concrete printing (3DCP), to help on the production of building elements has shown large potential to address some difficulties, such as manufacturing of complex geometries. Moreover, the rational use of materials quickly show potential to help this industry address the environmental targets aimed by the society.

Additionally, the use of unreinforced mortar in this new construction technique has also demonstrated limitations. The brittle nature of the material used for extrusion implicates in the building phase in limitation on the usage of the technology, incorporation of external reinforcement or in designs where limited tensile forces are required. To address this issue, this work proposes the use of strain hardening cementitious composites (SHCC). A rational methodology is proposed to adapt available mix-designs in literature for the requirements of extrusion as a casting technique.

Two SHCC mixtures available in literature were used for the studies. Mix-design parameters such as the influence of water-to-solid ratio, fibre volume percentage, superplasticizer and viscosity modifying admixture (VMA) content on the fresh state properties were investigated. The use of a ram extrusion experiment together with the Benbow-Bridgwater model was proposed to evaluate the rheological properties of the materials. The rheological characterization has shown that the use of chemical admixtures and a low water-to-solid ratio was necessary to achieve a dough-like consistence needed for extrusion based 3DCP. These admixtures were also closely correlated to the shape of the output material from the ram extrusion test. Selected mixtures were evaluated with pumping trials when the extrusion capabilities were confirmed. Using cast samples, the mechanical performance of the modified mixtures was evaluated, and the strain hardening was confirmed through four-point bending tests and uniaxial tensile test.

Using two adapted SHCC mixtures for extrusion, several elements were printed aiming to investigate the influence of this new construction technique in the performance of the material. Long beam elements with one, two, three and four printed layers were manufactured. Samples from these elements were taken and mechanical tests in different directions as well as microstructure investigations were performed. It was concluded that extrusion based 3DCP induces the creation of a preferred plane of orientation of the fibres. This preferential orientation guarantees strain hardening performance when the composite is loaded in two directions: parallel and perpendicular to the printing direction for the same printing plane. No ductility was observed when samples were loaded in tension perpendicular to the printing plane (layer interface bond strength). Nevertheless, it was also found that the interface between the printed layers was not a weak spot in the material. Besides the strain hardening performance the overall ductility was considered low in comparison with the original SHCC and with other results available in the literature. This low energy absorption was explained later when large air void content was observed with the help of a micro computered tomography (μ CT scan) tests. This test also helped in clarifying that the interface region between two printed layers had the lowest air void content through the height of the sample. Therefore, the study of the printed SHCC concluded that an anisotropic behaviour should be expected when this new building technique is used and that printing settings might have significant influence on the performance of the manufactured element.

During the previous investigations it became clear that the use of chemical admixtures were crucial for the development of extrudable fibre reinforced cementitious composites. Especially the use of VMA was proved essential to achieve the required rheological properties. As the use of such admixture in Portland cement-based materials was not fully understood a microstructure characterization was necessary. Several characterization techniques were used to investigate the hydration development. An anomalous formation of portlandite was observed in electron and optical microscopy. The large quantities of this mineral were confirmed using other techniques. The use of the admixture was also correlated with delays on the setting time, promoting internal curing, higher degree of hydration and high air void content. The use of VMA might lead to consequences in the hydration process of Portland cement and therefore, the use of this shall be used carefully. Nevertheless, some of the side effects might be wisely used to improve other properties of the cementitious composites.

Moreover, the development of specific materials to be used in 3DCP also opens the possibility to incorporate extra functionalities. In vision with the possibilities found for this type of material, in this work two extra properties in cementitious composites were investigated namely self-sensing and autogenous self-healing. The influence of the use of VMA and cellulose pulp in the autogenous self-healing performance of matrices rich in Portland cement or blast furnace slag was investigated. It is known that the natural fibres embedded in Portland cement matrix are susceptible to degradation when exposed to wetting and drying cycles. Therefore, two extra conditions were also evaluated during this research: fibre pre-treatment (hornification cycles) and accelerated ageing cycles (wetting and drying). Two techniques were used to quantify the healing performance: analysis of images obtained from μ CT scan tests and water permeability tests. The results showed that the autogenous self-healing performance of Portland cement rich ma-

trices are largely influenced by the volume of VMA. The large volume of air voids and the anomalous formation of portlandite observed in the microstructure evaluation might be the explanation for this enhanced property. On the other hand, blast furnace slag rich matrices did not show this influence.

Regarding the samples using un-treated natural fibres an improved performance was observed for both evaluated fibre content. Moreover, the same results were not found in samples with pre-treated fibres. As the pre-treatment decreases the water absorption of these fibres the autogenous self-healing performance is also hindered since keeping the moisture for longer periods in the sample is crucial. In general a very low autogenous self-healing performance for samples submitted to accelerated ageing cycles was observed. Only samples with fibres exposed to 10 pre-treating cycles demonstrated some level of protection against the accelerated ageing cycles. It is not clear if the low autogenous self-healing performance of aged samples is related to the ageing of the fibres or the densification of the matrix. Unfortunately, very limited correlation between the two techniques used to quantify the autogenous self-healing performance was found.

The second extra property investigated was the development of SHCC with self-sensing properties. The influence of multi-wall carbon nanotubes on the piezoresistive properties of the composite was investigated. While loading the samples with an uniaxial tensile force an impedance measurement was performed. The comparison of the evolution of the capacitance and the resistance in comparison with the deformations on the composites lead to the development of factors. These factors were used to list the sensitivity of the composite to the deformation and to the damage on the sample with the amount of carbon nanotubes used on the sample. The research showed that SHCC doped with CNT are able to be used as a strain sensor and that the use of alternate current shows significant advantages in comparison with direct current.

As it was reported in this thesis the development of smart SHCC to be applied in the extrusion based 3DCP is possible. The potential of extra properties to be embedded in this composite was explored as well as characterization techniques for the fresh and hardened state of this material. It is believed that the development of new materials will bring further understanding in areas where the building industry is lacking knowledge such as rheology of cementitious materials. Finally, this is also an important opportunity for this economic sector to address the environmental challenges by means of use of new technologies and more sustainable materials.

SAMENVATTING

Het toevoegen van extra functionaliteit aan cementgebonden materialen zal bijdragen aan een beter begrip van de mogelijke toepassingen van deze materialen in constructies en tegelijkertijd de levensduur ervan verlengen. De bouwsector is in veel landen een van de belangrijkste economische sectoren. Daarom kunnen inspanningen om de productiviteit te verbeteren leiden tot aanzienlijke ontwikkelingen in de economie van een regio. Een hogere productiviteit kan bijvoorbeeld worden bereikt door middel van procesautomatisering, door waarde toe te voegen aan het product dat met een activiteit wordt gegenereerd of door de levensduur van een gegeven asset te verlengen.

Het gebruik van automatisering in de bouwsector is een uitdaging geweest waaraan veel bedrijven en onderzoekers tijd hebben besteed om te zoeken naar verbeteringen en begrip. De grote complexiteit van de activiteiten samen met de grote maatschappelijke impact van een duurzame oplossing zijn enkele van de uitdagingen die de implementatie van nieuwe technologieën in deze sector bemoeilijken.

Het gebruik van machines om de verplaatsing van zware producten te vergemakkelijken is reeds geïmplementeerd in de bouwsector. Pas de laatste tijd heeft de automatisering van complexe activiteiten echter zijn intrede gedaan. Het gebruik van op extrusie gebaseerde additieve productie, ook wel extrusie gebaseerd 3D-betonprinten (3DCP) genoemd, om te helpen bij de productie van bouwelementen, heeft een groot potentieel getoond bij het tackelen van enkele bottlenecks, zoals de productie van complexe geometrieën. Bovendien blijkt uit het rationele gebruik van materialen al snel het potentieel om deze industrie te helpen bij het behalen van de milieudoelstellingen die de samenleving nastreeft.

Bovendien heeft het gebruik van ongewapende mortel in deze nieuwe constructietechniek ook beperkingen aangetoond. De brosse aard van het materiaal dat wordt gebruikt voor extrusie brengt ook beperkingen met zich mee, zoals de noodzaak voor integratie van externe versterking of het slechts toepassen in ontwerpen waar slechts beperkte trekkrachten aanwezig zullen zijn. Om dit probleem aan te pakken, stelt dit onderzoek het gebruik voor van Strain Hardening Cementitious Composites (SHCC). Er wordt een rationele methodologie gepresenteerd om beschikbare mengsel-ontwerpen in de literatuur aan te passen aan de vereisten van 3D printen.

Voor de studies werden twee in de literatuur beschikbare SHCC-mengsels gebruikt. Mix-ontwerpparameters zoals de invloed van de water-tot-vaste-stof-verhouding, het vezelvolumepercentage, superplastificeerder en het gehalte aan viscositeitsmodificerende hulpstof (VMA) op de eigenschappen van de verse mortel werden onderzocht. Het gebruik van een ram-extrusie-experiment samen met het Benbow-Bridgewater-model werd voorgesteld om de reologische eigenschappen van de materialen te evalueren. De reologische karakterisering heeft aangetoond dat het gebruik van chemische hulpstoffen en een lage verhouding water/vaste stof nodig was om een deegachtige consistentie te bereiken die nodig is voor op extrusie gebaseerde 3DCP. Deze toevoegingen waren ook

nauw gecorreleerd met de vorm van het materiaal dat uit de ram-extrusietest kwam. Geselecteerde mengsels werden geëvalueerd met pompproeven toen de extrusiemogelijkheden postitief resultaat toonden. Met behulp van gestorte monsters werd de mechanische prestatie van de gemodificeerde mengsels geëvalueerd en werd de strain hardening eigenschap bevestigd door middel van vierpuntsbuigtesten en eenassige trektesten.

Met behulp van twee aangepaste SHCC-mengsels voor extrusie werden verschillende elementen geprint om de invloed van deze nieuwe constructietechniek op de prestaties van het materiaal te onderzoeken. Lange stroken met één, twee, drie en vier geprinte lagen werden vervaardigd. Er werden monsters genomen van deze elementen en er werden mechanische testen in verschillende richtingen uitgevoerd alsook microstructuuronderzoeken. Er werd geconcludeerd dat op extrusie gebaseerde 3DCP leidt tot een voorkeursoriëntatievlak van de vezels. Deze voorkeursoriëntatie garandeert strain hardening gedrag wanneer de composiet in twee richtingen wordt belast: evenwijdig aan en loodrecht op de printrichting voor hetzelfde printvlak. Er werd geen ductiliteit waargenomen wanneer monsters onder spanning loodrecht op het printvlak werden belast (hechtsterkte tussen de lagen). Toch bleek ook dat het hechtvlak tussen de geprinte lagen niet een zwakke schakel was in het materiaal. Relatief gezien is de ductiliteit van het geprinte materiaal echter laag in vergelijking met de oorspronkelijke SHCC en met andere resultaten die beschikbaar zijn in de literatuur. Deze lage energie-absorptie werd later verklaard toen een grote porositeit werd waargenomen met behulp van een microcomputertomografie (CT-scan). Deze test hielp ook om te verduidelijken dat het grensgebied tussen twee geprinte lagen het laagste gehalte aan porositeit had gezien over de hoogte van het proefstuk. Daarom is geconcludeerd dat van de geprinte SHCC een anisotroop gedrag moet worden verwacht wanneer deze nieuwe bouwtechniek wordt gebruikt en dat printinstellingen een aanzienlijke invloed kunnen hebben op de prestaties van het gefabriceerde element.

Tijdens de eerdere onderzoeken werd duidelijk dat het gebruik van chemische hulpstoffen cruciaal was voor de ontwikkeling van extrudeerbare vezelversterkte cementcomposieten. Vooral het gebruik van VMA bleek essentieel om de vereiste reologische eigenschappen te bereiken. Aangezien het gebruik van een dergelijke hulpstof in materialen op basis van portlandcement niet volledig duidelijk was, was een karakterisering van de microstructuur noodzakelijk. Verschillende karakteriseringstechnieken werden gebruikt om de hydratatieontwikkeling te onderzoeken. Een afwijkende vorming van portlandiet werd waargenomen in elektronen- en optische microscopie. De grote hoeveelheden van dit mineraal werden met andere technieken bevestigd. Het gebruik van de hulpstof was ook gecorreleerd met vertragingen in de uithardingstijd, de mogelijkheid om te worden gebruikt voor interne uitharding, een hogere mate van hydratatie en een hoog gehalte aan luchtballen. Het gebruik van VMA kan gevolgen hebben voor het hydratatieproces van portlandcement en daarom moet het zorgvuldig worden toegepast. Desalniettemin kunnen sommige van de bijwerkingen slim worden gebruikt om andere eigenschappen van cementgebonden composieten te verbeteren.

Bovendien opent de ontwikkeling van specifieke materialen voor gebruik in 3DCP ook de mogelijkheid om extra functionaliteiten in te bouwen. In dit onderzoek zijn twee extra eigenschappen van cementgebonden composieten onderzocht, namelijk mogelijkheden voor self-sensing en autogene self-healing.

De invloed van het gebruik van VMA en cellulosepulp op het autogeen zelfherstellend vermogen van matrices rijk aan portlandcement of hoogovenslakken werd onderzocht. Het is bekend dat de natuurlijke vezels ingebed in de matrix van portlandcement vatbaar zijn voor degradatie wanneer ze worden blootgesteld aan vocht-droogcycli. Daarom werden tijdens dit onderzoek ook twee extra condities geëvalueerd: vezelvoorbehandeling (verhoorningscycli) en versnelde verouderingscycli (bevochtigen en drogen). Er werden twee technieken gebruikt om de zelfherstellende eigenschap te kwantificeren: analyse van beelden verkregen uit CT-scanstesten en waterdoorlatendheidstesten. De resultaten toonden aan dat de autogene zelfherstellende prestatie van matrices die rijk zijn aan portlandcement grotendeels wordt beïnvloed door het volume VMA. Het grote volume aan luchtholtes en de abnormale vorming van portlandiet waargenomen in de microstructurevaluatie kunnen de verklaring zijn voor deze verbeterde eigenschap. Aan de andere kant vertoonden matrices die rijk zijn aan hoogovenslakken deze invloed niet.

Met betrekking tot de monsters die onbehandelde natuurlijke vezels gebruikten, werd een verbeterde prestatie waargenomen voor beide geëvalueerde vezelgehaltenes. Bovendien werden dezelfde resultaten niet gevonden in monsters met voorbehandelde vezels. Aangezien de voorbehandeling de wateropname van deze vezels vermindert, wordt ook het autogene zelfherstellende vermogen belemmerd, aangezien het cruciaal is om het vocht gedurende langere perioden in het monster vast te houden. Over het algemeen werd een zeer lage autogene zelfherstellende werking waargenomen voor monsters die werden onderworpen aan versnelde verouderingscycli. Alleen monsters met vezels die zijn blootgesteld aan 10 voorbehandelingscycli vertoonden een zekere mate van bescherming tegen de versnelde verouderingscycli. Het is niet duidelijk of de lage autogene zelfherstellende prestatie van verouderde monsters verband houdt met de veroudering van de vezels of de verdichting van de matrix. Helaas werd een zeer beperkte correlatie gevonden tussen de twee technieken die werden gebruikt om de autogene zelfherstellende prestatie te kwantificeren.

De tweede extra onderzochte eigenschap was de ontwikkeling van SHCC met zelfwaarnemende eigenschappen. De invloed van meerwandige koolstofnanobuisjes (CNT) op de piezoresistieve eigenschappen van de composiet werd onderzocht. Tijdens het belasten van de monsters met een uniaxiale trekkracht werd een impedantiemeting uitgevoerd. De vergelijking van de evolutie van de capaciteit en de weerstand in vergelijking met de vervormingen op de composieten leidt tot de ontwikkeling van factoren. Deze factoren werden gebruikt om de gevoeligheid van de composiet voor de vervorming en de schade aan het proefstuk in kaart te brengen in relatie tot de hoeveelheid koolstofnanobuisjes die in het proefstuk. Uit het onderzoek bleek dat SHCC's met CNT kunnen worden gebruikt als spanningssensor en dat het gebruik van wisselstroom aanzienlijke voordelen biedt ten opzichte van gelijkstroom.

Zoals gemeld in dit proefschrift is de ontwikkeling van slimme SHCC voor toepassing in de op extrusie gebaseerde 3DCP mogelijk. Het potentieel van extra eigenschappen die in dit composiet kunnen worden ingebed, werd onderzocht, evenals karakteriserings-technieken voor de verse en uitgeharde toestand van dit materiaal. Er wordt aangenomen dat de ontwikkeling van nieuwe materialen meer begrip zal brengen op gebieden waar het de bouwsector aan kennis ontbreekt, zoals de reologie van cementgebonden materialen. Ten slotte is dit ook een belangrijke kans voor deze economische sector om

de milieu-uitdagingen aan te pakken door middel van nieuwe technologieën en duurzamere materialen.

1

INTRODUCTION

*Viver - não é? - é muito perigoso.
Porque ainda não se sabe. Porque aprender-a-viver é que é o viver, mesmo.*

João Guimarães Rosa, Grande Sertão: Veredas

*Living is a dangerous business, isn't it?
Because we are still ignorant. Because learning-to-live is living itself.*

João Guimarães Rosa, The Devil to Pay in the Backlands

This chapter introduces the thesis and shows the thesis outline. Here a very brief introduction to the entire content of the thesis is given. The importance of research devoted to improve autonomous techniques for the construction market is also emphasized.

1.1. INTRODUCTION

THIS book is the summary of the research developed during the PhD studies of the author when the development of smart cementitious materials is explored. The work is done in the context of enhancing autonomous mechanisms in the construction industry, from the fabrication till the building usage.

The construction industry plays an important role on the social and economical context of modern society. An efficient use of what was built in the past and what will be built in the future is crucial for people, providing sheltering, ways of transportation and communication, for example. Therefore, rational use of resources is crucial for the success of a society in the long term.

In the past centuries, production in large scale has shaped society and provided different sort of goods and services. Intense use of natural resources coupled with the power of industrially modify them to the needs of the people have made expansion of the population possible. Latter in evolution the use of computers made possible a better understanding of the use of these resources and intensified the possibility of automation of repetitive tasks.

The construction industry has also followed this societal evolution and created different process and technologies to use most of the resources extracted form the nature. Mastering the possibility of mass production the built area of many countries expanded. Nowadays, the need of expansion still exists, meanwhile the need of preserving what was built becomes more important with the time.

Currently, a digital era is showing the importance of collecting and transforming data in information. Advancements in robotics brings the possibility to transfer drawings to commands that can be applied to as many repetitive tasks as the users creativity demands. From factories to laboratories, robotics can play an important role in raising the efficiency of society. Automation might be used to prevent accidents, easing the workload for the good of people or to raise productivity and resources allocation for the good of the capital. In either circumstance, it is inevitable to note that technology is important for the progress.

Often, the construction industry is accused to be very slow and conservative when applying new technologies and solutions. For many reasons, this was not different in the incorporation of automation to their activities.

In this context this PhD thesis decided to explore the possibilities to contribute to the use of automation in the construction industry. More specifically, the aim is to improve and/or develop techniques to enhance the use of autonomous technologies in this industry. With the focus on the materials, this research was dedicated to develop a fibre reinforced cementitious composite with enhanced properties that can be used in the construction phase and during the service life of this material. Somehow, this composite could play a smart role on the commissioning phase of the building and at the same time adapted for new construction methods that will be further explored in this book. Furthermore, this research aims also to address questions related to the development of the material, such as:

- How to develop fibre reinforced cementitious composites that can be used by additive manufacturing in the building industry?

- What might be incorporated to these cementitious composites that could bring additional functionalities to this material?
- What might be the consequences of the use of the selected materials on the composites characteristics?

1.2. THESIS OUTLINE

The thesis outline is given in figure 1.1. From the first chapter until the last one the development, characterization and some added functionalities to printable strain hardening cementitious materials are discussed.

An overview of the use of smart cementitious materials, focusing on the importance of automation since the construction phase, until the maintenance of the building is given in the second chapter of this book. In this chapter the use of composites for additive manufacturing, self-healing and self-sensing applied in the construction industry is approached.

In the following two chapters (3 and 4) the development of printable strain hardening cementitious composites is discussed. A rheological approach is proposed and the influence of each mixture component is evaluated in the fresh state. Moreover, two mixtures were developed. One of them containing large volumes of blast furnace slag and the other with large volumes of fly ash together with the use of sand as aggregate. Further, in chapter 3 printed elements were tested and the strain hardening performance was confirmed, in addition of several other discoveries such as the influence of the printing methodology, the fibres distribution and a larger than usual air-voids content.

To achieve such rheological properties, printable mixtures must be manipulated with care and the use of some chemical admixtures is needed. Therefore, the influence of the use of hydroxypropyl methylcellulose (HPMC) in the cement hydration is discussed in chapter 5. Interesting finds are shared in this chapter, for instance explaining the reason behind the higher amount of air-voids in printable materials and a higher and anomalous grow of portlandite. These finds made the author rise the question that would result in the following chapter of this thesis. Would this different portlandite formation somehow influence the autogenous self-healing performance of printable materials?

The answer for this question was discussed in chapter 6. Pure Portland cement paste and blended with blast furnace slag pastes with different contents of HPMC were evaluated. Additionally, the use of natural fibres to work as a water reservoir in the composite whenever the material gets saturated was proposed. The investigation concluded that the use of HPMC indeed enhanced the autogenous self-healing performance of cementitious materials. Moreover, the use of natural fibres could also enhance this performance but, could only keep the autogenous healing efficiency for longer periods of time if they were treated before used in the composite.

In the end, the use of SHCCs to be employed as strain sensor is discussed in the chapter 7. In order to enhance the piezoresistivity performance of the same material used as a base for the development of one of the printable mixtures, the SHCC was doped with carbon nano-tubes. The electrical impedance of the composite was measured while the specimens were loaded in tension. During this investigation the separate use of the resistance and the capacitance of the material is proposed. In this research it was observed

that these two electrical measurements could deliver different information during the tensile load. While one was more efficient in the elastic phase, the other was very valuable during the plastic phase.

Finally, chapter 8 brings the conclusions and a final overview of the study after all the investigations. Along with the conclusions, suggestions for future works are given for this challenging and inspirational research field.

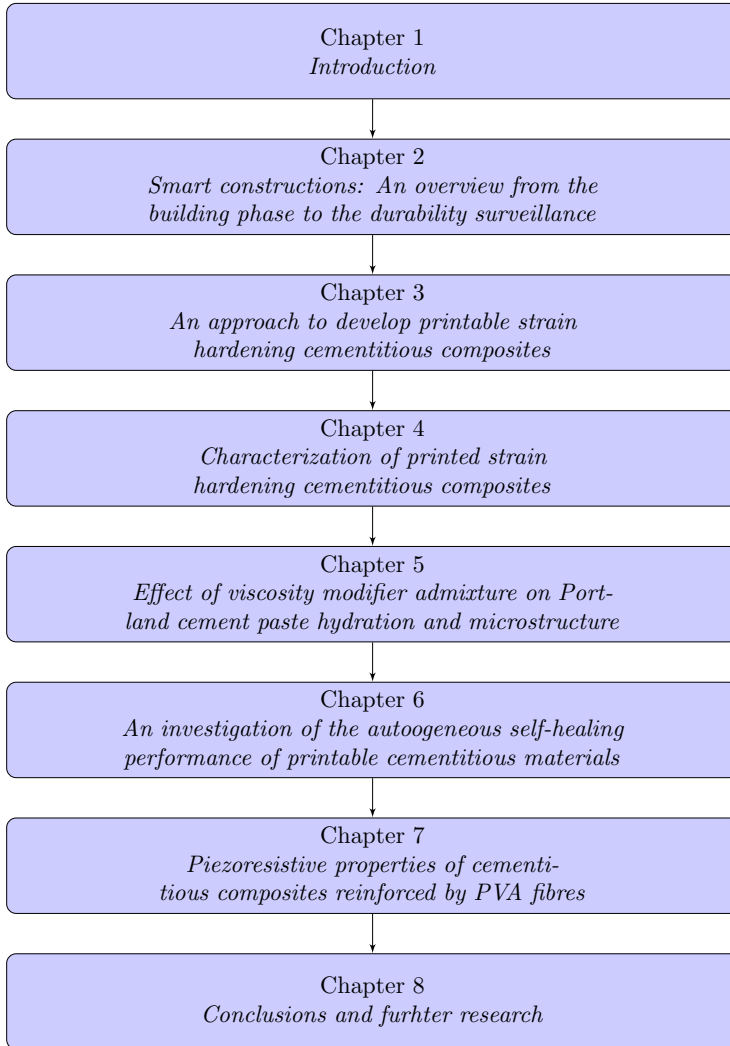


Figure 1.1: Thesis Outline.

2

SMART CONSTRUCTIONS: AN OVERVIEW FROM THE BUILDING PHASE TO THE DURABILITY SURVEILLANCE

Education is the most powerful weapon which you can use to change the world

Nelson Mandela

Lately, attention has been given on the development of a new construction technique namely 3 dimensional (3D) printing. This technique has demonstrated its potential to address the lack of automation during the building phase. Due to the development of this new way of building, adjustments on the materials must still be accomplished. In addition, this has also brought the possibility of incorporating of new materials to this industry. Aiming for an extended service life of construction materials much effort has been given on the development of new technologies that are able to monitor and even act when a damage occurs, such as self-sensing and self-healing. Great achievements were made through research on the development of smart solutions for the construction industry. These efforts have enabled new options for designing new building materials that are able to provide feedbacks to the users during their service life and even act to protect themselves. These new technologies collaborate with the efforts of decreasing the environmental impact of this industry and provide better materials for the increasing demand of automated structures.

Parts of this chapter have been published in Figueiredo S.C., Çopuroğlu O., Schlangen E. (2018) Smart constructions: An overview from the building phase to the durability surveillance. 13th International Congress on Advances in Civil Engineering. 2018. September 2018, Izmir [1]

2.1. INTRODUCTION

DURING the past few years the construction industry has not developed significantly regarding its automation. From the building phase until its service life surveillance structures are usually not able to provide information to their users in real time. A lot of efforts has been put on the design and building phase, bringing process control techniques and efficiency benchmarks from industrial engineering. Significant improvements were achieved on the design phase. However, on the building phase these techniques have only improved the industry management. Lately, attention has been paid on the development of a new technique of construction. The printing of structural elements has demonstrated its potential to address the lack of automation during the building phase. Due to the development of this new way of building, adjustments on the materials must still be accomplished. In addition, this has also brought the possibility and the need of incorporation of new materials to this industry.

From the structural service life point of view, very few has been achieved. Until today, durability reports are very dependent on field observations and damage alarms. Monitoring structures through sensors only happens when some problem is reported, and sometimes a repair is already too late to preserve and prolong the service life. The lack of real time assessment of structures makes almost impossible the development of any automation script to alarm in case of capacity overhead. Aiming for an extended service life of construction materials, much effort has been given on the development of new technologies that are able to monitor and even act when a damage occurs. Two examples are given:

Self-sensing techniques have been on the spot light for some years. These composites were developed doping cementitious materials with electrical conductive particles. The result is a cementitious composite that is able to change its electrical resistivity when its dimensional stability changes, due to tensile or compressive loads. This technique has a great potential to be employed during the service life of structures, providing data to be used in real time durability surveillance.

Another technology which has also received attention is the development of self-healing cementitious composites. Either using its natural capability of closing small cracks or improving it employing other products, this type of material has potential to prolong the service life of infrastructure. For instance, the enhancement of autogenous healing capabilities has been reported employing superabsorbent polymers and the healing of larger cracks were achieved employing selected bacteria.

This paper aims to discuss and make a review of the recent developments from the building phase till its service life assessment which will lead towards automation for this field.

2.2. CONSTRUCTION MANAGEMENT

There are several reasons why a process starts to be reviewed, trying to minimize the resources employed to manufacture a product. Resource problems like its cost, availability, quality and many others are usually some of the start points to review the way that a product is made. This review goes from changing the raw materials needed to make this product, or even change the process of making this product. Industrial and

process engineers are usually in charge of review and suggests solutions for this type of problem. Observing how industries approach such a problem, it is possible to understand the importance of this matter. To survive in the market, constantly manufactures are studying techniques to improve the production of their goods.

In the case of the construction industry, a lot of efforts have been done to bring concepts usually found on the automotive and technological manufactures. The pressure of competitors, tight schedules, cost of labor work and materials, environmental concerns and consumers requirements are usually the reasons why this industry looks for technologies from other sectors. Many techniques were successfully adapted from other industries to the construction sites, e.g. the lean construction, 5S and 6-sigma. These techniques aim to organize the process of production dividing tasks and providing tools to measure productivity, for instance [2, 3].

A construction process which can be taken as an example and has clearly changed over time is the raise of buildings. It is recommended to split the building construction in several parts like financial feasibility, project development, foundations execution, structural and nonstructural parts, electric and hydraulic installation, finishing, etc. From the point of view of the owner of the business, this strategy guarantees that each phase can be individually optimized, executed by specialized contractors and easier to be controlled. And from the costumer point of view, the product which will be bought has a higher chance of having a good quality/price ratio.

An industry which has been totally developed after importing the management tools to the construction market, was the precast of structural elements. The precast of those elements can be done in situ or ordered from different companies. Depending on the degree of complexity of the project to be executed, one of these options can be chosen. The availability of this type of components for the contractors, has changed the market and improved significantly the sector's productivity. Employing this technology, the number of tasks to be done on the construction site decreases considerably [4]. Therefore, the time planed for the execution is more probable to be reached employing less but more qualified workers. This type of approach, brings the same point of view of for instance the automotive industry, where a vehicle is assembled in a production line with its pieces coming from different industries.

Meanwhile the productivity on this sector has significantly rose due to those new management strategies, the process of building is still labor work intense. In a precast industry the workers must be deployed to execute several different types of activities, like assembly and disassembly molds, preparing and positioning steel reinforcement, casting concrete, operate the logistic of moving each manufactured piece, quality control, etc. Even though, the productivity of this industry has increased, very little automation has been developed. The high complexity of structural elements with its reinforcement and details has always been one of the obstacles.

2.3. ADDITIVE MANUFACTURING

Additive manufacturing (AM) is the terminology used to generally refer to any type of technology related with the manufacture of a product from a digital design employing robotic techniques to create the object. AM is commonly referred as three-dimensional printing (3D printing), as well [5]. Initially this technique was developed to facilitate the

understanding of two-dimension draws. At that time, the original technique fabricated three-dimension models composed of several layers of photopolymerized polymers [6]. Furthermore, the technique was considerably improved and automated. It was further developed to other materials, like other plastics, metals, food and ceramics.

In the case of cementitious materials two techniques has drawn attention: powder based and counter craft technologies. They are the 3D printing technologies which has so far demonstrated the greatest potential to be applied in large scale on the construction industry. They rely on different mechanism of deposition to fabricate the product.

Powder based AM technology uses a powder bed and a laser or an inkjet head to fabricate the objects. A continuous supply of powder keeps filled a reservoir where the object is being printed. The head connected to a robotic arm is responsible to put together the powder available on the reservoir, respecting the drawings created on the computer. Layer by layer, the object is fabricated, and in the end, it can be withdrawn from the reservoir [7]. In the case of the laser head, the contour of the object is obtained melting the supplied powder. This technique has been broadly used to obtain complex shapes made of metals, polymers, ceramics and it has demonstrated great potential for biologic tissue. In the case of an inkjet head the supplied powder must be a binder. The inkjet head fabricates the desired object placing layer by layer a small and continuous amount of liquid which can react with the powder. This technique has been applied to produce objects made from ceramics [8] and plastics [9]. For both powder based techniques problems are often reported regarding the high temperature reached with the laser head, leading afterwards to cracks due to thermal movements, high porosity and poorly chosen binders for the inkjet head [10].

The counter craft technology fabricates the object layer by layer using solid suspensions extruded through a nozzle. The solid suspension must have specific consistence to provide enough fluidity to be pushed out from a nozzle and keep the desired cross section shape to form the layer. The counter craft was developed in 2004 by a group of researchers from the Department of Industrial and Systems Engineering of the University of Southern California in the United States of America [11]. This technique has been largely applied for researches of construction purpose as it has demonstrated great potential to be applied in manufacturing of large scale projects. The same group where the technology was created, has progressed with further experiments demonstrating its enormous versatility and capability to handle large scale projects [12, 13]. At this same group a lot of efforts were put on the development of cementitious composites to be used as raw material for the fabrication of the objects.

The customization that AM brings to the construction market can turn complicated process of preparing and executing structures of complicated geometries into a normal task in a construction site. Nevertheless, this type of structure would also be employed to reduce the total volume of material employed. The possibility of customizing the elements fabricated by AM develops the possibility of smarter designs which will lead to the reducing of the self-weight of structures [14, 15]. Another positive side of this entirely new concept of functional structures is the high probability that this way of fabricating elements will lead to environmental friendly design, when structural materials will be placed only where it is strictly necessary.

The development of mix designs to be used on AM employing the counter craft tech-

nology does not follow the same rules of designing a standard mortar or concrete. The fresh state properties of the material are of extremely importance. Mixture compositions devoted to being used for 3D printing purposes must have a dough like consistence on the fresh state. This type of consistence is a key parameter to generate a homogenous composite [16].

Looking back in the history of cementitious composites, one specific technology draws attention among others. The extrusion of composites is a very well established industry, where mixtures are pumped through hoses, pushed out of nozzles, and afterwards the composites must retain their shapes, as it will not be further processed. Those characteristics are very close to what is needed for counter craft technology. In general extrusion is a technology which has received a lot of attention on the 1980's, when different models and experiments were conducted for application mainly on plastic and highly concentrated solid suspensions. In the case of cementitious composites, of course the technologies created for highly concentrated solid suspensions are of great importance [17, 18].

In the fresh state, a cementitious mixture can also be faced as a solid suspension. To keep the quality of such kind of mixture during the extrusion process some attention has to be given on the particle size distribution of the raw materials and the liquid to solid ratio. Tailoring those parameters will lead the composite to have a high packing density and diminish the risk of separation of the liquid and solid phases during the extrusion process.

Taking care on the development of the mixture to reach a well distributed particle gradation and an optimum liquid/solid ratio will guarantee a homogeneous, and a stable shape after the extrusion. However, a particular characteristic of printing materials must be also addressed. The printing technology fabricates the product layer by layer. Therefore, the self-weight of higher layers on the lower layers can reach values higher than the bulk yield stress of the mixture. When it happens, the printed object would unfortunately collapse. To achieve better capabilities to hold the pressure generated from the upper layer, adjustments on the setting time of the printing materials must be done. The setting time of a printable mix-design must be optimized to be able to be still fresh when the following layer arrives on top of it and must build strength over time to guarantee that it will never or minimally slump when the consecutive layers are placed on top of it. Experiments regarding adjustments of the setting time of printable mixtures are often reported in publications where the development of mixtures is addressed [13]. Alternatively, instead of using admixtures to accelerate the chemical reactions in printable mixtures which employs ordinary Portland cement, this field opens a window for the implementation of fast setting binders, such as: geopolymers, alumina, and phosphor cements, for instance.

Besides the fact that AM can bring innumerable advantages to the construction industry some problems must still be studied. Problems regarding the lack of ductile reinforcement, the high potential of cracking due to plastic and drying shrinkage or poor bonding between printed layers are some of the issues that must still be subject of research. One of the most direct and important issues that must be addressed is the lack of reinforcement. In structures, steel reinforcement takes care of tensile and shear loads. To bring AM as an automation solution for the industry an answer will need to be elab-

orated for solving this issue. This problem was addressed embedding a metallic wire on an extruded mortar [19]. The solution proposed by the authors of that publication has potential to be upscaled and eventually to be implemented on the industry.

The possibility to directly link drawings from the design of the structure to real life, through AM techniques no doubts bring a new era for the construction industry. This type of technique can increase considerably the productivity on this sector, which is determinant for the gross domestic product of some countries.

2.4. SERVICE LIFE ASSESSMENT

Infrastructure maintenance is a worldwide problem, due to the high complexity of the structures and the cost involved in a durability surveillance. Maintenance surveillance of infrastructure spread in large areas will always be challenging, and resources demanding. Therefore, techniques which improve the efficiency of infrastructure health monitoring must be developed [20].

Most of the infrastructure will need repair interventions during their service life. In the past few years, several projects have been carried out on the development and characterization of different repair materials. Among these, the performance of high ductility cementitious composites has drawn the attention of different sectors. The importance of high absorption of energy while loading, possibility of reaching high strains and failure only after the development of multiple micro-cracks were acknowledged [21].

Furthermore, to keep structures up to date, their service conditions must be assessed. In an ideal situation, the structural and materials design, together with the construction site diary and the reports form the service life assessments during the entire service life of the equipment could make part of a unique portfolio of the aging process of a structure. This type of portfolio would be very welcome when any type of diagnostic of a damage is needed. However, keeping track of the aging of infrastructure is not an easy task. It is usually an expensive service, involving specialized work, and equipment.

To collect data about the behaviour of the structure over time, different type of sensors can be employed. From the environment surrounding the structure, measurements from thermometers, hygrometers, pluviometers and seismometers are commonly reported. Meanwhile, displacement transducers, total stations, optic fibres, oscillometers and even video cameras are some of the examples of sensors employed monitoring the structure itself [22]. There are several papers reporting the implementation of sensors to measure already built structures, mainly bridges [23]. In some special infrastructure cases, where the investments on the health monitoring are higher, the use of several types of sensor guarantee the safe use of the equipment and a better planning of repair refurbishment and inspections [24].

2.5. SMART CEMENTITIOUS COMPOSITES

2.5.1. SELF-SENSING

Self-sensing cementitious composites are materials developed by doping brittle matrix with conductive fillers. Those conductive fillers might have a particle shape like graphite or steel balls, or they can be used also in fibre form similar to steel or carbon fibres. Their size can vary from nanometres to a couple of millimetres. The principle of the self-

sensing cementitious composites relies on the piezoresistive nature of these particles. The piezoresistive property is defined as a change in the electrical resistivity of certain material, when this material is subjected to a certain change on its size. Composites that receive this type of admixture usually demonstrates sensitivity to mechanical strains, damage and temperature differences.

Han, Ding and Yu, 2015 [25] describes that the electrical conductivity of cementitious composites with conductive fillers is represented by the contact conduction between the particles, the tunnelling or field emission conduction and ionic conduction. The contact conduction is only possible when the particles are in contact with each other. The field emission conduction can happen only within particles with very sharp edges and close enough of each other. Finally, the ionic conduction which depends on the availability of ions to transport the charge. It is important to remember that ionic conduction plays a very important role on cementitious composites, due to the moisture and porous matrix properties [25]. It was also demonstrated that in general self-sensing cementitious composite decreases its electrical resistivity when compressive loads are applied and in the case of tensile loads, the resistivity would go higher [26].

This material has been under development in different research groups worldwide. Different aspects were approached obtaining interesting results. Conductive fillers were tested in paste, mortar and on fibre reinforced composites level. Results of the incorporation of carbon nanotubes [27], graphene [28], carbon black [29], carbon fibres [30] and even intrinsic ability of composites on sensing damage was detailed in some works.

[31] has demonstrated that standard concrete can be used as damage sensor, if the electrical resistance of the material is measured continuously. Afterwards, researches have demonstrated that fibre reinforced cementitious composites are also able to detect damage through electrical resistance measurements. In the case of these composites, the damage propagation when tensile loads were applied on the material could even be followed. The reported composites had the property to develop several cracks during the loading. Therefore, the current flow on the composite had to be deviated always when a crack was being created, and those deviations were translated as drastic increases of electrical resistance [32].

Employing conductive fibres to enhance strain sensibility is also commonly found in literature. [33] have reported decrease on the overall electrical resistivity when cementitious composites reinforced by large amounts of steel fibres were loaded in tension. More often are reports on composites employing reinforcement by carbon fibres. Many publications were released demonstrating how the electrical resistance of cementitious composite reinforced by carbon fibres changes while loaded in tension, compression and bending. Small volumes (approximately 0.5% by volume) of fibre reinforcement were generally sufficient to provide strain or damage sensitivity to cementitious composites. Looking for improvements on the bond strength between fibres and cementitious matrix together with enhanced sensitivity, fibre surface treatment with ozone was also proved to improve this type of composite [34].

Another piezoresistive filler which has been broadly investigated for development of self-sensing cementitious composites are the carbon nanotubes (CNT). Due to their piezoresistive property and its very small dimensions CNT have demonstrated a great potential in this field. Investigations have demonstrated that very small volumes of ad-

dition of this admixture are able to develop piezoresistive response on cementitious materials. Incorporation ranging from 0.05 to 0.5% of Portland cement weight is usually reported on literature, with optimum content close to 0.1% [27, 30, 35].

The volume of CNT employed to reach a desired piezoresistive performance is directly connected with the dispersion of this material on the matrix. Many studies discussed about different techniques to improve dispersion of nanoparticles on cementitious matrix. From all approached methods three or the combination of some of them are commonly reported successful. The first method relies on the agitation of an aqueous suspension of CNT employing ultrasonication. This type of agitation is very energetic, enabling the lumps of CNT to be separated and further dispersed. On the other hand, often ultrasonication of aqueous CNT solutions are enhanced by a second dispersion method which relies on the employment of chemical admixtures. Usually the employment of surfactants enhances the dispersion of nanoparticles considerably. Surfactants can surround the nanoparticles and lower their surface tension, making them easier to be dispersed. Some researchers have reported a successful dispersion of CNT in aqueous solution containing surfactants and improved piezoresistive properties on cementitious composites containing the solution [36, 37]. The third and most advanced technique that guarantees a homogeneous dispersion of CNT was reported by [38]. This method facilitates the growing of CNT and carbon nanofibres during the Portland cement clinker production. The new type of cement created by this group has been applied mainly on the cementation of oil wells, due to the ultimate mechanical performance achieved [39].

Several authors have demonstrated not only advantages in their use on cementitious matrix regarding the reduction of the electrical resistivity but also on the gain of mechanical performance. The CNT can act as nucleation spots for the cement hydration. This property leads to a faster and higher hydration of the cementitious matrix, generating CSH with higher mechanical properties [40].

One extra matter which deserves to be addressed is the methodology to measure the electrical resistance. Several publications report the measurements during the mechanical test employing direct current (DC). This type of measurement is in general easy to be conducted and does not involve complicated knowledge on electromagnetism. However, to obtain reliable measurements with this technique the sample must be dry or after connecting the sample to the voltage supply a long time must be waited before the test gets start. This precaution is due the polarization effect. As soon as a DC supply is connected to a cementitious composite, due to its porous and ionic intrinsic property, the composites acts as a capacitor charging until its stabilization [41, 42]. This type of inconvenience on the measurement can be avoided employing an alternate current (AC). This technique indeed requires more complex equipment but reveals a more detailed diagnostic of the sample. Measuring the current and voltage signals it is possible to make a diagnostic of the capacitance and reactance behaviour of the material while loaded [43, 44]. This diagnosis might lead to a deeper understanding of the reasons behind the total changes on the electrical resistance of the composite measured employing DC.

Cementitious composites able to be used as damage or strain sensor are a step further on the surveillance of large amount of infrastructure. A real time monitoring of this type of material can be extremely important to have a broad and realistic diagnosis of

the conditions of structures exposed to hazardous environments or overloads such as capacity overhead from users or seismic movements. Moreover, the use of this technology can decrease the number of *in-situ* inspections, which are not always easy to be performed, usually not periodically realized, and sometimes extremely expensive. This type of continuous monitoring contributes significantly for the improvement of automation on the construction industry, providing more reliable data and diminishing or at least decreasing society exposure to unnecessary risks.

2.5.2. SELF-HEALING

One of the most dangerous situations that a concrete structure can be exposed is the cracking of its cover layer. This type of damage is most of the time dormant as it can have very small sizes, placed in hard to be access locations and usually not causing large problems at the beginning of the pathology. The cover layer is designed to protect the steel reinforcement. Its depth is calculated to provide isolation of the reinforcement inside of the concrete from the external environment during the service life of the structure. The concrete with its intrinsic properties provides this protection. For instance, its porosity and alkalinity protect the structure against carbonation, penetration of chloride ions and spoiling due to deicing salts [45]. Therefore, cracks on the cover layer are pathways to connect the external surrounds to the metallic reinforcement, facilitating the ingress of hazardous materials. Moreover, over time the cover layer is naturally damaged due to aging and if no action is taken this will lead to the exposure of the reinforcement.

Due to the high complexity of a detailed execution of structural projects, often it is possible to find reports describing crack formation on surface of concrete due to plastic or drying shrinkage [46]. Furthermore, tiny cracks due to excessive loading or thermal differences might also be the cause of appearance of damages on the cover layer of cementitious composites. It should be of primary importance the diagnoses of the existence of such problem in a concrete structure as early as possible. Therefore, periodically infrastructure surveillance is important to detect and quantify how broad is the problem. However, unfortunately maintenance campaigns are usually performed whenever a large problem is detected. At this point a large amount of hazardous materials could have penetrated the concrete causing a deeper and of course expensive damage.

For the past few years, a lot of attention has been given by researches to develop technologies to help on this matter. Several solutions providing the concrete itself capability to act when a crack is generated were created to minimize or solve such a big issue for the construction industry. The concrete ability to heal its own cracks is often addressed on literature as self-healing. The self-healing technology covers a large field of techniques to provide cementitious composite the ability of healing. Following an overview of autogenous self-healing and the different approaches to improve this natural property of cementitious composites, the use of microorganism and organic polymer to heal cracks of larger width will also be addressed.

Autogenous self-healing is an intrinsic property of cementitious materials. The cracks generated on the surface of cementitious materials can be filled with late hydration products from un-hydrated cement particles or deposition of calcium carbonate on the cracked surface. This way of healing the crack is depended on availability of moisture, as both chemical reaction in which the filling of the crack relies depends on water to happen

[47].

In the case of further hydration, any un-hydrated cement particle exposed to moisture can hydrate and its formed products might help on the crack filling. Further hydration can also rely on the pozzolanic activity of supplementary cementitious materials, like fly ash or blast furnace slag [48, 49]. This type of healing is often reported on high mechanical performance cementitious composites, as ultra-high-performance concrete (UHPC) or strain hardening cementitious composites (SHCC). The mix-design of these composites are designed to deliver the best mechanical properties possible, bringing the binder content to extremely high values and limiting considerably the availability of water.

Although, further hydration or pozzolanic reactions can contribute filling cracks, the most important mechanism of autogenous self-healing is the precipitation of calcium carbonate on the surface of the crack. The deposition of the mineral relies on the reaction between two dissolved ions. Carbon dioxide dissolved in water reacts with calcium anions coming from the concrete generating CaCO_3 . The crystal minerals formed during this reaction precipitate on the crack surface leading towards its closure [50].

The autogenous healing is able to close narrow cracks [51]. In general authors only report the closure of cracks and consequently the protection of internal parts of the structure against penetration of hazardous materials. However, Victor Lee has reported that mechanical properties of an Engineered Cementitious Composite (ECC) was also recovered after soak and dry cycles [52].

It is crucial for this type of healing the presence of water. Then, some researchers have employed superabsorbent polymers (SAP) to store moisture when a crack is exposed to water. SAP are materials able to store and slowly release the water in time. Additionally, when water is absorbed by this type of polymer they swell, blocking the way for more water to penetrate the concrete. Therefore, the cracked surface would stay longer exposed to the moisture increasing the self-healing efficiency of the damaged cementitious component [51, 53].

One of the self-healing techniques which has draw a lot of attention of the construction market is the healing of cracks employing microorganism. This type of healing relies on bacterial metabolism to heal the crack with calcium carbonate. Mainly, two mechanism of crack filling have been reported. The first developed mechanism employs bacteria able to produce urease during its metabolism, leading afterwards to a precipitation of calcium carbonate. On this case the process of filling the cracks relies only on the precipitation of CaCO_3 . The mineral is formed in the same way as described for the autogenous self-healing. However, the urease released by the bacteria in contact with water contributes increasing the availability of CO_2 dissolved in water [54].

Later, a second method employs two components: one is bacterial spores and the second is the organic compounds to be consumed by the microorganism [55]. As soon as the bacterial spores get in contact with the oxygen and the organic compounds they move out from the latent stage and start to produce CaCO_3 , CO_2 and water as a by-product of its metabolism. The calcium carbonate minerals are directly involved on the filling of the cracks and when the CO_2 gets dissolved in water it can enhance the autogenous healing, also contributing to the healing mechanism. This method has been largely published demonstrating its potential in laboratory scale [56], as well as in field

trials [57].

Another technique often reported on literature is the addition of manufactured particles during the mix of concrete or mortar. Those particles must have a stronger bond with the cementitious matrix than its own mechanical properties. They can be filled with organic polymers like epoxy, or with some other fast setting mineral compounds. Then, when a crack propagates through the concrete, those capsules must break and release their content [58, 59].

Self-healing techniques contribute to enlarge the service-life of structures which employ cementitious materials. They present solutions to decrease the time of exposure of the internal parts of a structural element to deleterious materials by means of autonomous healing of the damages. Self-healing techniques are already a reality on the construction market. They contribute significantly to improve the quality and automation of concrete structures, improving their safety and reliability.

2.6. CONCLUSIONS

Through the review brought by this chapter, the importance of automated solutions to the daily routines on the construction market was exposed. Structural damage in concrete happens in different ways, such as capacity overhead or ageing. It was also demonstrated that an extended and detailed survey of the health conditions of a vast infrastructure complex is difficult and resource consuming. However, an intense health monitoring rationalizes the scheduling of in-situ inspections and repair, saving costs and diminishing risks for the society. Therefore, the application of autonomous technologies contributes significantly in the development of smart cementitious composites. Research devoted to this area is a key factor on the development of a sustainable and health economy, enabling more reliable infrastructure investments.

3

AN APPROACH TO DEVELOP PRINTABLE STRAIN HARDENING CEMENTITIOUS COMPOSITES

In nature nothing is created, nothing is lost, everything changes.

Antoine-Laurent de Lavoisier

New additive manufacturing methods for cementitious materials hold a high potential to increase automation in the construction industry. However, these methods require new materials to be developed that meet performance requirements related to specific characteristics of the manufacturing process. The appropriate characterization methods of these materials are still a matter of debate. This study proposes a rheology investigation to systematically develop a printable strain hardening cementitious composite mix design. Two known mixtures were employed and the influence of several parameters, such as the water-to-solid ratio, fibre volume percentage and employment of chemical admixtures, were investigated using a ram extruder and Benbow-Bridgwater equation. Through printing trials, rheology parameters as the initial bulk and shear yield stress were correlated with variables commonly employed to assess printing quality of cementitious materials. The rheology properties measured were used to predict the number of layers a developed mixture could support. Selected mixtures had their mechanical performance assessed through four-point bending, uni-axial tensile and compressive strength tests, to confirm strain hardening behaviour was obtained. It was concluded that the presented experimental and theoretical framework are promising tools, as the bulk yield stress seems to predict buildability, while shear yield stress may indicate a threshold for pumpability.

This chapter has been published in S. C. Figueiredo, C. R. Rodríguez, Z. Y. Ahmed, D. Bos, Y. Xu, T. M. Salet, O. Çopuroğlu, E. Schlangen, and F. P. Bos, An approach to develop printable strain hardening cementitious composites, *Materials & Design*, vol. 169, p. 107651, 2019. [60]

3.1. INTRODUCTION

OVER the last decades, the employment of automation at construction sites has seen substantial achievements to enhance the productivity of the sector [61, 62]. Management tools have allowed tasks and activities to become more specialized and dynamic, thus providing an environment for shortening of construction time and decreasing construction errors. The employment of machinery to execute tasks on this industry was specially devoted to heavy duties nevertheless, some other activities still rely on the skills of humans.

A relatively recent development has been the introduction of Additive Manufacturing (AM) to the construction industry, also popularly known as 3D printing. AM is a classification of manufacturing technologies that fabricate objects by controlled, often layer-wise, addition of material, rather than by removal of material from a larger piece of bulk material. Generally, robotized equipment is applied that manufacture an object directly from digital design input [5, 6]. For construction, advances are being made AM of polymers [63], foams [64], glass [65], timber [66] and steel [67].

Developments have been particularly rapid for AM of concretes and other cementitious materials (AMoC) for construction. Technologies under development include the Stereolithography (STL) based D-shape process [68], Contour Crafting (CC) [11], Concrete Printing (CP) [69], 3D Concrete Printing (3DCP) [14], as well as the vertical extrusion based Smart Dynamic Casting [70] and Mesh Mould [71], in which a mesh reinforcement acts as the mould. Leaving the phase of showcasing the potential behind, described in a range of publications [72–79], AMoC (also referred to as Digitally Fabricated Concrete (DFC), to emphasize the automated production method) has now entered in a period of first real uses [80], and commercial initiatives abound (e.g. Contour Crafting, Total Kustom, WinSun, CyBe, Apis Cor, XtreeE, Incremental 3D, COBOD, and others). Alternative techniques are also available in which a mould of insulation material is printed and the concrete is cast inside [81].

This requires the development of a whole new generation of materials to meet both the manufacturing requirements (printability) as well as the mechanical and durability demands of a long-lasting. Recent researches have shown the development of cementitious composites with different aggregate particle sizes [72]. In some studies, fibres have been incorporated to stabilize the mixture at fresh state or to minimize the occurrence of cracks due to shrinkage [13].

However, as has been pointed out by other researchers as well, the different technologies and materials under development still suffer from a major drawback that forms an important obstacle for them to achieve their potential which includes form freedom, reduced material use and labour, decreased CO₂ emissions, and construction speed [82–86]. The print materials in AMoC, in general, have a low tensile strength compared to their compressive strength. Furthermore, they are usually brittle and thus fail relatively suddenly without large deformations. For structural use in construction, this is unacceptable, as the conventional concepts, such as the use of steel reinforcement bars, are either incompatible with AMoC or eliminate its advantages. A number of innovative approaches have been presented to overcome this problem, like the ones described by [15, 19, 87]. Further research is needed to be able to fully assess their potential and applicability.

Including fibres in the print material is an obvious solution strategy, too. It has been explored by Panda et al. [88], who compared glass fibres of different lengths (3, 6 and 8 mm) and varying volume percentage of fibres. Both studies reported a significant increase in flexural tensile strength, as well as an orientation effect of the fibres in the direction of the filament flow, but neither discussed the effects on ductility. Moreover, the use of PVA fibres in printable cementitious mortars exposed to fire attack was studied in [89]. In this case the authors have shown the advantages of using fibres to enhance ductility but also to minimize the occurrence of spoling. And recently the use of steel fibres to reinforce a printable mortar was also explored in [90].

Over the last decades, cementitious composites have been developed that exhibit strain hardening behaviour [91, 92]. Their performance is based on an optimized matrix composition, fibre performance, and matrix-to-fibre bond, and are known as Engineered Cementitious Composites (ECCs) or Strain Hardening Cementitious Composites (SHCCs). Significant plastic deformations can be achieved, as well as a high tensile strain, strength, and multiple crack development [21]. Resistance to quasi-static and dynamic loading is generally high [93]. Jointly, this results in favourable structural performance.

First results on the development of printable ECCs have been published by Soltan & Li [94]. Based on considerations of extrudability (indicating the ability of the mixture to pass through a printing system) and buildability (indicating the ability of a mixture to remain stable after deposition and during printing), that together define the printability, they developed several mixtures with polyvinylalcohol (PVA) fibres. The influence of several ingredients on fresh state workability and processing parameters were investigated. This resulted in at least one mixture that seems printable and shows strain hardening failure behaviour. However, the assessment of fresh state properties was based on the flow factor according to ASTM C1437 and ASTM C230, which is not a true rheological property. Also, the real printability was not truly yet established as only several layers were deposited with a manual piston. Pending a more extensive publication, a brief description of results about the development of a printable SHCC with high-density polyethylene (HDPE) fibres were given by [95].

The development of printable mix-designs is different from that of castable concretes. The challenges are not restricted to the hardened properties: competing requirements for extrudability and buildability have to be met as well. Globally speaking, the material should be fluid enough to pass through a print system without the use of excessive pressure and the occurrence of ruptures and/or void, while exhibiting sufficient strength and stiffness after deposition to avoid failure during printing or excessive geometrical deformations. When both these requirements are met, the material can be considered printable.

In order to evaluate the printability, different tests have been proposed, such as the cylinder test [13], the slump of the fresh mixture in a shape of a cylinder [96] or the slump of the printed layer itself [16]. In general, these tests consist in measuring the slump of the fresh material with or without a certain weight on top of it. However, such empirical tests do not result in true physical properties that describe the rheological or mechanical behaviour of the material. Only recently, first attempts to analyse printability in terms of physical rheology or mechanics properties have been presented [97]. Suitable method-

ologies are still under development.

The requirements for materials employed in the process of manufacturing an object in AMoC through a processes like 3DCP, are similar to those for extrusion manufacturing, a process that is commonly used for several types of concrete products. Although this has been acknowledged in some reports, the mix-design often does not follow the procedure that is usually suggested in the field of extrusion research [98]. Extruded cementitious mixtures can be considered as solid suspensions. These highly concentrated suspensions usually show dough-like texture. Therefore, the employment of conventional shear-based rheometers is not always suitable. Slippage and plug-forming of the evaluated mixture may lead to unreliable results [99]. Alternatively, a ram extrusion rheometer can be used. Using the pressure measurements from this device, true rheology parameters can be determined through the Benbow-Bridgwater rheology model [17, 100, 101]. A more detailed explanation of the model and the apparatus will be given in Sections 6.2 and 3.3.2.

As extrusion techniques are of great importance for the construction industry, the ram extruder proposed by Benbow-Bridgwater was extensively employed to quantify rheological parameters of different materials, amongst which a vast number of ingredients for cementitious composites. Particularly relevant to this study are reports on fibre reinforced mixtures, like the ones found in [99, 102–104], with PVA fibres, or in [18, 105] with natural fibres, or even with nano-fibres in [106]. The fresh state properties depend on several factors, like the volume of liquid employed, the particle size distribution, the volume of fibre reinforcement, time, and so on. Furthermore, rheology modifiers are commonly reported to have been used in studies on extruded fibre reinforced cementitious composites.

As SHCCs demonstrate enhanced mechanical performance in comparison to standard concrete or mortar, as well as superior durability properties [107, 108], the systematic (i.e. based on true properties) development of printable SHCC mixtures can move AMoC forward. Therefore, this research aimed to develop a printable SHCC mix-design based on the rheology properties measured with a ram extruder and determined through the Benbow-Bridgwater model. To understand the meaning of the physical properties on the flowability, visual inspections were performed on the extruded composite. A printability trial was subsequently conducted in a large scale 3DCP facility, on selected mixtures to assess pumpability, extrudability, and buildability. After hardening, several mechanical properties were determined to show the printable mixtures do indeed result in objects with strain-hardening failure behaviour. Only a limited number of tensile test results are shown here. The full results of the study on mechanical properties in the hardened state will be subject of a future publication.

3.2. THEORETICAL BACKGROUND

Behaving rheologically as a Bingham fluid, cementitious materials can have their yield stress measured. Measuring rheological properties of highly concentrated particle suspensions through conventional shear based rheometers has been shown as not the best approach [99, 109], and alternatives were given in [17, 100, 101]. The Benbow-Bridgwater model, used commonly to study fluids such as molten plastics, clay suspensions and prefabricated cementitious material, is especially suitable for this work.

In order to evaluate the rheology of composites at the fresh state a ram extruder was employed. The ram extruder is commonly composed of an upper barrel, where the material is introduced first and a connected die land, with smaller diameter, from which the material is extruded at last. A piston, moving downwards, pushes the material from the upper barrel through the die land. Coupling the total pressure drop in the die measured with this device alongside the Benbow-Bridgwater model, a description of the fluid rheology can be obtained. The total pressure drop in the die is composed by the pressure drop of the fluid on the die entry and the pressure drop on the die land. The pressure drop does not take in consideration any pressure drop in the barrel, as it is neglectable [110]. Therefore, the total pressure drop is given by the equation 3.1:

$$P = P_1 + P_2 = 2 \ln\left(\frac{D}{d}\right)(\sigma_0 + \alpha V) + \frac{4L}{d}(\tau_0 + \beta V) \quad (3.1)$$

where:

P = Total pressure drop [kPa]

P_1 = Pressure drop in the die entry [kPa]

P_2 = Pressure drop in the die land [kPa]

σ_0 = Bulk yield stress [kPa]

α = Parameter characterizing speed in the die entry [kPa.s/mm]

V = Extrusion speed in the die land [mm/s]

D = Barrel diameter [mm]

d = Die diameter [mm]

τ_0 = Shear yield stress [kPa]

β = Parameter characterizing speed in the die land [kPa.s/mm]

L = Die length [mm]

For the case of extruded paste developing pseudo-plastic behaviour the influence of the extrusion speed on the total pressure drop is not linear. For such cases, the Benbow-Bridgwater model is further enriched with the coefficients m and n , as shown in equation 3.2 [110].

$$P = P_1 + P_2 = 2 \ln\left(\frac{D}{d}\right)(\sigma_0 + \alpha V^m) + \frac{4L}{d}(\tau_0 + \beta V^n) \quad (3.2)$$

Rheological characterization of dough-like pastes are especially interesting for extruded materials, as they must keep their shape after being extruded. The resulting rheological properties are also very interesting for printed cementitious composites. Initial shear and bulk yield stresses are physical properties which can help quantifying important parameters for the AM with counter craft technology. The shear yield stress quantifies the friction of the material moving through the die while the bulk yield stress is an intrinsic material property. These quantities can be related to the main mixture requirements like shape stability and printability. Moreover, these properties can also be useful to estimate the amount of layers the material is able to support.

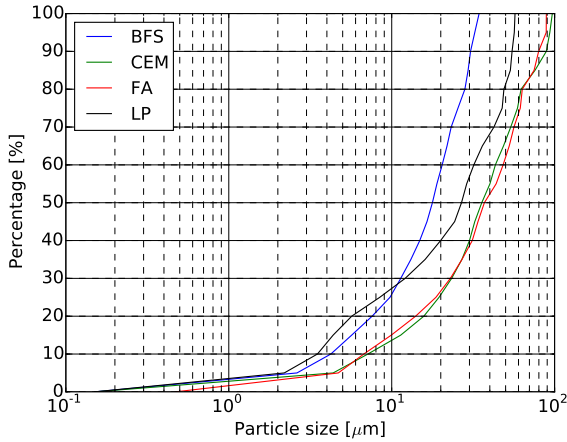


Figure 3.1: Particle size distribution

3.3. EXPERIMENTAL METHODS

3.3.1. MATERIALS AND SAMPLE PREPARATION

Two SHCC mixtures from [111, 112] were chosen as a departure point for the development of the SHCC mixtures for 3D printing. Both mixtures were reinforced with 2% by volume of polyvinyl alcohol (PVA) fibres. The first mixture matrix was composed by ordinary Portland cement (OPC), blast furnace slag (BFS), and limestone powder (LP), while the second reported mixture is composed by OPC, fly ash (FA) and sand. In order to increase the amount of fines used in the second SHCC, additional LP was used. In table 3.2 and table 3.3 the composition of each mixture are detailed. Initially, the rheology of their matrices (the composite without fibres) were studied. The influence of viscosity modifying agent (VA), superplasticizer (SP), water-to-solid ratio, PVA fibre volume and sand grain size on the fresh state properties were investigated.

The chemical composition of powder materials and their loss on ignition (LOI) can be found in table 3.1. They were assessed by X-ray fluorescence analysis (XRF) and thermogravimetric analysis performed at 10 K/min under Argon atmosphere. The LOI was calculated using the loss of mass between 45 and 1000 °C. The particle size distribution of the raw materials can be found on figure 3.1.

VA with viscosity 201000 mPa.s was provided by Shanghai Ying Jia Industrial Development Co., Ltd. SP used was a Glenium 51 obtained from BASF with solid concentration of 35%.

For the rheology tests, a volume of 0.5 litres was mixed in a planetary mixer according to the following procedure:

- All dry materials were mixed for two minutes at low speed (speed 1 - 60 rpm);
- While mixing at speed 1, during approximately one minute, water mixed with SP was added;
- The wet powders were mixed for the next two minutes at speed 1. In this phase

Table 3.1: Chemical composition of powder raw materials

Compound	CEM I 42.5 N [%]	Fly Ash [%]	Blast Furnace Slag [%]	Limestone Powder [%]
CaO	69.53	5.30	42.00	55.80
SiO ₂	15.6	53.23	30.73	0.28
Fe ₂ O ₃	3.84	7.77	0.54	0.03
Al ₂ O ₃	3.09	26.67	13.30	-
SO ₃	2.6	0.81	1.45	-
MgO	1.67	1.27	9.44	0.14
K ₂ O	0.55	1.42	0.34	-
TiO ₂	0.31	1.22	1.01	-
P ₂ O ₅	0.14	0.25	-	-
Rest	0.53	0.52	0.62	0.03
Loss on Ignition	2.14	1.55	0.57	43.71

it was possible to observe a significant change in the mixture's viscosity. A dough like consistence was achieved;

- At moderate speed (speed 2 - 124 rpm), the dough like mixture was further mixed. At this phase the dough opens inside the mixing bowl, and the fibres get dispersed.

3.3.2. RHEOLOGY MEASUREMENTS

In order to obtain the four parameters (σ_0 , α , τ_0 , β) describing the paste flow a ram extruder was built. The design was based on the equipment reported by [99, 100, 113] and can be found in figure 3.2. Three dies were applied with an internal diameter of 12.8 mm and length-to-diameter (L/d) ratios of 1, 4, and 8. The diameter of the piston (38.3 mm) was designed to minimize friction with the internal walls of the barrel (D = 38.4 mm) and to fit on an servo-hydraulic press (Instron 8872). Besides that, a Fluon[®] (polytetrafluoroethylene) ring was used as the end of the piston to seal the gap between walls and minimizing friction. During the tests this region was always lubricated with a silicone release compound (Dow Corning 7, Dow Corning[®]). For each new experiment the piston and the ring were removed from the Instron actuator and washed with tap water and soap.

The ram extruder barrel was filled with the mixture under evaluation. For each portion placed inside the barrel, compaction with the help of a 30 mm diameter steel rod was done. Compaction of the paste inside of the barrel is important to avoid big pockets of air which would result in drastic drop on the pressure during the extrusion experiment. As soon as the barrel was filled, the piston was attached to the Instron actuator. Four different speeds of the piston were used by controlling the displacement rate of the Instron actuator while the reaction force to the imposed displacement of the fluid was measured by a load cell. This load was used to calculate the total pressure applied to the fluid. In figure 3.3 an example of the output data from the experiment is given. The ram extruder experiment was performed four times for each die. The first extrusion was not

Table 3.2: Mix design summary of X series in [kg/m^3]

Mixtures nomenclature	CEM I 42.5	Blast Furnace Slag	Limestone powder	PVA	VA	Superplasticizer (Glenium 51) [g]	Water
XVA1	265.2	618.9	884.2	0	1.8	17.7	353.7
XVA2	264.9	618.0	882.9	0	3.6	17.7	353.2
XVA3	264.5	617.2	881.7	0	5.2	17.6	352.7
XVA4	264.1	616.3	880.5	0	7.0	17.6	352.2
XVA3SP1	266.7	622.2	888.9	0	5.3	8.9	355.5
XVA3SP3	262.4	612.3	874.7	0	5.2	26.2	349.9
XVA3W1	224.9	524.7	749.6	0	4.5	15.0	449.7
XVA3PVA10	261.9	611.0	872.9	13.0	5.2	17.5	349.2
XVA3PVA15	260.6	608	868.5	19.5	5.2	17.4	347.4
XVA3PVA20	259.2	604.9	864.1	26	5.1	17.3	345.6
XVA4PVA20	258.9	604	862.9	26	6.9	17.3	345.2

Table 3.3: Mix design summary of Y series in [kg/m^3]

Mixtures nomenclature	CEM I 42.5	Fly ash	Limestone powder	Sand (125 - 250) μm	Sand (250 - 500) μm	Sand (500 - 1000) μm	PVA	VA	Superplasticizer (Glenium 51) [g]	Water
YVA1	492.0	581.4	111.8	110.4	174.3	207.3	0	1.7	13.3	335.4
YVA2	491.4	580.7	111.7	110.3	174.1	207	0	3.3	13.3	335.0
YVA3	490.7	579.9	111.5	110.1	173.8	206.7	0	5	13.3	334.5
YVA4	490.0	579.1	111.4	110.0	173.6	206.4	0	6.7	13.3	334.1
YVA3SP1	493.7	583.5	112.2	110.8	174.9	208	0	5	6.6	336.6
YVA3SP3	487.8	576.5	110.9	109.5	172.8	205.5	0	5	19.8	332.5
YVA3W1	420.4	496.8	95.5	94.4	148.9	177.1	0	4.3	11.4	429.9
YVA3PVA10	485.8	574.1	110.4	109	172.1	204.7	13.0	4.9	13.2	331.2
YVA3PVA15	483.3	571.2	109.8	108.5	171.2	203.6	19.5	4.9	13.1	329.5
YVA3PVA20	480.9	568.3	109.3	107.9	170.4	202.6	26	4.9	13.0	327.8
YVA3PVA20-S05	480.9	568.4	109.3	186.5	294.4	0	26	4.9	13.0	327.9
YVA4PVA20-S05	480.2	567.6	109.1	186.3	294	0	26	6.5	13.0	327.4

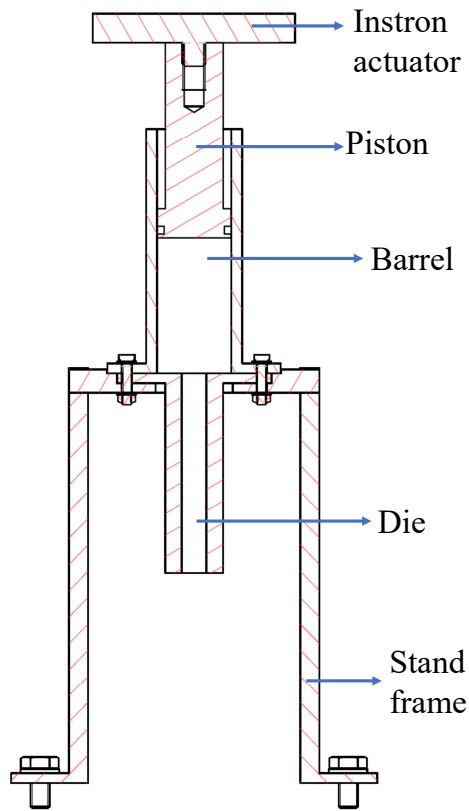


Figure 3.2: Ram extruder and components.

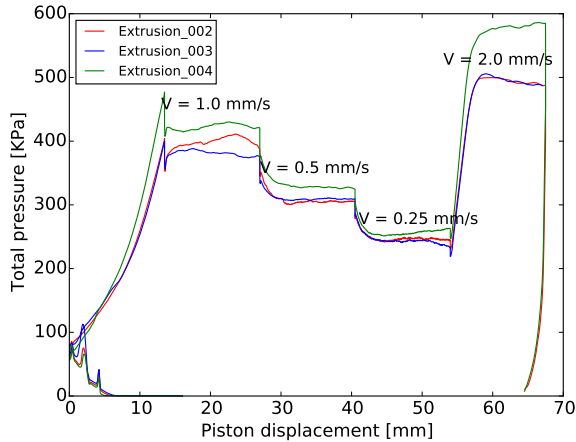


Figure 3.3: An example of the output data from one of the rheology experiments employing the ram extruder.

considered for the test, as its only function was to aid with the appropriate filling of the die. Hence, an average of the pressure at each extrusion speed of the three repetitions was used in the calculation.

From equation 2 a linear relation between the total pressure applied on the fluid and L/d ratios was obtained. Curve fitting employing a least square method was used for each of the curves in order to obtain the rheology parameters that characterize the fluid. As the experiment was done for four different extrusion speeds and three L/d ratio, an average of each of the components (σ_0 , α , m , τ_0 , β and n) could be obtained. Figure 3.4 exemplifies the linear curve of total pressure drop versus L/d obtained from the experiment.

3.3.3. PRINTING TRIALS

After the rheological characterization, printing trials were performed to assess the actual printability of the material. First, an initial test of the pumpability and extrudability was performed on 6 of the developed mixtures that were expected to show sufficient buildability based on their rheological characterization, as assessed both through visual inspection and their quantitative properties. The purpose of this trial was to establish whether the developed mixtures were compatible with the equipment, particularly whether the fibres would not cause blockage in the linear displacement pump, which features narrow cavities. Based on the observations in this initial trial, one mixture was subsequently selected for an object printing experiment.

For the preceding initial trials, mixed batches of the selected mixtures were fed to the pumping unit of the mixer-pump that is part of the 3DCP print facility of the Eindhoven University of Technology (TU/e) as described by [72]. The mixer unit of the mixer-pump was bypassed as the extent of mixing provided by this unit is insufficient for the developed mixtures. Therefore, batches were mixed using the procedure that was also applied for the rheological tests, and material from the mixed batch was inserted into the pumping unit of the mixer pump. The pump was connected to a 5 m, \varnothing 2.5 cm hose. It was

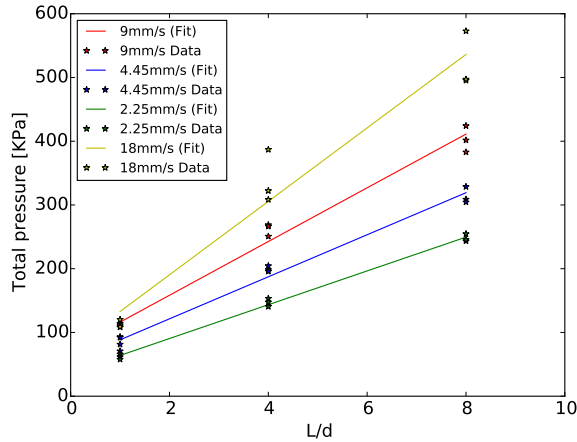


Figure 3.4: An example of the curve fitting employing a least square method of the total pressure drop and L/d ratio.

observed whether the material would be pumped without clogging, and whether the material could be transported through the hose.

In the object printing experiment, the TU/e 3DCP print facility, shown in Figure 3.5, was used in its entirety (except, again, for the mixing unit of the mixer-pump). The mixer-pump was connected to the print head with the standard 10 m, ϕ 2.5 cm hose. The standard print nozzle with a 40×10 mm mouth opening was used. Cylinder shapes with a print path (heart line) diameter of 500 mm were printed until failure. The appropriate print speed was established as 5000 mm/min (or 83.3 mm/s). The print time of a single layer, thus, was approximately 0.31 min (or 19 s). This geometry has been used previously by [114] to study buildability of another mixture. Overall behaviour was visually recorded and the number of stacked layers before failure counted.

3.3.4. MECHANICAL TESTS

The composites reinforced with 2% by volume of PVA fibres were also evaluated mechanically, to verify whether strain hardening failure behaviour had indeed been obtained. For these cases, a volume of 3 litres was mixed following the same procedure described earlier. Four-point bending, and compressive tests were performed to evaluate the performance of the composite. Motivated by the outcomes of the research at the rheology measurement stage, only YVA4PVA20-S05 and XVA3PVA20 mixtures were chosen to have their tensile behaviour tested.

The samples were cast and kept sealed in their moulds for three days. Afterwards, they were demoulded and cured in a curing room at (20 ± 2) °C and relative humidity of $(98 \pm 2)\%$. The compressive strength was measured at 14 and 28 days on 35 mm cubes, sawn from $40 \times 40 \times 160$ mm beams. The samples for four-point bending test were sawn from $180 \times 180 \times 10$ mm slabs, with approximate dimensions of $180 \times 40 \times 10$ mm and tested at 28 days of curing. Finally, the samples for direct tensile test were sawn from $240 \times 60 \times 10$ mm slabs, in the end reaching final dimensions of $150 \times 40 \times 10$ mm and

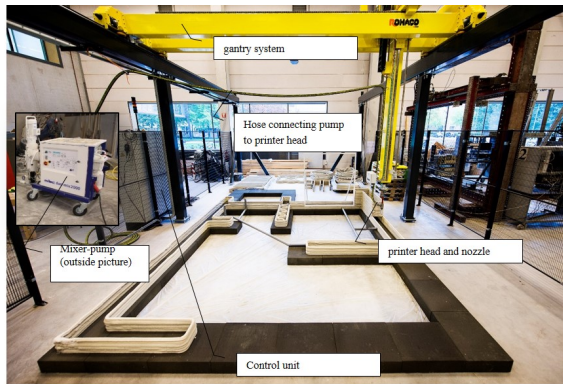


Figure 3.5: 3D Concrete Printing facility of the Eindhoven University of Technology (TU/e) (taken from: [72])

tested at 35 days of curing. The compressive test was done at loading rate of 2 kN/s. The four-point bending, with a test span of 12 mm, and tensile tests were performed on the same servo-hydraulic Instron 8872 machine in which the extrusion tests were done. The employed deflection rate for the four-point bending was 0.01 mm/s and the tensile elongation rate was 1 $\mu\text{m/s}$, controlled by linear variable differential transformer (LVDT) sensors. It is important to observe that the specimens tested on uni-axial tensile test had upper and lower side glued on steel plates. The lower side was glued inside the servo-hydraulic machine to avoid bending while testing.

Due to the high viscosity of the mixtures obtaining a homogeneous thickness while casting the samples was difficult, especially for the four-point bending specimens. Therefore, prior to the mechanical tests each individual specimen was measured at several locations.

Specimens undergoing tensile test had their frontal surface prepared for employment of digital image correlation (DIC). Their surface was painted white and randomly distributed black dots were made with a permanent marker. This pattern helps enhancing the contrast needed for the DIC software to calculate the displacements during test. The open source software Ncorr2 was employed for the DIC [115]. A Cannon camera model EOS 6D with Tamron aspherical 28 - 75mm lens were employed to obtain one picture each two seconds of test. An approximate resolution of 48 $\mu\text{m/pixel}$ was obtained.

3.4. RESULTS

3.4.1. RHEOLOGY

The six parameters-approach according to equation 3.2 was chosen to characterize all mixtures, as a non-linear behaviour was identified. Figure 3.6 illustrates the increase of total pressure of different extrusion speeds. In the following subsections, the influence of each of the mixture variables (viscosity modifier agent, water content, superplasticizer, and fibres) is detailed. A summary of all results is shown in table 3.4.

Table 3.4: Summary with all measured rheology parameters

Mixtures	α [kPa.s/mm]	β [kPa.s/mm]	σ_0 [kPa]	τ_0 [kPa]	m	n
XVA1	0.88 ± 0.09	0.14 ± 0.02	8.74 ± 0.90	0.42 ± 0.21	0.26 ± 0.02	0.24 ± 0.09
XVA2	0.93 ± 0.17	0.39 ± 0.10	9.33 ± 1.66	2.03 ± 0.41	0.28 ± 0.04	0.69 ± 0.05
XVA3	1.30 ± 0.42	0.69 ± 0.01	13.06 ± 4.18	3.44 ± 0.06	0.35 ± 0.08	0.81 ± 0.01
XVA4	2.10 ± 0.44	0.87 ± 0.05	21.07 ± 4.38	4.36 ± 0.27	0.49 ± 0.08	0.92 ± 0.03
XVA3SP1	2.43 ± 0.41	0.94 ± 0.06	24.11 ± 4.28	4.68 ± 0.30	0.55 ± 0.07	0.96 ± 0.04
XVA3SP3	0.20 ± 0.12	0.75 ± 0.04	1.99 ± 1.21	3.74 ± 0.18	0.12 ± 0.03	0.85 ± 0.02
XVA3W1	0.78 ± 0.03	0.15 ± 0.01	7.77 ± 0.26	0.50 ± 0.12	0.24 ± 0.01	0.28 ± 0.05
XVA3PVA10	3.09 ± 0.54	0.42 ± 0.10	30.90 ± 5.42	2.07 ± 0.48	0.68 ± 0.09	0.63 ± 0.06
XVA3PVA15	3.23 ± 0.58	0.46 ± 0.11	32.25 ± 5.76	2.32 ± 0.56	0.70 ± 0.10	0.66 ± 0.07
XVA3PVA20	3.45 ± 0.51	0.51 ± 0.10	34.52 ± 5.06	2.53 ± 0.52	0.74 ± 0.08	0.69 ± 0.06
XVA4PVA20	3.93 ± 0.80	0.97 ± 0.05	39.03 ± 8.31	4.87 ± 0.26	0.81 ± 0.14	0.98 ± 0.03
YVA1	0.41 ± 0.07	0.18 ± 0.02	4.08 ± 0.72	0.74 ± 0.20	0.17 ± 0.02	0.37 ± 0.09
YVA2	0.61 ± 0.05	0.23 ± 0.02	6.04 ± 0.54	1.13 ± 0.12	0.21 ± 0.01	0.51 ± 0.07
YVA3	0.70 ± 0.06	0.34 ± 0.05	7.03 ± 0.63	1.85 ± 0.12	0.23 ± 0.01	0.71 ± 0.10
YVA4	0.79 ± 0.08	0.50 ± 0.01	7.92 ± 0.83	2.52 ± 0.07	0.25 ± 0.02	0.70 ± 0.01
YVA3SP1	1.33 ± 0.10	0.23 ± 0.01	13.26 ± 1.02	1.25 ± 0.06	0.36 ± 0.02	0.59 ± 0.04
YVA3SP3	0.82 ± 0.06	0.21 ± 0.02	8.17 ± 0.63	0.99 ± 0.19	0.25 ± 0.01	0.47 ± 0.08
YVA3W1	0.70 ± 0.07	0.100 ± 0.001	6.88 ± 0.73	0.102 ± 0.004	0.23 ± 0.01	0.101 ± 0.002
YVA3PVA10	1.65 ± 0.15	0.28 ± 0.03	16.46 ± 1.47	1.40 ± 0.15	0.43 ± 0.03	0.56 ± 0.01
YVA3PVA15	2.09 ± 0.23	0.32 ± 0.03	20.88 ± 2.28	1.59 ± 0.14	0.51 ± 0.04	0.57 ± 0.02
YVA3PVA20	2.92 ± 0.18	0.19 ± 0.03	29.22 ± 1.83	0.90 ± 0.18	0.65 ± 0.03	0.46 ± 0.04
YVA4PVA20	3.60 ± 0.19	0.50 ± 0.02	35.96 ± 1.90	2.51 ± 0.08	0.77 ± 0.03	0.69 ± 0.01
YVA3PVA20S05	2.56 ± 0.19	0.43 ± 0.02	25.63 ± 1.89	2.16 ± 0.09	0.59 ± 0.03	0.65 ± 0.01
YVA4PVA20S05	3.43 ± 0.20	0.50 ± 0.02	34.26 ± 1.98	2.49 ± 0.08	0.74 ± 0.03	0.69 ± 0.01

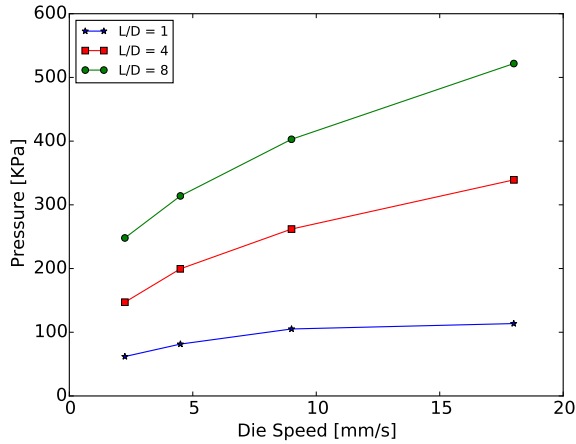


Figure 3.6: An example total pressure on the fluid measured for different extrudate velocities.

EFFECT OF VA CONTENT

The effect of VA was investigated on matrix level. Four dosages of methylcellulose were employed: 0.1, 0.2, 0.3 and 0.4% of the total solids weight. The water-to-solid ratio and superplasticizer added were kept constant at 0.2 and 2% by total powder weight, respectively.

For both matrices, the increase of VA content directly influenced the initial bulk and shear yield stresses, as is visually shown in figure 3.7, and quantitatively compared in figure 3.8. The increase in these rheological parameters have direct effect on the shape stability of the printed material. Therefore, the employment of VA can contribute positively to the development of printable mix designs. Greater rheological parameters values were obtained for the X matrix, indicating that solid suspensions with smaller liquid-to-particles surface area ratio are more vulnerable to changes in the viscosity of the liquid phase. This result is important to show how sensitive highly concentrated solid solutions, like the ones obtained for SHCCs or macro defect free cementitious composites, are to the adjustment of VA content.

EFFECT OF WATER CONTENT

The influence of extra water in the mixtures was investigated at matrix level. By keeping the superplasticizer and methylcellulose constant, the effect of increasing the water-to-solid ratio from 0.2 to 0.3 was investigated.

As expected, a higher volume of water in the solution changes significantly the flowability of mixtures where the amount of liquid to wet the surfaces of the particles is already limited. Therefore, the decrease of X series' bulk yield stress was considerably larger than the one observed for SMCE, as reported on figure 3.10. Anyhow, as the amount of liquid to lubricate the movement of the particles against each other is higher, the largest influence of the increase of the amount of water on the mixture can be observed on the shear yield stress. The influence of the water-to-solid ratio on the paste fluidity can be observed in figure 3.9.



Figure 3.7: Visual inspection of extruded material with different amounts of VA.

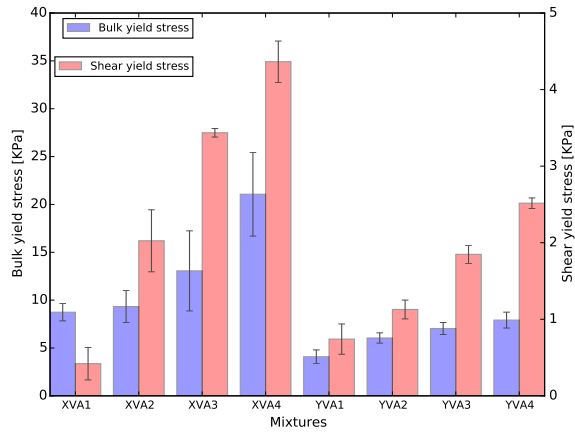


Figure 3.8: A summary of the effect of VA content on initial bulk and shear yield stress.

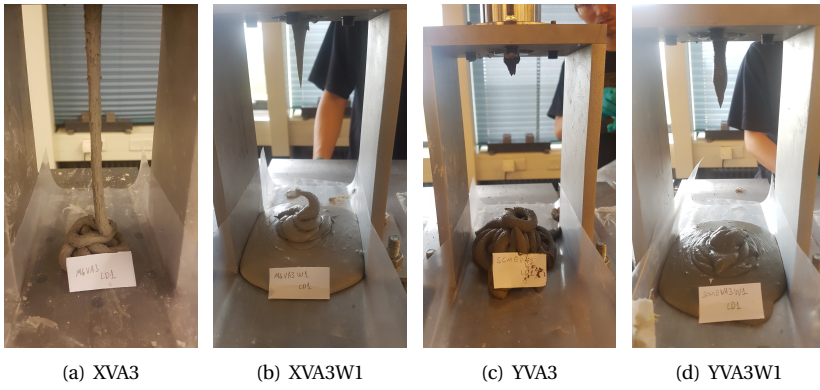


Figure 3.9: Visual inspection of extruded material for different water-to-solid ratio.

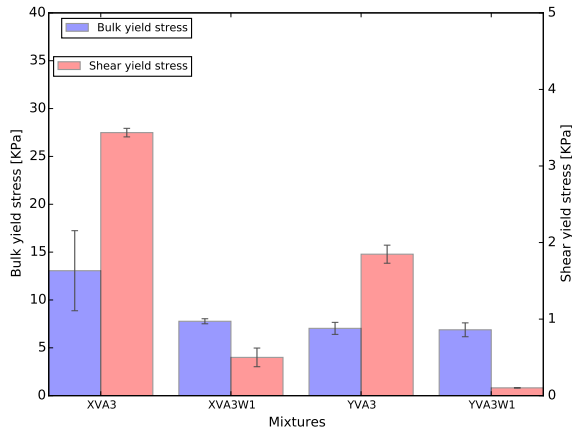


Figure 3.10: A summary of the effect of water-to-solid ratio on initial bulk and shear yield stress.



Figure 3.11: Visual inspection of extruded material for different SP concentrations.

EFFECT OF SUPERPLASTICIZER CONTENT

A subsequent investigation targeted the effect of the superplasticizer dosage at 1, 2, and 3% of the total powder phase. Keeping constant the percentages of methylcellulose and water-to-solid ratio it could be noticed that the influence on the rheology properties were not as remarkable as the one measured when the water-to-solid ratio was investigated.

The initial bulk yield stress increased or decreased whenever the amount of superplasticizer was changed from 1 to 3% (figure 3.12). However, a decrease of approximately 32% of the initial shear yield stress when 1% of superplasticizer was employed on Y matrix was measured. This decrease might be correlated with the excess of liquid present in this solid suspension, as the particle size went up to 1 mm and there is a considerable high usage of fly ash. Visually, the influence of the amount of superplasticizer can be observed in figure 3.11.

EFFECT OF PVA FIBRE REINFORCEMENT

As described in the introduction, the goal of this research was to develop a printable SHCC mix design. Therefore, the influence of 1.0, 1.5 and 2.0% by total volume of fibre

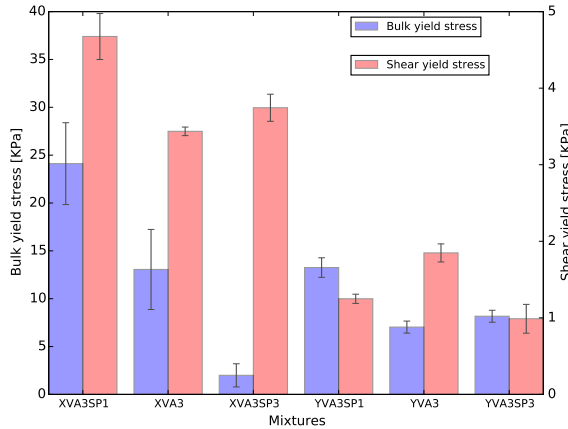


Figure 3.12: A summary of the effect of SP content on initial bulk and shear yield stress.

reinforcement on the above described matrices was studied. For both matrices (X and Y) the content of superplasticizer, methylcellulose and water-to-solid ratio were chosen to be 2%, 0.3% and 0.2 respectively.

For both mixtures, the fibre reinforcement increased considerably the initial bulk and shear yield stresses. The values of σ_0 at least doubled when the fibre reinforcement was incorporated, as can be seen on figure 3.14. Zhou et al. 2005, explained this behaviour by attributing this increase to the raise of friction between fibres and particles in the matrix while the mixture is being extruded.

However, when the rheological properties of both mixtures were observed with the increasing volume of fibres, they demonstrated a different behaviour. The increased volume of fibres did not significantly change σ_0 and τ_0 for the X composites. On the other hand, the enlarged volume of reinforcement in the Y matrix significantly increased σ_0 . These dissimilar effects can be attributed to the different particle size distributions of the respective composites. The X matrix was tailored to minimize the space between all the composing matrix particles, including the fibres. The Y matrix, on the other hand, presents larger gaps between the aggregates, where the increasing volume of fibres can be allocated. Visual inspections can be done with the help of figure 3.13. There the shape stability of the extruded filaments as well as the influence of the volume of fibre reinforcement and 0.4% of VA can be assessed. Comparing the rheological results obtained and summarized in figure 3.14 with the images in figure 3.13, provides a clear correlation between the shape stability and the increase values of initial bulk yield stress.

EFFECT OF SAND MAXIMUM GRAIN SIZE ON Y REINFORCED BY 2% OF PVA FIBRES

Although the TU/e 3DCP facility [19] is capable of processing mixtures with a particle size of up to 2 mm, it was observed in preliminary trials that the probability of blockage in the pump system significantly decreased when a less viscous mixture was used or the maximum grain size was reduced. However, during the trials only with the pump, the probability of blockage was considerably higher when aggregates up to 1 mm were



Figure 3.13: Visual inspection of extruded material for different levels of PVA fibre reinforcement.

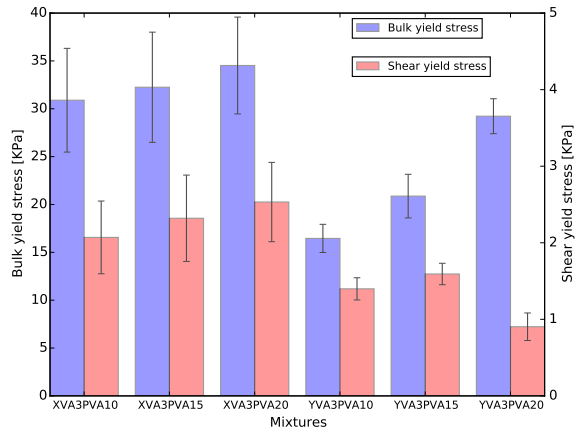


Figure 3.14: A summary of the effect of PVA fibres volume on initial bulk and shear yield stress.

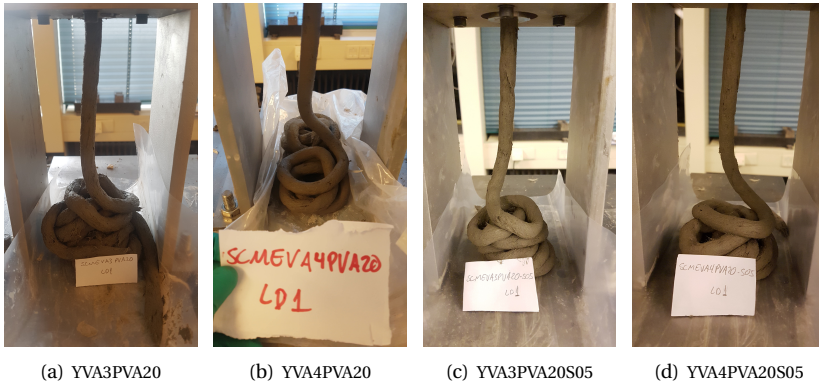


Figure 3.15: Visual inspection of extruded material for sand maximum grain size of 0.5 mm and 1 mm.

employed. This risk was only decreased when a less viscous mixture was employed at the expense of worsening the shape stability. As reported above, if more water or superplasticizer is added to this mixture the consequences would be the decrease on the initial bulk and shear yield stresses. Hence, those changes would lead to losses on the shape stability culminating with a less stable mixture which could segregate while the composite is pumped.

Therefore, the influence of the maximum grain size of sand used on Y composites was evaluated through the rheological parameters. Mixtures employing 0.3 and 0.4 wt.% of the total solid content of VA, with the maximum sand grain size of 0.5 mm, and keeping 2% of PVA fibres by volume, 2% of superplasticizer by total solid weight and 0.2 water-to-solid ratio were evaluated.

The results showed that by decreasing the maximum grain size of the sand slightly lowered the bulk yield stress of composites with 0.3 wt.% of VA, as it can be seen on figure 3.16. However, when employing 0.4 wt.% of VA, the values of σ_0 remained in the same range as the ones observed for composites employing 1 mm sand. Furthermore, the τ_0 of composites with 0.3% of VA increased considerably in comparison with composites with 1 mm sand. This result demonstrates that the use of smaller maximum grain size for sand contributes to the development of a more packed composite with an initial bulk yield stress comparable to what was obtained for the X mixtures. In figure 3.15, the influence of the sand grain size and the amount of VA can be observed.

3.4.2. PRINTING EXPERIMENTS

INITIAL TRIAL

Based on the visual assessment and quantitative rheology properties, six mixtures were selected for the initial trial with the pump and a 5 m hose. The results are summarized in table 3.5. Two mixtures could not be pumped as they led to blockage of the linear displacement pump. It could therefore not be established whether they could be extruded through the 5 m hose. The blockages were likely caused by the maximum grain size of the respective mixtures that turned out to be incompatible with the pumping system. Exces-

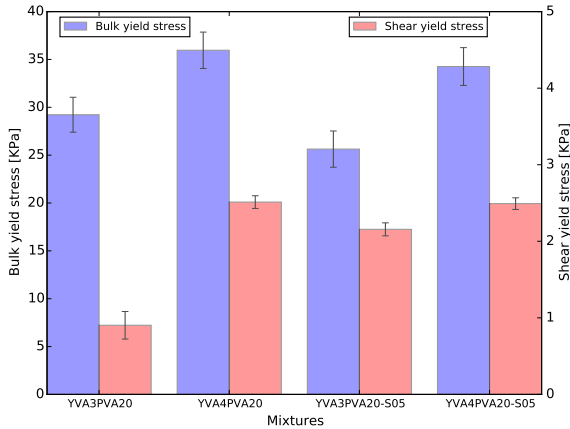


Figure 3.16: A summary of the effect on PVA fibres volume.

Table 3.5: Results of initial pumpability and extrudability trials.

Mixture	σ_0 [kPa]	τ_0 [kPa]	mixture can pass through...	
			pump	5 m hose
XVA3PVA20	34.74 ± 5.20	4.41 ± 0.18	✓	✓
XVA4PVA20	39.03 ± 8.31	4.87 ± 0.26	✓	×
YVA3PVA20	29.22 ± 1.83	0.90 ± 0.18	×	(n/a)
YVA4PVA20	35.96 ± 1.90	2.51 ± 0.08	×	(n/a)
YVA3PVA20S05	25.63 ± 1.89	2.16 ± 0.09	✓	✓
YVA4PVA20S05	34.26 ± 1.98	2.49 ± 0.08	✓	✓

sive bulk and shear yield stresses of these mixtures were not the cause, as they were in the same range as those of the other mixtures.

One other (XVA4PVA20) could pass through the pump, but generated too much friction in the hose to be transported through it. This seems to correspond to a limit of shear yield stress having been exceeded for the system to which the mixture was applied, as it is higher than that of three mixtures that could both be pumped and transported. Further experiments are required to further elucidate the apparent relations between the rheological parameters bulk and shear yield stress on one hand, and mixture behaviour in the printing process.

Considering these results, for printing, the mixture with the highest bulk yield stress that still fulfils the pumpability and extrudability requirement (i.e. does not exceed the shear yield stress limit), should be selected, as it should result in optimal buildability. Thus, two mixtures (XVA3PVA20 and YVA4PVA20-S05) seem to be comparably suitable. Their shape stability is also visually apparent from the rheology tests, as shown in figure 3.13(c) and 3.15(d). For practical purposes, the YVA4PVA20-S05 mixture was selected for the object printing experiment. The third mixture (YVA3PVA20-S05), whilst being pumpable, was expected to have lower buildability due to the lower bulk yield stress,

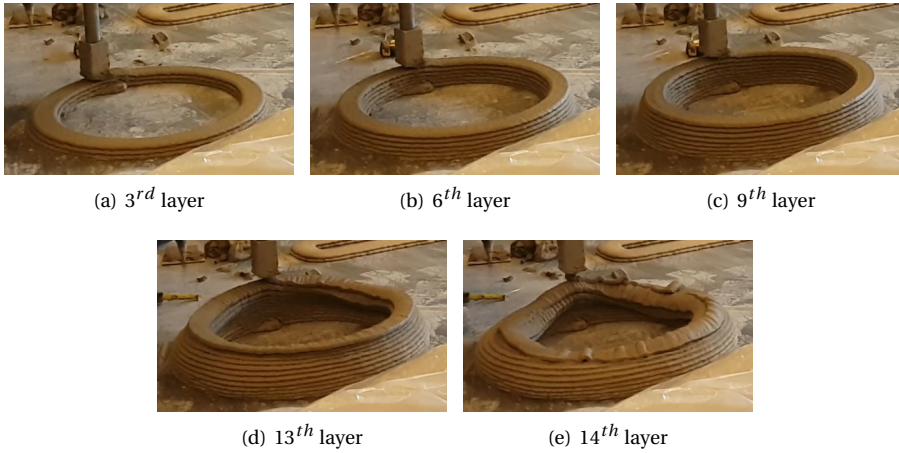


Figure 3.17: Cylinder printing test.

and was thus disregarded.

OBJECT PRINTING EXPERIMENT

Analysis methods to predict the buildability are still under development. Wolfs et al. [114] have presented a solid mechanics based approach considering both stability and material failure effects, whereas others (Roussel, 2018 [116]) have proposed a rheology based failure criterion. As the print material develops from a highly viscous to a solid state after deposition, both approaches have merit. An extensive discussion of this issue falls outside the scope of this study. For now, a rheology based approximation of the expected buildability was calculated to be 17 layers, based on the measured bulk yield stress of (34.26 ± 1.98) kPa, an assumed mass density of $2,000 \text{ kg/m}^3$, and an average layer height of 0.01 m . The mixture has an excessive open time of more than 12 hours. Therefore, structural build-up during printing was ignored in this estimation. The progress of the object printing experiment is shown in figure 3.17. The object collapsed during printing of the 14^{th} layer. The calculated 17 layers apparently is a considerable overestimation, but it is nevertheless in the same order of magnitude. The deviation is likely due to stability effects that depend on the 3D geometry, density variations, and dynamically changing loads caused by the deposition of the print filament. It may nevertheless be concluded that the mixture is printable, and further adaptations of it should be considered to improve buildability.

3.4.3. MECHANICAL PROPERTIES

Among all evaluated mixtures, only those reinforced by 2 vol.% of fibres were evaluated mechanically. The influence of 0.3 and 0.4% by solid weight of VA, as well as the maximum grain size of the sand, were evaluated through compressive strength and four-point bending tests.

All tested mixtures delivered flexural hardening and developed a ductile behaviour,

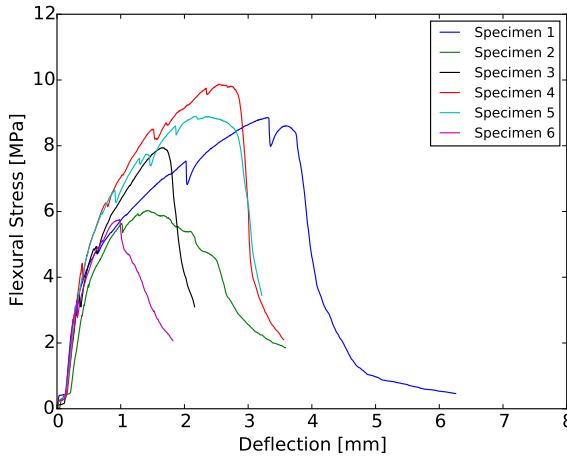


Figure 3.18: An example from the obtained flexural hardening behaviour obtained from mixture XVA3PVA20

Table 3.6: Compressive strength performance [MPa]

Mix design	Load perpendicular to the casting direction	Load parallel to the casting direction
XVA3	41.12 ± 4.18	41.71 ± 3.21
XVA4	38.26 ± 5.48	37.76 ± 3.45
YVA3	15.89 ± 0.95	14.37 ± 1.81
YVA4	14.49 ± 1.48	14.78 ± 1.3
YVA3S05	8.39 ± 1.82	8.49 ± 0.5
YVA4S05	15.47 ± 0.65	15.84 ± 1.58

as given in Figure 3.18. Nevertheless, multiple cracks were more often observed in X series and in mixtures in which the smaller grain size of the sand was employed. This behaviour was expected since the size of aggregates influences the number of cracks and the crack pattern, as demonstrated by [117]. Additionally, larger aggregates can also make the dispersion of fibres more difficult, decreasing the number of fibres effectively bridging the cracks [118]. Figure 3.19 summarizes the results from the four-point bending test.

Meanwhile, the compressive strength values of all analysed mixtures, listed in table 3.6, were significantly higher for X's, in comparison with the Y's. The amount of VA employed in the composites did not significantly influenced the compressive strength or the flexural behaviour of the analysed composites, with exception of the ones with sand up to 0.5 mm. Only in this case, composites with 0.4 wt.% of VA delivered higher performance. As demonstrated, the mechanical performance was not influenced by the amount of VA employed on X mixtures and 0.4 wt.% improves Y-S05 series.

Moreover, as discussed in the previous section, only XVA3PVA20 and YVA4PVA20-S05

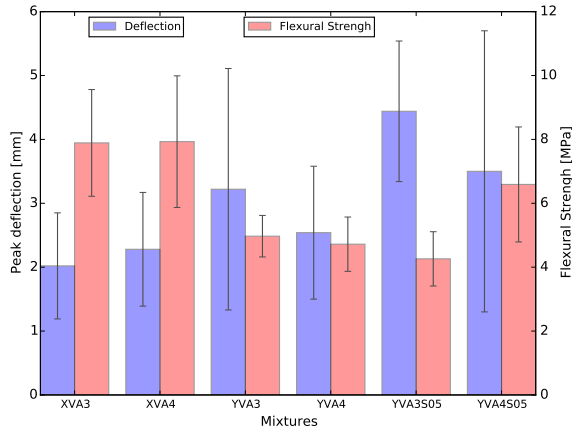


Figure 3.19: Average performance on four point bending test of selected mixtures.

were suitable for printing. Therefore, only these two mixtures were chosen to be investigated employing an uni-axial tensile test, in order to confirm their strain hardening and multiple crack behaviour. In figures 3.20 and 3.21 the "tensile stress versus strain" curve of both mixtures are plotted. It could be confirmed that the modified composites mix-design also showed high ductility and strain hardening behaviour.

In figures 3.22, 3.23, 3.24, 3.25 the last picture from the DIC analyses are shown. In pictures depicting the vertical displacements only elongations were shown. Regions in blue suffered less deformation than regions with colours closer to red, where the cracks are. On pictures showing the horizontal displacements elongations and compressions are shown. There, zero displacements were demonstrated with yellow colours with elongations been demonstrated in red and compressions in blue. Through the DIC analysis the horizontal displacements could also be captured. Where the cracks were concentrated it was possible to observe areas with compressive values and some others in tension. These regions are believed to have fibres oriented with different angles, which emphasizes the importance of fibre dispersion in this type of composite. It is possible to observe that all samples developed at least two cracks, and specimens from the X series resulted in higher tensile performances and considerably greater number of cracks.

3.5. CONCLUSIONS

Through the experimental procedure carried out in this study, a methodology was presented to develop printable cementitious composite mix-designs based on fundamental rheological properties. The influence of rheology modifiers on the fresh and hardened state were evaluated for application in high performance cementitious composites. Visual inspection together with rheology parameters evaluation were employed to obtain an optimized SHCC mixture in terms of printability, shape stability and strain hardening behaviour. Printing experiments were conducted to compare the pumpability and extrudability of various mixtures. One mixture was used to print an object and evaluate buildability. Mechanical tests were performed to confirm the strain hardening behaviour

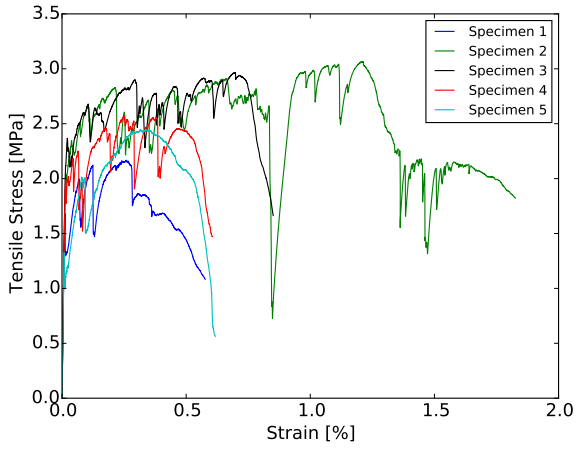


Figure 3.20: Tensile performance of X series.

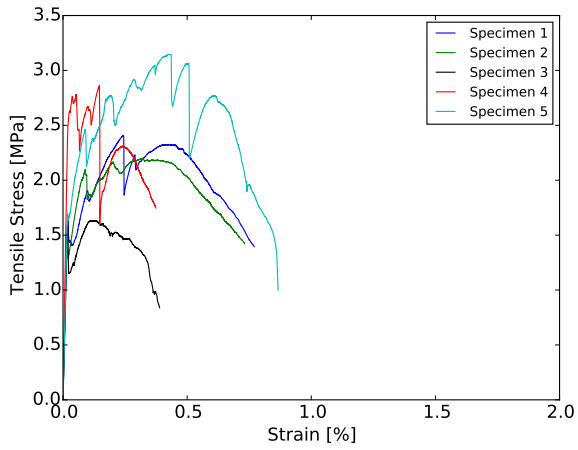


Figure 3.21: Tensile performance of Y series.

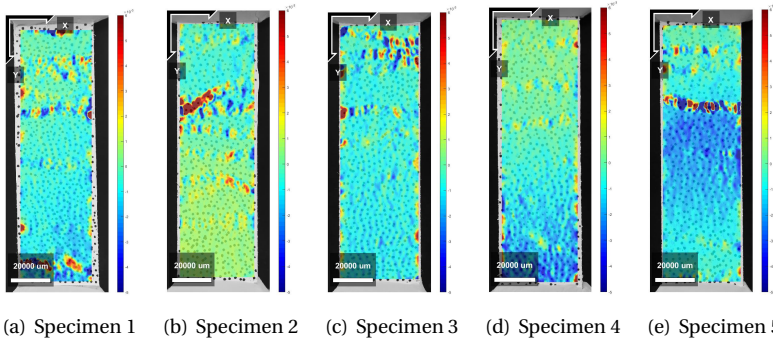


Figure 3.22: Crack pattern obtained from DIC analysis on X samples - Horizontal Deformations.

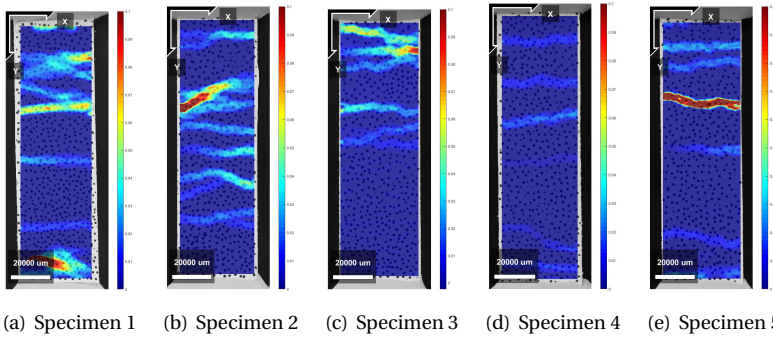


Figure 3.23: Crack pattern obtained from DIC analysis on X samples - Vertical Deformations.

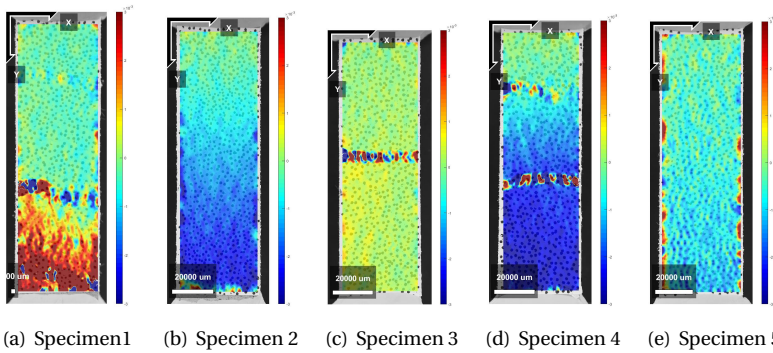


Figure 3.24: Crack pattern obtained from DIC analysis on Y samples - Horizontal Deformations.

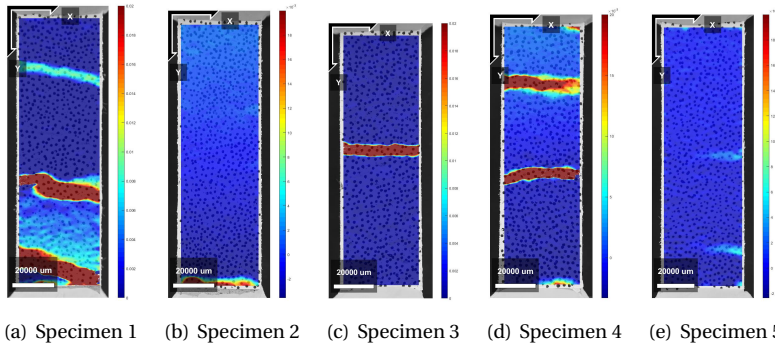


Figure 3.25: Crack pattern obtained from DIC analysis on Y samples - Vertical Deformations.

of the developed mixtures. In summary the following conclusions can be drawn:

- Ram extruder with the Benbow-Bridgwater model are appropriate tools to develop printable cementitious composites. However, it is important to notice that the method has limitations. One example was the inability to predict the blockage of some mixtures in the pump;
- The employment of rheology modifiers is crucial for the development of high ductility cementitious composites, with dough-like consistency in the fresh state;
- The liquid-to-solid ratio of the solid suspension is more relevant to the shape stability of printable mixtures, than the amount of superplasticizer;
- For the development of a printable cementitious mixtures, the particle size distribution and the liquid-to-total surface area of all solids is more relevant than the employment of rheology modifiers;
- The amount of rheology modifiers employed in the mix did not significantly influence the mechanical properties of most evaluated composites.
- XVA3PVA20 and YVA4PVA20-S05 are composites which have proven to have high mechanical performance and superior printing quality and therefore, must be considered for further developments in the construction printing industry.

4

MECHANICAL BEHAVIOUR OF PRINTED STRAIN HARDENING CEMENTITIOUS COMPOSITES

"Who am I, really?" The search for an answer produces feelings of alienation and anxiety and can only be relieved when one accepts that inner self and receives public recognition for it.

Francis Fukuyama, Identity: The demand for dignity and the politics of resentment.

Extrusion based additive manufacturing of cementitious materials have demonstrated strong potential to become widely used in the construction industry. However, the use of this technique in practice might be conditioned to a feasible solution to implement reinforcement in such automated process. One of the most successful ductile materials in civil engineering, strain hardening cementitious composites (SHCC) has a high potential to be employed for 3 dimensional printing. The match between the tailored brittle matrix and ductility of the fibres enables these composites to develop multiple cracks when loaded under tension. Using previously developed mixtures, this study investigates the physical and mechanical performance of printed SHCC. The anisotropic behaviour of the materials is explored by means of mechanical tests in several directions and micro computered tomography tests. The results demonstrated a composite showing strain hardening behaviour in two directions explained by the fibre orientation found in the printed elements. Moreover, the printing technique used have also guaranteed an enhanced bond in between the printed layers.

This chapter has been published in S. C. Figueiredo, C. R. Rodríguez, Z. Y. Ahmed, D. H. Bos, Y. Xu, T. M. Salet, O. Çopuroğlu, E. Schlagen, and F. P. Bos. Mechanical Behavior of Printed Strain Hardening Cementitious Composites. Materials. vol. 13, p. 2253. 2020. [119]

4.1. INTRODUCTION

THE additive manufacturing of cementitious materials (AMoC) is rising as one of the solutions to achieve fully automated building processes. One of the most rapidly spreading technologies is extrusion-based deposition of subsequent layers, popularly known as 3D concrete printing (3DCP) [120]. In 3DCP, printable mortars are used that attain a dough-like consistency in a single stage mixing process, or in a double stage process in which accelerators or viscosity modifiers are added at or near the printing head. The printed material should be able to resist their self-weight, as well as the loads caused by additional layers. Many publications have already testified the success and potentials of this new construction technique [72, 73, 121, 122]. Different types of materials have been used to print such as geopolymers [123], calcium aluminate cement [94], calcined clay cement [124, 125], Portland cement with copper tailing [16] and many other examples.

As cementitious materials demonstrate brittle failure behaviour, their application in construction requires a form of reinforcement to ensure structural safety. In conventional cast concrete, reinforcement with steel bars is generally used, as well as some other strategies such as pre-stressed reinforcement, fibre reinforcement, or a combination thereof. These solutions are not necessarily applicable to 3DCP, as they may interfere with the manufacturing process, limit the geometrical freedom presented by 3DCP, produce insufficient residual strength, or apply only to rather specific situations. As it is generally recognized, lack of suitable reinforcement methods could seriously hinder the potential applicability of the technology [126, 127], several options are being developed by different groups. Until now, only two strategies have been presented that are fully integrated with the 3DCP process: the automated entrainment of reinforcement cable [19, 90, 128, 129], and the application of fibres which will be further discussed in this manuscript. Several studies have already demonstrated strategies to reinforce extruded cementitious composites, a process similar to 3DCP, as demonstrated by Shen et al. [130] with layered elements with different PVA fibre content or using natural fibres [131]. Fibre reinforcement for printed concrete was initially studied by Hambach and Volkmer [132]. They tested not only different fibres (carbon, glass and basalt) to reinforce a blended cement paste with silica fume but, also different printing patterns. Other studies assessed the influence of various fibre types on mechanical properties, such as the tensile and compressive strengths, the interlayer strength, and ductility [133–137]. A dominant orientation of the fibres in the flow direction is commonly reported. In this direction, tensile strength is found to be higher [132, 133, 137]. An important aspect to consider is whether the applied fibres are compatible with the 3DCP equipment that is used.

A special family of fibre reinforced mortars are the Strain-Hardening Cementitious Composites (SHCCs, in literature also referred to as Engineered Cementitious Composites, ECCs). This type of material is able to absorb significantly higher amounts of energy during failure by tensile forces in comparison to a conventional fibre reinforced material. The strain hardening performance is obtained by tailoring the bond strength between the fibre and the matrix. This behaviour enables this type of composite to develop a very small and well distributed cracking pattern [21]. This results in superior behaviour in terms of mechanical performance [138], durability [139] and when employed as a repair

mortar [140].

Therefore, SHCC has significant potential in automated concrete manufacturing. Some researches have already reported the use of this material in the development of mixtures to be applied in 3D printing of cementitious composites. In one of the first published investigations regarding the printability of SHCCs, fresh state properties were assessed when some of the constituents of the matrix were changed [94]. Typically 2% by volume of PVA fibres (12mm length and 40 μ m diameter) were reported as reinforcement. With the exception of reference' mixtures 0.4 wt% of hydroxypropyl methylcellulose (HPMC) was used as a rheology modifier. To increase the setting speed some of the evaluated mix-designs contained calcium aluminate cement and silica fume as well. A manual caulking apparatus was used to print specimens out of selected mixtures. Some of the authors' conclusions stated that calcium aluminate cement has effectively accelerated the hardening what positively contributes to the buildability of this type of material. The mixing parameters such as water temperature and batch volume have significantly influenced rheological properties and therefore, must be controlled to achieve reproducible printing results. Finally, modifications of the SHCC' mix-design, to facilitate the printing process, did not affect the strain-hardening properties of the composite (around 4% maximum strain capacity). In a subsequent study, printed ECC with varying fibre content per layer was presented as a strategy to optimize fibre usage [141].

The anisotropic stress-strain behaviour of a PVA reinforced SHCC was subject of a study performed by Yu and Leung [142]. Remarkably, they reported limited strain-hardening performance when load was applied perpendicularly to the interfaces. Nevertheless, the mechanical performance was found when the load was applied in the same direction of the printing.

Another investigation on printable SHCCs was presented by Ogura et. al. [143], who used an automated printing setup based on a moving printing head connected to a progressive cavity pump. An extensive experimental investigation was performed with mix-designs composed of CEM II/A-M (S-LL) 52.5R, silica fume, fly ash, sand of maximum grain size of 1 mm and high-density polyethylene microfibres (HDPE). Three different reinforcement levels were investigated (0.3, 1 and 1.5 vol.%) along with three sand-to-binder ratios and two water-to-binder ratios. Extrudability tests were performed using a ram-extruder and the flowability was measured by means of a standardized flow test. Composite's mechanical performance was assessed by means of direct tensile and compressive tests to evaluate printed and cast specimens. The authors showed that the extrusion force strongly depends on the proportions of raw materials. The total volume of fibres were not a crucial factor in this property, but sand-to-binder ratio has played an import role. Results pointed out that using smaller amount of sand in the mixtures usually leads towards lower extrusion forces due to increased cohesion. Moreover, the mechanical properties of printed materials were specially improved. Probably due to the preferential alignment of the fibres in printed samples, the total strain capacity of the composites reinforced with 1.5 vol.% were significantly improved. All tested specimens delivered strain-hardening behaviour with multiple small cracks.

Another interesting use of the anisotropic behaviour that extrusion based materials own were reported by [144] and [145]. These studies have demonstrated that the different mechanical properties for different directions can be used to develop larger scale

materials with enhanced properties and optimized performance.

Chapter 3 and [60] have extensively evaluated the rheological parameters involved in the development of printable SHCCs. Several modifications in the mix-design of such composite were investigated using a ram-extruder coupled with the Benbow-Bridgewater model [110]. With the developed methodology, rheological properties of printable materials on their relation to the ability of the given mixture to possess adequate printability and buildability. From that research two outstanding mixtures were selected to be used in the current study.

The aim of this study was to give a comprehensive evaluation of physical and mechanical properties of SHCC specially tailored to be 3D printed. As it was expected that the extrusion of the material might generate preferential orientation of fibres and consequently anisotropy, a protocol was followed to characterize the composite. Non-destructive techniques were employed to study the air void content and fibre orientation. Particularly the interface region between layers was of interest. In addition, a range of destructive mechanical tests were performed to determine compressive, tensile, and flexural strength and toughness. Various loading directions (relative to the print path) were assessed, as well as 2 print layer interval times and 4 beam geometries (for flexural bending).

4.2. EXPERIMENTAL METHODS

4.2.1. MATERIALS AND METHODS

Two types of SHCC were evaluated. They were created based on [111] and [112]. Their rheological properties were explored in an earlier publication [60]. In that study the influence of water, superplasticizer and viscosity modifier admixture (VA) contents, as well as the fibre volume and sand grain size distribution on the rheology of these mixtures were evaluated. As it was reported, only one mix-design of each SHCC were chosen to be printed. They had the best initial shear and bulk yield stresses along with a successful printability tests. These two rheological properties were considered essential to extrude fibre reinforced cementitious composites. In Table 7.2 the composition of each mixture was given. The initial bulk and shear yield stresses of both mixtures were (34.74 ± 5.20) kPa and (4.41 ± 0.18) kPa for XVA3PVA20 and (34.26 ± 1.98) kPa and (2.49 ± 0.08) kPa for YVA4PVA20-S05, respectively. Physical and chemical characteristics of the raw material used can be found in in [60].

A total volume of 50 litres of SHCC were prepared. Due to high viscosity in the fresh state of both mixtures, two batches of 25 litres were mixed in a planetary mixer. The material was printed at the Eindhoven University of Technology facilities, previously reported in [72]. The material was printed as long beams shape of one, two, three and four layers, as illustrated in Figure 4.1. Each layer had a rectangular cross section shape with 10 mm thickness and 50 mm width. The printer head was moved at 100 mm/s. The time interval between two contiguous layers was 3, 2, and 4.5 minutes, respectively for elements printed with two, three and four layers. An extra element with two layers was printed. The time interval between the two layers was 36 minutes. The later element was printed to investigate the time dependency of the tensile strength of the bond interface.

Both mixtures were printed in two consecutive days. After 24 hours of the printing



Figure 4.1: Printing table with final printed elements with one, two, three and four layers.

Table 4.1: Mix design summary in $[kg/m^3]$

	XVA3 PVA20	YVA4 PVA20-S05
CEM I 42.5	259.2	480.2
Blast Furnace Slag	604.9	0
Fly ash	0	567.6
Limestone powder	864.1	109.1
Sand (125 - 250) μm	0	186.3
Sand (250 - 500) μm	0	294
PVA	26	26
HPMC	5.1	6.5
Superplasticizer [g]	17.3	13
Water	345.6	327.4

session, the long printed beams were sawn into several pieces and stored in a curing chamber at $(20 \pm 2)^\circ\text{C}$ and relative humidity of $(98 \pm 2)\%$ for the rest of the curing period.

4.2.2. MECHANICAL CHARACTERIZATION

To investigate the mechanical properties of printed composites an extensive experimental investigation is proposed. Through this study the printed material's performance was detailed and the influence of the printing process is compared with results reported in [60] for the same mixtures, traditionally cast.

COMPRESSIVE STRENGTH TEST

Compressive tests were performed in a servo hydraulic machine with a constant load rate of 2 kN/s. Cubes of 35 mm side were sawn from four layers beams and compressive strength was measured at 14 and 28 days. As an anisotropic behaviour is expected due to

the printing technique, the compressive load was applied perpendicular and parallel to the printing plane, corresponding to direction I and II, respectively as defined by [146].

FRACTURE TOUGHNESS TEST

Specimens with dimensions of $30 \times 40 \times 160 \text{ mm}^3$ were sawn from four layers printed beams for fracture toughness test at 28 days of curing. A notch was created in those specimens with a width of 4.5 mm and height of 7 mm for XVA3PVA20 samples and 10 mm for YVA4PVA20-S05. A three-point bending test was performed by controlling the crack mouth opening displacement (CMOD) at a rate of $0.8 \mu\text{m/s}$ until the first crack (elastic phase) and $3.3 \mu\text{m/s}$ for the rest of the test (plastic phase). Two linear variable differential transformers (LVDT) were used in the middle of the span to measure the deflection during bending.

The results from this test were treated to obtain several composites parameters that are useful for the mechanical performance characterization. Figure 4.2 exemplify these values. The following data can be extracted from the flexural stress - CMOD curves obtained from the tests:

- Limit of proportionality (LOP) and its respective CMOD value: The LOP is the flexural stress obtained from the the first point out of the linear elastic phase;
- Modulus of rupture (MOR) and its respective CMOD value: The MOR is the maximum flexural stress of the composite;
- Matrix crack tip fracture toughness (J_{tip}): This value gives information regarding the matrix of the composite, measuring the amount of energy needed from the material to go over the elastic phase [147–149];

$$J_{tip} = \sigma_{LOP} \epsilon_{LOP} - \int_0^{\epsilon_{LOP}} \sigma(\epsilon) d\epsilon \quad (4.1)$$

- The complementary energy (J_b): This is the complementary energy needed to achieve MOR of the composite. Therefore, this value gives information regarding the amount of energy needed from the fibres being pulled-out from the matrix up to the maximum flexural stress [147–149].

$$J_b = \sigma_{MOR} \epsilon_{MOR} - \int_0^{\epsilon_{MOR}} \sigma(\epsilon) d\epsilon \quad (4.2)$$

FOUR-POINT BENDING TEST

Samples with one, two, three and four layers were evaluated through four-point bending ageing 14 and 28 days of curing. These specimens were sawn from the printed elements to homogenize their width (approximately 40 mm) and the length (approximately 150 mm). This test was performed in an Instron 8872, applying a deflection speed of 1 mm/s. The span of the test was 120 mm and the load was applied by two metal rods spaced 40 mm from each other. Two LVDTs were used to measure the deflection in the middle of the span. During this test the load was applied perpendicularly to the printing plane.

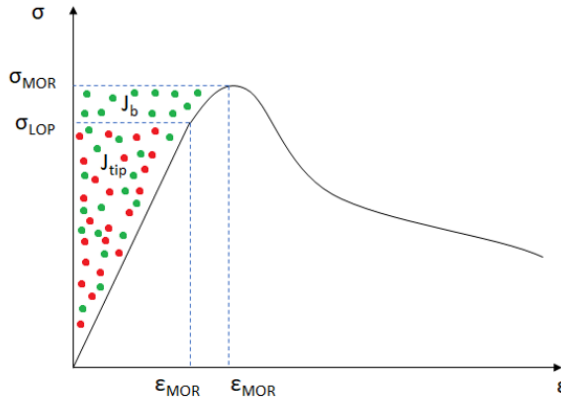


Figure 4.2: Typical CMOD curve with a representation of the calculated parameters

UNI-AXIAL TENSILE TEST

Assuming that the printing technique would induce preferential orientation on the fibre direction, tensile tests were performed in specimens with one layer. Printed beams were sawn to create two batches of specimens which were tested after 35 days of curing. One batch had its tensile properties measured in the printing direction (LPA). The specimens had a width of 40 mm and a length of 150 mm. Another batch was tested with uni-axial tensile set-up with the load applied perpendicular to the printing direction (LPE). The specimens had a width of 35 mm and a length of 30 mm.

With the help of a LVDT sensors the uni-axial tensile test was carried out in displacement control with loading rates of 1 and 0.2 $\mu\text{m/s}$ respectively for samples in LPA and LPE. These two rates corresponds to the same deformation ratio of 6.67 $\mu\text{strain/s}$.

Specimens undergoing tensile testing had their front surface prepared for digital image correlation (DIC) analysis. A layer of white paint was applied on the front surface of the sample and randomly distributed black dots were made with a permanent marker. This pattern helps enhancing the contrast needed for the DIC software to calculate the displacements during test. The open source software Ncorr2 was employed for the DIC analysis [115] with a subset radius of 57 and subset space of 1 pixel. A Cannon EOS 6D camera with 28 - 75 mm Tamron aspherical lens was employed to obtain a frame every two seconds. An approximate resolution of 48 $\mu\text{m/pixel}$ was obtained.

UNI-AXIAL TENSILE TEST OF TWO PRINTED LAYERS

As reported elsewhere [146, 150, 151], bond interface between printed layers can be the weakest region on the composite. The time interval between two layers, which amongst others is a function of the object size and print nozzle speed, is crucial [146, 151]. When a critical threshold time interval is exceeded, a so-called cold-joint may be formed leading to a significantly reduced strength compared to the bulk material. This phenomenon is well known in the field of concrete repair [152, 153]. Recommendations to avoid prob-

lems in this area usually point out larger surface contact employing grooved surfaces and substrate pre-wetting to enhance the bond between both materials. Most of the techniques cited before have not yet been approached within the 3D printing context. The application of an articulated interlock has been successfully applied by Zareyan et al. [12] to significantly increase the bond strength.

In order to study the mechanical performance of the interface of two printed layers, elements with two layers were printed with the second layer being placed within two different time intervals (3 and 36 minutes). Afterwards, the specimens were sawn from such elements in order to create prismatic specimens sized $10 \times 10 \times 20 \text{ mm}^3$. At the age of 28 days, these specimens were tested applying a tensile load perpendicular to the interface plane between two printed layers. The deformation was at $0.1 \mu\text{m/s}$ by means of LVDT sensors. This rate corresponds to a strain rate of $5 \mu\text{strain/s}$. Through this test the interface bond strength could be assessed, and failure zone could be identified.

4

4.2.3. AIR VOID CONTENT AND FIBRE ORIENTATION ASSESSMENT

To allow a more extensive interpretation of the results of the mechanical tests described in the subsequent subsections, non-destructive scanning was performed to determine the air void content and fibre orientation in the printed composite. The interface area where two layers meet is the most interesting region in this kind of composite. Several studies have used non-destructive methods to study the local microstructure [151], to relate growing layer interval times to increased porosity [154], and larger capillary water ingress [155].

To evaluate the anisotropic behaviour of printed fibre reinforced cementitious materials X-ray computerized micro tomography (X-ray CT) was performed by means of a Phoenix Nanotom X-ray. X-ray CT was performed on prismatic specimens with dimensions $10 \times 10 \times 20 \text{ mm}^3$, sawn from two-layers printed beams of each studied mixture. A notch was made in the sample to indicate the printing direction. The values of accelerating voltage and current to generate the x-ray beam were chosen to achieve a resolution of $7.5 \mu\text{m}$. 3D reconstruction of the acquired radiographs was done through the software VG Studio.

The reconstructed 3D volume was then analysed with the help of Trainable Weka Segmentation tool [156] from FIJI [157]. Two different segmentation procedures were implemented in order to 1) quantify the air voids and 2) to qualitatively and quantitatively assess fibres orientation in the composite.

The latter segmentation was carried out only on two randomly selected representative elementary volume (REV) extracted from each of the layers of the reconstructed volume. The REVs were composed by two stacks of 75 pictures, one in each printed layer. Therefore, in total four volumes consisting of a minimum of approximately 150 mm^3 were analysed per mixture. The latter segmentation distinguished between four phases, namely: air voids, bulk paste, large limestone grains and finally the imprints left from the fibres in the matrix. The segmented REVs were transformed into binary images to distinguish further between fibre imprints and the other phases. The segmented fibres were further filtered by constraining the individual fibre imprints to have at least an area of 10 pixel^2 and a low circularity, between 0 and 0.3. To determine the orientation of a given fibre the Feret's angle was used. This angle is given in a range from 0 to 180° .

Table 4.2: Compressive strength of printed samples [MPa]

	Age [days]	XVA3 PVA20		YVA4 PVA20-S05	
Printed layers perpendicular to the load	14	37.63	± 3.8	14.57	± 0.39
	28	44.09	± 4.33	17.66	± 0.24
Printed layers parallel to the load	14	34.98	± 1	12.03	± 1.04
	28	41.93	± 1.88	15.02	± 0.52

According with the samples preparation horizontal fibres (angles of 0 or 180°) represent totally alignment with the printing direction, and vertical fibres (90°) represent totally perpendicular alignment to the printing direction. These results were used to investigate the influence of the extrusion of the material on the final fibre orientation of the printed composite.

4.3. RESULTS

4.3.1. COMPRESSIVE STRENGTH

The results obtained from the compression test were summarized in Table 4.2. Although slight differences in compressive strength between loading directions in perspective to the printing plane were observed for both compositions, they are rather small (between 5 and 15 %). For the X series, the difference is less than the standard deviation, for the Y series somewhat larger. This seems to be more or less in line with results reported in literature: either a limited [158] or no directional dependency was found [7, 146]. The compressive strength of these printed specimens was also found to be close to the compressive strength of cast specimens, as presented in [60]. As Wolfs et al. [146] reported a significant strength reduction for printed specimens compared to the cast ones, it seems that the dough like consistency of the proposed SHCC discussed in this study was less vulnerable to casting parameters, such as compaction.

4.3.2. FRACTURE TOUGHNESS TEST

The flexural stress - CMOD curves obtained from the fracture toughness test are shown in the Figure 4.3 and the results are summarized in the Table 4.3. Both mixtures presented ductile behaviour, although mixture XVA3PVA20 achieved superior performance. According to [147–149] in order to obtain pseudo strain-hardening behaviour the composite must satisfy the condition $J_b > J_{tip}$. As can be observed in the summarized results the performances of both composites are in agreement with this condition. However, the XVA3PVA20 specimens exhibited considerably more stiff post-crack behaviour than the YVA4PVA20-S05 specimens. This means that the fibres immediately took over the tensile stresses, what might indicate a much stronger mechanical bond between the fibre and the matrix.

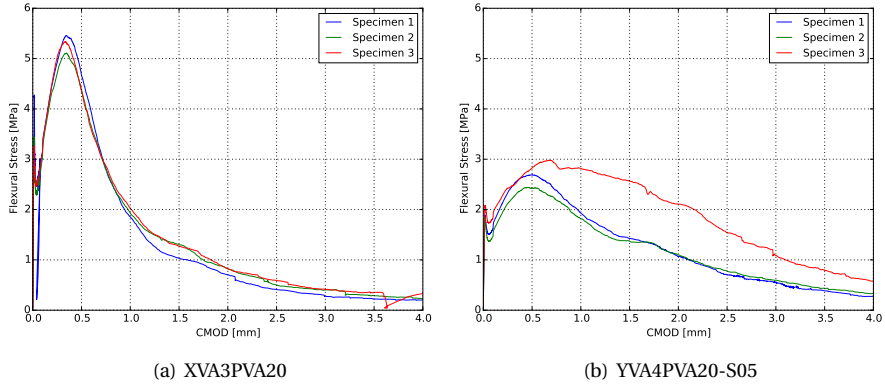


Figure 4.3: Flexural stress × CMOD curves from fracture toughness tests.

Table 4.3: Summary of results obtained for fracture toughness test.

	XVA3PVA20		YVA4PVA20-S05	
LOP [MPa]	1.10	± 0.17	0.56	± 0.04
CMOD at LOP [μm]	10.60	± 1.29	9.49	± 0.93
MOR [MPa]	1.84	± 0.09	0.97	± 0.10
CMOD at MOR [μm]	341.99	± 4.00	545.06	± 112.15
J_{tip} [kJ/m^2]	16.37	± 4.51	7.11	± 1.51
J_b [kJ/m^2]	430.74	± 14.62	260.94	± 67.97

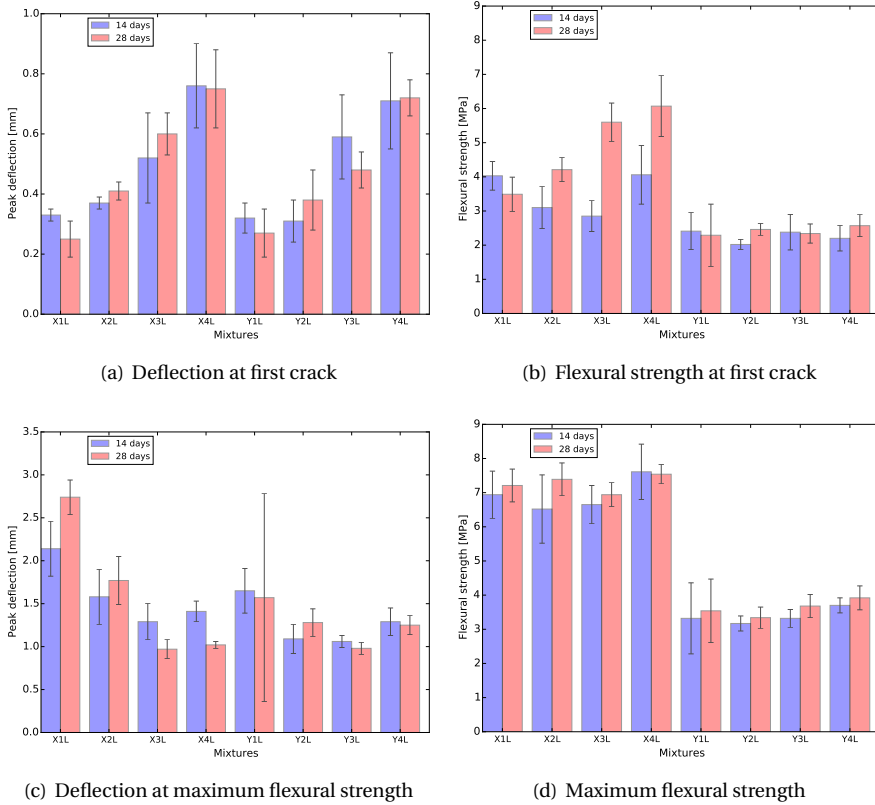


Figure 4.4: Flexural hardening behaviour for X samples cured for 14 days.

4.3.3. FOUR-POINT BENDING

The results obtained from the four-point bending test of 28 days cured samples are shown in Figures 4.5 and 4.6, as an example. At both curing ages flexural hardening performance was obtained for all samples. Nevertheless, the results show better performance for XVA3PVA20. This indicates a lower probability to obtain strain hardening performance for composites YVA4PVA20-S05. Although on average, YVA4PVA20-S05 specimens showed strain hardening behaviour, a small number of individual specimens did not. Furthermore, no significant differences were found when the flexural performance of one-layer 3D printed samples is compared to that of conventionally cast samples [60].

As it can be observed from the flexural stress - deflection curves and also summarized in the Figure 4.4, the number of layers of the printed element influences greatly the flexural hardening response. A lower number of cracks was registered for samples with more than one printed layer as well as lower values of deflection at the maximum flexural strength. These results indicate decreased ductility for thicker components.

This behavior is related to two main causes. The first one is purely geometrical: higher tensile stresses are generated in the tension zone due to the increased moment

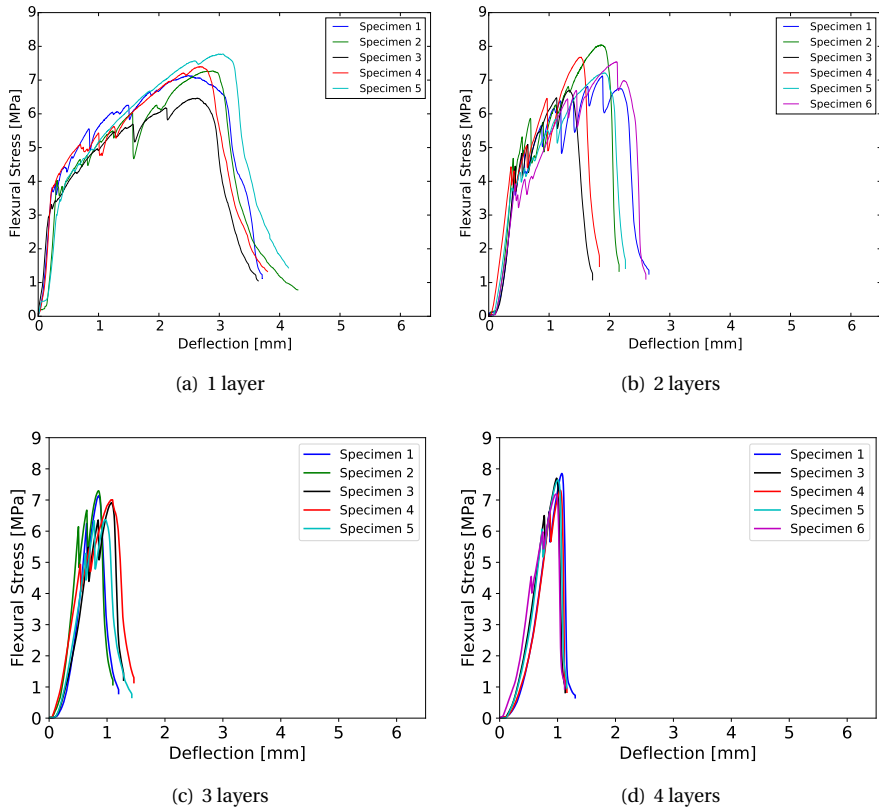


Figure 4.5: Flexural hardening behaviour for X samples cured for 28 days.

of inertia of the cross section. As a result, fibres are pulled-out more promptly to absorb the tensile stresses, limiting the crack propagation and the regain of flexural strength.

A second factor that plays a role is related to the printing technique employed. In order to obtain thicker elements, four layers were extruded on top of each other. This deposition generates interface regions that can be weaker, stronger or have the same mechanical properties as the bulk of the composite. In [159] the authors studied the influence in the overall mechanical performance of materials with embedded regions where properties are different from the bulk, like the interface in between layers observed in 3d printing of cementitious materials. In their study they showed that if the interface has better mechanical performance than the rest of the material, the total fracture crack energy increases. In the case of SHCCs, the results found by them led towards some loss in ductility. This is in accordance with the experimental results shown in Figure 4.4.

4.3.4. UNI-AXIAL TENSILE TEST

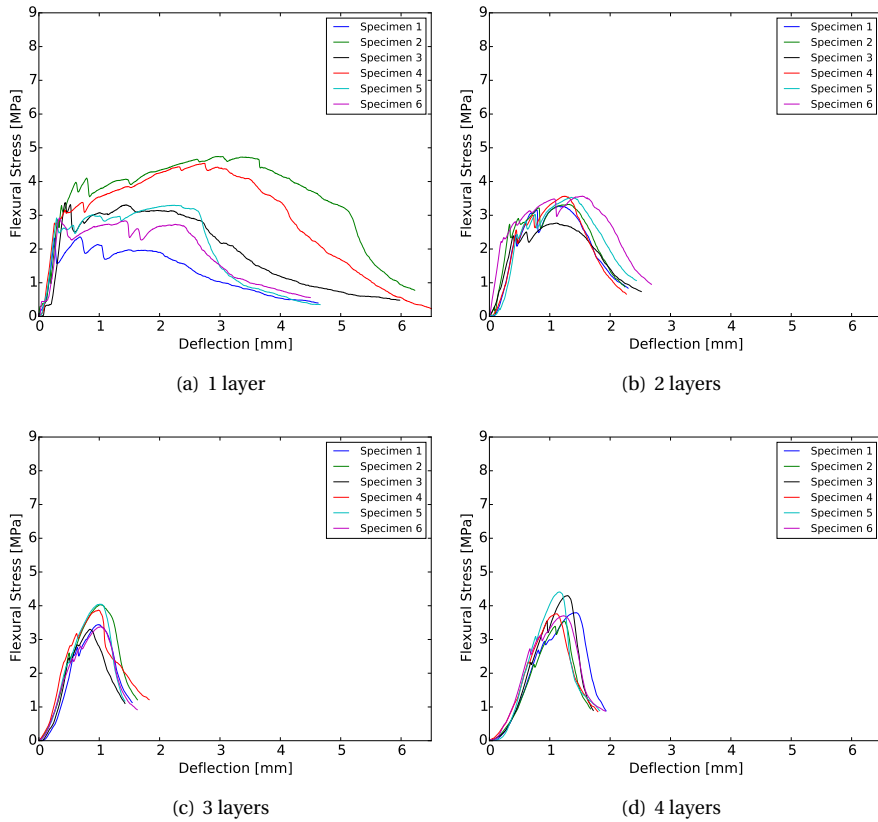


Figure 4.6: Flexural hardening behaviour for Y samples cured for 28 days.

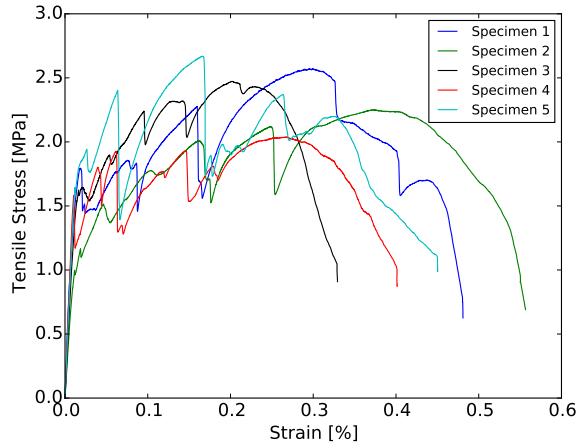


Figure 4.7: Strain hardening behaviour of X specimens cured for 35 days when LPA is applied.

Table 4.4: Mechanical performance at first crack of printed composites.

	Tensile strength at first crack [MPa]		Deformation at first crack [%]	
XLPA	1.53	± 0.23	0.023	± 0.006
XLPE	1.84	± 0.47	0.017	± 0.003
YLPA	1.28	± 0.33	0.022	± 0.017
YLPE	1.15	± 0.2	0.012	± 0.003

LOADING PARALLEL TO THE PRINTING DIRECTION (LPA)

Figures 4.7 and 4.8 show the stress - strain curves resulting from the uniaxial tensile tests in LPA for mixture X and Y, respectively. In tables 4.4 and 4.5 all the results from uniaxial tensile tests are shown, including both loading directions for both mixtures, respectively. It results evident that tensile behavior of the composites varied dramatically when tested in LPA or in LPE. Strain hardening behaviour was obtained for XVA3PVA20 specimens whereas only few samples from YVA4PVA20-S05 composites could be classified as such. The large deviations found for the values of deformation at maximum tensile strength for YVA4PVA20-S05 specimens is also an evidence of the better mechanical performance of XVA3PVA20. DIC results also helped to clarify this conclusion. The last picture of the test is used to illustrate the crack pattern in figures 4.9, 4.10, 4.11 and 4.12. These figures show the large cracks distribution at the end of the test. Using DIC results together with the stress - strain curves it is possible to conclude that multiple cracking was obtained in all samples, with the exception of specimen number 4 from YVA4PVA20-S05 samples. Towards the end of the test several large cracks formed and usually one of them concentrated the large displacements until reaching final failure of the composite. The mechanical performance obtained in this research are similar to what was previously reported for the same mixtures in [60].

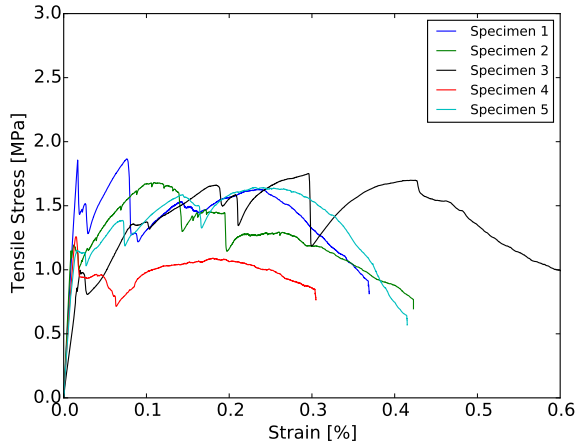
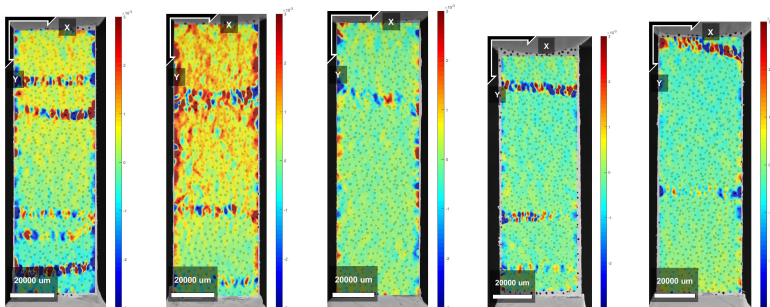


Figure 4.8: Direct tensile tests results of Y specimens cured for 35 days when LPA is applied.

Table 4.5: Maximum mechanical performance of printed composites.

	Maximum tensile strength [MPa]		Deformation at maximum tensile strength [%]		
XLPA	2.4	± 0.26	0.26	± 0.08	
XLPE	2.41	± 0.36	0.31	± 0.26	
YLPA	1.64	± 0.23	0.15	± 0.12	
YLPE	1.65	± 0.27	0.29	± 0.26	



(a) Specimen 1 (b) Specimen 2 (c) Specimen 3 (d) Specimen 4 (e) Specimen 5

Figure 4.9: Crack pattern obtained from DIC analysis on X samples - Horizontal Deformations.

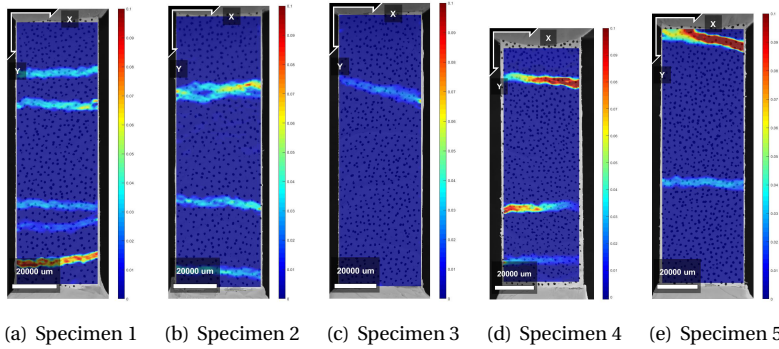


Figure 4.10: Crack pattern obtained from DIC analysis on X samples - Vertical Deformations.

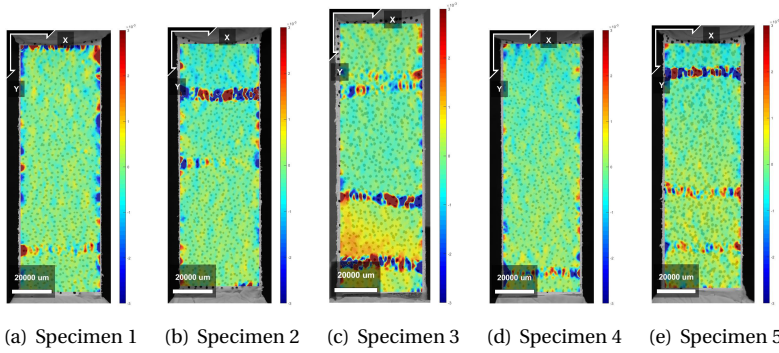


Figure 4.11: Crack pattern obtained from DIC analysis on Y samples - Horizontal Deformations.

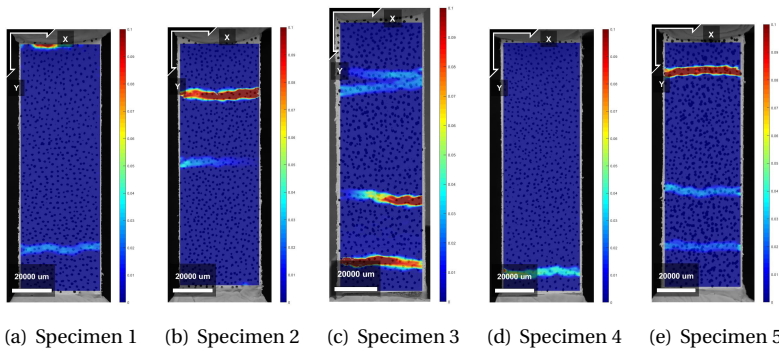


Figure 4.12: Crack pattern obtained from DIC analysis on Y samples - Vertical Deformations.

For both series XVA3PVA20 and YVA4PVA20-S05 the total strain capacity of the composites was affected by the printing technique when compared with the original results of these composites [111] and [112]. Several factors contributed to the degradation in composites ductility, such as: mix-design modification to make these materials printable, casting and mixing procedures. Regarding the lower total volume of water used and the use of HPMC, both modification would generate stronger matrices due to lower capillary porosity as a consequence of the lower water/binder ratio, and the internal curing promoted by the release of arrested water in the HPMC molecules [160]. Moreover, further in this study another important difference was also discovered and will be addressed to justify the loss in the overall composite's ductility.

LOADING PERPENDICULAR TO THE PRINTING DIRECTION (LPE)

The possibility of creating preferential fibre orientation in the extruded composite is one of the most important differences of such technique when compared to conventional casting. While extruding the pressure applied in the fresh mixture has the power to change the direction of the fibres, increasing the probability to find fibres longitudinally oriented towards the extrusion direction [132].

This issue is a matter of large interest of researches and industry. One of the techniques used to characterize the fibre orientation is the mechanical testing itself. In the case of fibre reinforced cementitious composites the lack of fibres in one of the directions would result in lower ductility or especially in the case of SHCCs the lack of strain hardening.

Figures 4.13 and 4.14 show the results recorded during a tensile test with LPE. Results obtained during these experiments showed that the printing technique have indeed oriented a large amount of fibres longitudinally, especially the ones found in YVA4PVA20-S05. Nevertheless, high ductility was still found for those composites. Moreover, in the case of XVA3PVA20 samples strain hardening properties were still found. This indicates that even if the extrusion process oriented the fibres in the mixture, the amount of reinforcement left in other directions was enough to guarantee SHCC performance. However, it is noteworthy to point-out that large deviations were found for values of deformation at maximum tensile strength for both mixtures, as seen in Table 4.5. This means that the preferential fibre orientation formed during the extrusion process created high anisotropy in the composite.

4.3.5. TENSILE BOND STRENGTH OF INTERFACE

Figures 4.15(a), 4.15(b), 4.15(c) and 4.15(d) show the tensile - strain curves resulted from the direct tensile tests of two printed layers of all evaluated mix-designs and time intervals. Samples named 2T had their second layer deposited after 3 minutes and 2TT after 36 minutes. The average tensile strength of these samples are also summarized in the Figure 4.16.

The first conclusion that can be taken from the test is that the specimens showed little ductility and no strain hardening behaviour in this direction. This was expected and should be attributed to the fact that only very few fibres bridge the fracture surface. In line with the other mechanical tests, the interface tensile strength of the YVA4PVA20-S05 specimens is smaller than that of the XVA3PVA20 specimens. On average, a small

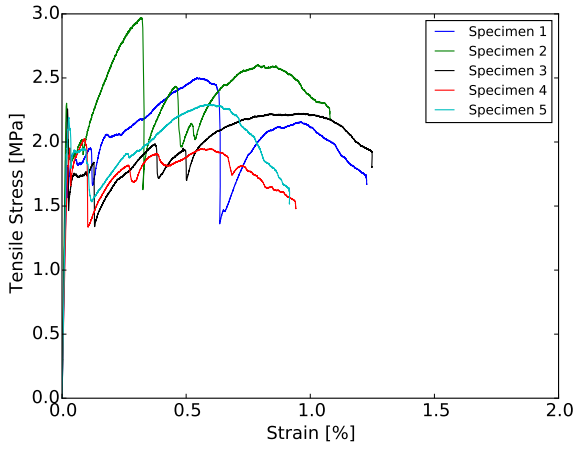


Figure 4.13: Strain hardening behaviour of XLPE cured for 35 days.

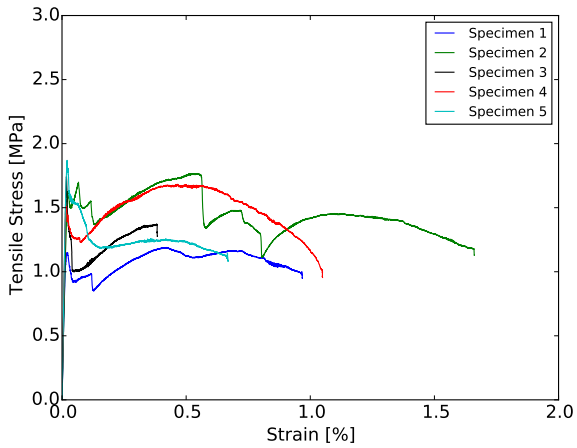


Figure 4.14: Strain hardening behaviour of YLPE cured for 35 days.

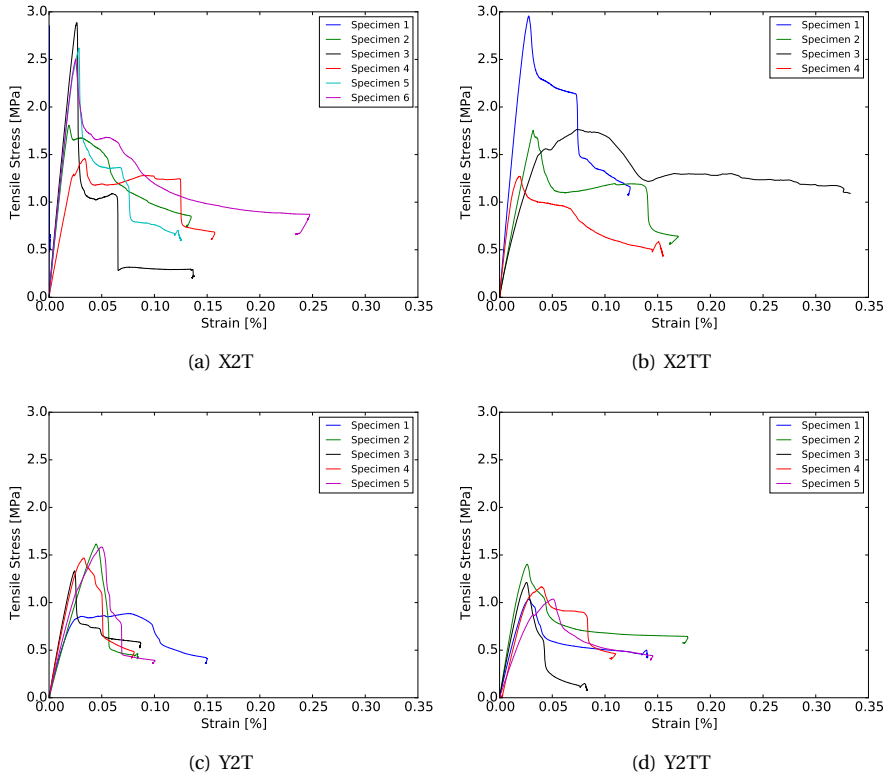


Figure 4.15: Layer interface tensile bond strength.

influence of the interlayer interval time was found, but the scatter is such that this cannot be considered significant.

The interface strength specimens with either material is comparable to or even slightly more than the tensile strength for LPA and LPE, i.e. of the bulk material. Often, it is reported that the layers interface tensile strength is lower than the bulk tensile strength [7, 146]. In the case of the currently studied materials, this difference will be further discussed in the section where CT-scan results are discussed. As reported by [150] the nozzle height influences the bond tensile strength between printed layers. Therefore, pushing one layer against the other generates a compacted area at the interface. A visualization of the consequence of this printing technique will also be illustrated in the section where CT-scan results are discussed.

As mentioned before, the use of HPMC in the mixture might also have contributed to the enhancement of this interface region. This admixture is known to work as a water reservoir while the mixture is still in the fresh state. This property also contributes to the phenomenon known as internal curing of cementitious composites and has been investigated before [160].

These results are very important to the development of new materials and technolo-

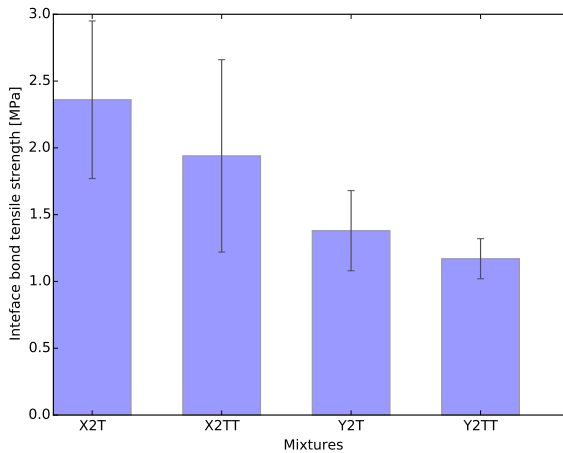


Figure 4.16: Average layer interface tensile bond strength.

gies for the printing of cementitious materials. Strain hardening was achieved in two directions, whereas only minor ductility was observed in the third. This confirms the intrinsic anisotropy that the technology brings.

4.3.6. CT-SCAN

In order to directly investigate the particular anisotropy of the studied composites, X-ray micro CT was employed. So far, the results pointed out that a composite with anisotropic mechanical behaviour was developed, with ductility being achieved for tensile loads applied in parallel and perpendicular to the printing direction and brittle behaviour when two printed layers were pulled apart.

Comparing the results obtained from the direct tensile test of LPA, the achieved ductility was lower than the one reported in [111]. The reason why the ductility found for those composites was below expectations can be given analysing the total air void content found in printed samples. This amount was significantly higher than what is usually found for SHCCs in literature. As these air voids can work as an obstacle to the fibre orientation they undermine the mechanical performance of the printed composites as well. The causes of increased porosity in cementitious composites which had its rheological properties modified by HPMC were discussed along with modifications in the hydration progress of cement paste by [160].

Observing the air void distribution along the height of two printed layers another interesting result was found. From Figures 4.17(a), 4.17(b), 4.18(a), 4.18(b), it was possible to visualize that the printing technique used in this investigation contributed positively to the mechanical performance of the bond strength of the interface between layers. As it can be noticed, the interface between the layers is the region with the lowest air void content in the sample. Therefore, this interface was not the weakest zone in the composite making it less probable that a crack would propagate through that zone. Nevertheless, it is also important to emphasize that the regions just under and above the interface

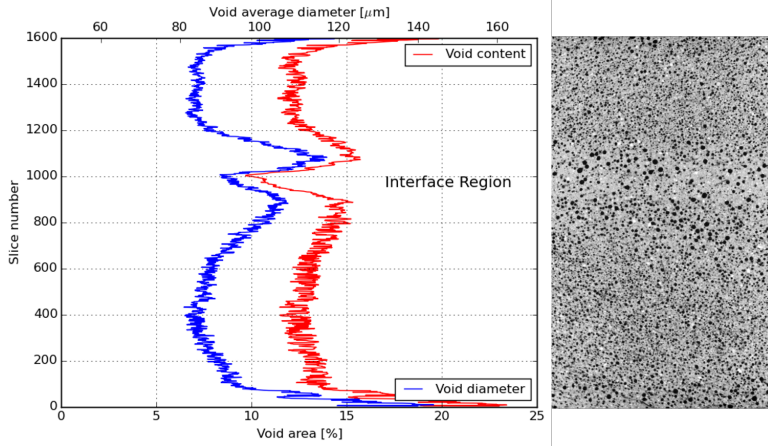
between layers have, in general, higher air void content.

In order to investigate the effect of air void distribution along the height of the printed beam on the fibre orientation, also the fibre orientation distribution was analyzed through X-ray micro CT. Figure 4.19, shows the orientation of the fibres in the printed layers. The results found go in accordance with the results found in the mechanical test, especially the tensile test with LPA and LPE when ductility was found in both directions. Therefore, the extrusion process of this type of mixtures preferably oriented the fibres diagonally in relation with the printing direction. Two hypothesis are given to justify this distribution. The first one might be related to the fact that PVA fibres are flexible and the extrusion forces applied to them are too high, causing a kind of turbulence. The second reason and most probably the strongest factor is again related to the printing technique and to facilitate the understanding it is also schematically represented in Figure 4.20. As discussed before the printed layers are always extruded against the previous one. Therefore, the extrusion forces exert shear stresses to the printing plane causing a small spread of the material in this plane. Moreover, the combined effect of the extrusion forces and the movement of the printing nozzle generate the observed fibre preferential orientation.

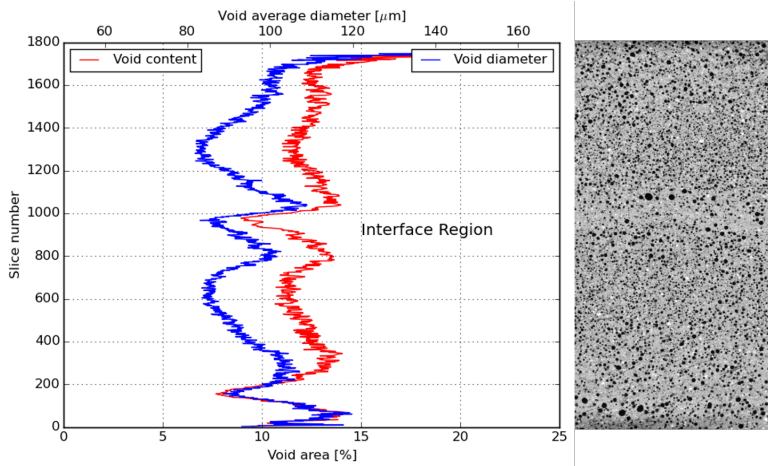
4.4. CONCLUSIONS

In this experimental study PVA-reinforced cementitious composites printed via additive manufacturing process was extensively characterized. The methodology developed in [60] was followed for the development of printable cementitious composites. A summary of the main conclusions of the present investigations are given:

- Two types of fibre reinforced cementitious composites were successfully printed and characterized. Both demonstrated anisotropic mechanical behaviour when tested in direct tensile load with ductility found in two directions loaded parallel and perpendicular to the printing direction (LPA and LPE) and brittleness in the third direction (between two printed layers);
- Both composites showed flexural and strain hardening behaviour, as well as multiple cracking, in LPA. Moreover, only the samples with 0.3 wt.% of HPMC and reinforced by 2 vol.% (XVA3PVA20) showed strain hardening in LPE;
- Besides the fact that both mixtures resulted in flexural hardening, 4-point bending tests also showed that thick samples fail in a more brittle way. This behaviour is due to the larger tensile forces in the tension zone. Higher forces cannot be distributed homogeneously to the fibres. Consequently, the energy dissipated during the cracking can not be distributed along the specimen to create multiple cracking. Further research is needed to develop ductile composites that could dissipate such high energy;
- Extruding a printed layer against the previous one is a good strategy to enhance its bond strength. As observed in this study the interface tensile strength of both mixtures were in the same range of values of the first crack when composites were loaded in LPA and LPE, independently on the time taken to deposit the top layer. Therefore, this was not a weak zone in the composite;

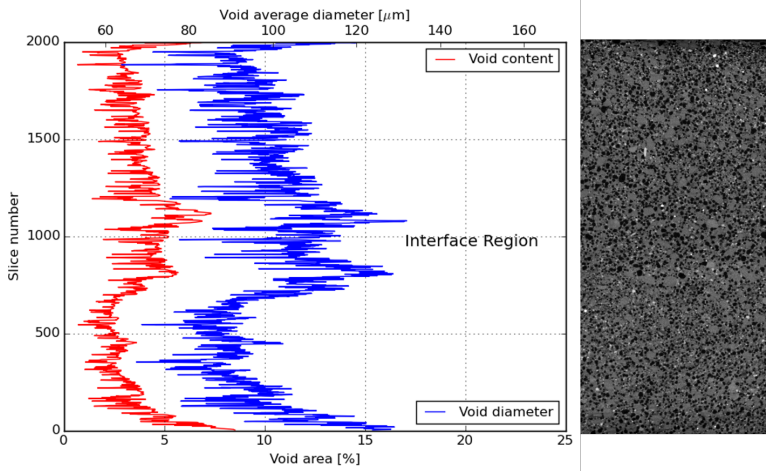


(a) X2T

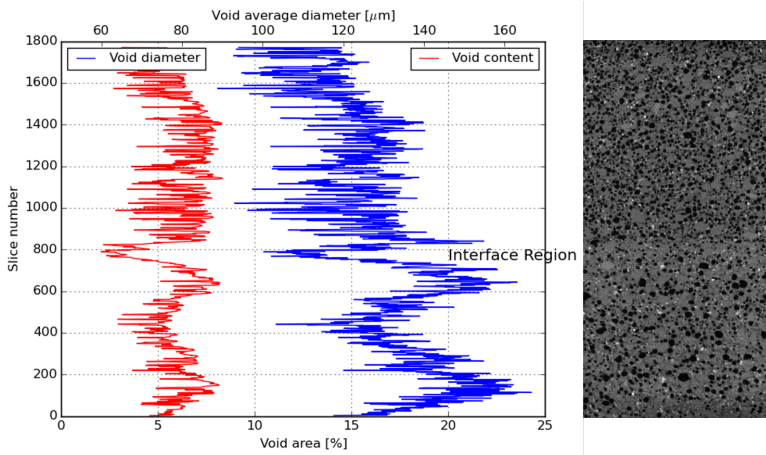


(b) X2TT

Figure 4.17: Average air void content and diameter distribution in the height of a 2 layers printed element of X series.



(a) Y2T



(b) Y2TT

Figure 4.18: Average air void content and diameter distribution in the height of a 2 layers printed element of Y series.

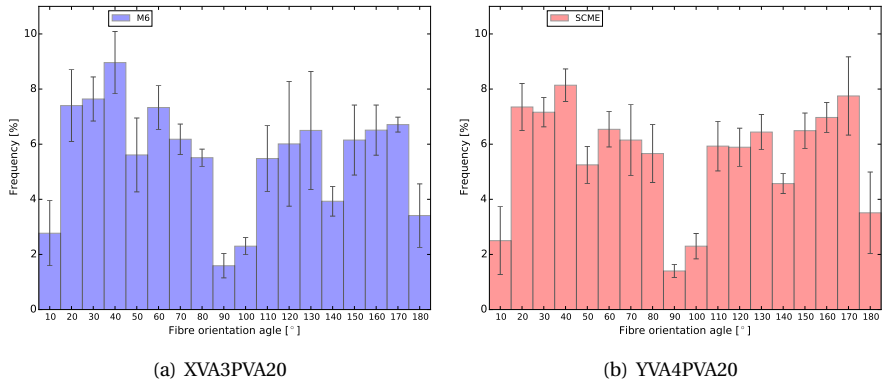


Figure 4.19: Average fibre orientation of both printed mixtures

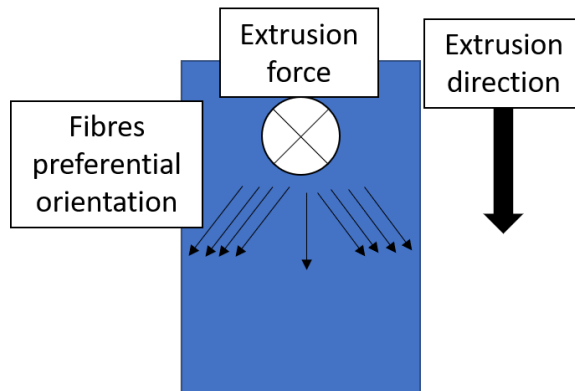


Figure 4.20: Schematic view of fibre orientation due to the printing technique.

- The same extrusion technique that helped to improve tensile bond strength between printed layers, may also have played a role in the fibre orientation, which was observed to be mainly diagonal to the print direction, rather than parallel to it. Flow speed differences in the filament likely also contribute to this fibre orientation;
- As observed in chapter 3 and [60] and confirmed during the experiments reported in the current study, composites with matrices richer in blast furnace slag showed better mechanical performance than the composites rich in fly ash.

5

EFFECT OF VISCOSITY MODIFIER ADMIXTURE ON PORTLAND CEMENT PASTE HYDRATION AND MICROSTRUCTURE

No one is born fully-formed: it is through self-experience in the world that we become what we are.

Paulo Freire

Significant attention has been given to the development of new materials and techniques to be employed in the construction market. One of the techniques which has drawn noticeable attention is the additive manufacturing process (a.k.a. 3-dimensional printing (3D printing)). One of the approaches of this construction technique is the extrusion of cementitious composites to form contour of a desired geometry. To achieve high viscosity in cementitious materials, usually viscosity modifying admixtures (VMA) are employed. However, the consequences of using these admixtures at high dosages is still not fully understood. This study characterized the influence of different VMA dosages on Portland cement paste, through a microstructure analysis. Hydration development was assessed, and effect of the admixture was quantified at different curing ages. Techniques such as thermogravimetric analysis, optical and electron microscopy, X-ray diffraction, Fourier transform infrared spectroscopy, micro computed tomography scan and nanoindentation were employed. Important negative side effects were found such as: VMA increasing the cement setting time, anomalous dispersion of hydration products in the bulk and increasing the void content. On the other hand, positive effects were also found such as: evidence of internal curing, higher degree of hydration and lack of undesired hydration products.

This chapter has been published in S. C. Figueiredo, O. Çopuroğlu, and E. Schlangen, Effect of viscosity modifier admixture on Portland cement paste hydration and microstructure, Construction and Building Materials, vol. 212, pp. 818-840, 2019. [160]

5.1. INTRODUCTION

A promising construction technique which has drawn notable attention in the past few years is the additive manufacturing (AM). This revolutionary technique is likely to open a new era in the construction industry, optimizing process and materials [83]. AM is a general classification for technologies which fabricates objects with the help of automated equipment, directly from a digital design technology [5, 6]. There are several different techniques to manufacture the objects developed based on AM, such as the powder bedding with an inkjet head [82] or the laser melting [161], and the counter craft technology which employs extrusion techniques to fabricate objects [11]. Both AM technologies build an object through a layer by layer deposition process. The counter-craft AM has drawn a lot of attention in the construction market as its implementation looks feasible to be applied in large scale. It should be noted that materials with unique properties need to be developed to meet the mechanical and durability-related requirements of a long-lasting and safe structure.

Recent investigations have shown the development of cementitious composites with different aggregate particle sizes. Concrete and mortars have been developed with printable characteristics. In some studies fibres have been incorporated to stabilize the mixture at fresh state or to minimize the occurrence of cracks due to shrinkage. However, the materials and printing methods have not yet delivered solutions to improve the hardened performance of composites when loaded in tension [13, 72].

Moreover, researchers have addressed this problem developing a technique to produce mortar filaments through AM reinforced by a steel wire. Higher ductility was achieved with samples reinforced by the steel wire. Further, more research is needed to enhance the interface bonding between the wire and the mortar [19].

Another strategy to increase the ductility of printed brittle materials is fibre incorporation. Great plastic deformations can be achieved on cementitious composites reinforced by fibres, namely strain hardening cementitious composites (SHCC). This type of composite can deliver high tensile strain, strength and frequent but tiny multiple cracks under tensile loading [21].

SHCCs are cementitious composites reinforced by high volume of fibres. Usually the reinforcement level is around 2% of the total composite's volume, which brings challenges regarding the flowability of such mix designs. An alternative often approached to enhance the fibre dispersion is the employment of viscosity modifier admixtures (VMA) [60, 162]. These admixtures are usually composed of long organic chains with -OH ramifications, that arrest the free water in the mixture through hydrogen intermolecular bridge. One of the most used VMA is composed of hydroxypropyl methylcellulose (HPMC) [102]. In addition, the use of VMA is a key factor when developing printable cementitious composites [60]. The adjusting of the amount of the chemical admixture, coupled with a good distribution of particles grain size in the matrix, and optimum water-to-solid ratio may lead towards a material with the needed viscosity for printing.

Khyat detailed several types of VMA that can be used in cementitious materials. The author separated them in five different classes according with the mechanism of action and their composition. In general they are employed in the construction industry to control some of the fresh state properties for development of high performance cementitious composites, such as specific types of grouts or under water projects [163].

Furthermore, other studies have demonstrated the ability of VMAs to arrest the water available in cementitious mixtures. For instance, the employment of HPMC in some cement-based mortars enhances significantly their water retention improving or keeping the quality of this type of material inside certain limits [164–167]. Moreover, D. Marchon *et. al.* approached the need to control rheological properties of fresh cementitious mixtures to be applied for 3D printing. In that article several different types of admixtures are discussed and the importance of VMAs for the pumping, extrusion and deposition phase of printed cement-based composites is acknowledged [168]. Thus, the use of VMAs in the construction industry helps concrete technologists to keep viscosity and yield stresses of mixtures under control.

Besides the fact that VMA can help in controlling the rheological properties of a solid suspension, the consequences on the microstructure of hydrated Portland cement is not yet fully understood. The influence of some water-soluble polymers on the microstructure development of Portland cement was investigated in [169]. Their findings showed a delay on the hydration process, formation of unusual minerals at early ages, a slightly lower $\text{Ca}(\text{OH})_2$ content and a higher amount of chemically bounded water. Besides that, a higher cohesion of the cement paste resulting in a lower number of microcracks and different morphology of portlandite crystals was also observed under microscope.

Researches investigated the influence of HPMC with different viscosities in the hydration of two individual phases of the Portland cement clinker. They demonstrated through calorimetry measurements that independently of VMAs viscosity the hydration of C_3S and C_3A was delayed with the use of rheology modifier admixture. Nevertheless, blending each individual phase with gypsum would lead towards a slightly different result. Naturally, the addition of gypsum delayed hydration of both phases as it would happen in an ordinary Portland cement hydration. However, reactions of blended C_3A and gypsum powders were sensitive to VMA viscosity. The authors justified their finds stating that C_3A hydration was more susceptible to lower ions mobility through viscous solutions [170].

Furthermore, the cement hydration delay was explained with the effect of HPMC on the precipitation of calcium hydroxide, the polymer's water absorption capacity [171–173], and the methyl content [174]. Moreover, a study have also reported the influence of molecular weight on the rheology of cement paste modified by HPMC admixture and its potential to combine via intermolecular and intramolecular crosslinks with Ca^{+2} ions [175]. This study also reports potential challenges using HPMC together with polycarboxylate superplasticizers as HPMC molecules have the potential to adsorb superplasticizer molecules. Hence, the probability of SP molecules to be deposited in the surface of the cement particles decreases.

As demonstrated by other studies and summarized here, the employment of VMAs to control rheological properties of cementitious materials is essential to the development of printable mixtures. However, the consequences of using this organic admixture in the microstructure of cement-based materials is not clear. The present research aims to build a better understanding to the consequences of HPMC use in cement paste. This information together with the literature already available, contributes to the new generation of construction materials which are under development to be applied on 3D printing.

Table 5.1: Chemical composition of Portland Cement used in this study

Compound	CEM I 42,5 N [%]
CaO	69.53
SiO ₂	15.60
Fe ₂ O ₃	3.84
Al ₂ O ₃	3.09
SO ₃	2.60
MgO	1.67
K ₂ O	0.55
TiO ₂	0.31
P ₂ O ₅	0.14
Rest	0.53
LOI	2.14

5

5.2. EXPERIMENTAL METHODS

Chemical composition of the Ordinary Portland Cement (OPC) CEM I 42,5 N and its loss on ignition (LOI) can be found in Table 1. They were assessed by X-ray fluorescence analysis (XRF) and thermogravimetric analysis performed at 10 K/min under Argon atmosphere. The LOI was determined using the loss of mass between 45 and 1000°C.

The VMA used for this study is composed by HPMC with viscosity of 201000 mPa.s. The samples were cast mixing a volume of 0.5 litres in a planetary mixer according to the following procedure:

- All dry materials were mixed for two minutes at low speed (speed 1 - 60 rpm);
- While mixing at speed 1, during approximately two minutes, the water was added;
- The wet powders were mixed during the next two minutes at speed 1. In this phase it was possible to observe a significant change in the mixture's viscosity. A dough like consistence was achieved;
- Using a spoon the wet powder is manually mixed, in order to ensure a homogeneous mix;
- At high speed (speed 2 - 124 rpm), the dough like cement paste was further mixed. At this phase the rigid dough becomes softer and "opens" in the mixing bowl.

A reference cement paste with a water-to-cement (w/c) ratio of 0.3 (REF) and three levels of VMA, 0.1, 0.3 and 1% of the cement mass, named 1M, 3M and 10M respectively were evaluated. The VMA content employed in this study follows the same levels found in [60] where the rheology of crowded solid suspensions using this type of admixture was studied, aiming the development of printable SHCCs.

The mixed paste was cast inside plastic containers (33 mm diameter ad 69 mm height) and sealed with the help of paraffin paper. Right after moulding they were left for 24

hours rotating around their own axis (5 - 7 rpm), as reported by [176], to ensure a homogeneous material avoiding any segregation and bleeding, as discussed in [177]. With the exception of 10M samples, afterwards, they were demoulded and cut in slices of approximately 5mm and cured at $(20 \pm 2)^\circ\text{C}$ and relative humidity of $(98 \pm 2)\%$. 10M samples could only be demoulded and cut 48 hours after casting.

To stop cement hydration the cut slices were manually crushed into small pieces and partially submerged in liquid nitrogen for 3 minutes and completely submerged for 5 minutes. Immediately after, crushed particles were conditioned in plastic bags with holes to allow the release of moisture from the samples and stored in a freeze drier for further drying. Those samples were used for thermogravimetric analysis (TGA). The small cut slices destined to electron microscopy observations, X-ray diffraction (XRD), Fourier Transform Infrared Spectroscopy (FTIR), micro Computed Tomography scan (Micro-CT scan), nanoindentation and thin section microscopy observations had their hydration arrested by solvent exchange procedure, employing ethanol [178]. To investigate the hydration progress of all samples the following procedures were used for each test:

- Thermogravimetric analysis (TGA):

The test was performed increasing the temperature from 40 to 1000°C at 10 K/minute. In order to quantify the hydration products and total degree of hydration the mass loss was measured according with the following thresholds:

- 110°C to 450°C: water loss from AFm products;
- 450°C to 520°C: water loss from portlandite;
- 550°C to 800°C: carbon dioxide loss from calcium carbonate minerals.

Portlandite and calcium carbonate contents were measured taking the stoichiometry balance of each reaction into account. Moreover, the total degree of hydration was calculated deducting the mass loss from the calcium carbonate minerals. Two tests were run for each sample. Additionally, a TGA test only with pure VMA was run to quantify the mass loss of different temperatures. This test was important for adjustments on samples where HPMC was employed.

- X-ray diffraction (XRD) and Fourier Transform Infrared Spectroscopy (FTIR):

Powder samples analysed with the XRD and FTIR were hand milled to avoid heating up the samples. The materials used in both tests were sieved with a 75 μm opening sieve. XRD samples were measured from 2θ equal to 5° to 70°, at 2°/min. FTIR samples were tested measuring bands from 550 to 4000 cm^{-1} .

- Isothermal calorimetry analysis:

The total energy in form of heat released during the first 10 days of cement hydration was measured with the assistance of a TAM Air Isothermal Calorimeter with eight channels, at 20°C and using as reference ampoules with sand. The samples used for this test were mixed outside of the calorimeter. Therefore, the initial peak of heat released corresponded to the exothermic dissolution of the grains and formation of first AFt phases were not present in these results.

- Thin section analysis:

Thin section specimens otherwise known as "petrographic thin section" were produced for all four mixtures, from specimens which had its hydration arrested by solvent exchange. A thin section sample had approximately 30 μm thickness and it was obtained through a controlled grinding process employing a semi-automatic thin section machine where three rollers with diamonds of 64, 46, 16 μm were used. Low viscosity epoxy with fluorescent pigment was used to guarantee sample stability during preparation and facilitate porosity investigations under ultra-violet (UV) light. Thin section samples were observed with a Leica DM2500P polarized light microscope equipped with linear and circular polarization filters. Lenses of $2.5\times/0.07$, $10\times/0.22$ and $20\times/0.4$ (magnification/numerical aperture) were available. Plane polarized light (PPL), PPL with UV light, cross polarized light (XPL) and circular polarized light (CPL) were used to observe the air entrapped voids and the portlandite distribution in the paste. The advantages of using CPL for quantitative image analysis have been shown in [179]. Using this technique all available portlandite crystals can be observed in a single field of view, in contrast with XPL where only a portion of the available crystals are visible due to the extinction phenomenon.

- Scanning electron microscope (SEM):

Samples destined to SEM observations were mounted in a working glass and ground with the help of a thin section grind machine with the same three rollers employed for manufacturing of thin section samples. These samples were also impregnated using a low viscosity epoxy with epo-dye colour and had their surfaces ground and polished. To ensure the thickness of epoxy on the surface of the sample, they were measured before and after epoxy impregnation. After epoxy impregnation, the samples were ground again only with the roller with 16 μm diamonds. Only after ensuring a flat surface, the samples were ground employing the 1200 silicon carbide paper cooled with ethanol. For polishing purposes, a paste with 6, 3, 1 and 0.25 μm diamonds were used. Back scattered electrons (BSE) and secondary electrons (SE) images were obtained.

In order to quantify information which can contribute to the understanding of the hydration development, image analysis with the help of Trainable Weka Segmentation tool [156] from FIJI [157] was performed. 30 images with 200 times magnification covering a total area of 214.03 mm^2 was used per mixture. The average area of unhydrated OPC particles, inner and outer products, portlandite and voids were measured.

- Micro computed tomography scanner (Micro-CT scan)

To obtain the average size and the total volume of voids on the analysed pastes with VMA a Phoenix Nanoton m Micro-CT scanner was employed. Cylindrical specimens with 35 mm diameter and approximately 3 mm height were scanned, reaching 16.67 $\mu\text{m}/\text{pixel}$ resolution. Afterwards, an image stack with the top view of the cylinder was analysed with the help of Trainable Weka Segmentation tool [156] from FIJI [157]. For those images, only two phases were distinguished voids and matrix.

- Mechanical performance (Nanoindentation and compressive strength)

The mechanical performance of the studied pastes were assessed through compressive strength of cubes with 40mm edges at 2, 3, 7 and 29 day-old of curing and nanoindentation of 29 days-old samples.

To quantify the matrix stiffness a nanoindenter MTS G200 with continuous stiffness measurement was used. This measurement was employed to investigate the local mechanical performance of the paste and quantify the influence of VMA at this scale. The surface of the samples tested through this technique were flat and scratch free. To achieve this surface quality a similar approach as the one employed in the sample preparation dedicated for specimens investigated under SEM was used with exception of the epoxy impregnation step. The polishing done in the lapping table using diamond paste with 6, 3, 1 and 0.25 μm diamonds and cooled with ethanol was executed for 10, 10, 15 and 30 minutes for each specimen respectively. After polishing the samples were stored in a vacuum oven at 25°C before testing. A grid of 15×15 indents were made using a strain ratio of 0.05/s until the maximum depth of 2000 nm. The indents were separated of each other by a distance of 50 μm . In order to calculate the average stiffness of each indent the Poisson ratio of 0.2 was used and the values were calculated from a depth of 200 to 400 nm. Hydration products were identified by their stiffness as reported in [40] and [180].

- Rheological properties

The rheology properties are very important to define a printable mixture. Materials developed for printing purposes must be stable under high pressures to avoid any type of segregation when the mixture is under pressure and they must also have shape stability in order to manufacture the desired contour. All those empirical parameters needed for a printable mixture were quantified by means of rheological tests. For this study, a ram extruder (Figure 3.2) was employed to assess the paste rheology parameters. Three dies with a length-diameter ratio of 1, 4 and 8 plus, four different extrusion speeds 0.25, 0.5, 1 and 2 mm/s were employed. Using six parameters analysis from the Benbow-Bridgewater (equation 3.2) model the properties which governs the flow of this type of solid suspension were obtained. The parameters "m" and "n" are responsible to guarantee the non linear behaviour of the pressure drop with the extrusion speed characteristic from pseudo-plastic fluids.

5.3. RESULTS

Before the description of all results found for evaluated specimens it is important to show that the VMA employed was investigated under electron microscope, TGA and XRD. The results from these tests have demonstrated that the chemical admixture suffers from sodium chloride impurity. The impurity was found through TGA from the weight loss from 800 to 950°C, as shown on the differential thermogravimetry (DTG) curve plotted in Figure 5.1(b). At this interval of temperature halite melts and small portions of it might vaporize, as demonstrated by the loss of mass. XRD pattern plotted on Figure 5.1(a) also shows the presence of NaCl crystals, among all the amorphous organic phase. Finally, as shown in Figure 5.2 the salt crystals were observed using an Environmental SEM, and with the help of Energy-Dispersive X-ray Spectroscopy (EDS) measurements the pres-

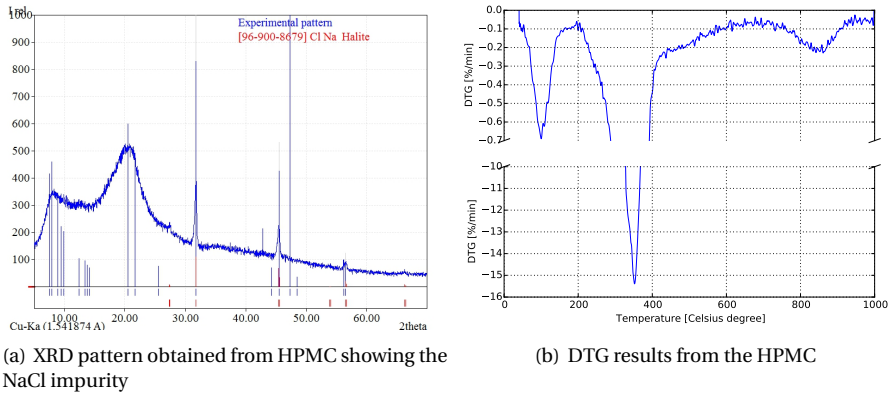


Figure 5.1: HPMC Impurity characterization

5

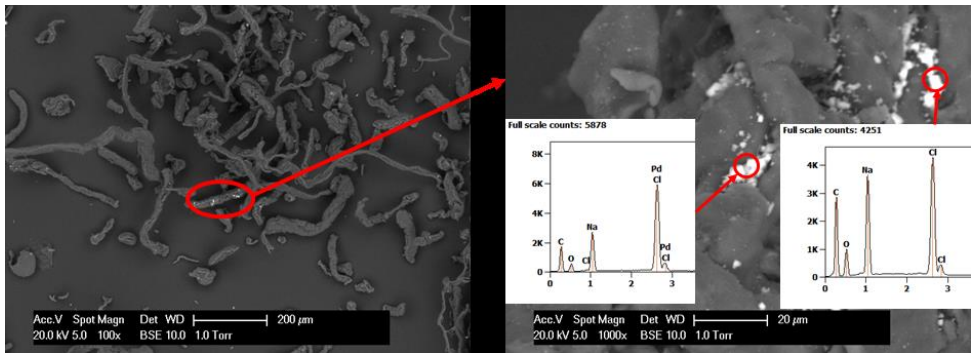


Figure 5.2: Electron microscope image and chemical composition from EDS measurement.

ence of peaks of sodium and chlorine were found. It should be noted that NaCl accelerates OPC hydration [181] [182], and leads to corrosion of steel reinforcement [183] [184].

5.3.1. ISOTHERMAL CALORIMETRY TEST

In Figure 6.8 the result from the isothermal calorimetry test was reported. The increasing volume of viscosity modifier on the cement paste, lead towards delaying Portland cement hydration. The greatest consequences were measured on pastes with 1% of VMA, where the dormant stage went up to the first 9 hours of hydration.

Specimens 1M and 3M had also their early age properties changed. Both had a slightly longer dormant period, than the reference as also reported by [170]. However, the C_3S peak obtained for both was also slightly higher than reference samples, meaning that the hydration reactions were significantly accelerated after the extended dormant period. Other fact that shows this acceleration is the overlapping of the peak of heat generated by the hydration of C_3S and the renewed formation of ettringite [185]. In reference samples after about 10 hours the slope of the heat release decreases, followed

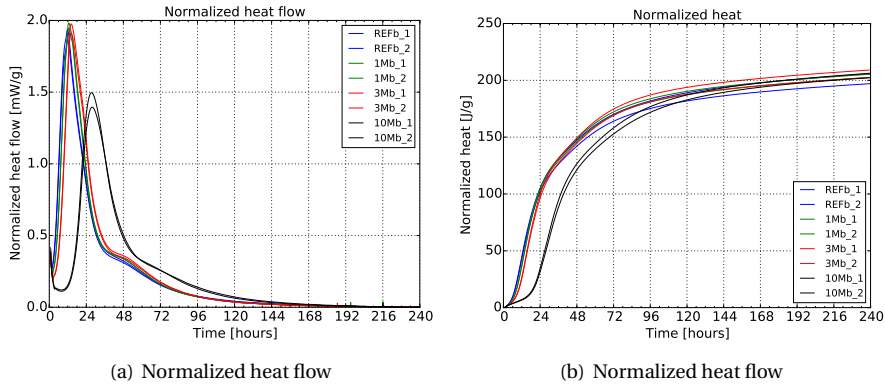


Figure 5.3: Isothermal calorimetry test from the initial 10 days of hydration

by a re-acceleration after some minutes. In 1M samples the different slopes can also be noticed however, the second slope was shown only during the descending part of the curve, after approximately 10.5 hours. Specimens with 0.3% of VMA do not show these two slopes. The heat released by these clinker components overlay creating a wider peak.

In Figure 5.3(a) the total heat generated during the measurement period was plotted. Besides the fact that the employment of VMA delays Portland cement hydration, after approximately 30 hours of hydration samples 1M and 3M had already a slightly higher total heat released. In general, samples with HPMC have released a higher amount of energy during the first 10 days of curing.

5.3.2. THERMOGRAVIMETRY ANALYSIS

Thermogravimetry results were especially important to quantify the results found on this study. A summary with all results obtained with the test is given in Table 5.2. The influence of 1% VMA on the hydration delay of cement paste could also be noticed on the TGA results. Degree of hydration (α) was calculated for all samples and the results show a significant loss on 1 day cured samples for 10M specimens. Moreover, a significant increase in α since the 1st day of hydration for 1M and 3M specimens was noticed. 10M specimens only develop higher degree of hydration after the 3rd day.

To explain the higher values found for samples with HPMC an understanding of how this chemical admixture changes the viscosity of solid solutions must be approached. The HPMC molecules are able to “arrest” water through hydrogen intermolecular interactions. These interactions decrease the availability of water during the first hours of cement hydration increasing significantly the viscosity of the water which surrounds OPC particles. As soon as pore solution pH rises, the increasing availability of OH^- ions decreases the capabilities of VMA in change the viscosity of the solid suspension by rescuing the kidnapped water molecules and making water molecules available for hydration again. Gradually this phenomenon happens in the paste, and therefore gradually the water “arrested” on HPMC molecules are released to become available for hydration. This description is also found to explain the phenomenon known as internal curing. There-

Table 5.2: Summary of properties measured using TGA technique.

Age [days]	α	H ₂ O from 105 to 450°C [%]	Portlandite [%]	Calcium carbonate [%]	Portlandite before carbonation [%]
REF					
1	0.2932 ± 0.0112	4.12 ± 0.21	7.64 ± 0.05	5.12 ± 0.03	10.61 ± 0.07
2	0.3745 ± 0.0073	5.33 ± 0.01	7.58 ± 0.34	5.44 ± 1.16	10.80 ± 0.52
3	0.4081 ± 0.0027	5.79 ± 0.08	7.93 ± 0.06	5.52 ± 0.68	11.22 ± 0.45
29	0.6489 ± 0.0002	8.88 ± 0.11	11.79 ± 0.97	5.43 ± 0.03	15.07 ± 0.99
1M					
1	0.3472 ± 0.0159	4.86 ± 0.06	8.09 ± 0.12	5.76 ± 0.71	11.55 ± 0.41
2	0.4192 ± 0.0167	5.55 ± 0.16	9.44 ± 0.89	5.86 ± 0.59	12.99 ± 0.45
3	0.4327 ± 0.0065	5.90 ± 0.16	8.40 ± 0.52	7.65 ± 1.64	13.29 ± 0.71
7	0.5584 ± 0.0145	7.46 ± 0.14	9.51 ± 0.26	7.40 ± 0.32	14.23 ± 0.49
29	0.734 ± 0.0118	9.43 ± 0.04	12.73 ± 0.81	8.49 ± 1.13	18.29 ± 0.04
3M					
1	0.3311 ± 0.0094	4.70 ± 0.12	6.87 ± 0.35	6.92 ± 0.75	11.19 ± 0.21
2	0.4218 ± 0.0096	5.72 ± 0.02	8.32 ± 0.16	6.74 ± 1.09	12.53 ± 0.97
3	0.4972 ± 0.0077	6.55 ± 0	9.47 ± 0.22	6.56 ± 0.94	13.56 ± 0.48
7	0.611 ± 0.0019	8.02 ± 0.08	11.08 ± 1.32	6.47 ± 1.15	15.12 ± 0.46
29	0.7838 ± 0.03	10.07 ± 0.1	14.41 ± 0.8	6.19 ± 1.49	18.27 ± 0.31
10M					
1	0.1472 ± 0.0069	2.17 ± 0.02	1.30 ± 0.25	5.44 ± 0.15	4.49 ± 0.35
2	0.3238 ± 0.0008	4.49 ± 0.08	5.70 ± 0.31	8.07 ± 0.16	10.88 ± 0.19
3	0.4403 ± 0.0017	5.90 ± 0.11	8.51 ± 0.62	8.84 ± 2.32	14.28 ± 1.11
7	0.5503 ± 0.0092	7.19 ± 0.01	9.44 ± 0.48	13.04 ± 1.13	18.35 ± 0.36
29	0.7353 ± 0.0423	9.36 ± 0.23	13.45 ± 0.61	10.86 ± 1.98	20.77 ± 0.88

fore, it is believed that the VMA does not only contribute to the viscosity modification of the solid suspension, but also to improve OPC hydration.

The mechanism which VMA provides internal curing to the cement paste is very similar to the ones reported to other materials with equivalent water retention, such as natural fibres [186, 187], super absorbent polymers [130] or porous aggregates [188, 189].

The total loss of water from AFm and CSH, as well as the total amount of calcium hydroxide is smaller for 10M samples only until the 3rd day of hydration. As it was measured and exemplified on Figure 5.5, the higher degree of hydration found on samples with VMA is coming mainly from the water lost from 105 until 450°C, corresponding to hydration products such as AFm and CSH.

Another important characteristic of samples where the viscosity modifier was employed is the total amount of calcium carbonate. The proportions from this mineral rise with the increasing employment of the admixture. To explain this result two hypotheses were raised. The first hypothesis considered that this carbonation happened during the TGA test. The second acknowledges that the total time needed for sample preparation before storing them in the freeze drier was enough to cause a certain level of carbonation.

According with the first hypothesis products formed during the heating up of the VMA would induce some carbonation in the samples. To test this hypothesis thermogravimetric tests were performed in calcium hydroxide and calcium hydroxide mixed with 1% by weight of VMA. The calcium hydroxide used was supplied by VWR chemicals and according to the certificate of analysis provided by the manufacturer the material employed should have a purity higher than 96%, and specifically for the lot used in this research 97% was measured. The goal was to emulate the same environment found during the TGA tests for the cement pastes but, with a much higher VMA-to-CH ratio. This high concentration of both components would hypothetically lead to a great formation of calcium carbonate.

Figures 5.4(a) and 5.4(b) show the obtained TGA / DTG curves and the summary of the total amount of calcium hydroxide and calcium carbonate found for this experiment respectively. As it can be seen, the calcium hydroxide levels were stable and the amount of calcium carbonate were slightly higher for samples with VMA. A consumption of $\text{Ca}(\text{OH})_2$ was expected to generate the CaCO_3 , and a much higher amount of the carbonated mineral was expected to be formed. Therefore, as a conclusion of this study it is possible to say that the higher content of calcium carbonate found for samples with VMA was not caused by a reaction between the CH and the products formed when VMA is submitted to high temperatures.

As the first hypothesis could not be validated, only the second hypothesis seems to explain this accelerated carbonation. This phenomenon might be correlated with the large amount of entrapped air voids found on samples with HPMC. Accelerated carbonation was previously reported for foamed concrete, as the total surface area exposed to the gas is larger [190]. The total amount of calcium carbonate in the cement used during this study was 1.22%. Therefore, carbonation happened for all samples with more emphasis on the samples with VMA. This phenomenon might be influenced by the combination of several factors: larger surface area of samples used for TGA (crushed particles of about 1 mm edge); significantly larger volume of air voids; and the abnormal precipi-

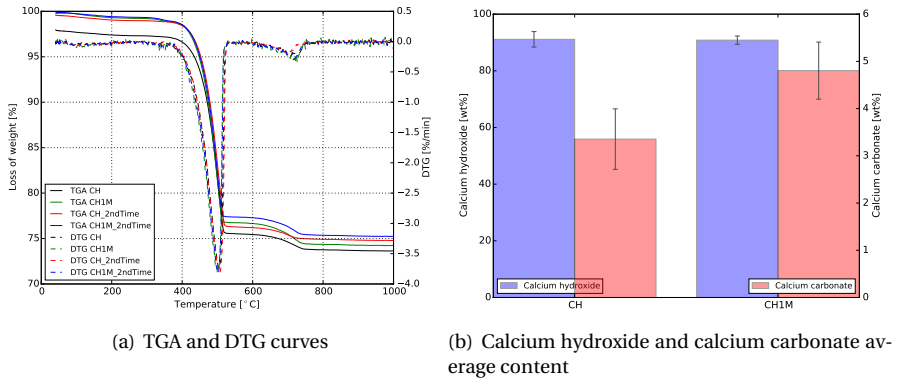


Figure 5.4: Summary of results found in the calcium hydroxide experiment

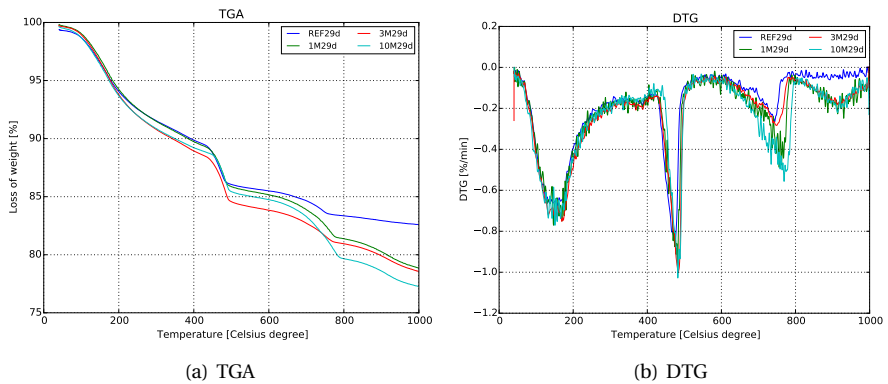


Figure 5.5: Thermogravimetric results from 29 day-old samples

tation of portlandite in the inner walls of the voids.

Assuming that the only source of calcium carbonate in those samples are coming from the original amount of filler in the cement and the rest was generated due to carbonation the last column of Table 5.2 shows how higher the total percentage of CH would be.

5.3.3. X-RAY DIFFRACTION

The absence of some intermediate cement hydration minerals might be happening due to: delayed hydration due to VMA use; and the lack of distinguishment of the heat release peaks from ettringite and C_3S . Therefore, an investigation into the mineralogical composition was carried out in order to verify if the modal composition followed a similar trend in VMA containing samples as well as the REF ones.

In Figure 5.6 the XRD pattern for samples with 29 days samples are shown. As the results were analysed only qualitatively, the patterns did not present formation of new

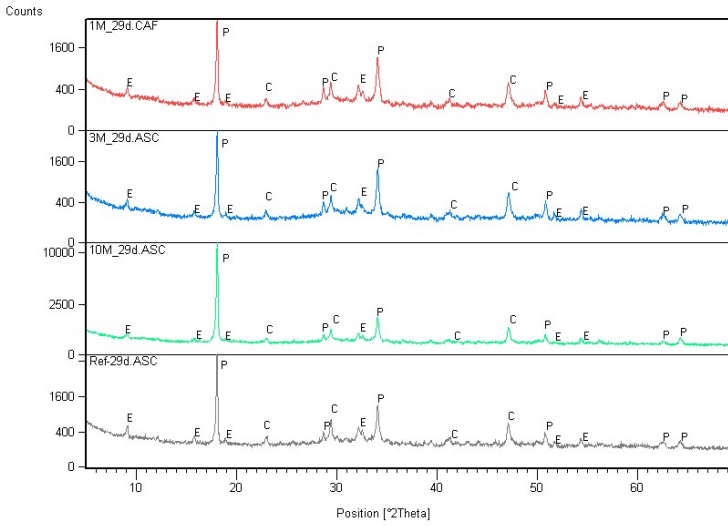


Figure 5.6: XRD pattern of samples with 29 days, where ettringite (E), calcium carbonate (C) and portlandite (P) peaks are in evidence.

or lack of minerals. Therefore, the employment of rheology modifier does not generate any hazardous minerals which could lead to a decrease on the durability or reliability of printed cementitious composites.

5.3.4. FOURIER TRANSFORM INFRARED SPECTROSCOPY

In Figure 5.7 the FTIR results from 3 and 7 days samples are plotted to exemplify the hydration evolution and the differences among specimens with different VMA content. According with Singh et al, 2003 [191], the band corresponding to the presence of $\text{Ca}(\text{OH})_2$ is found at 3645cm^{-1} and from 1635 to 3445cm^{-1} are bands due to the presence of calcium sulphate in the form of ettringite. Observing the figures corresponding to the first 1, 2 and 3 days of hydration, the presence of especially the bands corresponding to ettringite are very important.

As demonstrated with the calorimetry tests, the employment of VMA delays hydration of Portland cement. Therefore, especially the presence of these bands closely explains hydration evolution. 3M samples show higher transmittance bands, until the 3rd day of hydration. Moreover, from the 7th hydration day 10M samples took over, as the reactions for those samples were significantly delayed, like reported with the calorimetry results. The FTIR results followed the same trend observed in TGA and calorimetry test results.

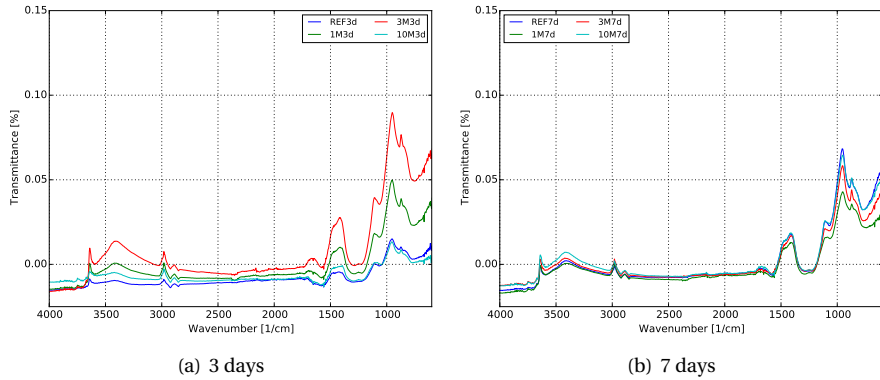


Figure 5.7: FTIR results

5

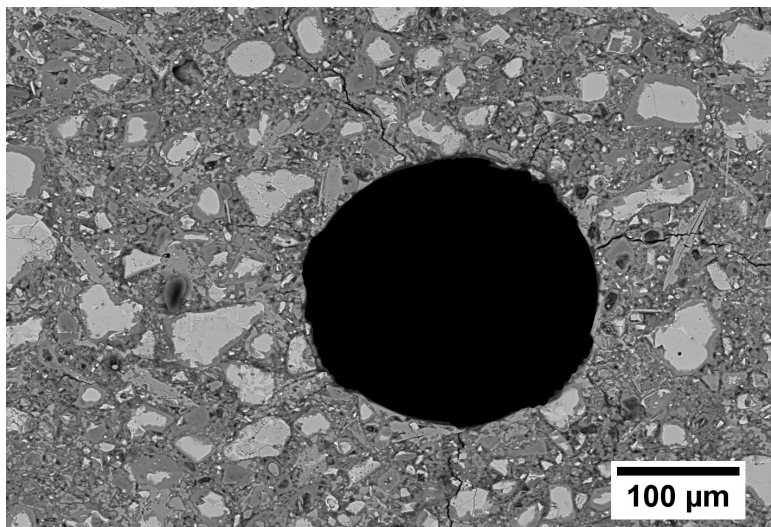
5.3.5. QUALITATIVE AND QUANTITATIVE IMAGE ANALYSIS

The microstructure of 29 days-old samples was observed under scanning electron microscope and are exemplified on Figures 5.8(a), 5.9(a), 5.10(a) and 5.11(a). One of the first differences noticed was the number of voids in samples where the chemical admixture was used. This might be caused due to the high viscosity achieved while mixing the paste, which facilitated air entrapment.

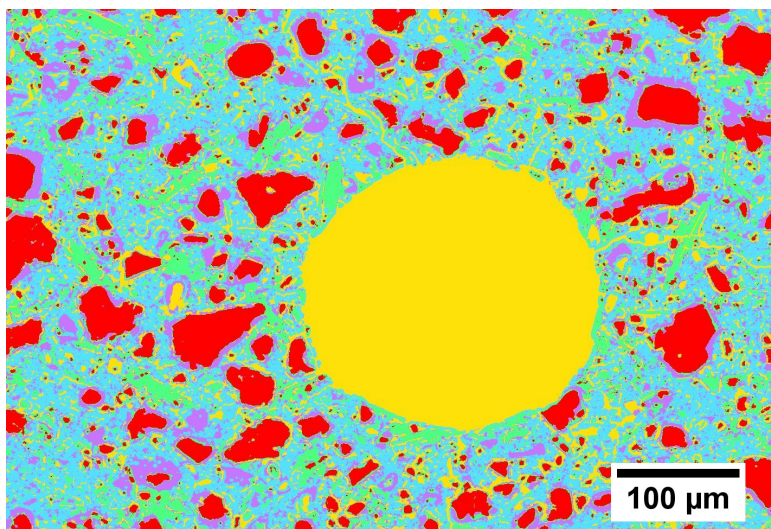
Besides that, around the voids found on samples with VMA a higher capillary porosity region is always found, leading to the conclusion that these are less dense than the bulk paste. This means that the voids found on these samples were perhaps filled or at least highly concentrated with water. This is an important result that is connected to the fact that the HPMC molecules can “arrest” part of the mixing water through its -OH ramifications. As the hydration further progresses, the water molecules are released which contributes for the curing of the surrounding area.

Some examples from the image analysis performed on the SEM micrograph are shown in Figures 5.8(b), 5.9(b), 5.10(b) and 5.11(b) and a summary of results obtained are shown on Figure 5.12. They confirm an increasingly larger volume of voids found in specimens with VMA, as well as the decreasing total area of unhydrated OPC grains. However, the large standard deviation found for the void content makes clear the need of another technique to quantify this phase. In agreement with the results found on TGA and the accelerated carbonation hypothesis, large amount of calcium hydroxide was measured by image analysis. Results found with this technique were in agreement with an enhancement on Portland cement hydration whenever VMA is employed.

Another noteworthy observation was the location where portlandite clusters were found. Usually, $\text{Ca}(\text{OH})_2$ grows disperse in the paste and eventually inside the void or pore walls. However, voids in VMA samples were progressively filled with portlandite, from 0.1 to 1 wt.% of VMA. It is important to notice, as mentioned in the introduction, that other research have already reported formation of portlandite with different morphology in cement pastes with VMA [169]. In order to illustrate this phenomena thin section photomicrograph, with $2.5\times$ magnification, are shown on Figures 5.13, 5.14, 5.15

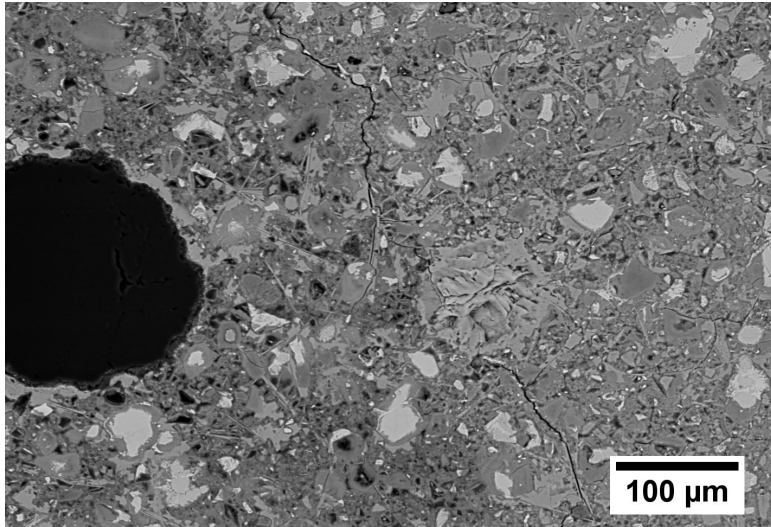


(a) REF

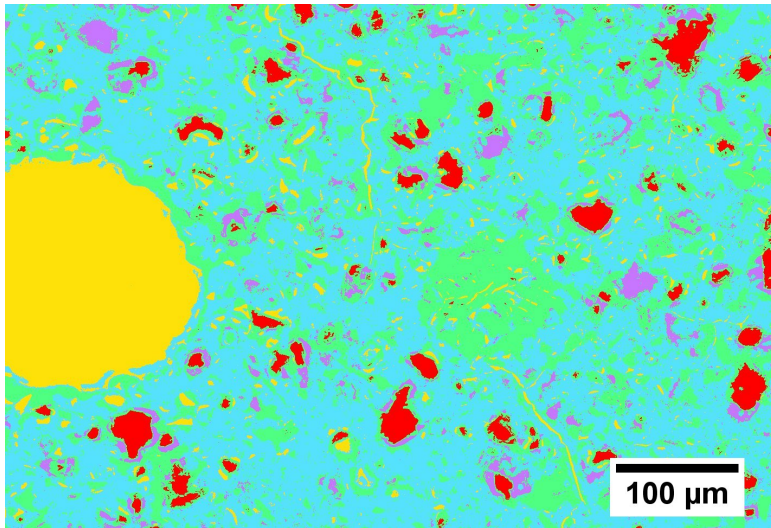


(b) REF + Weka segmentation

Figure 5.8: SEM picture from REF sample with 29 days of curing and the result from the image analysis

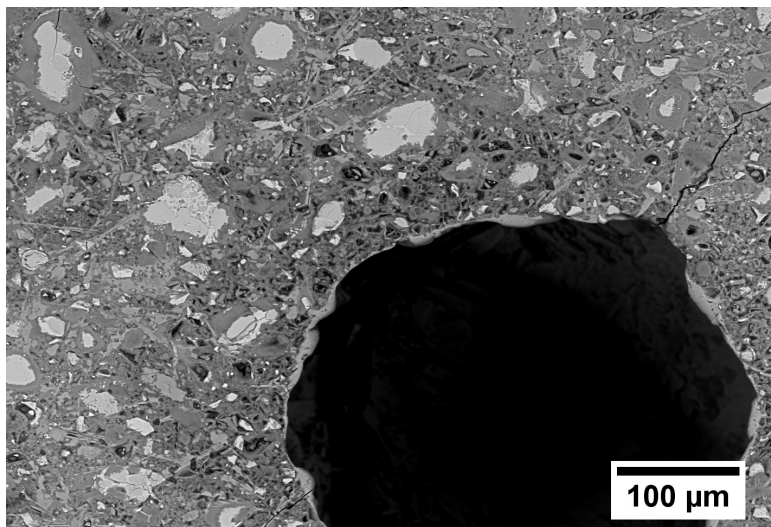


(a) 1M

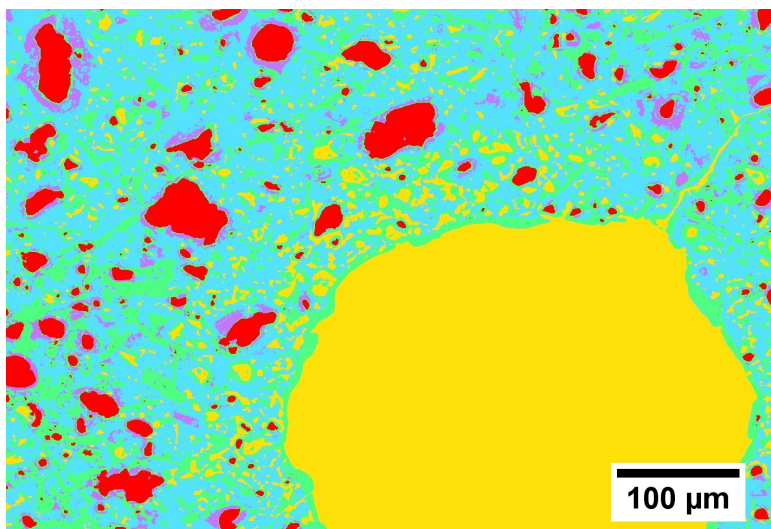


(b) 1M + Weka segmentation

Figure 5.9: SEM picture from 1M sample with 29 days of curing and the result from the image analysis

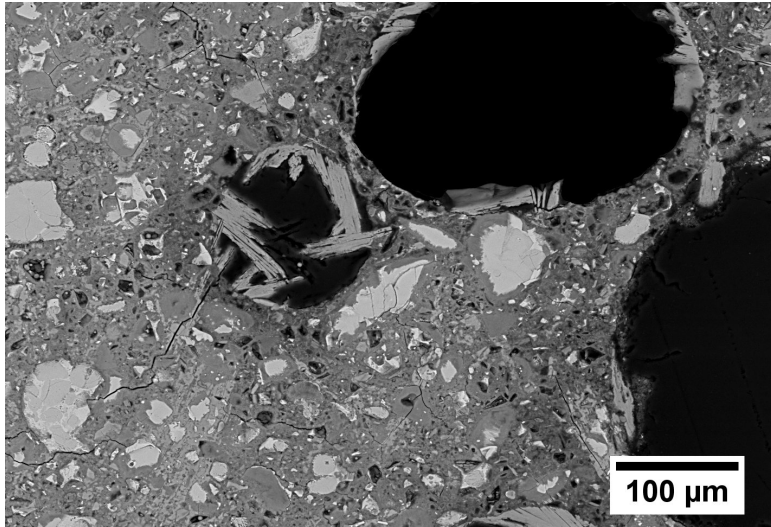


(a) 3M

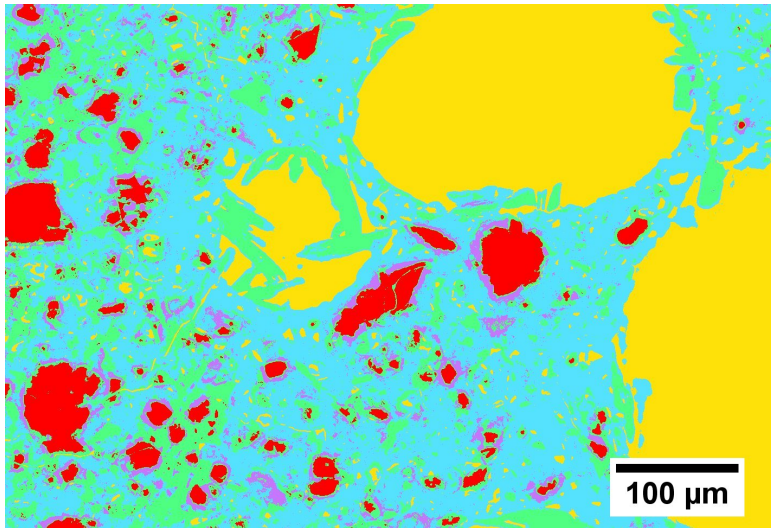


(b) 3M + Weka segmentation

Figure 5.10: SEM picture from 3M sample with 29 days of curing and the result from the image analysis



(a) 10M



(b) 10M + Weka segmentation

Figure 5.11: SEM picture from 10M sample with 29 days of curing and the result from the image analysis

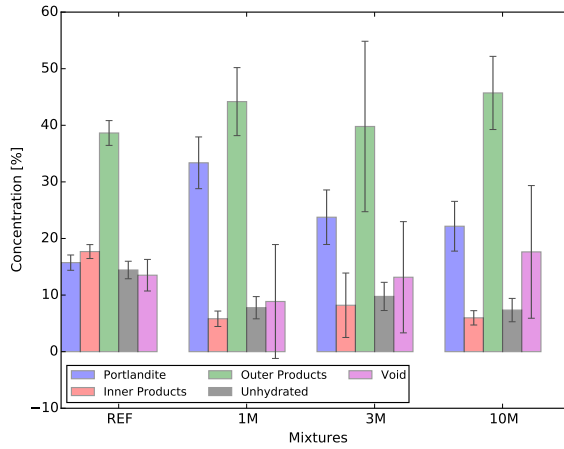


Figure 5.12: Summary of the results from image analysis obtained from SEM images

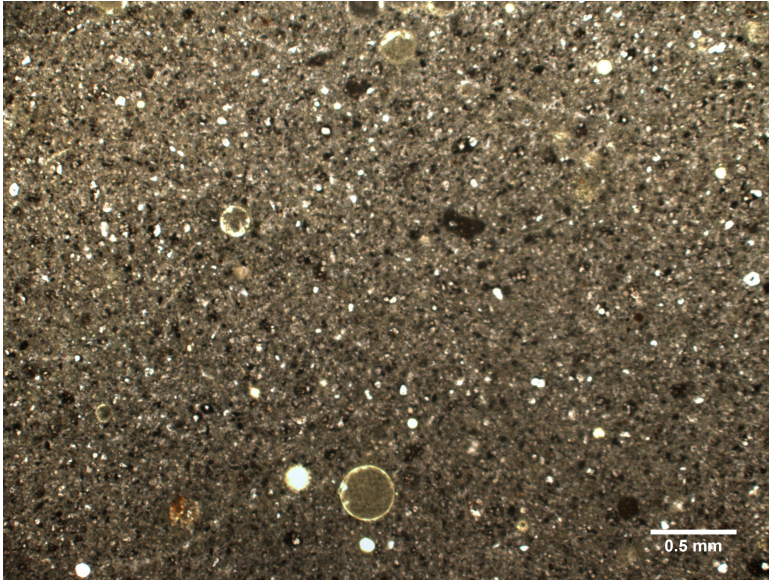
and 5.16. Remarkably, voids from 10M samples were almost completely filled with portlandite, such as the ones showed in Figure 5.17, with 20× magnification.

Employing images obtained from CT-scan the average void area and the average void diameter of the image stack from the studied paste are shown on Figure 5.18. In order to avoid the influence of measurement noise, only voids larger than 5 pixels were taken into account during the measurements. Results obtained from this experiment demonstrate that not only the porosity increases with the employment of VMA but also the average size of these voids. Those results contribute to the explanation for the lower compressive strength obtained for mixture where the VMA is employed.

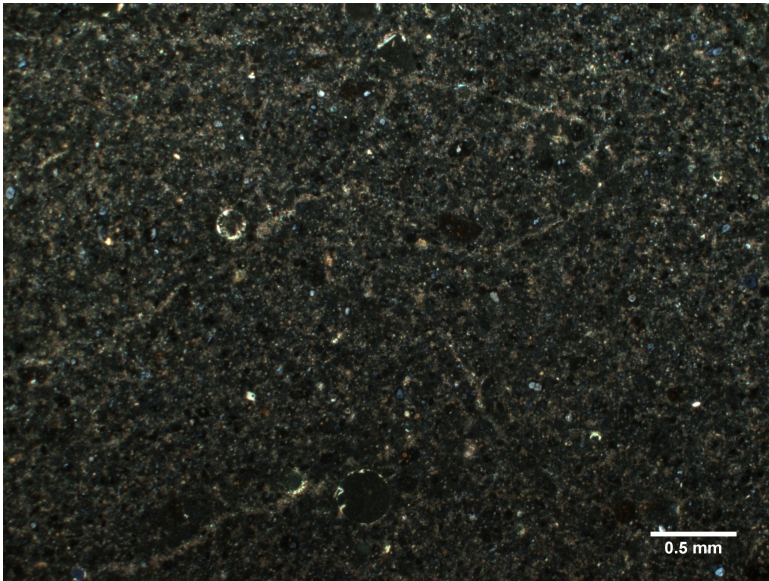
5.3.6. RHEOLOGY PROPERTIES

The rheology parameters measured on the cement paste with HPMC can be found in Table 5.3 and 5.4. Using VMA did not seem to lead to a direct increase on the initial bulk yield stress (σ_0) but had an immediate effect on the initial shear yield stress (τ_0). This influence is more evident when the ratio between σ_0 and τ_0 is taken in account. This result together with the pictures (Figure 5.19) emphasize the importance of VMA to achieve the needed rheology for 3D printing purposes. As the Benbow-Bridgwater equation with six parameters analysis was used to characterize the rheology parameters, the bulk dynamic stress (αV^m) and the shear dynamic stress (βV^n), for a given extrusion speed (which for this case was adopted 18mm/s). Using the same parameters the extrusion pressure for each paste can be predicted, as shown on Table 5.4.

Using the same approach employed in [60] one can estimate that from all studied pastes, only 1M, 3M and 10M would be able to be printed. An extra conclusion could be drafted from the rheological experiments. Consider a printing layer with a rectangular cross section with 40 mm width and 10 mm height. Moreover, supposing a maximum theoretical density of 2100 kg/m³ for the studied mixtures each printed layer will produce a hydrostatic pressure of approximately 2 kPa. Therefore, among all studied mix-

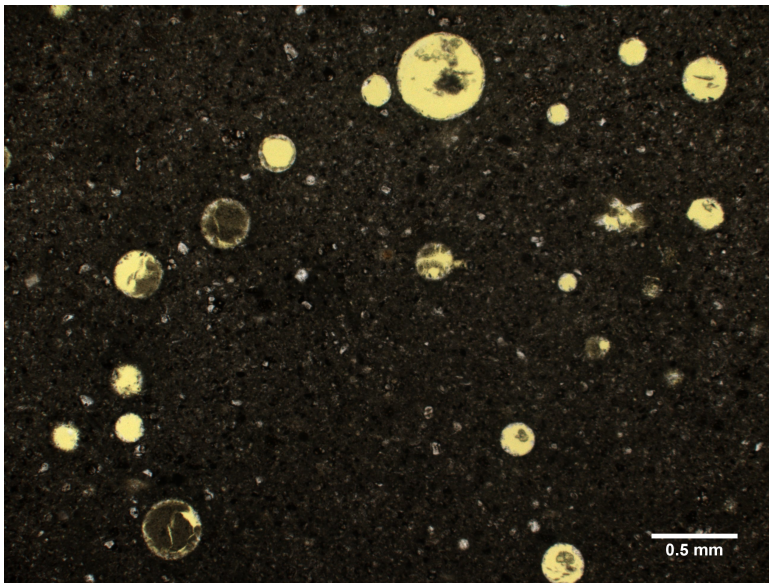


(a) REF sample in PPL

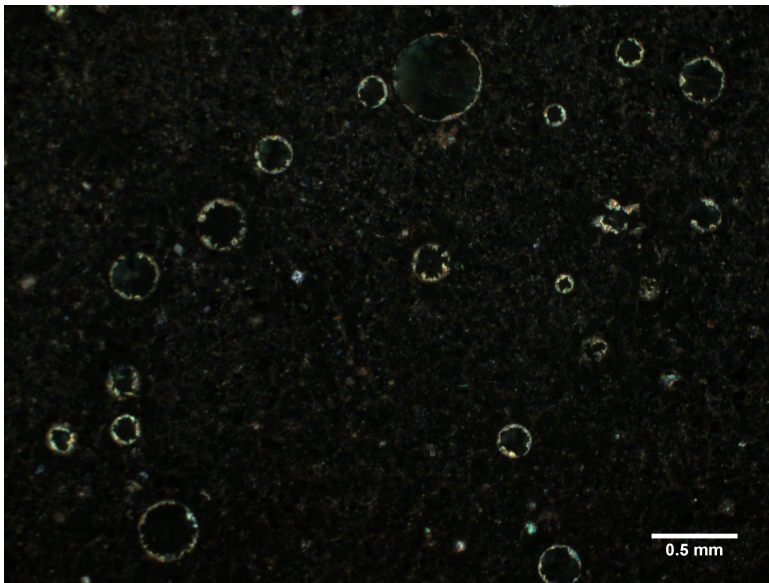


(b) REF sample in CPL

Figure 5.13: Thin section images from REF samples

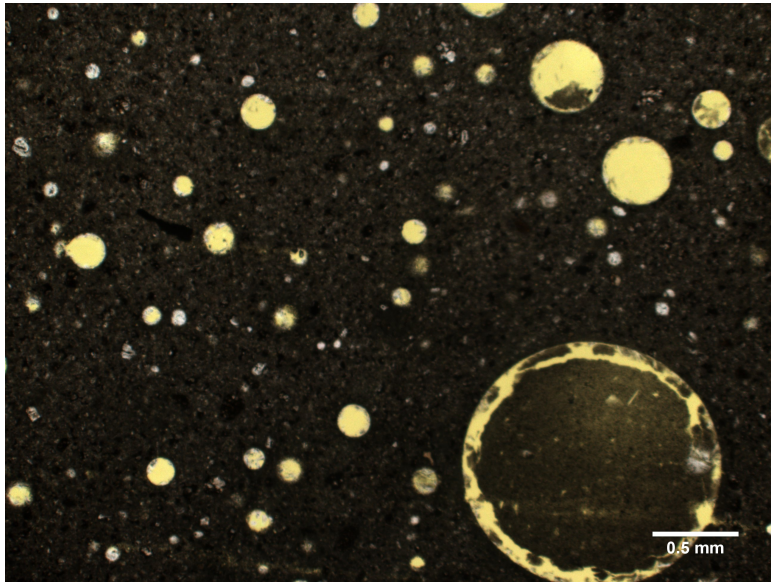


(a) 1M sample in PPL

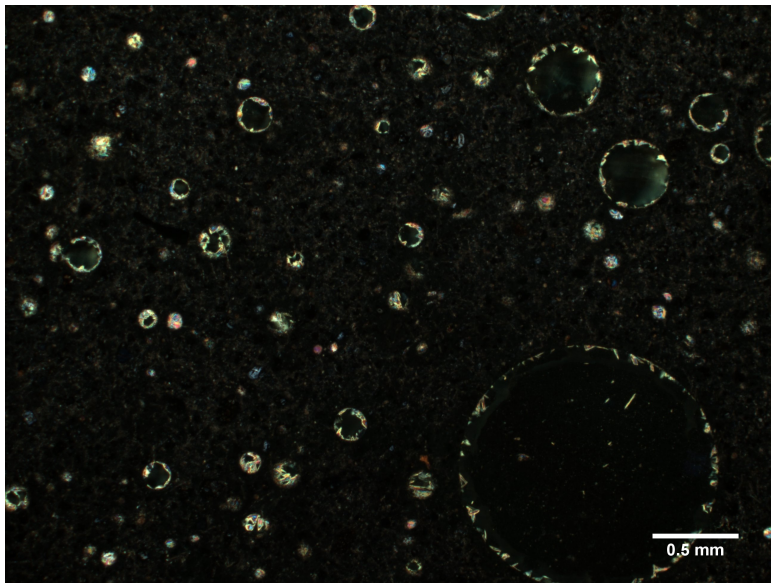


(b) 1M sample in CPL

Figure 5.14: Thin section images from 1M samples

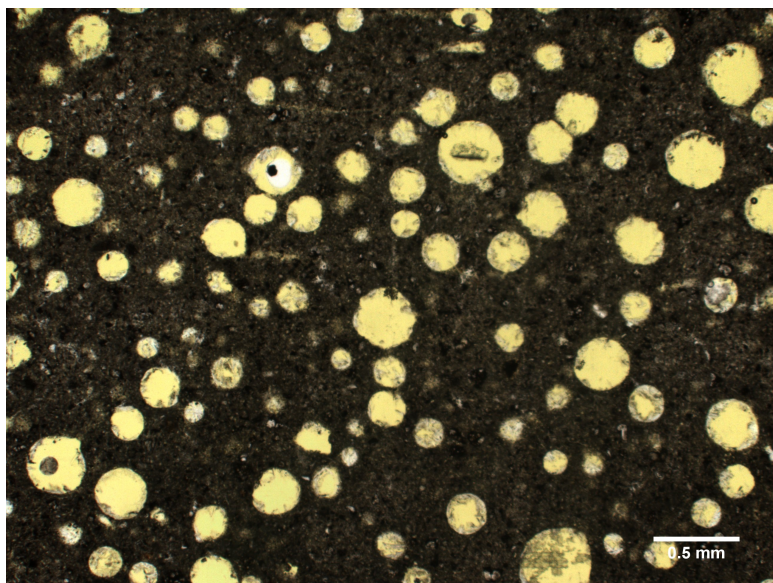


(a) 3M sample in PPL

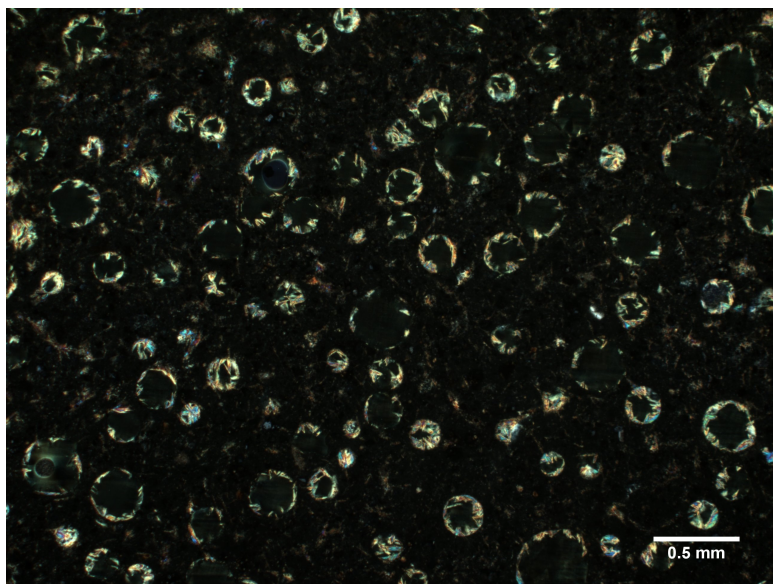


(b) 3M sample in CPL

Figure 5.15: Thin section images from 3M samples

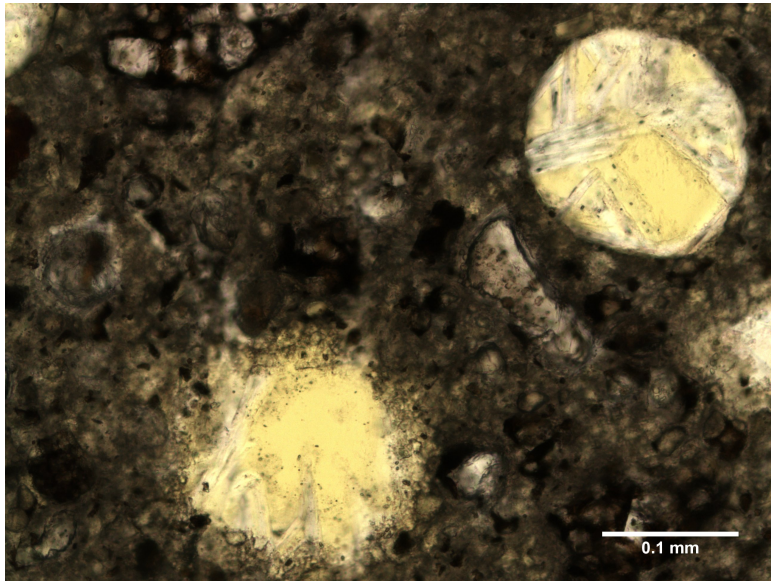


(a) 10M sample in PPL

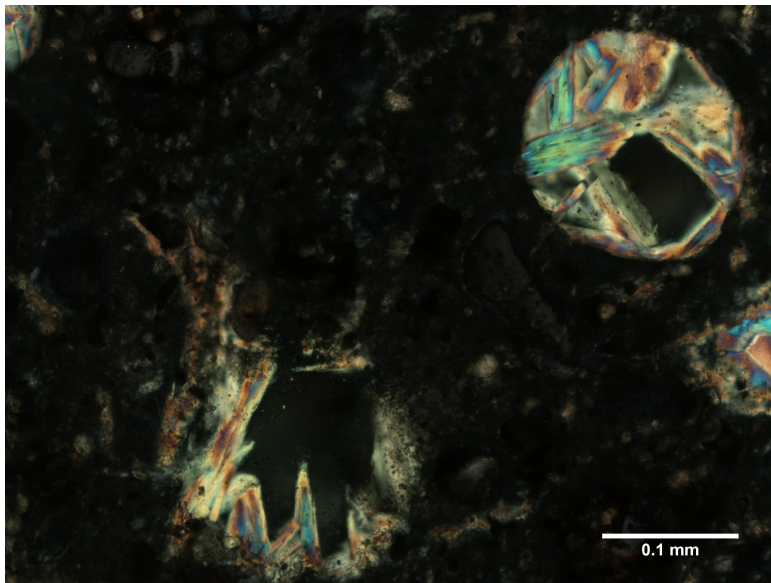


(b) 10M sample in CPL

Figure 5.16: Thin section images from 10M samples



(a) 10M sample in PPL 20×



(b) 10M sample in CPL

Figure 5.17: Thin section images from 10M samples with 20× magnification

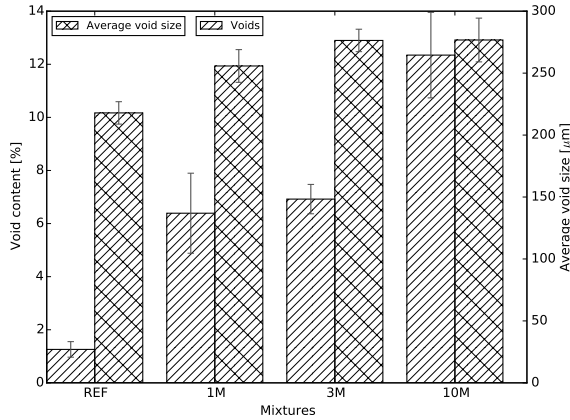


Figure 5.18: Void content and average void diameter assessed by micro CT-scan

Table 5.3: Summary of measured rheology parameters (First part)

Specimens	α [Kpa.s/mm]	β [Kpa.s/mm]	σ_0 [KPa]	τ_0 [KPa]
REF	1.631 ± 0.095	0.111 ± 0.001	16.313 ± 0.9637	0.200 ± 0.071
1M	1.282 ± 0.108	0.160 ± 0.006	12.841 ± 1.086	0.636 ± 0.059
3M	1.302 ± 0.116	0.181 ± 0.011	13.016 ± 1.170	0.828 ± 0.104
10M	2.268 ± 0.255	0.474 ± 0.023	22.673 ± 2.545	2.372 ± 0.115

tures only 1M, 3M and 10M would be considered printable and would be able to support approximately a maximum of 6, 6 and 11 layers, respectively.

5.3.7. MECHANICAL PROPERTIES

The overall compressive strength for 2, 3, 7 and 29 days of curing decreases significantly as the weight percentage of VMA increases, as shown on Figure 6.10. These results are aligned with the rise of the total volume and the average size of the air entrapped voids found on the samples. Therefore, any improvement on the OPC hydration provided by the internal curing when VMA is used cannot be quantified by means of mechanical performance at this scale. In order to investigate any improvement on the hydrated products a mechanical performance characterization at a smaller scale must be made. This investigation was possible using the nanoindentation results.

In Figure 5.21(a) and 5.21(b) the Young's modulus frequency distribution and the frequency of some hydration products are given. It is known that the VMA percentage has a direct influence on the formation of hydration products, as it was already shown in the previous sections. For all samples with VMA the frequency appearances of indents on unhydrated particles was smaller than the reference sample. This result reinforces the argument that the VMA contributes to the hydration of cement, by means of internal curing.

Table 5.4: Summary of measured rheology parameters (Second part)

Specimens	m	n	σ_0/τ_0	αV^m [KPa]	βV^n [KPa]	Pressure for V=18mm/s and L/D=8 [KPa]
REF	0.42 ± 0.019	0.145 ± 0.031	81.46	5.49	0.17	59.72
1M	0.349 ± 0.023	0.338 ± 0.026	20.19	3.52	0.42	69.87
3M	0.353 ± 0.025	0.423 ± 0.047	15.73	3.61	0.61	82.69
10M	0.54 ± 0.043	0.672 ± 0.014	9.56	10.81	3.31	255.36

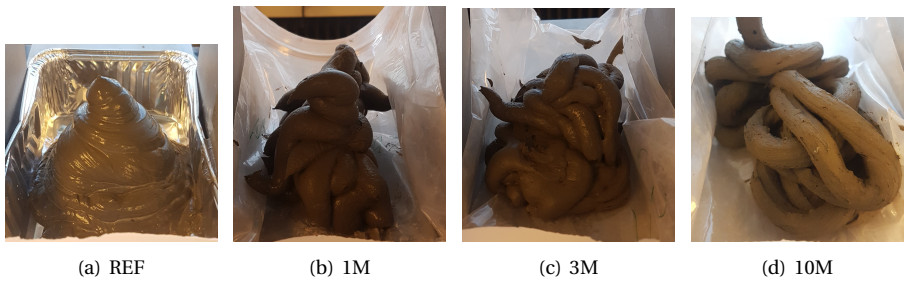


Figure 5.19: Visual difference on the shape stability of Portland cement paste with different VMA content after test in the ram extruder.

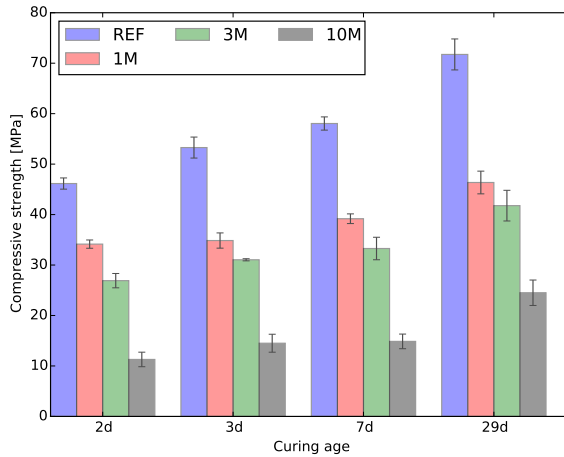
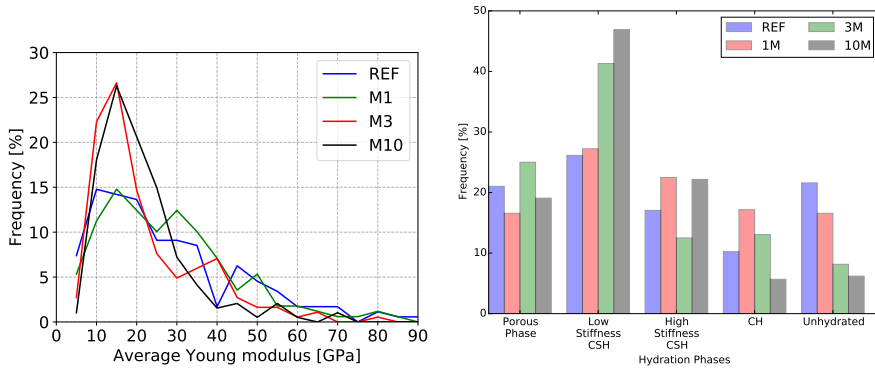


Figure 5.20: Compressive strength development



(a) Frequency distribution of Young modulus assessed by nanoindentation (b) Frequency of some OPC hydration products

Figure 5.21: Nanoindentation results

Furthermore, the frequency of indents on portlandite was smaller than the reference for 3M and 10M samples. An immediately conclusion could be drafted saying that there is a smaller concentration of this mineral for these samples. However, observing the results found on the image analyses of SEM pictures and on the thin section images this conclusion would be disrupted. Therefore, all the results found here on this study lead the authors to confirm that the portlandite precipitation on samples with high content of VMA has an abnormal behaviour. The $\text{Ca}(\text{OH})_2$ distribution on samples with VMA is very different than an ordinary cement paste. In 3M and 10M samples the portlandite crystals precipitates more often on the air void inner walls and not spread on the bulk of the cement paste. This abnormal precipitation of portlandite might be specifically related with the different viscosity that samples with VMA show, and quantified by the σ_0/τ_0 ratio on Table 5.4. In addition, this might lead to an increased Ca^{+2} leaching from the pore solution towards the entrapped air voids. This type of behaviour is not shown in concrete with air entrainment admixtures as the viscosity of the liquid phase (excluding the air voids) of this type of material does not change, for example.

5.4. CONCLUSIONS

The results obtained during this study were important for understanding the influence of using VMA on cementitious materials. A wide range of industries make use of this chemical admixture, such as those that extrude fibre reinforced cementitious composites and nowadays additive manufacturing based on extrusion. Summarizing the main conclusions are:

- Rheological properties of cementitious materials using VMA are significantly different than the ordinary ones. The employment of the admixture brings shape stability and guarantee higher initial bulk yield stresses which is essential for extrusion based 3d printing;

- VMA concentration is of high importance on OPC hydration. Even small concentrations of the admixture lead to retardation of the initial hydration. 1 wt.% already leads to a large latent time of the Portland cement;
- It is likely that the rheology modifier admixture “arrests” the available water with hydrogen bonds. The admixture only loses its preference for the water when the pH of the solution increases, making stronger connections with other ions;
- As demonstrated with the degree of hydration and the total heat released VMA can also be employed for internal curing purposes;
- Under electron microscope, it was possible to observe that entrapped air voids formed during mixing works also as water reservoir. As soon as the pH of the paste rises, the water released from VMA develops a region around these voids with a higher water/cement ratio, in comparison with the rest of the matrix;
- To modify the rheology parameters of solid suspensions, the grain size distribution or the employment of viscosity modifier admixtures are usually employed. However, the results found in this research suggest that VMA loses its preference for H₂O molecules when enough OH⁻ ions are available in solution. Therefore, solid suspensions which have high pH from the beginning of the mixing, such as alkali activated materials, will be challenged to decrease the solution's pH or provide a well distributed particles grain size.
- The employment of VMA changes the portlandite growing mechanism on Portland cement pastes. Samples with VMA show an abnormal preferential grow of Ca(OH)₂ crystals on the internal walls of the entrapped air voids, most probably suggesting that these samples are more exposed to Ca⁺² leaching from the pore solution to the entrapped air voids.

6

AUTOGENOUS SELF-HEALING OF CEMENTITIOUS MATERIALS: THE INFLUENCE OF RHEOLOGY MODIFIERS AND CELLULOSE PULP

It is not the inner self that has to be made to conform to society's rules, but society itself that needs to change.

Francis Fukuyama, Identity: The demand for dignity and the politics of resentment.

Additive manufacturing of cementitious materials is a technique which is drawing a lot of attention in the past few years. Many investigations have already demonstrated the high automation potential that this technique might bring to the construction industry. Along with the development of the technique, methodologies to create materials which can be used for this purpose have also received some attention. The development of this new generation of materials opens the opportunity to embed recent advances on the field of construction, such as those with enhanced self-healing capabilities. Therefore, this study investigated the influence of the use of rheology modifier admixtures and the use of natural fibres to enhance the autogenous self-healing capabilities of printable cementitious composites. Two levels of reinforcement were employed: 0.5 and 1% by total composite's volume. The influence of fibre pre-treatment (5 and 10 hornification cycles) was studied. In addition, to enrich the evaluation of the cellulose pulp performance for self-healing purposes the durability of these composites was also assessed. Samples were exposed to 10 and 20 accelerated ageing cycles (wetting and drying). The autogenous self-healing performance of all composites were assessed through water permeability, μ CT-scans and microscopy tests. Correlations between water permeability results and the volume of autogenous healing obtained using CT-scans were discussed in this investigation for a better understanding of the phenomenon.

6.1. INTRODUCTION

THE development of printable cementitious mixtures is very much dependent on the control of rheological parameters [78, 116]. In order to obtain such control, especially in fibre reinforced cementitious composites, the use of chemical admixtures such as the hydroxypropyl methylcellulose (HPMC) is needed [60, 192, 193]. Although the use of HPMC results in undesired air entrainment and subsequent consequences, there is one additional potential of this admixture to confer self-healing capabilities to the composite. During microstructure analysis of this material [160] it was proven that an anomalous growth of portlandite was obtained, which can be useful for enhancing self-healing performance of printable cementitious composites.

Furthermore, another challenge in the development of 3D printing mixtures is drying shrinkage [158]. The printed elements are usually fabricated in areas where the temperature and relative humidity are not controlled or even its control is not realistic. Additionally, it is intrinsic by the method that one printed layer will need to wait exposed to the surrounding environment while the printing of the second layer does not start. This means that these mixtures might be exposed to prolonged drying periods and the risks of cracks are higher.

Such improvement in self-healing capacity is very much needed in 3D concrete printing because the conditions in which such fabrication occurs might result in drying shrinkage and therefore early age cracking. Moreover, cracking of cementitious materials usually expose the structure to harmful chemicals. This extra exposure might decrease the service life due to accelerated degradation process such as chloride migration causing reinforcement corrosion (in case of steel reinforcement), carbonation and leakage.

6

6.2. THEORETICAL BACKGROUND

6.2.1. AUTOGENEOUS SELF-HEALING

Autogenous self-healing is an inherent ability of cementitious materials either due to the presence of hydrated or un-hydrated clinker. Several parameters control the efficiency or even the possibility of such event to happen. There are crucial ingredients that contribute to this phenomenon, such as: high availability of calcium ions, moisture, carbon dioxide, unhydrated cement particles or even the presence of pozzolanic materials. Without these ingredients the closure of open cracks in cementitious composites is not likely.

Further hydration of unreacted cement grains and pozzolanic reactions have been reported to be dominant self-healing mechanisms in young concrete, especially with low water-to-cement ratios. This has been previously reported in investigations on ultra high performance concretes [194, 195] or fibre reinforced cementitious composites [196, 197]. In the case of the fibre reinforced materials, especially strain hardening cementitious composites (SHCC) (or also called engineered cementitious composites (ECC)), have demonstrated enhanced self-healing behaviour. A number of studies have concluded that high amount of binders combined with the volume of fibres used in this kind of composite and the formation of narrow and closely spaced cracks to enhance the healing performance [54, 198, 199]. Others have reported mechanical recovery of such materials due to its autogenous self-healing capabilities [200].

At later stages, when further hydration and pozzolanic reactions have been exhausted, precipitation of calcium carbonate becomes the dominant mechanism for autogenous self-healing [51, 201]. Three main components are needed for successful calcium carbonate precipitation, namely: availability of calcium source, carbon dioxide (in the form of carbonate ions ($\text{CO}_3^{-2}(\text{aq})$) or carbonic acid in solution) and moisture [51]. Additionally, narrow crack widths (of around $50 \mu\text{m}$) are also preferable in the case of autogenous healing.

Whereas calcium sources are readily available for dissolution in non-fully carbonated cementitious matrices and carbon dioxide is available in the environment, the moisture is an important ingredient that depends on the surrounding conditions.

The use of admixtures to potentially keep cementitious materials moist for longer periods of time has been an interesting research question in the past years. Some solutions were reported such as the use of light-weight aggregate [202, 203], nano-clay [199] and a range of different super absorbent polymers (SAP) [53, 204–206]. The use of SAP has been by far the most efficient solution to this issue. Since superabsorbent polymers swell upon absorption of significant amount of mixing water and release it back gradually while the matrix dries, a macropore is left behind upon shrinking. The presence of such system of macroeffects steers crack propagation. Therefore, in the event of a crack the surface of the polymeric particles will always be exposed to the external environment keeping the crack surrounds with a relatively high moisture content consequently, contributing to the autogenous self-healing performance of the composite.

In addition to their ability to internally cure concrete during early ages, SAP are also able to swell in the crack when moisture penetrates, producing a short-term sealing of the crack [207]. This property is very advantageous as the crack sealing might block the ingress of hazardous species inside the crack and/or limit the exposure of the steel reinforcement to the external environment [208, 209]. In an extensive modelling work validated through experiments the influence of SAPs in the moisture uptake of sound and cracked mortars was discussed [210]. This study have demonstrated the influence of the SAPs properties in the self-sealing efficiency and showed a comprehensive and alternative approach to improve the self-sealing performance. Finally, SAPs have also demonstrated their potential as internal water reservoirs which provide internal curing and mitigate autogenous shrinkage in cementitious materials [49].

Unfortunately, to the best of the author's knowledge, almost no studies in literature regarding long term durability of SAPs in cementitious composites. As a polymeric admixture the SAPs might be susceptible to different hazardous environment commonly found in the brittle matrix, such as the high alkalinity, ultra-violet rays or wet and drying cycles. The degradation of this admixture might influence on its self-healing and/or self-sealing performance.

6.2.2. THE USE OF NATURAL FIBRES

Natural fibres are commonly used in constructions from advanced composite manufacturing to materials for simple mud houses where the walls are manually cast with reinforced clay. Some researches report the use of these fibres by different civilizations independent to their technological development [211–213].

From the beginning of natural fibres use until nowadays, where the nano-fibres can

be extracted from wood, a lot of research was conducted in this field. The use of cellulose pulp fibres, extracted from hard or softwoods, became a very important source of reinforcement at industrial scale when asbestos price rose significantly during and after the second world war. These fibres were incorporated in the production of fibre-cement boards produced by an industrial process called Hatschek, for the first time in Australia. Since then, they became indispensable when the use of asbestos started to face limitations due to its carcinogenic effect [214].

Moreover, the use cellulose pulp in cementitious matrices faces challenges regarding its durability [215, 216]. Two main phenomena are responsible for the degradation of the cellulose pulp within cementitious matrices during the service life of the composite. One of the issues is related to the dimensional stability of these fibres. When exposed to moisture, cellulose pulp swells, increasing significantly its volume and shrink in absence of it. Consequently, within a given number of cycles the fibres are not able to return to their original volume damaging the bond with the cementitious matrix and hence effecting their reinforcing capacity [217–219]. The second cause of the reinforcement failure is attributed to the migration of cement hydration products to inside of the fibres along with crystallization of the reinforcement, causing its mineralization and consequently the loss of ductility of the fibre-cement boards [219–222]. To solve the issue two main actions drove the problem solving, namely: matrix modifications and fibre pre-treatment.

Regarding the matrix modifications the use of pozzollanic materials was proposed and has been proven efficient to minimize fibres mineralization. Several supplementary cementitious materials were investigated like blast furnace slag (BFS) [223], metakaolin [220], fly ash (FA) [224] and silica fume (SF) [225] to consume the calcium hydroxide and maximize composite's performance. Besides that, the opportunity to use locally available waste materials was also investigated and the use of rice husk ash (RHA) [226] and sugarcane bagasse ash (SCBA) [227] was explored.

Another method used to consume portlandite from the matrix of those composites is the use of autoclave curing. This curing technology uses of high temperatures and water vapour pressure to accelerate cement hydration and with the help of a silica source consume all the portlandite available in the matrix. The durability of these composites were assessed and researchers have also concluded that their quality could also meet the desired long-term performance [221].

The second strategy used to improve fibre-cement composites was the fibre pre-treatment. Some researches have suggested the use of chemical products to make natural fibres water tight. Chemical treatments with silane were also reported in literature achieving interesting results [228, 229]. However, the costs involving this kind of treatment made its use not practical. Another simpler treatment called hornification has drawn the attention of several researchers. This method consist of subjecting the fibres to several wet and drying cycles before their use in the composite. By performing these cycles the crystallinity of the fibres would be boosted, the intermolecular distance between the cellulose layers would decrease and a dimensionally more stable material would be obtained. This treatment has been proven successfully in a series of studies applied in different type of natural fibres, from cellulose pulp for fibre-cement boards [219] or even in sisal or jute fibres for production of SHCCs [230].

Table 6.1: Mix design summary in $[kg/m^3]$

	XVA0	XVA3	XVA10	REF	10M	XVA3C05	XVA3C10
CEM I 42,5 N	265.6	264.5	261.9	1619.5	1599	263.2	261.9
Blast Furnace Slag	619.8	617.2	611.2	0	0	614.1	611
Limestone powder	885.4	881.7	873.2	0	0	877.3	872.9
HPMC	0	5.2	17.5	0	16	5.2	5.2
Superplasticizer (Glenium 51)	17.7	17.6	17.5	0	0	17.5	17.5
Water	354.2	352.7	349.3	485.9	479.7	350.9	349.2
Cellulose pulp	0	0	0	0	0	7.5	15

6.3. EXPERIMENTAL METHODS

6.3.1. MATERIALS AND SAMPLE PREPARATION

To investigate the influence of natural fibres in printable mixtures a previously developed cementitious matrix was used. This mixture is composed by Portland cement CEM I 42,5 N, blast furnace slag, limestone powder and was proposed in a study where rheological tests were used to develop printable cementitious composites [60]. The chosen mix-design for the current investigation was used in chapter 3 as a matrix of the printed strain hardening cementitious composite and presented bulk and shear yield strength of (13.06 ± 4.18) kPa and (3.44 ± 0.06) kPa respectively. These two fresh state parameters are crucial to characterize a printable cementitious composite. Assuming a density of 1500 kg/m^3 for the natural fibres, two levels were used 0.5 and 1% by total volume. Moreover, the use of hydroxypropyl methylcellulose (HPMC) and superplasticizer (SP) are needed to achieve the required rheological requirements for printing through extrusion. Table 6.1 summarizes the composition of all tested mixtures. Chemical and physical characterization of the raw materials can be found in table 3.1 and figure 3.1.

One of the most crucial parameters for an effective dispersion of the cellulose pulp in the composite is the fibre preconditioning. To ensure that the fibres could disperse homogeneously through the mixture, they were first mixed with high volumes of water and latter drained with the help of a vacuum pump and a cloth filter. At this stage the fibres were wet but would only release the water left inside of them if pressure is applied. Using the fibres at this stage also guaranteed that they would not absorb the mixing water but also not release its absorbed water during mixing. This characteristic behaviour of working as a water reservoir was once reported along with the advantages of using such material for internal curing in cementitious components [186]. The total mass of dry fibres used was as given in table 6.1 however, the total wet fibres mass was different, following their moisture content given in table 6.3.

The mixing procedure for this type of composite was the same as previously reported in [60] and [160], with the addition of an extra step regarding the fibre dispersion. Therefore, in summary the mixing procedure was:

- All dry materials were mixed for two minutes at low speed (speed 1 - 60 rpm);
- The wet fibres together with the mixing water were mixed in a high shear mixer at 4000 rpm for 2 minutes. In the end the SP was added to the solution and homogenized with the help of a spoon;
- While mixing at speed 1, during approximately one minute, water mixed with SP and wet fibres were added;
- The wet powders were mixed for the next two minutes at speed 1. In this phase it was possible to observe a significant change in the mixture's viscosity. A dough like consistence was achieved;
- At moderate speed (speed 2 - 124 rpm), the dough like mixture was further mixed. At this phase the dough opens inside the mixing bowl, and the fibres get dispersed.

All mixed materials were cast in prismatic moulds ($40 \times 40 \times 160$) mm³ and kept sealed for the first 24 hours. After that they were demoulded and cured in a curing chamber at $(20 \pm 2)^\circ\text{C}$ and relative humidity of $(98 \pm 2)\%$.

6.3.2. FIBRE TREATMENT

In order to evaluate the influence of fibres' pre-treatment in the overall autogenous self-healing performance, three different scenarios were created. Composites with fibres not previously treated (0HC) and composites with fibres after 5 (5HC) and 10 (10HC) hornification cycles. The hornification cycles were performed and the fibre properties were assessed according to the recommendations of [231], where the authors successfully pre-treated natural fibres and obtained enhanced mechanical performance after the investigated composites were exposed to accelerated ageing cycles.

The hornification cycles consist of cycles of wetting and oven drying the fibres. In order to saturate the fibres, it is first necessary to disperse them in water. The mixing process was composed of two steps. In buckets of 10 litres containing 300 g of fibres, water was added until the total volume of material reached 50% of the bucket's working capacity. Afterwards, with the help of a mixer the first mixing is executed at 300 rotations per minute (rpm) for 2 minutes. Right after the first mixing time is finished the bucket must be filled with water until its maximum working volume and the second mixing step starts at 650 rpm for another 10 minutes. As soon as the mixing is finished the buckets must be closed and fibres are left soaked in water for 3 hours. After the saturation time, the solution of fibres and water is drained with the help of a cotton cloth filter and a dead weight of 30 kg for 30 minutes. In the end the wet fibres are dried in an ventilated oven at 80°C for 16 hours.

To assess the fibre conditions before and after the hornification cycles some of the suggested tests in [231] were performed, namely:

- X-ray diffraction (XRD) with a scanning rate of $2^\circ/\text{s}$, from 2θ equal to 5° to 70° . The results from this tests are valuable to calculate the relative crystallinity degree following the recommendations of [231, 232]. This crystallinity value is obtained by dividing the peak area by the total area under the XRD pattern obtained from the test (equation 6.1);

$$RelativeCrystallinity[\%] = 100 \times \frac{Area_{peak}}{Area_{total}} \quad (6.1)$$

- Thermogravimetric analysis (TGA) with a heating rate of 10 K/minute and a purge of 50 ml/minute of argon gas to ensure an inert atmosphere was performed in oven dried fibres (105°C). This test was used to quantify the total mass loss from 200 to 1000°C which, according to [231], is related to the chemical stability of the cellulose in the fibres;
- Fourier transform infra-red spectroscopy (FTIR) was also performed in the fibres to measure the total energy needed to break the hydrogen bonds based on their resonance values. The test was performed measuring bands from 550 to 4000 cm^{-1} ;
- The total moisture absorption of the fibres was measured according to the following procedure:
 - Fibres were dispersed in large volume of water using a high shear mixer at 4000 rpm for 60 seconds;
 - This solution was drained under vacuum, using a cloth filter until the fibres could not release the water arrested internally. At this stage the mass (M_{wet}) of the fibres is determined;
 - The wet fibres were then dried in the oven at 105°C for 24 hours and the moisture content was calculated according to equation 6.2, where M_{wet} is the fibre mass in wet stage and M_{dry} is the dried fibre mass.

$$M[\%] = 100 \times \frac{M_{wet} - M_{dry}}{M_{wet}} \quad (6.2)$$

6.3.3. ISOTHERMAL CALORIMETRY ANALYSIS

The total energy in form of heat released during the first 208 hours of cement hydration was measured with the assistance of a TAM Air Isothermal Calorimeter with eight channels, at 20°C and using as reference ampoules with sand. The samples used for this test were mixed outside of the calorimeter. Therefore, the initial peak of heat released corresponded to the exothermic dissolution of the grains and formation of first AFt phases were not present in these results.

6.3.4. ACCELERATED AGEING CYCLES

As previously discussed, the natural fibres are susceptible to degradation in the cementitious matrix. As proposed by several authors one of the most deleterious degradation mechanism is the exposure of composites reinforced with natural fibres to wet and dry cycles. The present study proposed to investigate the influence of aged composites in the self-healing performance of such materials. In order to achieve that, once more three scenarios were built, namely: specimens not degraded (0DC) and specimens exposed to 10 (10DC) and 20 (20DC) wet and dry cycles.

Prismatic samples of (40 × 40 × 160) mm and cylinders of 11 mm height and diameter were used during the ageing cycles. Following the recommendations from [231] the wet and dry cycles were composed by a period when the specimens were soaked in water at 20°C for 3 hours, followed by a period of drying at 60°C for 17 hours. Prismatic samples were used to quantify the influence of the accelerated ageing cycles in the mechanical performance of the composites. Three-point bending and compression test were performed on those samples at a loading rate of 0.5 and 2 kN/s, respectively. These results can also be useful to discuss the influence of the natural fibres in the overall mechanical performance of non aged composites.

6.3.5. SELF-HEALING CYCLES

The self-healing cycles were performed only on the cylindrical specimens and following the recommendations from [233]. In that study the influence of SAPs was investigated in mortar samples. As the proposed mechanism of the SAPs and the water reservoir behaviour of natural fibres are the same, the same method to accelerate the autogenous self-healing was proposed.

Like the accelerating ageing cycles, the accelerated self-healing cycles were composed of wetting and drying cycles, as well. However, the self-healing cycles were performed at laboratory temperature and relative humidity for a period of one hour and drying at lab conditions for the rest of the day (23 hours). Self-healing was measured by assessing the specimens before and after 20 accelerated self-healing cycles.

6.3.6. SELF-HEALING PERFORMANCE ASSESSMENT

X-RAY MICRO COMPUTED TOMOGRAPHY (μ CT)

To assess the self-healing performance of the investigated materials, cylindrical cores of 11 mm diameter and equal height were drilled from (40 × 40 × 160) mm beams. These cylinders were cracked along the diameter by means of a Brazilian splitting test. To ensure that both parts of the splitted cylinder were kept together a PVC tape was used around the specimen.

To measure the filling of crack area inside of the specimens a X-ray micro computed tomography (μ CT) was used. The equipment employed was a Phoenix nanotom m provided by GE. The accelerating voltage (in kV) and current (in mA) of 90, 100 and 90, 90 were used in all samples, making sure that the same parameters were used before and after the self-healing cycles. Every projection was obtained from an average of two radiographies collected after 500 μ s of exposure for each picture. In total 720 projections were obtained per specimen, corresponding to one every 0.5° of rotation. In total each specimen's μ CT-scan test took 19 minutes. The acquired projections were reconstructed as a three dimensional volume with the help of software phoenix datos|x provided by the machine manufacturer with an automatic centre adjustment and a beam hardening correction of 8.7. A 6.25 μ m/pixel resolution was obtained for matrix samples and 6.75 μ m/pixel for samples with natural fibres. This difference was caused by small variations in the height of some of the cylindrical specimens that had fibres. Unfortunately, this problem was exclusively related to an error during sawing of some of the cylinders during the sample preparation.

Moreover, top view images were obtained from the volume and a median filter, with

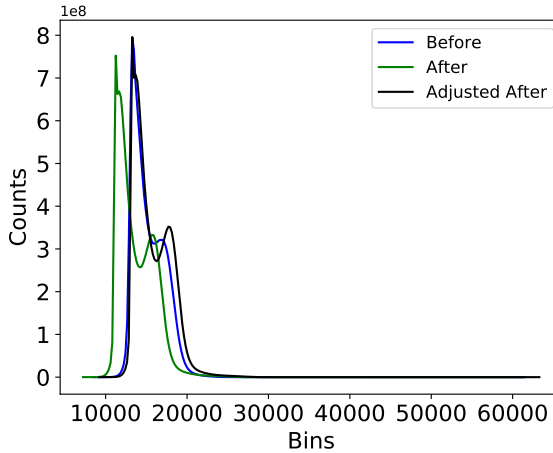


Figure 6.1: Histogram adjustment for image registration.

a 3 pixel diameter was applied with the help of the software VGstudio. The applied filter minimizes the noise traded off to minimize the total scanning time during the measurements.

To ensure reliable comparison when the self-healing performance is assessed, the image stacks must correspond to the exact same specimen's proportion. This can be achieved by registering the image stacks obtained before and after the accelerated self-healing cycles. In order to carry out a successful registration, two steps were adopted. The first step consisted in adjusting the histograms of the before and after self-healing scans by aligning the main histogram peaks. Figure 6.1 exemplifies the histogram correction of the images after healing using before healing images as a reference. As the electron accelerating voltage and current in the X-ray source were kept the same before and after the self-healing cycles, very small differences were obtained in the count of pixels obtained (Y-axis in the histogram) for the main peak. This image treatment was done by using FIJI [157]. The second step was done with the help of the software DataViewer from Bruker. This software produces a pseudo-3d registration of before and after-self-healing stacks through X,Y and Z displacements, as well as the rotations around such axes using the before healing volume as a reference. This alignment is done manually and automatically in all directions. The final result of the second step are two image stacks representing the top view of the sample before and after self-healing cycles positioned in the exact same origin. From now on the images can be compared and self-healing might be spotted by direct comparison.

In order to compare the efficiency of the self-healing cycles 1400 slices were separated from both volumes (before and after). This strategy is needed to avoid slices very close to the specimen edge (bottom and top), where the partial volume effect is observed. This effect is a result of the reconstruction problems generated by the sharp edge of the extremities of the sample and the differences in the results obtained for the X-ray beam passing through a high and low density materials (cementitious material and air).

To evaluate the total healing capacity of the selected volumes, the images were post-processed with the help of FIJI [157]. The method consists of cropping the image stack leaving only the region surrounding the crack. Using an appropriate threshold value separating the dark pixels from the air (voids and crack) and the lighter pixels from the matrix a binary image is created. Implementing a circularity filter only the crack area is measured before and after the healing process. The average crack area is assessed through the specimen height for every 350 images (approximately 2.36 mm for fibre reinforced samples and 2.19 mm for matrix samples) meaning that the healing performance of each specimen can be declared in function of its height. Moreover, the self-healing performance was given by the equation 6.3.

$$SHPCT[\%] = 100 \times \frac{(A_{before} - A_{after})}{A_{before}} \quad (6.3)$$

Where:

- SHPCT: Self-healing performance calculated from the μ CT-scans images;
- A_{before} : Average crack area before the healing process;
- A_{after} : Average crack area after the healing process.

Additionally, the images obtained with the μ CT-scans was also used to assess the crack width of the samples. The first 10 images from each each stack were selected and a portion of the crack was cropped from the rest of the image. Employing the same image segmentation method previously described the crack width was calculated based on the measured crack area and the length. These values are important as the crack width was not controlled during the experiments.

WATER PERMEABILITY TEST

A second commonly used test to assess the healing performance of cracked specimens was also employed. The water permeability test consist of measuring the total volume of water that passes through a cracked sample before and after the self-healing period for a certain given time [234]. The total water-head used in this experiment was 1.1 m and the total volume of water that passed though the crack within 10 minutes was measured twice before and after the self-healing period. Therefore, the self-healing performance for each sample was calculated according to the equation 6.4

$$SHPWP[\%] = 100 \times \frac{(V_{before} - V_{after})}{V_{before}} \quad (6.4)$$

Where:

- SHPWP: Self-healing performance calculated from the water permeability test;
- V_{before} : Average water volume through the crack before the healing process;
- V_{after} : Average water volume through the crack after the healing process.

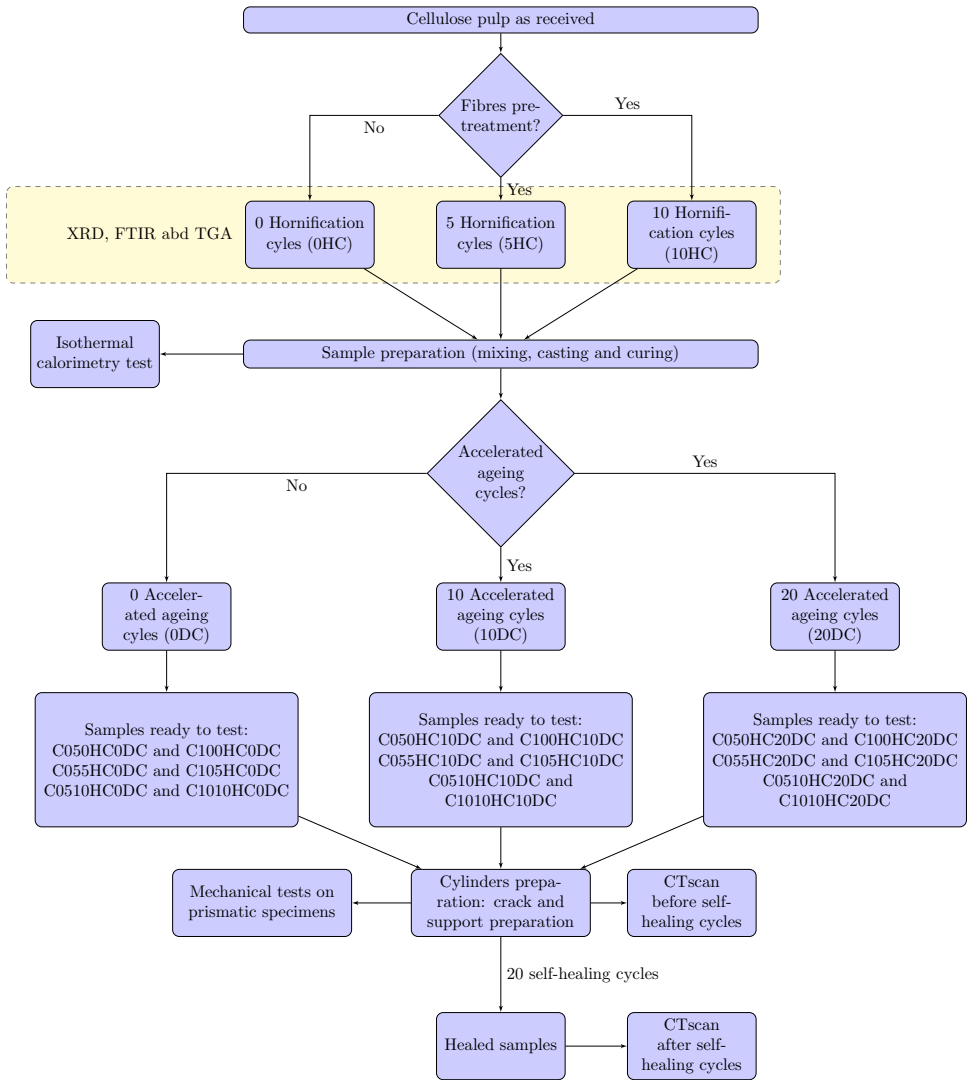


Figure 6.2: Summary of the experimental methodology.

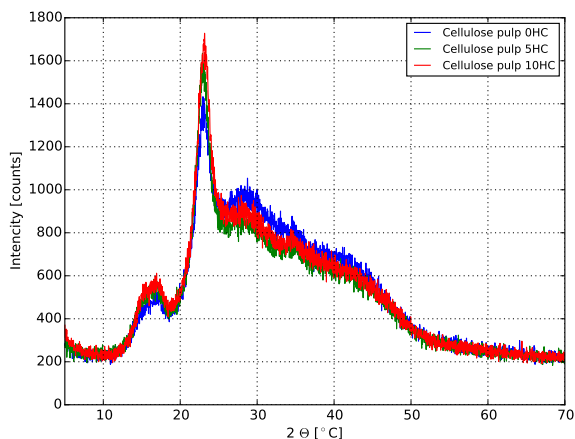


Figure 6.3: XRD pattern from the cellulose pulp before and after pre-treatment.

Table 6.2: Fibre relative crystallinity in [%] as measured by [231, 232]

0HC	5HC	10HC
14.29	15.87	16.27

6.4. RESULTS

6.4.1. FIBRE TREATMENT

From the XRD results reported in table 6.2 and figure 6.3, an increasing relative crystallinity level was measured. This result means that the cellulose in the fibres is more stable, stiffer and consequently less susceptible to dimensional changes.

Moreover, the lower water absorption percentages obtained for samples after hornification cycles and reported in table 6.3 confirms the same trend observed in the XRD results. Fibres 10HC presented the most favourable conditions from a durability point of view.

However, results from TGA, DTG and DSC summarized in the figures 6.4, 6.5 and 6.6 respectively concluded that fibres exposed to 5HC are in fact more chemically stable. Considerably more energy is needed for the depolymerization of the macromolecules leading to higher values on the DSC measurements. This means that there is a higher

Table 6.3: Fibres average moisture content [%]

Fibres	Moisture content [%]		
0HC	77.2	±	0.8
5HC	75.7	±	0.8
10HC	74.8	±	0.3

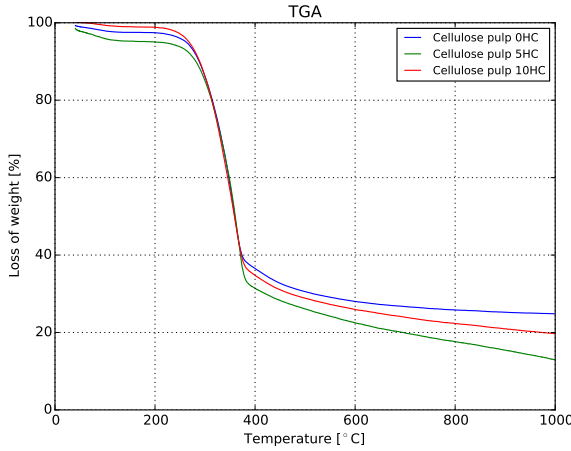


Figure 6.4: TGA curves from the cellulose pulp before and after pre-treatment.

number of intermolecular bonds increasing the crystallinity of the fibres [231, 232]. Additionally, after cellulose degradation (approximately from 200 up to 400) a higher amount of water was dissociated for 5HC samples.

Finally, the results from FTIR also lead to the conclusion that fibres exposed to 5HC are more chemically stable than 0 and 10HC. In figure 6.7 the lower transmittance found for 5HC samples is related to stronger OH bonds of the different components of a natural fibre, such as lignin (bands around 3567 cm^{-1}) and cellulose (bands around 3278 cm^{-1}) [paper].

The results obtained from the tests have pointed out that the pre-treatment was successful. In summary, the cellulose pulp increased crystallinity, lowered water absorption and higher chemical stability was also found. Nevertheless, the results obtained so far were not conclusive enough to determine the optimum number of hornification cycles. Anyhow, this optimization will also be approached when the self-healing results are discussed.

6.4.2. ISOTHERMAL CALORIMETRY ANALYSIS

It is known that the use of HPMC might delay ordinary Portland cement hydration. On the other hand, these polymers can arrest part of the mixing water and only releases it after the matrix starts to dry out due to the cement hydration. In this type of composites this mechanism has been proven to be beneficial, improving the overall degree of hydration and preventing printed materials to loose large amount of water due to drying. Moreover, previous studies have also confirmed that cellulose pulp can provide similar beneficial characteristics as the HPMC for the cementitious matrices [186].

The normalized heat flow curves in figure 6.8(a), the normalized total heat released in figure 6.8(b) and a summary of the total heat released in the table 6.4 gives an overview of the magnitude of change in hydration kinetics of the studied composites. The results from isothermal calorimetry show that indeed the HPMC have contributed significantly

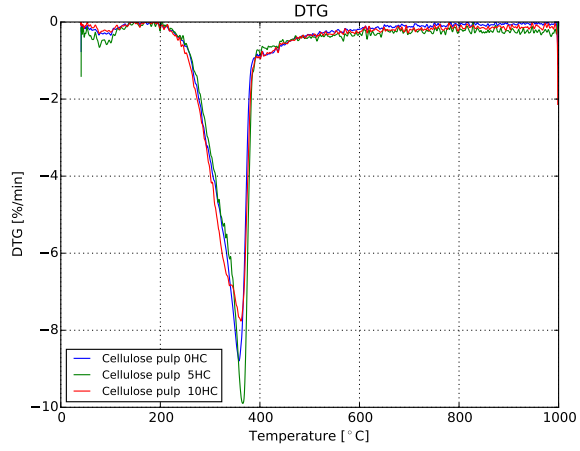


Figure 6.5: DTG curves from the cellulose pulp before and after pre-treatment.

6

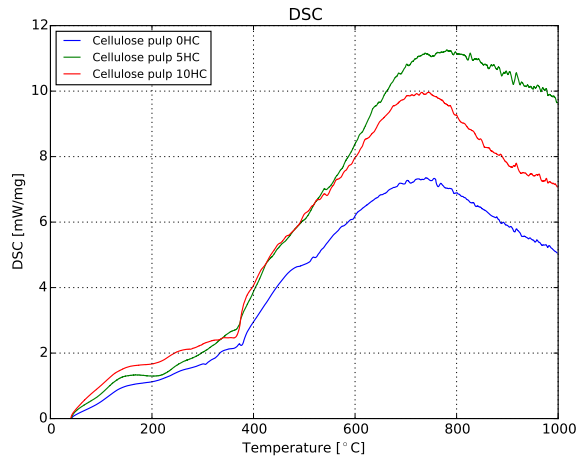


Figure 6.6: DSC curves from the cellulose pulp before and after pre-treatment.

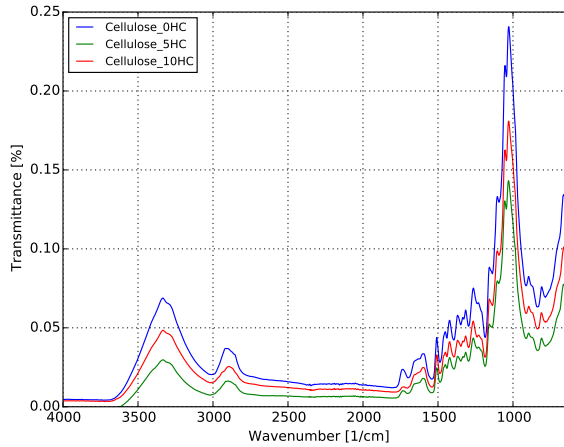


Figure 6.7: FTIR curves from the cellulose pulp before and after pre-treatment.

Table 6.4: Normalized heat released by the samples with HPMC and cellulose pulp

Sample	Normalized total heat released [W/g]
XVA0	73.74
XVA3	82.35
XVA3C050HC	79.24
XVA3C100HC	79.84
XVA3C055HC	76.87
XVA3C105HC	74.21
XVA3C0510HC	77.49
XVA3C1010HC	76.92

to the internal curing process of blast furnace slag mixtures, as well. All samples containing fibres could also release a higher amount of energy during hydration than the reference mixture without any admixture or reinforcement. Therefore, during this investigation the internal curing potential by using natural fibres were also confirmed. However, no more energy than XVA3 was released when HPMC and natural fibres were used together. Additionally, the use of pre-treated fibres have also decreased the total energy released during hydration, as those fibres have less water stored inside.

6.4.3. ACCELERATED AGEING CYCLES

Besides the influence of the ageing on the self-healing performance of the cementitious composites, the mechanical performance regarding flexural and compressive strengths was also assessed in this study. It was not the aim of the investigation the use of the natural fibres as a reinforcement. This statement can be justified with two arguments: 1) The maximum volume used (1%) is not sufficient to provide any crack bridging for this type of fibre. Usually the literature reports cellulose pulp reinforcement around 5%

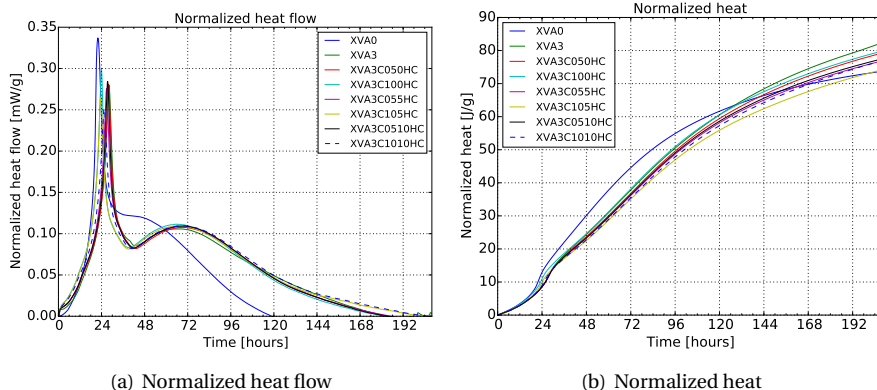


Figure 6.8: Isothermal calorimetry results

by volume to gain some ductility [216]. 2) The use of those fibres in a wet stage during casting. As explained before these fibres are not volumetrically stable in presence of moisture. Therefore, upon release of absorbed water, the bond between matrix and fibre will be lacking.

6

In figure 6.9 the flexural strength results are summarized. Samples with 0.5% of fibres had slightly higher initial values when the fibres were treated with 5HC. Nevertheless, these samples were somehow more exposed to the degradation, showing up to 31.4% losses. Only composites with fibres treated with 10HC were actually less effected by the accelerated ageing, when a maximum loss of 7.85% was registered after 20DC. Therefore, in the case of composites reinforced with 0.5% by volume of natural fibres 10HC appears to be the best solution to diminish losses in the flexural strength. Moving the analysis to composites with 1% by volume of fibres, these composites were somehow less susceptible to the ageing with maximum losses of 25%. The best results were found in specimens with fibres pre-treated with 5HC when a 15.7% of loss was found after 20DC. An interesting observation must be noted for these composites. They show remarkable loss after the first 10DC however, they tend to change less after 20DC, especially those reinforced with 10HC fibres. This means that the use of larger volume of fibres makes the composites more vulnerable to ageing but, the pre-treatment is no doubt helpful.

In figure 6.10 the compressive strength of the composites are summarized. Only for comparison the results obtained from composites without HPMC and without fibres were also shown. As reported before in a study of the influence of HPMC in cementitious materials the compressive strength reduces significantly due to the large amount of air voids generated whenever the chemical admixtures is used. Moreover, comparing the results when the fibres were added in fact, the mechanical performance of composites containing HPMC unexpectedly improves. This behaviour is the contrary of what was found in [53] where SAP particles were added in cementitious mortars with HPMC.

Regarding the porous nature of the cementitious matrix, it is believed that the material was somehow densified with the use of the fibres. This assumption might hold true as it was previously reported in literature [160] an anomalous growth of portlandite in

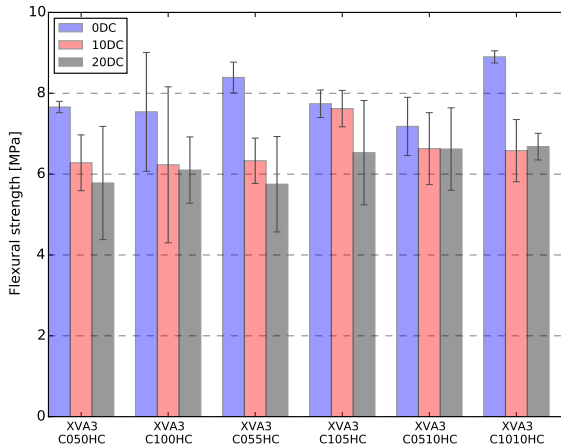


Figure 6.9: Flexural strength of the composites before and after accelerated ageing cycles.

the inner walls of the air voids. In that case the natural fibres could work as a nucleation spot for the growth of the crystals, providing surface area and also high moisture content even in latter curing ages. This hypothesis is confirmed somehow when the results of the compressive strength of the composites reinforced with fibres showed significantly rise after the accelerated ageing cycles (minimum of 19.7% and a maximum of 27.2% after 20DC). This phenomenon might be explained with the densification of the matrix with the above mentioned mechanism along with further cement and pozzolanic reactions.

6.4.4. SELF-HEALING PERFORMANCE

EFFECT OF HPMC CONTENT ON CEMENTITIOUS MATRICES

As mentioned before, and reported in [160] the use of HPMC promotes higher degree of hydration, an anomalous formation of portlandite and a high air void content in cement pastes. These differences might be beneficial for the autogenous self-healing performance of cementitious materials. The results obtained from the analysis of the Portland cement paste samples show a better healing performance and a more homogeneous healing through the height of the samples. In table 6.5 and 6.6 the performance of these samples are summarized. Even for greater crack widths in 10M samples the healing performance obtained from the image analysis and the water permeability shows that the use of HPMC has positively influenced the self-healing capabilities of this material. Most probably the reason why this performance was improved was previously explained in [160] when a larger portlandite formation was reported.

Moreover, in table 6.7 and 6.8 the results from the investigation of the matrices rich in blast furnace slag have demonstrated that this type of material is less succeedable to the use of HPMC. In contrary of what was observed in Portland cement past samples, these samples have not improved their overall self-healing performance or also the distribution of the healing products through the samples height.

Additionally, observing the healing performance calculated from the image analysis

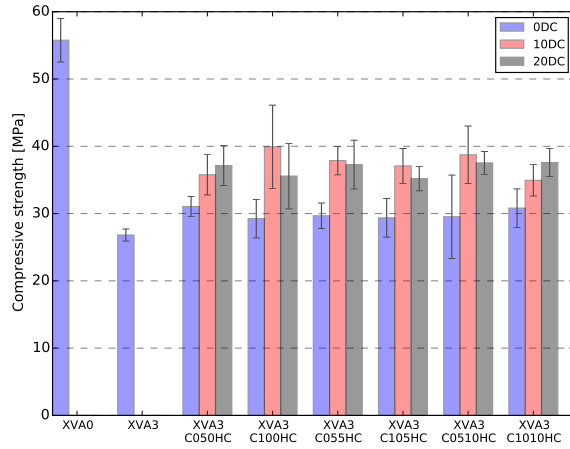


Figure 6.10: Compressive strength of the composites before and after accelerated ageing cycles.

6

Table 6.5: Results summary for REF. SAR: Segmented area recovery; TAAR: Total average area recovery; WPR: Water permeability recovery.

Sample	Crack width [μm]	Depth [slices]	SAR [%]	TAAR [%]	WPR [%]
REF_1	59.25 \pm 2.24	0 - 350	44.13	38.31 \pm 4.55	88.65
		350 - 700	38.86		
		700 - 1050	37.06		
		1050 - 1400	33.19		
REF_2	127.87 \pm 0.86	0 - 350	16.38	10.86 \pm 9.52	20.82
		350 - 700	20.04		
		700 - 1050	8.46		
		1050 - 1400	-1.44		
REF_3	55.07 \pm 2.28	0 - 350	60.40	41.21 \pm 26.11	24.95
		350 - 700	59.76		
		700 - 1050	4.73		
		1050 - 1400	39.94		
REF_4	127.76 \pm 3.08	0 - 350	10.74	6.70 \pm 9.23	14.88
		350 - 700	17.48		
		700 - 1050	1.83		
		1050 - 1400	-3.26		

Table 6.6: Results summary for 10M. SAR: Segmented area recovery; TAAR: Total average area recovery; WPR: Water permeability recovery.

Sample	Crack width [μm]		Depth [slices]	SAR [%]	TAAR [%]		WPR [%]		
10M_1	298.54	\pm	16.95	0 - 350	37.51	35.18	\pm	8.27	97.16
				350 - 700	29.60				
				700 - 1050	27.77				
				1050 - 1400	45.85				
10M_2	220.98	\pm	11.90	0 - 350	36.74	45.16	\pm	12.45	15.33
				350 - 700	57.93				
				700 - 1050	53.50				
				1050 - 1400	32.46				
10M_3	266.33	\pm	12.52	0 - 350	31.93	30.49	\pm	7.35	27.28
				350 - 700	23.23				
				700 - 1050	26.68				
				1050 - 1400	40.12				
10M_4	328.53	\pm	39.21	0 - 350	43.91	39.65	\pm	4.80	15.75
				350 - 700	43.69				
				700 - 1050	35.73				
				1050 - 1400	35.27				

Table 6.7: Results summary for XVA0. SAR: Segmented area recovery; TAAR: Total average area recovery; WPR: Water permeability recovery.

Sample	Crack width [μm]		Depth [slices]	SAR [%]	TAAR [%]		WPR [%]		
XVA0_1	74.59	\pm	1.74	0 - 350	26.87	21.47	\pm	8.36	19.14
				350 - 700	14.62				
				700 - 1050	14.06				
				1050 - 1400	30.34				
XVA0_2	186.43	\pm	37.79	0 - 350	19.91	17.40	\pm	4.94	6.94
				350 - 700	16.88				
				700 - 1050	10.72				
				1050 - 1400	22.09				
XVA0_3	68.04	\pm	0.68	0 - 350	31.75	23.49	\pm	8.98	49.77
				350 - 700	18.82				
				700 - 1050	13.17				
				1050 - 1400	30.24				
XVA0_4	69.13	\pm	1.43	0 - 350	23.57	18.33	\pm	7.78	3.16
				350 - 700	12.44				
				700 - 1050	10.93				
				1050 - 1400	26.38				

Table 6.8: Results summary for XVA10. SAR: Segmented area recovery; TAAR: Total average area recovery; WPR: Water permeability recovery.

Sample	Crack width [μm]	Depth [slices]	SAR [%]	TAAR [%]	WPR [%]
XVA10_1	153.35 \pm 4.59	0 - 350	13.46	10.39 \pm 2.56	3.46
		350 - 700	11.04		
		700 - 1050	9.73		
		1050 - 1400	7.34		
XVA10_2	118.64 \pm 1.71	0 - 350	16.48	14.92 \pm 1.99	2.12
		350 - 700	16.54		
		700 - 1050	14.25		
		1050 - 1400	12.39		
XVA10_3	172.47 \pm 10.42	0 - 350	19.20	20.91 \pm 5.43	0.93
		350 - 700	27.16		
		700 - 1050	22.91		
		1050 - 1400	14.39		
XVA10_4	201.96 \pm 2.36	0 - 350	57.45	52.80 \pm 5.48	6.85
		350 - 700	45.06		
		700 - 1050	55.72		
		1050 - 1400	52.98		

and the water permeability plotted in figure 6.11 not much correlation was found for all analysed matrices. It was expected that a significant decrease in the water permeability would be found whenever a large healing performance, either in the top or bottom of the specimens, would be measured by the image analysis from the μCT scan. However, it is worth to note that a portion of the very bottom and top of the specimens could not be analysed in the μCT scan images. Other imaging techniques such as microscopy or the digital reconstruction of the sample using laser scanners could potentially lead to more detailed information of the formation of self-healing products close to the crack surface.

EFFECT OF FIBRE CONTENT

In table 6.9 and 6.10 a summary of the results regarding the healing performance of composites with 0.5 and 1% of cellulose fibres is given. It is possible to notice that greater volume of fibres helped on the self-healing of the evaluated samples. The larger formation of healing products can be observed in the results from the image analysis and also from the water permeability test. Comparing the results from figure 6.12 (samples with fibres) and the figure 6.11 (only the matrix) it is also possible to conclude that the use of 0.5% of fibres have contributed to the self-healing and the use of 1% of fibres delivered the highest healing performance. Therefore, it is interesting to observe that the use of natural fibres positively influence on the formation of autogenous self-healing products.

EFFECT OF FIBRE PRE-TREATMENT AND NO ACCELERATED AGEING

The use of pre-treated fibres was also investigated. As showed before, treated fibres can absorb less water and therefore the total healing performance of the composite might be effected. The results obtained from the experiments and summarized in the tables 6.11,

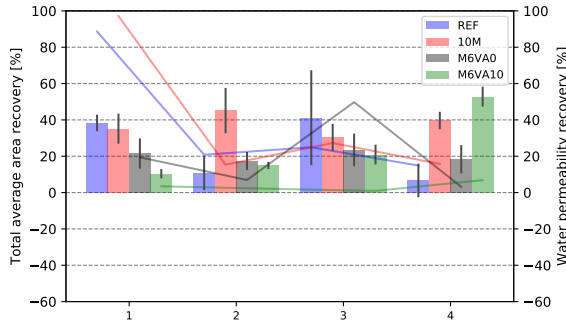


Figure 6.11: Autogenous self-healing recovery of samples with no fibres. The average area recovery measured on the CT scan images are represented with bars and the water permeability recovery is represented by the lines.

Table 6.9: Results summary for C050HC0DC. SAR: Segmented area recovery; TAAR: Total average area recovery; WPR: Water permeability recovery.

Sample	Crack width [μm]	Depth [slices]	SAR [%]	TAAR [%]	WPR [%]
C050HC0DC_1	166.36 ± 6.70	0 - 350	33.16	22.50 ± 8.56	36.46
		350 - 700	19.51		
		700 - 1050	24.49		
		1050 - 1400	12.85		
C050HC0DC_2	107.45 ± 2.20	0 - 350	50.08	43.95 ± 7.57	47.31
		350 - 700	44.20		
		700 - 1050	48.29		
		1050 - 1400	33.20		
C050HC0DC_3	191.87 ± 2.15	0 - 350	11.22	7.82 ± 3.92	3.75
		350 - 700	9.95		
		700 - 1050	7.75		
		1050 - 1400	2.34		
C050HC0DC_4	242.79 ± 4.67	0 - 350	13.56	9.51 ± 4.17	-0.07
		350 - 700	12.03		
		700 - 1050	8.18		
		1050 - 1400	4.26		

Table 6.10: Results summary for C100HC0DC. SAR: Segmented area recovery; TAAR: Total average area recovery; WPR: Water permeability recovery.

Sample	Crack width [μm]	Depth [slices]	SAR [%]	TAAR [%]	WPR [%]
C100HC0DC_1	139.85 \pm 1.97	0 - 350	22.45	16.05 \pm 5.90	25.14
		350 - 700	18.42		
		700 - 1050	14.78		
		1050 - 1400	8.56		
C100HC0DC_2	114.23 \pm 4.35	0 - 350	33.30	36.25 \pm 3.22	35.14
		350 - 700	40.36		
		700 - 1050	34.12		
		1050 - 1400	37.21		
C100HC0DC_3	139.11 \pm 13.36	0 - 350	27.42	19.82 \pm 6.55	73.77
		350 - 700	22.95		
		700 - 1050	15.78		
		1050 - 1400	13.13		
C100HC0DC_4	103.48 \pm 3.72	0 - 350	37.79	32.30 \pm 7.43	82.67
		350 - 700	39.50		
		700 - 1050	24.72		
		1050 - 1400	27.20		

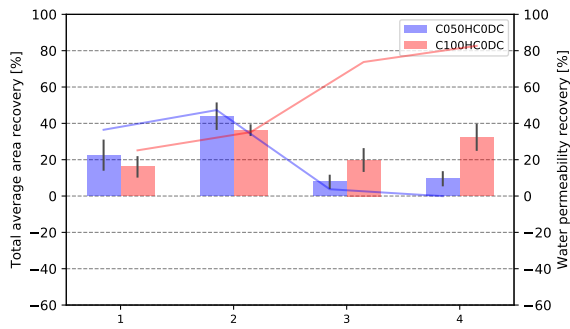


Figure 6.12: Autogenous self-healing recovery of samples with fibres. The average area recovery measured on the CT scan images are represented with bars and the water permeability recovery is represented by the lines.

Table 6.11: Results summary for C055HC0DC. SAR: Segmented area recovery; TAAR: Total average area recovery; WPR: Water permeability recovery.

Sample	Crack width [μm]		Depth [slices]	SAR [%]	TAAR [%]		WPR [%]
C055HC0DC_1	140.92	\pm 1.62	0 - 350	30.84	25.72	\pm 16.93	-26.26
			350 - 700	39.50			
			700 - 1050	1.02			
			1050 - 1400	31.53			
C055HC0DC_2	154.52	\pm 11.89	0 - 350	-19.85	-23.53	\pm 9.76	-8.69
			350 - 700	-15.16			
			700 - 1050	-21.53			
			1050 - 1400	-37.60			
C055HC0DC_3	221.29	\pm 2.01	0 - 350	25.46	22.83	\pm 3.30	34.06
			350 - 700	18.09			
			700 - 1050	24.58			
			1050 - 1400	23.20			
C055HC0DC_4	139.86	\pm 11.12	0 - 350	13.93	20.08	\pm 4.63	24.05
			350 - 700	25.04			
			700 - 1050	21.46			
			1050 - 1400	19.90			

6.12, 6.13 and 6.14 and figures 6.13 and 6.14 show that for both fibre reinforcement levels the use of treated fibres did not increase the formation of autogenous self-healing products. In the case of samples reinforced with 0.5% of cellulose pulp the maximum healing capacity measured in the μCT scan images and water permeability test have decreased with the increase in the number of HC. On the other hand, in samples reinforced with 1% of cellulose pulp this trend was only found in the results from the image analysis. Moreover, there is more homogeneity in the results from the μCT scan when fibres with more HC are used. For composites reinforced by 0.5% a frequently healing performance of 20 to 30% was found for 0, 5 and 10HC. Moreover, in samples reinforced by 1% the healing performance through the crack achieved 30 to 40% with non-treated fibres, and frequently the samples with treated fibres (5HC and 10HC) have demonstrated results from 10 to 20%.

EFFECT OF ACCELERATED AGEING ON THE SELF-HEALING PERFORMANCE FIBRES WITH NO PRE-TREATMENT

Firstly regarding the specimens reinforced with 0.5% of cellulose pulp, in general the self healing performance measured with the μCT scan is smaller when the samples are exposed to accelerated ageing. These results are shown in tables 6.9, 6.15 and 6.16 and figure 6.15. Anyhow, the distribution of the healing products through the sample height became more homogeneous, with less spreading and results in the range of 10 to 20% are frequently observed in samples exposed to 10 and 20 ageing cycles. Moreover, this smaller spread in the healing performance was also observed in the water permeability results.

Table 6.12: Results summary for C0510HC0DC. SAR: Segmented area recovery; TAAR: Total average area recovery; WPR: Water permeability recovery.

Sample	Crack width [μm]			Depth [slices]	SAR [%]	TAAR [%]			WPR [%]
C0510HC0DC_1	117.80	\pm	5.89	0 - 350	16.81	13.19	\pm	3.56	0.46
				350 - 700	15.03				
				700 - 1050	12.29				
				1050 - 1400	8.65				
C0510HC0DC_2	141.80	\pm	3.38	0 - 350	24.76	20.05	\pm	5.13	3.44
				350 - 700	24.04				
				700 - 1050	16.86				
				1050 - 1400	14.52				
C0510HC0DC_3	136.49	\pm	7.35	0 - 350	23.73	20.34	\pm	7.20	11.01
				350 - 700	19.78				
				700 - 1050	27.30				
				1050 - 1400	10.57				
C0510HC0DC_4	212.05	\pm	4.90	0 - 350	13.17	8.55	\pm	3.64	-3.75
				350 - 700	8.36				
				700 - 1050	8.42				
				1050 - 1400	4.27				

Table 6.13: Results summary for C105HC0DC. SAR: Segmented area recovery; TAAR: Total average area recovery; WPR: Water permeability recovery.

Sample	Crack width [μm]			Depth [slices]	SAR [%]	TAAR [%]			WPR [%]
C105HC0DC_1	144.43	\pm	4.17	0 - 350	21.15	17.89	\pm	3.02	40.35
				350 - 700	18.37				
				700 - 1050	18.20				
				1050 - 1400	13.85				
C105HC0DC_2	179.00	\pm	17.47	0 - 350	17.60	14.09	\pm	2.85	16.63
				350 - 700	13.05				
				700 - 1050	14.84				
				1050 - 1400	10.86				
C105HC0DC_3	121.34	\pm	2.80	0 - 350	33.41	20.37	\pm	9.01	48.45
				350 - 700	18.22				
				700 - 1050	17.13				
				1050 - 1400	12.74				
C105HC0DC_4	214.78	\pm	12.90	0 - 350	34.23	22.81	\pm	8.69	22.28
				350 - 700	24.12				
				700 - 1050	19.06				
				1050 - 1400	13.83				

Table 6.14: Results summary for C1010HC0DC. SAR: Segmented area recovery; TAAR: Total average area recovery; WPR: Water permeability recovery.

Sample	Crack width [μm]	Depth [slices]	SAR [%]	TAAR [%]	WPR [%]
C1010HC0DC_1	179.43 \pm 4.67	0 - 350	-	- \pm -	-
		350 - 700	-		
		700 - 1050	-		
		1050 - 1400	-		
C1010HC0DC_2	134.34 \pm 4.40	0 - 350	13.45	10.78 \pm 4.77	37.11
		350 - 700	12.13		
		700 - 1050	13.85		
		1050 - 1400	3.72		
C1010HC0DC_3	108.32 \pm 9.05	0 - 350	17.11	10.90 \pm 4.54	72.64
		350 - 700	10.60		
		700 - 1050	9.65		
		1050 - 1400	6.23		
C1010HC0DC_4	143.95 \pm 12.12	0 - 350	34.33	24.89 \pm 7.83	18.57
		350 - 700	26.68		
		700 - 1050	23.08		
		1050 - 1400	15.49		

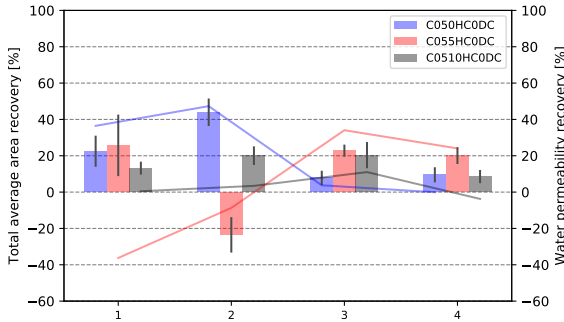


Figure 6.13: Autogenous self-healing recovery of samples with 0.5% of fibres after different HC. The average area recovery measured on the CT scan images are represented with bars and the water permeability recovery is represented by the lines.

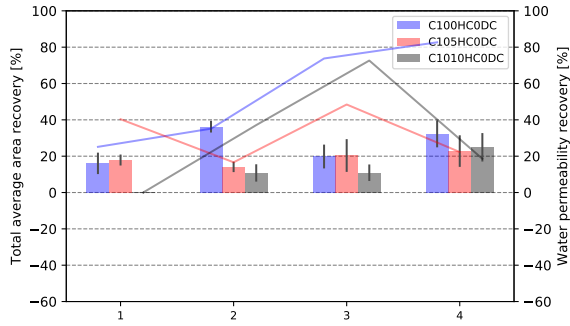


Figure 6.14: Autogenous self-healing recovery of samples with 1.0% of fibres after different HC. The average area recovery measured on the CT scan images are represented with bars and the water permeability recovery is represented by the lines.

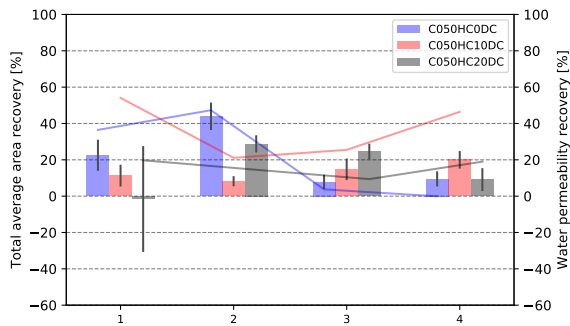


Figure 6.15: Autogenous self-healing recovery of samples with 0.5% of fibres with no HC and exposed to different DC. The average area recovery measured on the CT scan images are represented with bars and the water permeability recovery is represented by the lines.

Table 6.15: Results summary for C050HC10DC. SAR: Segmented area recovery; TAAR: Total average area recovery; WPR: Water permeability recovery.

Sample	Crack width [μm]		Depth [slices]	SAR [%]	TAAR [%]		WPR [%]
C050HC10DC_1	130.17	\pm 3.17	0 - 350	18.70	11.29	\pm 5.98	54.07
			350 - 700	11.85			
			700 - 1050	10.51			
			1050 - 1400	4.11			
C050HC10DC_2	133.41	\pm 0.78	0 - 350	11.65	8.82	\pm 2.79	21.09
			350 - 700	9.09			
			700 - 1050	9.56			
			1050 - 1400	4.99			
C050HC10DC_3	259.56	\pm 20.90	0 - 350	22.80	14.77	\pm 5.95	25.49
			350 - 700	14.61			
			700 - 1050	13.17			
			1050 - 1400	8.51			
C050HC10DC_4	145.64	\pm 9.42	0 - 350	19.52	20.01	\pm 4.84	46.41
			350 - 700	26.98			
			700 - 1050	16.38			
			1050 - 1400	17.15			

Table 6.16: Results summary for C050HC20DC. SAR: Segmented area recovery; TAAR: Total average area recovery; WPR: Water permeability recovery.

Sample	Crack width [μm]		Depth [slices]	SAR [%]	TAAR [%]		WPR [%]
C050HC20DC_1	356.40	\pm 10.19	0 - 350	16.32	-1.57	\pm 29.13	19.73
			350 - 700	12.93			
			700 - 1050	9.53			
			1050 - 1400	-45.07			
C050HC20DC_2	98.50	\pm 2.58	0 - 350	25.96	28.78	\pm 4.73	14.52
			350 - 700	24.67			
			700 - 1050	29.22			
			1050 - 1400	35.26			
C050HC20DC_3	126.11	\pm 1.06	0 - 350	26.80	24.64	\pm 4.26	9.38
			350 - 700	29.56			
			700 - 1050	21.62			
			1050 - 1400	20.58			
C050HC20DC_4	246.25	\pm 2.28	0 - 350	5.39	9.10	\pm 6.32	18.99
			350 - 700	13.10			
			700 - 1050	15.66			
			1050 - 1400	2.25			

Table 6.17: Results summary for C100HC10DC. SAR: Segmented area recovery; TAAR: Total average area recovery; WPR: Water permeability recovery.

Sample	Crack width [μm]	Depth [slices]	SAR [%]	TAAR [%]	WPR [%]
C100HC10DC_1	138.78 ± 9.13	0 - 350	14.33	11.45 ± 8.87	19.81
		350 - 700	12.01		
		700 - 1050	20.25		
		1050 - 1400	-0.79		
C100HC10DC_2	187.27 ± 2.64	0 - 350	5.19	-0.05 ± 3.78	14.88
		350 - 700	0.00		
		700 - 1050	-1.92		
		1050 - 1400	-3.48		
C100HC10DC_3	198.83 ± 14.59	0 - 350	12.86	12.09 ± 3.84	21.65
		350 - 700	16.75		
		700 - 1050	11.24		
		1050 - 1400	7.49		
C100HC10DC_4	237.19 ± 39.38	0 - 350	20.05	13.69 ± 5.47	32.88
		350 - 700	14.28		
		700 - 1050	13.74		
		1050 - 1400	6.68		

When the samples reinforced by 1% of cellulose pulp is observed the self-healing performance were significantly influenced by the ageing cycles. The worsening in the healing performance was measured in the results from the μCT scan and from the water permeability tests and summarized in the tables 6.10, 6.17 and 6.18 and figure 6.16.

One interesting observation might be done when the comparison between the results from the μCT scan and the water permeability tests is observed. Larger values of water permeability recovery are found when healing performances in the range of 20 to 30% are systematically observed through the height of the samples when the μCT scan results are evaluated.

FIBRES WITH 5 CYCLES OF PRE-TREATMENT

Analysing the results from the self-healing performance obtained from the μCT scan and water permeability it is possible to notice that 5HC was not able to help in keeping the stability of the composites after the accelerating ageing cycles. The results from samples with 0.5% of fibres are summarized in tables 6.11, 6.19, 6.20 and figure 6.17. The results from samples with 1.0% of fibres are summarized in tables 6.13, 6.21, 6.22 and figure 6.18. For both reinforcement levels the use of treated fibres did demonstrate frequent healing capacity through the height of the specimen of around 10 to 20% after 10 ageing cycles. However, the water permeability results revealed worsening after the ageing cycles.

FIBRES WITH 10 CYCLES OF PRE-TREATMENT

Regarding the results of samples which have used fibres submitted to 10HC, it seems that the self-healing performance was dependent on the total volume of fibres. A summary of the results obtained can be found in tables 6.12, 6.23, 6.24 and figure 6.19 for samples

Table 6.18: Results summary for C100HC20DC. SAR: Segmented area recovery; TAAR: Total average area recovery; WPR: Water permeability recovery.

Sample	Crack width [μm]	Depth [slices]	SAR [%]	TAAR [%]	WPR [%]
C100HC20DC_1	368.72 \pm 1.57	0 - 350	5.14	13.70 \pm 6.31	-12.47
		350 - 700	13.30		
		700 - 1050	19.89		
		1050 - 1400	16.47		
		0 - 350	14.63		
C100HC20DC_2	256.25 \pm 2.59	350 - 700	20.80	19.69 \pm 8.55	12.04
		700 - 1050	12.04		
		1050 - 1400	31.27		
		0 - 350	5.56		
		350 - 700	18.13		
C100HC20DC_3	208.64 \pm 1.44	700 - 1050	13.05	10.80 \pm 5.92	-0.35
		1050 - 1400	6.46		
		0 - 350	11.54		
		350 - 700	19.69		
		700 - 1050	10.28		
C100HC20DC_4	393.44 \pm 52.53	1050 - 1400	16.70	14.55 \pm 4.41	-4.89

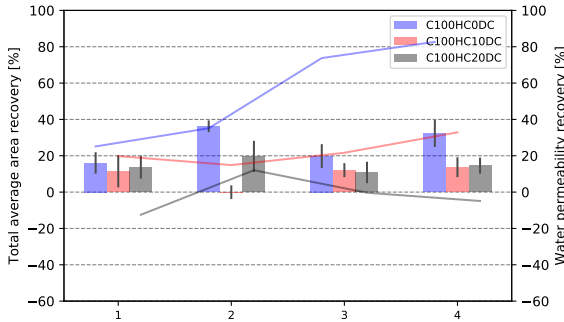


Figure 6.16: Autogenous self-healing recovery of samples with 1.0% of fibres with no HC and exposed to different DC. The average area recovery measured on the CT scan images are represented with bars and the water permeability recovery is represented by the lines.

Table 6.19: Results summary for C055HC10DC. SAR: Segmented area recovery; TAAR: Total average area recovery; WPR: Water permeability recovery.

Sample	Crack width [μm]		Depth [slices]	SAR [%]	TAAR [%]		WPR [%]		
C055HC10DC_1	111.66	\pm	1.40	0 - 350	11.22	12.95	\pm	1.32	31.42
				350 - 700	13.20				
				700 - 1050	12.94				
				1050 - 1400	14.42				
C055HC10DC_2	188.36	\pm	5.26	0 - 350	16.60	12.76	\pm	3.05	13.14
				350 - 700	11.86				
				700 - 1050	9.28				
				1050 - 1400	13.30				
C055HC10DC_3	306.05	\pm	13.61	0 - 350	15.35	10.89	\pm	4.75	18.69
				350 - 700	12.45				
				700 - 1050	11.56				
				1050 - 1400	4.19				
C055HC10DC_4	95.72	\pm	0.96	0 - 350	10.07	7.46	\pm	3.03	15.78
				350 - 700	3.82				
				700 - 1050	6.11				
				1050 - 1400	9.84				

Table 6.20: Results summary for C055HC20DC. SAR: Segmented area recovery; TAAR: Total average area recovery; WPR: Water permeability recovery.

Sample	Crack width [μm]		Depth [slices]	SAR [%]	TAAR [%]		WPR [%]		
C055HC20DC_1	125.49	\pm	6.83	0 - 350	18.83	11.25	\pm	5.14	-2.93
				350 - 700	8.53				
				700 - 1050	9.91				
				1050 - 1400	7.72				
C055HC20DC_2	192.37	\pm	12.35	0 - 350	18.58	17.12	\pm	0.98	-3.10
				350 - 700	16.52				
				700 - 1050	16.87				
				1050 - 1400	16.53				
C055HC20DC_3	156.75	\pm	11.80	0 - 350	20.71	16.18	\pm	3.09	18.67
				350 - 700	14.93				
				700 - 1050	13.76				
				1050 - 1400	15.33				
C055HC20DC_4	200.75	\pm	5.38	0 - 350	18.23	12.87	\pm	5.38	-5.30
				350 - 700	14.56				
				700 - 1050	13.25				
				1050 - 1400	5.43				

Table 6.21: Results summary for C105HC10DC. SAR: Segmented area recovery; TAAR: Total average area recovery; WPR: Water permeability recovery.

Sample	Crack width [μm]		Depth [slices]	SAR [%]	TAAR [%]		WPR [%]		
C105HC10DC_1	181.24	\pm	8.11	0 - 350	15.07	17.47	\pm	2.79	-1.77
				350 - 700	17.88				
				700 - 1050	15.68				
				1050 - 1400	21.24				
C105HC10DC_2	257.64	\pm	3.04	0 - 350	7.38	6.30	\pm	2.39	16.50
				350 - 700	5.90				
				700 - 1050	8.76				
				1050 - 1400	3.18				
C105HC10DC_3	218.51	\pm	12.28	0 - 350	27.00	22.80	\pm	4.18	8.45
				350 - 700	21.25				
				700 - 1050	17.66				
				1050 - 1400	25.26				
C105HC10DC_4	120.70	\pm	8.50	0 - 350	16.16	13.94	\pm	3.82	-2.41
				350 - 700	8.37				
				700 - 1050	16.67				
				1050 - 1400	14.57				

Table 6.22: Results summary for C105HC20DC. SAR: Segmented area recovery; TAAR: Total average area recovery; WPR: Water permeability recovery.

Sample	Crack width [μm]		Depth [slices]	SAR [%]	TAAR [%]		WPR [%]		
C105HC20DC_1	182.29	\pm	6.93	0 - 350	10.37	16.25	\pm	5.39	-20.03
				350 - 700	20.50				
				700 - 1050	21.13				
				1050 - 1400	12.99				
C105HC20DC_2	225.61	\pm	2.50	0 - 350	11.45	12.01	\pm	7.25	-6.89
				350 - 700	22.24				
				700 - 1050	5.46				
				1050 - 1400	8.91				
C105HC20DC_3	204.20	\pm	3.61	0 - 350	10.26	7.96	\pm	2.15	2.40
				350 - 700	9.32				
				700 - 1050	6.28				
				1050 - 1400	5.99				
C105HC20DC_4	140.00	\pm	13.70	0 - 350	8.82	5.06	\pm	2.52	-25.96
				350 - 700	4.16				
				700 - 1050	3.72				
				1050 - 1400	3.55				

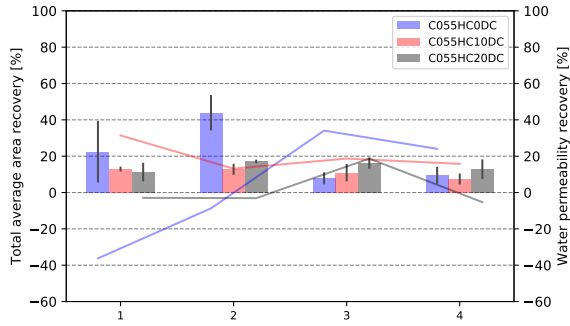


Figure 6.17: Autogenous self-healing recovery of samples with 0.5% of fibres after 5HC and exposed to DC. The average area recovery measured on the CT scan images are represented with bars and the water permeability recovery is represented by the lines.

6

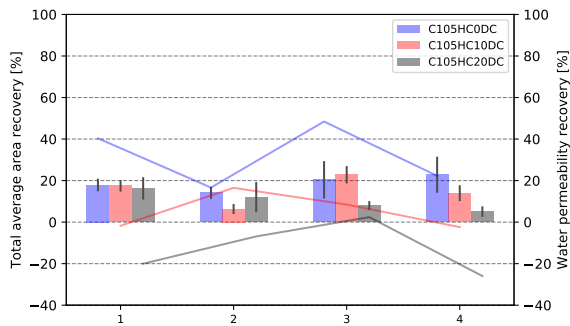


Figure 6.18: Autogenous self-healing recovery of samples with 1.0% of fibres after 5HC and exposed to DC. The average area recovery measured on the CT scan images are represented with bars and the water permeability recovery is represented by the lines.

Table 6.23: Results summary for C0510HC10DC. SAR: Segmented area recovery; TAAR: Total average area recovery; WPR: Water permeability recovery.

Sample	Crack width [μm]		Depth [slices]	SAR [%]	TAAR [%]		WPR [%]
C0510HC10DC_1	252.17	\pm 34.71	0 - 350	11.02	6.71	\pm 4.10	36.59
			350 - 700	9.19			
			700 - 1050	4.49			
			1050 - 1400	2.16			
C0510HC10DC_2	274.06	\pm 15.43	0 - 350	72.13	71.23	\pm 4.74	32.54
			350 - 700	64.31			
			700 - 1050	74.76			
			1050 - 1400	73.73			
C0510HC10DC_3	168.78	\pm 7.89	0 - 350	19.23	14.10	\pm 5.15	29.25
			350 - 700	16.38			
			700 - 1050	13.63			
			1050 - 1400	7.18			
C0510HC10DC_4	163.40	\pm 4.97	0 - 350	18.00	16.60	\pm 1.74	33.66
			350 - 700	15.35			
			700 - 1050	14.86			
			1050 - 1400	18.21			

with 0.5% of fibres. In the case of results from samples with 1.0% of fibres the results are shown in tables 6.14, 6.25, 6.26 and figure 6.20. Samples with 0.5% of pre-treated fibres resulted in a certain level of protection and delivered better healing performance when the samples were exposed to 10 accelerated ageing cycles. This healing performance was observed in the results from the μCT scan as well as in the water permeability test. Nevertheless, after 20 accelerating ageing cycles the water permeability results have shown significant worsening in the healing performance, while in the μCT scan frequent healing performance of 10 to 20% through the sample height was still found. Regarding composites reinforced with 1% of fibres μCT scan results have shown crack healing performance through the height of the samples frequently in the range of 10 to 20% for 0, 10 and 20 accelerated ageing cycles. However, the water permeability results from these samples have showed worsening after ageing.

In overall the use of pre-treated fibres does not show significant protection to the autogenous self-healing performance. The lack of formation of healing products is mainly observed in the water permeability tests when very little or no water blockage was provided for samples exposed to 10 and 20DC. This low performance might not be exclusively related to an eventual degradation of the fibres, but also by modifications in the matrix. As the accelerated ageing cycles impose the samples to an aggressive wetting and drying regime, a densification of the microstructure via pozzolanic reactions, further hydration or at some level carbonation plays an important role. An evidence of this further developments in the matrix can be exemplified by the higher compressive strength result of the samples exposed to the ageing. Moreover, the densification is somehow also related to the capture of the available calcium ions in the matrix to the creation of more

Table 6.24: Results summary for C0510HC20DC. SAR: Segmented area recovery; TAAR: Total average area recovery; WPR: Water permeability recovery.

Sample	Crack width [μm]		Depth [slices]	SAR [%]	TAAR [%]		WPR [%]
C0510HC20DC_1	193.93	\pm 3.28	0 - 350	7.59	4.50	\pm 2.77	-17.61
			350 - 700	5.69			
			700 - 1050	3.54			
			1050 - 1400	1.16			
C0510HC20DC_2	181.05	\pm 7.65	0 - 350	13.09	11.84	\pm 2.64	-17.25
			350 - 700	12.71			
			700 - 1050	13.65			
			1050 - 1400	7.93			
C0510HC20DC_3	177.18	\pm 5.87	0 - 350	15.05	13.45	\pm 2.39	-15.54
			350 - 700	13.87			
			700 - 1050	14.93			
			1050 - 1400	9.96			
C0510HC20DC_4	173.70	\pm 10.00	0 - 350	14.46	13.89	\pm 0.78	-15.37
			350 - 700	13.80			
			700 - 1050	14.47			
			1050 - 1400	12.82			

Table 6.25: Results summary for C1010HC10DC. SAR: Segmented area recovery; TAAR: Total average area recovery; WPR: Water permeability recovery.

Sample	Crack width [μm]		Depth [slices]	SAR [%]	TAAR [%]		WPR [%]
C1010HC10DC_1	203.72	\pm 22.51	0 - 350	22.90	20.82	\pm 4.40	20.22
			350 - 700	26.00			
			700 - 1050	17.66			
			1050 - 1400	16.71			
C1010HC10DC_2	183.54	\pm 7.66	0 - 350	11.63	8.63	\pm 2.60	17.71
			350 - 700	9.24			
			700 - 1050	8.29			
			1050 - 1400	5.34			
C1010HC10DC_3	132.94	\pm 12.77	0 - 350	12.86	9.98	\pm 2.18	5.49
			350 - 700	7.71			
			700 - 1050	9.15			
			1050 - 1400	10.20			
C1010HC10DC_4	247.26	\pm 4.31	0 - 350	18.11	13.64	\pm 3.41	5.13
			350 - 700	13.93			
			700 - 1050	9.93			
			1050 - 1400	12.59			

Table 6.26: Results summary for C1010HC20DC. SAR: Segmented area recovery; TAAR: Total average area recovery; WPR: Water permeability recovery.

Sample	Crack width [μm]	Depth [slices]	SAR [%]	TAAR [%]	WPR [%]
C1010HC20DC_1	0.00 \pm 0.00	0 - 350	9.57	11.35 \pm 2.26	-41.19
		350 - 700	14.27		
		700 - 1050	9.56		
		1050 - 1400	11.98		
C1010HC20DC_2	131.32 \pm 2.80	0 - 350	-8.18	-20.01 \pm 9.16	-37.90
		350 - 700	-26.64		
		700 - 1050	-27.83		
		1050 - 1400	-17.41		
C1010HC20DC_3	209.99 \pm 1.73	0 - 350	11.20	17.92 \pm 6.24	-17.42
		350 - 700	15.75		
		700 - 1050	18.65		
		1050 - 1400	26.06		
C1010HC20DC_4	141.47 \pm 4.61	0 - 350	19.39	17.68 \pm 2.23	3.21
		350 - 700	15.23		
		700 - 1050	16.37		
		1050 - 1400	19.75		

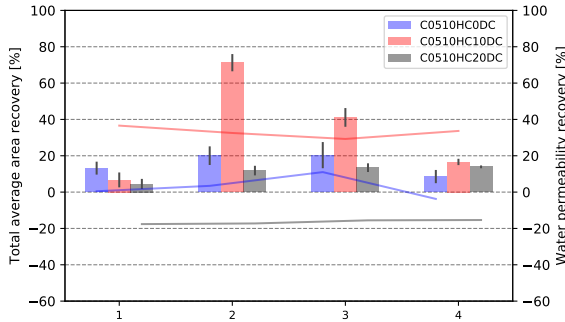


Figure 6.19: Autogenous self-healing recovery of samples with 0.5% of fibres after 10HC and exposed to DC. The average area recovery measured on the CT scan images are represented with bars and the water permeability recovery is represented by the lines.

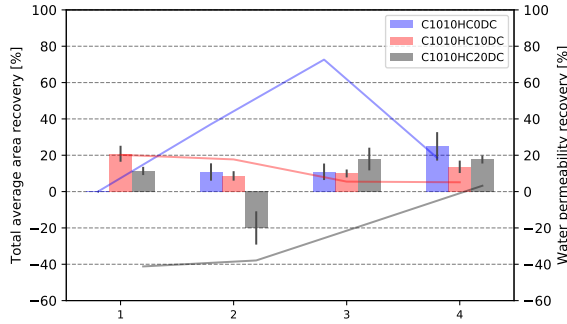


Figure 6.20: Autogenous self-healing recovery of samples with 1.0% of fibres after 10HC and exposed to DC. The average area recovery measured on the CT scan images are represented with bars and the water permeability recovery is represented by the lines.

stable minerals. Therefore, the autogenous self-healing performance is jeopardized by the lack of available essential components.

Very poor correlation of the recovery results measured with the water permeability test and the μ CT scan were observed. Both techniques used in this research to assess the healing performance of the composites could provide valid information about the process. However, if the water permeability of a sample is taken as reference to quantify the healing performance, parameters such as crack tortuosity, width and the opening of both extremities emerge as crucial parameters for the water to flow from one side to the other.

The comparison of images obtained from μ CT scan before and after a certain number of healing cycles is able to provide information about some of the previously listed parameters. Nevertheless, this technique is not the most suitable to make measurements close to the crack edge. Far from assuming that only water permeability tests can fully quantify the healing performance of cracked cementitious composites, the combination of techniques such as the ones used in this research along with imaging techniques from both crack extremities is crucial to properly quantify the healing process.

6.5. CONCLUSIONS

This study evaluated the use of natural fibres as water reservoirs in cementitious composites to enhance their autogenous self-healing performance. Besides that, in this research a pre-treatment of the fibres was proposed to improve their durability and an investigation on the potential consequences of the exposure of the composites to an accelerated ageing.

In summary the following conclusions could be drafted from this study:

- Portland cement matrices samples with HPMC deliver better autogenous self-healing performance than in samples without. This behaviour might be correlated to the higher degree of hydration found in samples with this type of admixture, larger volume of air voids and the anomalous formation of portlandite observed in [160];

- The autogenous self-healing performance of matrices rich in blast furnace slag were not influenced by the use of HPMC.
- The use of wet natural fibres up to 1% by volume did not harm the mechanical performance of the composites;
- The use of natural fibres helped to improve autogenous self-healing performance of cementitious composites regardless of the used volume.
- The use of the hornification cycles as a pretreatment of the cellulose pulp decrease the total volume of water that those fibres are able to absorb. This behaviour worsened the total autogenous self-healing performance of the composites when compared to those reinforced by non-treated fibres.
- Only fibres pre-treated by 10HC have demonstrated some level of protection against the accelerated ageing cycles when the results from μ CT scan are observed. However, it is not clear if the low autogenous self-healing performance from aged samples was caused by the ageing of the fibres or the densification of the matrix.
- Very little correlation between the results from the μ CT scan and the water permeability tests were found. Both techniques presents advantages and disadvantages. The images obtained from μ CT scan are useful to assess the healing performance through the sample height while the water permeability test is more sensitive to a sealing of one of the crack extremities.

7

PIEZORESISTIVE PROPERTIES OF CEMENTITIOUS COMPOSITES REINFORCED BY PVA FIBRES

It does not matter how slowly you go as long as you do not stop.

Confucius

The use of fibres to enhance the ductility of cementitious composites has been extensively studied for the past few years. The addition of polymeric or metallic fibres with random orientation to the composite or even natural long and aligned fibres demonstrated a very successful reinforcement capable to reach a high mechanical performance. Other property that has been studied is the use of those composites to work as strain sensors. To develop piezoresistive properties on cementitious composite, the addition of conductive materials is necessary. This research evaluated the incorporation of different volumes of multi-wall carbon nanotubes on the piezoresistive properties of strain hardening cementitious composites (SHCC) reinforced by PVA fibres. Through impedance measurements the opening of the cracks under tensile loading was studied. The characterization of this material can help on the understanding of self-sensing properties, adding value to the SHCC used by the repair industry and will contribute to the continuous infrastructure monitoring.

This chapter has been published in Figueiredo S.C., Çopuroğlu O., Šavija B., Schlangen E. (2018) Piezoresistive Properties of Cementitious Composites Reinforced by PVA Fibres. In: Mechtcherine V., Slowik V., Kabele P. (eds) Strain-Hardening Cement-Based Composites. SHCC 2017. RILEM Bookseries, vol 15. Springer, Dordrecht [235]

7.1. INTRODUCTION

INFRASTRUCTURE maintenance is a worldwide problem, due to the high complexity of the structures and the cost involved in a durability surveillance. The service life of a large number of existing concrete structures are soon to reach 50 or more years in many countries, bringing problems and high costs for refurbishment to extend their service life. An example can be drafted by the conditions of roads in United States of America and in Brazil, where 32% [236] in 2013 and 57,3% [237] in 2015 respectively were considered in unsatisfactory conditions. Maintenance surveillance of infrastructure spread in large areas will be always challenging, and resources demanding. Therefore, techniques which improve the efficiency of infrastructure monitoring must be developed.

Most of the infrastructure will need repair interventions during their service life. In the past few years, several projects have been carried out on the development and characterization of different repair materials. Among these, the performance of high ductility cementitious composites have drawn the attention of different sectors, bringing conclusions about the importance of the capability of absorbency of high strains of this kind of material [21].

Emerging as one of the most successful ductile materials in civil engineering, strain hardening cementitious composites (SHCC) are an example of the important role of ductility on performance of such composites. The match between the tailored brittle matrix and ductility of the Polyvinyl Alcohol fibres (PVA) enables these composites to develop multiple cracks when loaded under tension. In the very beginning, the matrix of this class of composite, also called Engineered Cementitious Composites (ECC) in this case, was composed by ordinary Portland cement, silica fume and sand [91]. Afterwards, different compositions for this matrix were developed, like demonstrated by [111], where the incorporation of blast furnace slag and limestone powder was investigated on the cementitious matrix. [238] demonstrated the importance of low toughness of the brittle matrix of cementitious composites, in order to obtain a pseudo-strain hardening behaviour.

Moreover, several other projects evaluated the performance of different fibres to reinforce cementitious matrix. Carbon [239], polyethylene (PE) [197], polypropylene (PP) [240], steel [241] and natural fibres [242] are usually found on literature as reinforcement for high ductility cementitious composites. Recently the search for hybrid reinforcement was pursued by [243] and in a multi-scale fibre reinforcement by [244], where the cementitious composites were reinforced by steel fibres and wollastonite micro-fibres. Besides the high mechanical properties, the SHCC's demonstrated a good performance when subjected to accelerated ageing tests and capability to develop autogenous self-healing, confirming extraordinary performance of this composite [107]. Some researches [32] investigated the self-sensing properties of ECC loaded in uniaxial tension. In their research, the influence of number of cracks and their average width was correlated with the increase of the electrical resistivity.

The development of smart cementitious composites has been under the spotlight, as well. The addition of electrical conductive fillers in cementitious materials decreases the overall resistivity of the composite. There are many works describing the influence of addition of materials like, nano ZrO_2 , Al_2O_3 , Fe_2O_3 and TiO_2 , ensuring mechanical performance improvement and in some cases lowering the electrical resistivity. However,

Table 7.1: CNT properties

Average diameter [nm]	Average length [μm]	Carbon purity [%]	Surface area [m^2/g]	Volume resistivity [$\Omega\cdot\text{cm}$]
9.5	1.5	90	250-300	10-4

the focus has been on the carbon nanotubes and nanofibres [35].

The electrical conductivity of cementitious composites with conductive fillers is represented usually by those three different forms: contacting conduction, tunnelling conduction (and/or field emission conduction), and ionic conduction. The contacting conduction is characterized by the direct contact of conductive particles. Tunnelling conduction happens only when the conductive particles are separated by a maximum distance of 10nm, and field emission conduction is induced when a strong electrical field is generated. The sharp tips found in nanomaterials, like carbon nanotubes (CNT), are important to create this strong field. Finally, ionic conduction plays a very important role in the case of cementitious matrixes, as well. The water present in the voids might dissolve the ions from the matrix, resulting in ionic conduction through interconnected capillary pores [25].

The use of carbon nanofibres on cementitious composites has been successfully employed on the development of smart composites for crack detection [36]. The development of a SHCC which would be able to contribute with the infrastructure health monitoring is investigated on this research program. An experimental routine is proposed to evaluate the performance of self-sensing SHCC.

7.2. EXPERIMENTAL

The SHCC developed by [111] was used as reference. The mix design of this composite employs ordinary Portland Cement (OPC) CEM-I 42.5N and blast furnace slag (BFS) as binders, limestone powder (LP) as filler and 2 vol.% of PVA fibres as reinforcement. To investigate the influence of CNT on the piezoresistive and mechanical performance of this composite two levels of incorporation 0.05 and 0.1 wt.% of binder weight were tested. The CNT used were delivered dispersed in aqueous solution with surfactant, with concentration of 3 wt.% by Nanocyl S.A. The properties of the dispersed CNT can be found in 7.1 and the mix design in 7.2.

500ml of the mixture were mixed in a Hobart mixer according to the following procedure: all the dry components were mixed at low speed for 4 minutes, then the liquids (water + superplasticizer + CNT solution) were added to the dry components and mixed for 1 minute at low speed, followed by 4 minutes at high speed. The total volume of water, superplasticizer and CNT solution were sonicated for 25 minutes in advance to enhance the nanoparticle dispersion.

The mixture was casted on dog-bone shape cylinders (see figure 7.1 with dimensions in millimetres). After casting, these moulds were covered with plastic foil during the first 24 hours of curing. The samples were demoulded after 24 hours of curing and the follow-

Table 7.2: Mix design of the composite [kg/m^3]

	M6	M6 - 2CNT	M6 - 4CNT
OPC	237	237	237
BFS	553	553	553
LP	790	790	790
Water	411	398.2	385.4
PVA	26	26	26
CNT	0	13.2	26.4
Superplasticizer	1.4	1.4	1.4

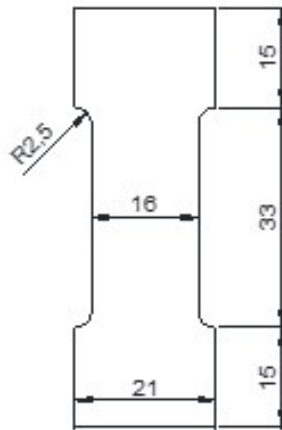


Figure 7.1: Dog-bone mould dimensions (in millimetres).

ing 27 days were in the curing room with a relative humidity higher than 95% and 20°C. Such small specimens were adopted on this research due to the use of CNT and the investigation of the electrical properties of the composite during the mechanical load. Regarding the necessity of employment of small specimens, it is believed that the internal diameter of 16mm will be enough to promote reasonable dispersion of PVA fibres.

Tensile test was performed using two LVDT's to control the average crack opening. The first 30µm of crack opening were performed at 0,02µm/s. From 30µm to 100µm the speed was increased to 0,1µm/s then, from 100µm to 600µm the speed was 0,5µm/s and the test was finished at 800µm at 1µm/s. Plexmon 7742 F two component glue was used to attach the specimen to the supporting screws mounted to the Instron machine (see 7.2). Young's modulus of the elastic phase and the tensile strength were calculated from the mechanical test results.

To measure the electrical impedance during the tensile test a function generator was employed delivering a voltage signal of 15V peak-to-peak amplitude using sine wave with frequency of 500Hz. The specimen impedance was measured in series with a known standard resistor of 100kΩ (see 7.3). To separate the resistance and capacitance mea-

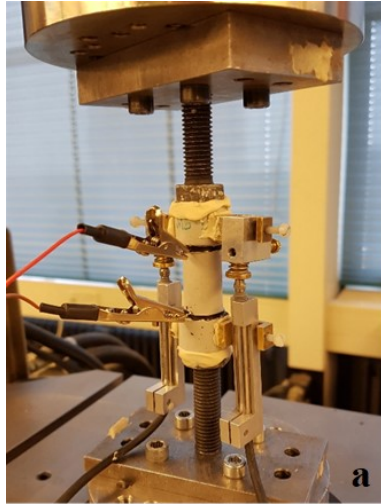


Figure 7.2: Direct tensile test set-up.

surement of the specimen, the phase angle between the current and voltage wave was utilized. Therefore, a real x imaginary plane with the impedance phasor can be used to calculate the real resistance and capacitance during loading.

A two probe electrical measurement was performed. The electrodes were glued on the surface of the specimen on the necking from the external diameter towards the internal diameter, using a conductive paint and a copper wire. In figure 7.2 the sample is prepared to be tested. The specimens were prepared on the 28th day and left under the lab conditions for one day, before the tensile test.

The measurement of the electrical impedance, resistance and capacitance were plotted as function of the average width of the crack. Moreover, the curve was divided in four segments to calculate the gauge factors according to Equation 7.1, where δZ is the

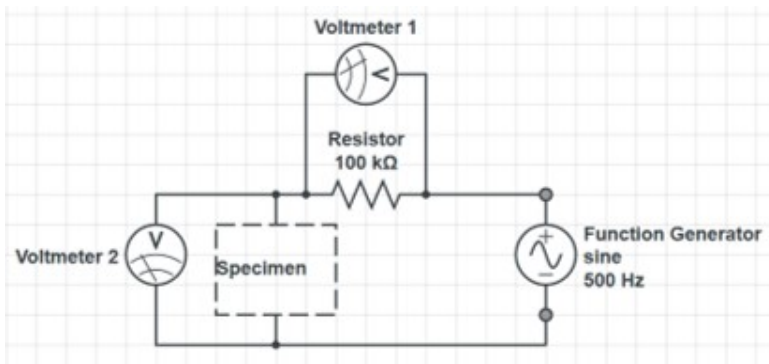


Figure 7.3: Diagram representing the electric circuit used.

Table 7.3: Average mechanical and initial electrical properties.

	M6	M6 - 2CNT	M6 - 4CNT
E [GPa]	11.2 ± 0.5	13.7 ± 4.1	12.3 ± 0.7
Maximum tensile strength [MPa]	3.4 ± 0.3	3.2 ± 0.4	2.9 ± 0.2
Z ₀ [kΩ]	247.6 ± 44.8	252.8 ± 57.0	180.2 ± 52.1
R ₀ [kΩ]	258.8 ± 49.4	259.8 ± 62.7	185.7 ± 55.9
C ₀ [pF]	371.8 ± 29.0	268.0 ± 13.0	416.8 ± 43.6

impedance changes, Z₀ is the impedance value before the test start and ε is the applied strain during the tensile test. This relation gives a quantitative method for ranking the sensitivity of the composite. The gauge factor from impedance changes is named GF, from resistance RF and capacitance CF. The number after indicates the maximum average crack opening from the analysed interval.

$$GF = \left(\frac{\Delta Z}{Z_0}\right)\left(\frac{1}{\epsilon}\right) \tag{7.1}$$

The segments correspond to the average crack opening from 0μm to 6μm, 6μm to 20μm, 20μm to 100μm and finally from 100μm to 800μm. The analysis of those factors will be helpful to evaluate the influence of different concentrations of CNT employed. To calculate the gauge factor, linear regression from the plot of the values of relative change on the electric properties (Impedance, Resistance and Capacitance) against the strain was adopted.

7.3. RESULTS AND DISCUSSION

Table 7.3 shows a summary of the mechanical and initial properties of the composite, where E, Z₀, R₀ and C₀ are the modulus of elasticity, initial impedance, resistance and capacitance, respectively. The addition of CNT on the SHCC did not change significantly the modulus of elasticity of the composite. However, a decrease on the tensile strength and ductility was observed. Nevertheless, strain hardening behaviour and multiple cracking was observed for all cases. An example is shown in Figure 7.4. The decrease of the mechanical properties was probably not caused by the CNT, but by the surfactant. This material is employed on the CNT solution to help on the dispersion of the nanoparticles. However, during the composite mixing process foam might be generated, introducing air pockets in the matrix and on the interface with the fibres.

Measured changes of the modulus of impedance were very similar to those reported by [32]. The development of cracks lead to an increase of the total resistance of the composite as can be observed in Figure 7.5. The employment of CNT enabled higher gauge factors calculated from the impedance measurement only for crack width up to 100μm.

Moreover, observing the evolution of the resistance and the capacitance during the tensile test, two different trends can be pointed out. The electrical resistance of the composite increases while the crack width increases and the capacitance goes backwards the opposite direction. By observing the Figure 7.6 and Figure 7.7, it is possible to note that the electrical resistance continuously increases while the damage propagates in the



Figure 7.4: Multiple cracks developed during tensile test.

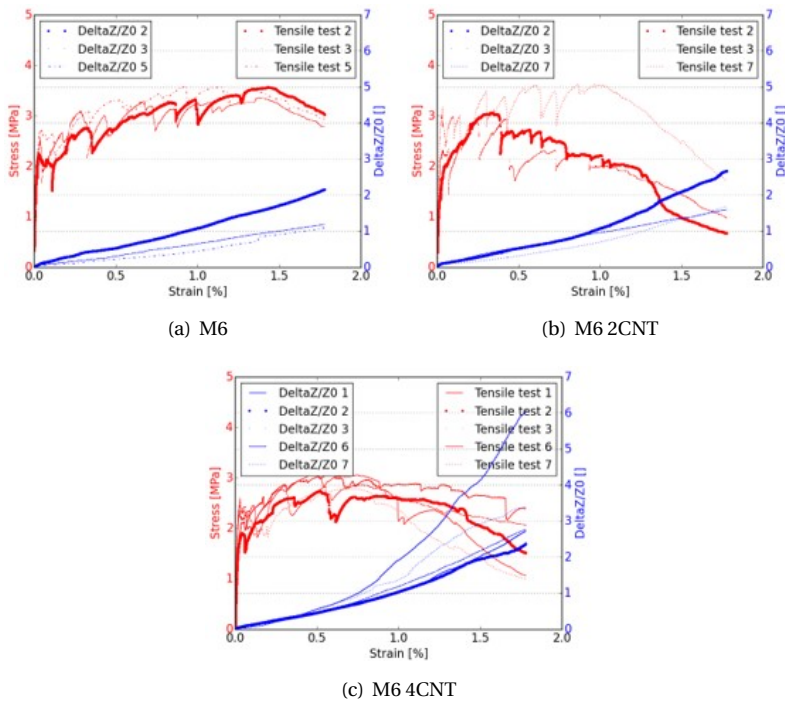


Figure 7.5: Fractional change on the electrical impedance during tensile test.

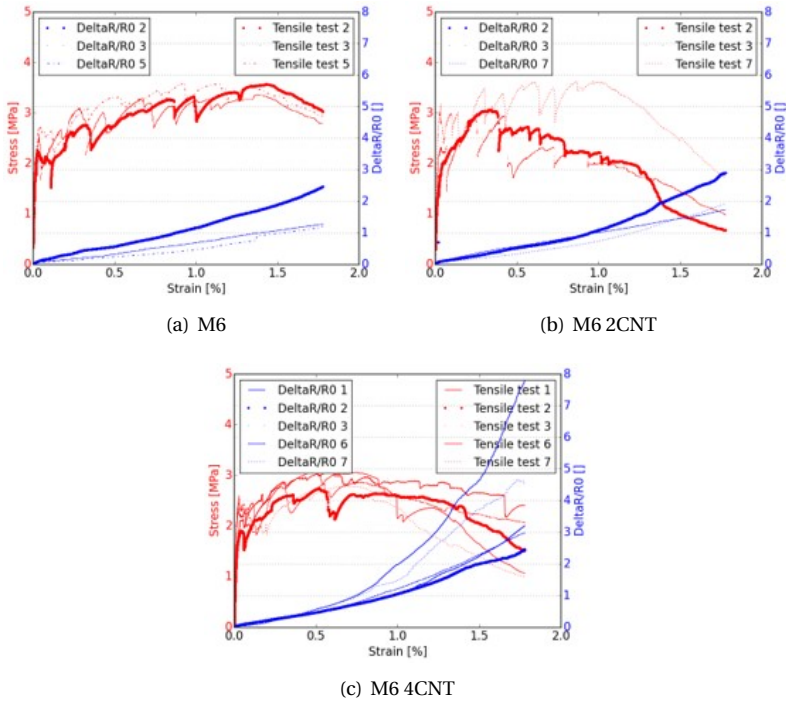


Figure 7.6: Fractional change on the electrical resistance during tensile test.

composite. On the other hand, the electrical capacitance fractional change tends to find a constant value for wide cracks. Therefore, the electrical capacitance changes are more valuable sensing mechanism for smaller damages than for large crack control.

During the tensile load the CNTs dispersed in the microstructure of the cementitious matrix tend to separate from each other. In [43] proposed an electrical model where the matrix between each CNT could be represented by an analogue electric circuit with a resistor in parallel to a capacitor. In this model, when the distance between the CNTs increases, the total impedance of the composite should increase, due to higher values of resistance and lower values of capacitance. The result found on this research matches with the experimental results and model proposed by [43].

To evaluate the efficiency of CNT employment on cementitious matrix as a piezoresistive sensor the gauge factor reported on Figure 7.8 must be taken into account. The electrical resistance of all mix designs evaluated on this study increased during the tensile test, demonstrating the capability of the SHCC to be employed as a damage sensor. The same result was found by [32]. However, only samples doped with CNT could bring slightly higher GF6 and RF6 for M6-2CNT and considerably higher CF100 and CF800 for M6-4CNT. This might mean that ordinary SHCC are good sensors for detection of small cracks, but CNT doped SHCC sensors could track the development of cracks.

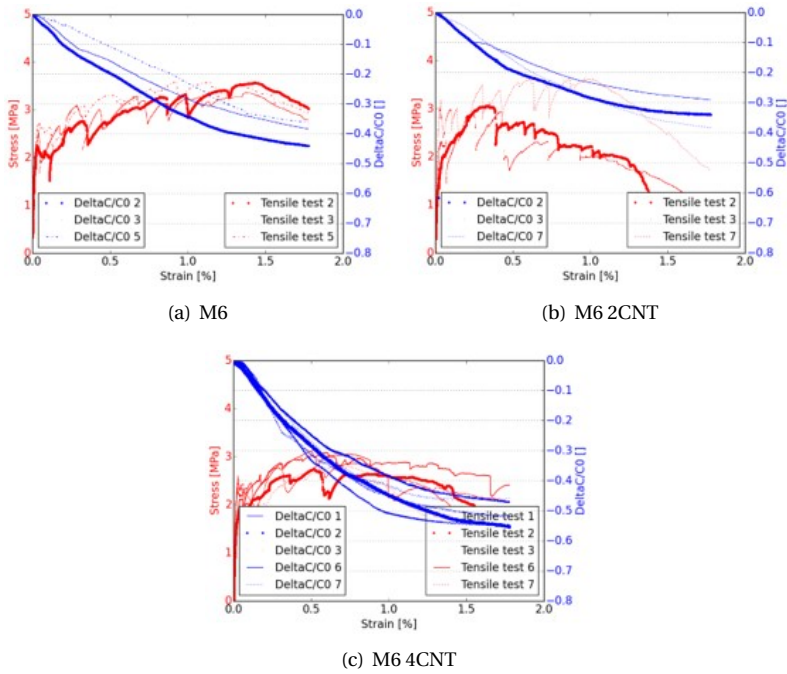


Figure 7.7: Fractional change on the electrical capacitance during tensile test.

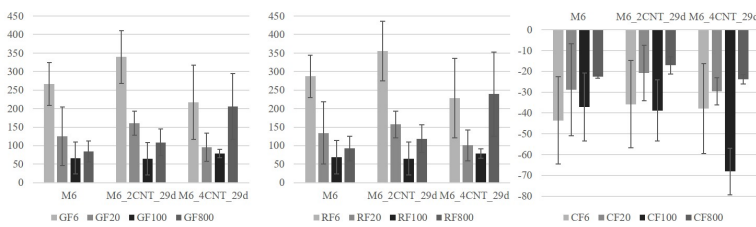


Figure 7.8: Average gauge factor calculated from: (a) Impedance modulus, (b) resistance and (c) capacitance.

7.4. CONCLUSIONS

The results found in this experimental work lead to the conclusion that the SHCC could be employed as a damage sensor, due to the increase of the modulus of the impedance. However, the use of piezoresistive admixtures as CNT can contribute to the measurement of the crack opening development.

The employment of AC, instead of DC on investigations performed on this field must be taken in account. The results of this paper have clearly shown the damage dependence of the resistance and capacitance. The fully understanding of changes on the total impedance values can clarify the entire mechanism behind it. The results have demonstrated that the changes on capacitance can also be used on measurement of smart cementitious materials.

Further research is needed on the piezoresistive mechanism of fibre reinforced cementitious composites. Older samples must be studied to understand the feasibility of this technique with the development of the hydration, temperature and moisture content. Recently, [245] demonstrated that moisture on mortar specimens with CNT lead the composite to lower sensitivity to strain variations. Moreover, the influence of ageing mechanism like carbonation, freeze and thaw or chloride attack must be comprehended to deliver durable and long term reliable sensors.

Nevertheless, in general the development of a self-sensing SHCC would be very beneficial due to the high importance of those composites for the repair industry, for structures built on seismic region and for a better control of the quality of the infrastructure during their service life.

8

CONCLUSION AND SUGGESTIONS FOR FURTHER RESEARCH

8.1. CONCLUSIONS

During this thesis the importance of a methodological and theoretical based process to develop materials was demonstrated. The use of those theories were fundamental to approach the problem of developing materials that could be applied for extrusion based additive manufacturing.

The research could successfully show that the use of a ram-extruder with the Benbow-Bridwater model can be very successful to study the rheological properties of printable materials. Moreover, the use of the initial bulk and shear yield stresses are important to predict the printability and buildability of mixtures.

The project could also address the lack of reinforcement in the printed elements. The use fibres or more especially the development of printable strain hardening cementitious composites has proved to be an interesting and feasible solution to the problem. Printed elements could deliver ductility when loaded in two different directions but still lacked reinforcement when two printed layers were pulled apart.

During the printable mixtures development it was also discovered the enormous importance of viscosity modifier admixtures to control the rheological properties. Mixtures with such material could present significant stability during the fresh state what has contributed to the positively to the printing technique. Samples with this admixture were less susceptible to drying, had a significantly longer dormant stage and the binders could reach higher degree of hydration. Furthermore, through microstructure investigations was also possible to prove that the formation of hydration products had a anomalous distribution in the matrix. Nevertheless, no hazardous modifications were found in investigated in cement pastes.

Due to the anomalous growth of portlandite in cementitious materials with hydroxypropyl methylcellulose (HPMC) and the larger amount of air voids a higher efficiency in the autogenous self-healing performance was also found in printable matrices. The images obtained from μ CT-scan could show the growth of healing products inside of a crack surface as well as in the inner walls of the air voids. Besides that the use of natural fibres as water reservoir were also found to be beneficial to the autogenous healing. They proved to work similarly to what was previously observed for super absorbent polymers. More stable healing performance was obtained in samples which were pre-treated, as they were less susceptible to the ageing during the proposed accelerated cycles.

Finally, in the end of the thesis investigations also proved the capabilities of carbon nanotubes doped strain hardening cementitious composites to work as a damage sensor. The use of impedance measurements were successfully proposed to quantify the progress of damage in samples loaded in tension. Therefore, in principle one would be able to print layers of this material to monitor the development of damages over a certain period of time.

In summary this thesis has covered a number of possibilities to add value and functionality to printing materials aiming the automation improvement. Ideally, a printable strain hardening cementitious composites with enhanced autogenous self-healing performance and damage sensibility was developed. However, creating new materials indeed solve some issues but definitely raises many more challenges and questions. Some of those are further approached in the following section.

8.2. SUGGESTIONS FOR FURTHER RESEARCH

Fortunately this research was conducted in a very recent and innovative environment. Nowadays, there are several groups and new projects starting to develop studies in this field. Along with the academia, companies have demonstrated strong interest in going further applying this new technique on their facilities as well. Therefore, from this study the following suggestions for future research are given:

- Arguably rheology is one of the research fields that has been under-researched when compared to concrete durability, reinforcement corrosion or high performance concretes for instance. Therefore, much more attention must be given into this area to develop the theoretical background needed for improvements in the extrusion based techniques. Developments such as the understanding of the composition of solid suspensions and the interaction between the solid and fluid phase shall contribute to the science of the fresh state of construction and building materials.
- One important step currently needed in extrusion based additive manufacturing of cementitious materials is incorporation of larger aggregates. So far, not many researches have approached this problem which culminates with the excessive use of fine particles or even binders in printable mixtures. The better understanding of the influence of the raw materials in the rheological properties might be the way to solve this important issue.
- The investigations shown in chapters 3, 4 and 5 have demonstrated the large amount of air-voids in printable materials, due to the use of HPMC. This large porosity in such type of composites might lead to accelerated ageing. In the case of materials with steel reinforcement this can be a significantly negative effect as those voids would facilitate the migration of hazardous materials such as chloride. In order to minimize presence of these voids vacuum is needed either in the mixing phase or in the extrusion process. This technique could improve mechanical and durability properties;
- Including reinforcement in printable materials is one of the most important topics of concern in this area. In order to keep the automation of the construction technique, and at the same time provide enough ductility to the material fibre reinforcement might be one of the most suitable solutions. However, to make sure that in a structural scale several ranges of crack widths could be covered some research will be needed in multi-scale fibre reinforcement. Ideally, fibres with different lengths, diameters, mechanical properties and compositions would be able to cover a larger range of cracks providing the needed ductility;
- Extrusion based additive manufacturing brings the opportunity to place the material precisely where it is needed. This possibility emphasizes the opportunity to incorporate the most advanced materials developed so far in very low contents. For instance, using high ductility materials only in layers where they are needed or incorporating self-healing mixtures only where cracking could be deleterious.

Therefore, the use of different types of materials simultaneously in the same element must be a matter of research to understand the consequences of such use.

- Incorporating automation in the construction industry up to the durability of the element is one of the most challenge topics. Including the ability to self-repair in the next generation of materials sounds very promising and needed. The incorporation of different self-healing techniques in printable materials is needed.
- Further research on strain or damage sensitive cementitious composites is needed. This technique has shown potential to be applied in an on-line durability surveillance of infrastructure. However, further research is needed regarding the influence of ageing of the cementitious composites on the electrical impedance measurements. Moreover, investigations regarding the use of different piezoresistive fillers such as carbon fibres or the influence of the surrounding conditions in the measurement are also necessary.

REFERENCES

REFERENCES

- [1] S. C. Figueiredo, O. Çopuroğlu, E. Schlangen, Smart constructions: An overview from the building phase to the durability surveillance, in: Proceedings of the 13th International Congress on Advances in Civil Engineering, September 2018, Izmir, 2018.
- [2] O. Salem, J. Solomon, A. Genaidy, M. Luegring, Site Implementation and Assessment of Lean Construction Techniques, *Lean Construction Journal* 2 (2) (2005) 1–21.
- [3] L. S. Pheng, M. S. Hui, Implementing and Applying Six Sigma in Construction, *Journal of Construction Engineering and Management* 130 (4) (2004) 482–489. doi:10.1061/(ASCE)0733-9364(2004)130:4(482).
- [4] R. O. Asamoah, J. S. Ankrah, K. Offei-nyako, E. O. Tutu, Cost Analysis of Precast and Cast-in-Place Concrete Construction for Selected Public Buildings in Ghana, *Journal of Construction Engineering* 2016 (2016).
- [5] E. Sachs, M. Cima, J. Cornie, D. Brancazio, J. Bredt, A. Curodeau, T. Fan, S. Khanuja, A. Lauder, J. Lee, S. Michaels, Three-Dimensional Printing: The Physics and Implications of Additive Manufacturing, *CIRP Annals - Manufacturing Technology* 42 (1) (1993) 257–260. doi:10.1016/S0007-8506(07)62438-X.
- [6] H. Kodama, Automatic method for fabricating a three-dimensional plastic model with photo-hardening polymer, *Review of Scientific Instruments* 52 (11) (1981) 1770–1773. doi:10.1063/1.1136492.
- [7] P. Feng, X. Meng, J.-F. Chen, L. Ye, Mechanical properties of structures 3D printed with cementitious powders, *Construction and Building Materials* 93 (2015) 486–497. doi:10.1016/j.conbuildmat.2015.05.132.
URL <http://dx.doi.org/10.1016/j.conbuildmat.2015.05.132>
- [8] Z. Zhou, F. Buchanan, C. Mitchell, N. Dunne, Printability of calcium phosphate: Calcium sulfate powders for the application of tissue engineered bone scaffolds using the 3D printing technique, *Materials Science and Engineering C* 38 (1) (2014) 1–10. doi:10.1016/j.msec.2014.01.027.
URL <http://dx.doi.org/10.1016/j.msec.2014.01.027>
- [9] X. Wang, M. Jiang, Z. Zhou, J. Gou, D. Hui, 3D printing of polymer matrix composites: A review and prospective, *Composites Part B: Engineering* 110 (2017) 442–458. doi:10.1016/j.compositesb.2016.11.034.
URL <http://dx.doi.org/10.1016/j.compositesb.2016.11.034>
- [10] S. F. S. Shirazi, S. Gharehkhani, M. Mehrali, H. Yarmand, H. S. C. Metselaar, N. Adib Kadri, N. A. A. Osman, A review on powder-based additive manufacturing for tissue engineering: Selective laser sintering and inkjet 3D printing, *Science and Technology of Advanced Materials* 16 (3) (2015). doi:10.1088/1468-6996/16/3/033502.
- [11] B. Khoshnevis, Automated construction by contour crafting - Related robotics and information technologies, *Automation in Construction* 13 (1) (2004) 5–19. doi:10.1016/j.autcon.2003.08.012.
- [12] B. Zareiyan, B. Khoshnevis, Effects of interlocking on interlayer adhesion and strength of structures in 3d printing of concrete, *Automation in Construction* 83 (2017) 212 – 221. doi:https://doi.org/10.1016/j.autcon.2017.08.019.
URL <http://www.sciencedirect.com/science/article/pii/S0926580516303703>

- [13] A. Kazemian, X. Yuan, E. Cochran, B. Khoshnevis, [Cementitious materials for construction-scale 3D printing: Laboratory testing of fresh printing mixture](#), *Construction and Building Materials* 145 (2017) 639–647. doi:10.1016/j.conbuildmat.2017.04.015.
URL <http://dx.doi.org/10.1016/j.conbuildmat.2017.04.015>
- [14] C. Gosselin, R. Duballet, P. Roux, N. Gaudillière, J. Dirrenberger, P. Morel, [Large-scale 3D printing of ultra-high performance concrete - a new processing route for architects and builders](#), *Materials and Design* 100 (2016) 102–109. doi:10.1016/j.matdes.2016.03.097.
URL <http://dx.doi.org/10.1016/j.matdes.2016.03.097>
- [15] D. Asprone, F. Auricchio, C. Menna, V. Mercuri, [3D printing of reinforced concrete elements: Technology and design approach](#), *Construction and Building Materials* 165 (2018) 218–231. doi:10.1016/j.conbuildmat.2018.01.018.
URL <https://doi.org/10.1016/j.conbuildmat.2018.01.018>
- [16] G. Ma, Z. Li, L. Wang, [Printable properties of cementitious material containing copper tailings for extrusion based 3D printing](#), *Construction and Building Materials* 162 (2018) 613–627. doi:10.1016/j.conbuildmat.2017.12.051.
URL <https://doi.org/10.1016/j.conbuildmat.2017.12.051>
- [17] J. J. Benbow, The dependence of output rate on die shape during catalyst extrusion, *Chemical Engineering Science* 26 (1971) 1467–1473.
- [18] R. Teixeira, G. Tonoli, S. Santos, J. Fiorelli, H. Savastano Jr., F. R. Lahr, [Extruded Cement Based Composites Reinforced with Sugar Cane Bagasse Fibres](#), *Key Engineering Materials* 517 (2012) 450–457. doi:10.4028/www.scientific.net/KEM.517.450.
- [19] F. P. Bos, Z. Y. Ahmed, E. R. Jutinov, T. A. Salet, [Experimental exploration of metal cable as reinforcement in 3D printed concrete](#), *Materials* 10 (11) (2017). doi:10.3390/ma10111314.
- [20] L. Alonso, J. Barbarán, J. Chen, M. Díaz, L. Llopis, B. Rubio, [Middleware and communication technologies for structural health monitoring of critical infrastructures: A survey](#), *Computer Standards and Interfaces* 56 (September 2017) (2018) 83–100. doi:10.1016/j.csi.2017.09.007.
URL <https://doi.org/10.1016/j.csi.2017.09.007>
- [21] V. C. Li, H. Horii, P. Kabele, T. Kanda, Y. Lim, [Repair and retrofit with engineered cementitious composites](#), *Engineering Fracture Mechanics* 65 (2-3) (2000) 317–334. doi:10.1016/S0013-7944(99)00117-4.
- [22] J. M. Ko, Y. Q. Ni, [Technology developments in structural health monitoring of large-scale bridges](#), *Engineering Structures* 27 (12 SPEC. ISS.) (2005) 1715–1725. doi:10.1016/j.engstruct.2005.02.021.
- [23] F. Magalhães, A. Cunha, E. Caetano, [Vibration based structural health monitoring of an arch bridge: From automated OMA to damage detection](#), *Mechanical Systems and Signal Processing* 28 (2012) 212–228. doi:10.1016/j.ymsp.2011.06.011.
- [24] H. Li, H. G. Xiao, J. Yuan, J. Ou, [Microstructure of cement mortar with nano-particles](#), *Composites Part B: Engineering* 35 (2) (2004) 185–189. doi:10.1016/S1359-8368(03)00052-0.
- [25] B. Han, S. Ding, X. Yu, [Intrinsic self-sensing concrete and structures: A review](#), *Measurement: Journal of the International Measurement Confederation* 59 (2015) 110–128. doi:10.1016/j.measurement.2014.09.048.
URL <http://dx.doi.org/10.1016/j.measurement.2014.09.048>
- [26] S. Wen, D. D. L. Chung, [Defect dynamics of cement paste under repeated compression studied by electrical resistivity measurement](#), *Cement and Concrete Research* 31 (10) (2001) 1515–1518. doi:10.1016/S0008-8846(01)00604-4.

- [27] M. S. Konsta-Gdoutos, C. A. Aza, [Self sensing carbon nanotube \(CNT\) and nanofiber \(CNF\) cementitious composites for real time damage assessment in smart structures](#), *Cement and Concrete Composites* 53 (2014) 162–169. doi:10.1016/j.cemconcomp.2014.07.003.
URL <http://dx.doi.org/10.1016/j.cemconcomp.2014.07.003>
- [28] I. Rhee, J. S. Lee, Y. A. Kim, J. H. Kim, [Electrically conductive cement mortar: Incorporating rice husk-derived high-surface-area graphene](#), *Construction and Building Materials* 125 (2016) 632–642. doi:10.1016/j.conbuildmat.2016.08.089.
URL <http://dx.doi.org/10.1016/j.conbuildmat.2016.08.089>
- [29] H. Xiao, H. Li, J. Ou, [Self-monitoring properties of concrete columns with embedded cement-based strain sensors](#), *Journal of Intelligent Material Systems and Structures* 22 (2) (2011) 191–200. doi:10.1177/1045389X10396573.
- [30] F. Azhari, N. Banthia, [Cement-based sensors with carbon fibers and carbon nanotubes for piezoresistive sensing](#), *Cement and Concrete Composites* 34 (7) (2012) 866–873. doi:10.1016/j.cemconcomp.2012.04.007.
URL <http://dx.doi.org/10.1016/j.cemconcomp.2012.04.007>
- [31] D. D. L. Chung, [Damage in cement-based materials, studied by electrical resistance measurement](#), Vol. 42, 2003. doi:10.1016/S0927-796X(03)00037-8.
- [32] R. Ranade, J. Zhang, J. P. Lynch, V. C. Li, [Influence of micro-cracking on the composite resistivity of Engineered Cementitious Composites](#), *Cement and Concrete Research* 58 (2014) 1–12. doi:10.1016/j.cemconres.2014.01.002.
URL <http://dx.doi.org/10.1016/j.cemconres.2014.01.002>
- [33] D. L. Nguyen, J. Song, C. Manathamsombat, D. J. Kim, [Comparative electromechanical damage-sensing behaviors of six strain-hardening steel fiber-reinforced cementitious composites under direct tension](#), *Composites Part B: Engineering* 69 (2014) 159–168. doi:10.1016/j.compositesb.2014.09.037.
URL <http://dx.doi.org/10.1016/j.compositesb.2014.09.037>
- [34] X. Fu, W. Lu, D. D. L. Chung, [Ozone treatment of carbon fiber for reinforcing cement](#), *Carbon* 36 (9) (1998) 1337–1345. doi:10.1016/S0008-6223(98)00115-8.
- [35] B. Han, Y. Wang, S. Dong, L. Zhang, S. Ding, X. Yu, J. Ou, [Smart concretes and structures: A review](#), *Journal of Intelligent Material Systems and Structures* 26 (11) (2015) 1045389X15586452–. doi:10.1177/1045389X15586452.
URL <http://jim.sagepub.com/content/early/2015/05/21/1045389X15586452.abstract>
- [36] J. Hoheneder, I. Flores-Vivian, Z. Lin, P. Zilberman, K. Sobolev, [The performance of stress-sensing smart fiber reinforced composites in moist and sodium chloride environments](#), *Composites Part B: Engineering* 73 (2015) 89–95. doi:10.1016/j.compositesb.2014.12.028.
URL <http://dx.doi.org/10.1016/j.compositesb.2014.12.028>
- [37] D. T. Figueiredo, A. A. S. Correia, D. Hunkeler, M. G. B. Rasteiro, [Surfactants for dispersion of carbon nanotubes applied in soil stabilization](#), *Colloids and Surfaces A: Physicochemical and Engineering Aspects* 480 (2015) 405–412. doi:10.1016/j.colsurfa.2014.12.027.
URL <http://linkinghub.elsevier.com/retrieve/pii/S0927775714009479>
- [38] P. Ludvig, J. M. Calixto, L. O. Ladeira, I. C. P. Gaspar, [Using converter dust to produce low cost cementitious composites by in situ carbon nanotube and nanofiber synthesis](#), *Materials* 4 (3) (2010) 575–584. doi:10.3390/ma4030575.
- [39] J. N. de Paula, J. M. Calixto, L. O. Ladeira, P. Ludvig, T. C. C. Souza, J. M. Rocha, A. A. V. de Melo, [Mechanical and rheological behavior of oil-well cement slurries produced with clinker containing carbon nanotubes](#), *Journal of Petroleum Science and Engineering* 122 (2014) 274 – 279. doi:<https://doi.org/10.1016/j.petrol.2014.07.020>.
URL <http://www.sciencedirect.com/science/article/pii/S0920410514002186>

- [40] M. S. Konsta-Gdoutos, Z. S. Metaxa, S. P. Shah, [Multi-scale mechanical and fracture characteristics and early-age strain capacity of high performance carbon nanotube/cement nanocomposites](#), *Cement and Concrete Composites* 32 (2) (2010) 110–115. doi:10.1016/j.cemconcomp.2009.10.007. URL <http://dx.doi.org/10.1016/j.cemconcomp.2009.10.007>
- [41] S. Wen, D. D. L. Chung, [Electric polarization in carbon fiber-reinforced cement](#), *Cement and Concrete Research* 31 (1) (2001) 141–147. doi:10.1016/S0008-8846(00)00382-3.
- [42] B. Han, X. Guan, J. Ou, [Electrode design, measuring method and data acquisition system of carbon fiber cement paste piezoresistive sensors](#), *Sensors and Actuators, A: Physical* 135 (2) (2007) 360–369. doi:10.1016/j.sna.2006.08.003. URL <http://dx.doi.org/10.1016/j.sna.2006.08.003>
- [43] A. Sanli, C. Müller, O. Kanoun, C. Elibol, M. F. X. Wagner, [Piezoresistive characterization of multi-walled carbon nanotube-epoxy based flexible strain sensitive films by impedance spectroscopy](#), *Composites Science and Technology* 122 (2016) 18–26. doi:10.1016/j.compscitech.2015.11.012.
- [44] S. Figueiredo, O. Çopuroğlu, B. Şavija, E. Schlangen, [Piezoresistive properties of cementitious composites reinforced by PVA fibres](#), Vol. 15, 2018. doi:10.1007/978-94-024-1194-2_81.
- [45] M. Saleem, M. Shameem, S. E. Hussain, M. Maslehuiddin, [Effect of moisture, chloride and sulphate contamination on the electrical resistivity of Portland cement concrete](#), *Construction and Building Materials* 10 (3) (1996) 209–214. doi:10.1016/0950-0618(95)00078-X.
- [46] P. C. Aitcin, [The durability characteristics of high performance concrete: A review](#), *Cement and Concrete Composites* 25 (4-5 SPEC) (2003) 409–420. doi:10.1016/S0958-9465(02)00081-1.
- [47] N. Hearn, [Self-sealing, autogenous healing and continued hydration: What is the difference?](#), *Materials and Structures* 31 (8) (1998) 563–567. doi:10.1007/BF02481539. URL <http://link.springer.com/article/10.1007/BF02481539>{%}5Cnhttp://link.springer.com/content/pdf/10.1007/2FBF02481539.pdf
- [48] S. Granger, A. Loukili, G. Pijaudier-Cabot, G. Chanvillard, [Experimental characterization of the self-healing of cracks in an ultra high performance cementitious material: Mechanical tests and acoustic emission analysis](#), *Cement and Concrete Research* 37 (4) (2007) 519–527. doi:10.1016/j.cemconres.2006.12.005.
- [49] D. Snoeck, O. M. Jensen, N. De Belie, [The influence of superabsorbent polymers on the autogenous shrinkage properties of cement pastes with supplementary cementitious materials](#), *Cement and Concrete Research* 74 (2015) 59–67. doi:10.1016/j.cemconres.2015.03.020. URL <http://dx.doi.org/10.1016/j.cemconres.2015.03.020>
- [50] D. Fukuda, Y. Nara, Y. Kobayashi, M. Maruyama, M. Koketsu, D. Hayashi, H. Ogawa, K. Kaneko, [Investigation of self-sealing in high-strength and ultra-low-permeability concrete in water using micro-focus X-ray CT](#), *Cement and Concrete Research* 42 (11) (2012) 1494–1500. doi:10.1016/j.cemconres.2012.08.014. URL <http://dx.doi.org/10.1016/j.cemconres.2012.08.014>
- [51] D. Snoeck, N. De Belie, [From straw in bricks to modern use of microfibers in cementitious composites for improved autogenous healing - A review](#), *Construction and Building Materials* 95 (2015) 774–787. doi:10.1016/j.conbuildmat.2015.07.018. URL <http://dx.doi.org/10.1016/j.conbuildmat.2015.07.018>
- [52] S. Zhu, D. D. L. Chung, [Theory of piezoresistivity for strain sensing in carbon fiber reinforced cement under flexure](#), *Journal of Materials Science* 42 (15) (2007) 6222–6233. doi:10.1007/s10853-006-1131-3.

- [53] D. Snoeck, D. Schaubroeck, P. Dubruel, N. De Belie, [Effect of high amounts of superabsorbent polymers and additional water on the workability, microstructure and strength of mortars with a water-to-cement ratio of 0.50](#), *Construction and Building Materials* 72 (2014) 148–157. doi:10.1016/j.conbuildmat.2014.09.012.
URL <http://dx.doi.org/10.1016/j.conbuildmat.2014.09.012>
- [54] M. Wu, B. Johannesson, M. Geiker, [A review: Self-healing in cementitious materials and engineered cementitious composite as a self-healing material](#), *Construction and Building Materials* 28 (1) (2012) 571–583. doi:10.1016/j.conbuildmat.2011.08.086.
URL <http://dx.doi.org/10.1016/j.conbuildmat.2011.08.086>
- [55] H. M. Jonkers, A. Thijssen, G. Muyzer, O. Copuroglu, E. Schlangen, [Application of bacteria as self-healing agent for the development of sustainable concrete](#), *Ecological Engineering* 36 (2) (2010) 230–235. doi:10.1016/j.ecoleng.2008.12.036.
- [56] D. Palin, H. M. Jonkers, V. Wiktor, [Autogenous healing of sea-water exposed mortar: Quantification through a simple and rapid permeability test](#), *Cement and Concrete Research* 84 (2016) 1–7. doi:10.1016/j.cemconres.2016.02.011.
URL <http://dx.doi.org/10.1016/j.cemconres.2016.02.011>
- [57] V. Wiktor, H. M. Jonkers, [Field performance of bacteria-based repair system: Pilot study in a parking garage](#), *Case Studies in Construction Materials* 2 (2015) 11–17. arXiv:Amsterdam, The Netherlands, ., doi:10.1016/j.cscm.2014.12.004.
URL <http://dx.doi.org/10.1016/j.cscm.2014.12.004>
- [58] C. Joseph, A. Jefferson, B. Isaacs, R. Lark, D. Gardner, [Experimental investigation of adhesive-based self-healing of cementitious materials](#), *Magazine of Concrete Research* 62 (11) (2010) 831–843. doi:10.1680/macr.2010.62.11.831.
URL <http://www.icevirtuallibrary.com/doi/10.1680/macr.2010.62.11.831>
- [59] K. Sisomphon, O. Copuroglu, E. A. B. Koenders, [Effect of exposure conditions on self healing behavior of strain hardening cementitious composites incorporating various cementitious materials](#), *Construction and Building Materials* 42 (2013) 217–224. doi:10.1016/j.conbuildmat.2013.01.012.
URL <http://dx.doi.org/10.1016/j.conbuildmat.2013.01.012>
- [60] S. C. Figueiredo, C. R. Rodríguez, Z. Y. Ahmed, D. Bos, Y. Xu, T. M. Salet, O. Çopuroğlu, E. Schlangen, F. P. Bos, [An approach to develop printable strain hardening cementitious composites](#), *Materials & Design* 169 (2019) 107651. doi:https://doi.org/10.1016/j.matdes.2019.107651.
URL <http://www.sciencedirect.com/science/article/pii/S0264127519300887>
- [61] B. E. Allmon, C. T. Haas, J. D. Borcherding, P. M. Goodrum, U. S. Construction Labor Productivity Trends, 1970–1998, *Journal of construction engineering and management* 126 (April) (2000) 97–104.
- [62] R. R. Ramrez, L. F. C. Alarcón, P. Knights, [Benchmarking System for Evaluating Management Practices in the Construction Industry](#), *Journal of Management in Engineering* 20 (3) (2004) 110–117. doi:10.1061/(ASCE)0742-597X(2004)20:3(110).
URL [http://ascelibrary.org/doi/10.1061/\(%\)28ASCE\(%\)290742-597X\(%\)282004\(%\)2920\(%\)3A3\(%\)28110\(%\)29](http://ascelibrary.org/doi/10.1061/(%)28ASCE(%)290742-597X(%)282004(%)2920(%)3A3(%)28110(%)29)
- [63] A. C. De Leon, Q. Chen, N. B. Palaganas, J. O. Palaganas, J. Manapat, R. C. Advincola, [High performance polymer nanocomposites for additive manufacturing applications](#), *Reactive and Functional Polymers* 103 (2016) 141–155. doi:10.1016/j.reactfunctpolym.2016.04.010.
URL <http://dx.doi.org/10.1016/j.reactfunctpolym.2016.04.010>
- [64] L. E. Murr, S. M. Gaytan, F. Medina, E. Martinez, J. L. Martinez, D. H. Hernandez, B. I. Machado, D. A. Ramirez, R. B. Wicker, [Characterization of Ti-6Al-4V open cellular foams fabricated by additive manufacturing using electron beam melting](#), *Materials Science and Engineering A* 527 (7-8) (2010) 1861–1868. doi:10.1016/j.msea.2009.11.015.
URL <http://dx.doi.org/10.1016/j.msea.2009.11.015>

- [65] J. Luo, H. Pan, E. C. Kinzel, [Additive Manufacturing of Glass](#), *Journal of Manufacturing Science and Engineering* 136 (6) (2014) 061024. doi:10.1115/1.4028531.
URL <http://manufacturingscience.asmedigitalcollection.asme.org/article.aspx?doi=10.1115/1.4028531>
- [66] J. Willmann, M. Knauss, T. Bonwetsch, A. A. Apolinarska, F. Gramazio, M. Kohler, [Robotic timber construction - Expanding additive fabrication to new dimensions](#), *Automation in Construction* 61 (2016) 16–23. doi:10.1016/j.autcon.2015.09.011.
URL <http://dx.doi.org/10.1016/j.autcon.2015.09.011>
- [67] D. Herzog, V. Seyda, E. Wycisk, C. Emmelmann, [Additive manufacturing of metals](#), *Acta Materialia* 117 (2016) 371–392. doi:10.1016/j.actamat.2016.07.019.
URL <http://dx.doi.org/10.1016/j.actamat.2016.07.019>
- [68] D-Shape, [What is D-Shape](#).
URL <https://d-shape.com/what-is-it/>
- [69] S. Lim, R. A. Buswell, T. T. Le, S. A. Austin, A. G. Gibb, T. Thorpe, Developments in construction-scale additive manufacturing processes, *Automation in Construction* 21 (1) (2012) 262–268. arXiv:NIHMS150003, doi:10.1016/j.autcon.2011.06.010.
- [70] E. Lloret Fritschi, L. Reiter, T. Wangler, F. Gramazio, M. Kohler, R. J. Flatt, [SMART DYNAMIC CASTING SLIPFORMING WITH FLEXIBLE FORMWORK - INLINE MEASUREMENT AND CONTROL](#), in: HPC/CIC Tromsø 2017. Eleventh High Performance Concrete (11th HPC) and the Second Concrete Innovation Conference (2nd CIC), Norwegian Concrete Association, Tromsø, 2017. doi:10.3929/ETHZ-B-000225616.
URL <https://doi.org/10.3929/ethz-b-000219663>
- [71] N. Hack, W. V. Lauer, [Mesh-Mould: Robotically Fabricated Spatial Meshes as Reinforced Concrete Formwork](#), *Architectural Design* 84 (3) (2014) 44–53. arXiv:arXiv:1011.1669v3, doi:10.1002/ad.1753.
URL <http://doi.wiley.com/10.1002/ad.1753>
- [72] F. Bos, R. Wolfs, Z. Ahmed, T. Salet, Additive manufacturing of concrete in construction: potentials and challenges of 3D concrete printing, *Virtual and Physical Prototyping* 11 (3) (2016) 209–225. doi:10.1080/17452759.2016.1209867.
- [73] Y. W. D. Tay, B. Panda, S. C. Paul, N. A. N. Mohamed, M. J. Tan, K. F. Leong, [3d printing trends in building and construction industry: a review](#), *Virtual and Physical Prototyping* 12 (3) (2017) 261–276. arXiv: <https://doi.org/10.1080/17452759.2017.1326724>, doi:10.1080/17452759.2017.1326724.
URL <https://doi.org/10.1080/17452759.2017.1326724>
- [74] D. Delgado, P. Clayton, W. J. O. Brien, C. Seepersad, M. Juenger, R. Ferron, S. Salamone, [Applications of additive manufacturing in the construction industry – A forward-looking review](#), *Automation in Construction* 89 (August 2017) (2018) 110–119. doi:10.1016/j.autcon.2017.12.031.
URL <https://doi.org/10.1016/j.autcon.2017.12.031>
- [75] H. A. Jassmi, F. A. Najjar, A.-h. I. Mourad, Large-Scale 3D Printing : The Way Forward Large-Scale 3D Printing : The Way Forward, in: IOP Conf. Series: Materials Science and Engineering, IOP Publishing, 2018, p. 324. doi:10.1088/1757-899X/324/1/012088.
- [76] B. Nematollahi, M. Xia, J. Sanjayan, Current Progress of 3D Concrete Printing Technologies, in: 34th International Symposium on Automation and Robotics in Construction (ISARC 2017), Taipei, Taiwan, 2017.
- [77] S. Hamidreza, J. Corker, M. Fan, Additive manufacturing technology and its implementation in construction as an eco-innovative solution, *Automation in Construction* 93 (May) (2018) 1–11. doi:10.1016/j.autcon.2018.05.005.

- [78] R. Buswell, [3D printing using concrete extrusion: a roadmap for research](#), *Cement and Concrete Research* (May) (2018) (this issue). doi:10.1016/j.cemconres.2018.05.006. URL <https://doi.org/10.1016/j.cemconres.2018.05.006>
- [79] M. A. Guowei, W. Li, J. U. Yang, State-of-the-art of 3D printing technology of cementitious material — An emerging technique for construction, *Science China Technological Sciences* 61 (4) (2018) 475–495. doi:10.1007/s11431-016-9077-7.
- [80] Agence France-Presse, [World's first 3D-printed bridge opens to cyclists in Netherlands](#) (2017). URL <https://www.theguardian.com/technology/2017/oct/18/world-first-3d-printed-bridge-cyclists-net>
- [81] K. Subrin, T. Bressac, S. Garnier, A. Ambiehl, E. Paquet, B. Furet, [Improvement of the mobile robot location dedicated for habitable house construction by 3d printing](#), *IFAC-PapersOnLine* 51 (11) (2018) 716 – 721, 16th IFAC Symposium on Information Control Problems in Manufacturing INCOM 2018. doi:<https://doi.org/10.1016/j.ifacol.2018.08.403>. URL <http://www.sciencedirect.com/science/article/pii/S2405896318315295>
- [82] R. A. Buswell, R. C. Soar, A. G. F. Gibb, A. Thorpe, Freeform Construction: Mega-scale Rapid Manufacturing for construction, *Automation in Construction* 16 (2) (2007) 224–231. doi:10.1016/j.autcon.2006.05.002.
- [83] P. Wu, J. Wang, X. Wang, [A critical review of the use of 3-D printing in the construction industry](#), *Automation in Construction* 68 (2016) 21–31. doi:10.1016/j.autcon.2016.04.005. URL <http://dx.doi.org/10.1016/j.autcon.2016.04.005>
- [84] G. D. Schutter, K. Lesage, V. Mechtcherine, V. Naidu, G. Habert, I. Agusti-juan, [Cement and Concrete Research Vision of 3D printing with concrete — Technical , economic and environmental potentials](#), *Cement and Concrete Research* 112 (August) (2018) 25–36. doi:10.1016/j.cemconres.2018.06.001. URL <https://doi.org/10.1016/j.cemconres.2018.06.001>
- [85] V. Nerella, V. N., Krause, M., Näther, M., Mechtcherine, 3D printing technology for on-site construction, *Concr. Plant Int* (2016) 36–41.
- [86] V. N. Schach, R.; Krause, M.; Näther, M.; Nerella, CONPrint3D: 3D concrete-printing as an alternative for masonry, *Bauingenieur* 9 (2017) 355–363.
- [87] R. Duballet, O. Baverel, J. Dirrenberger, [Space Truss Masonry Walls With Robotic Mortar Extrusion](#), *Structures* (November) (2018) 1–7. doi:10.1016/j.istruc.2018.11.003. URL <https://doi.org/10.1016/j.istruc.2018.11.003>
- [88] B. Panda, S. Chandra Paul, M. Jen Tan, [Anisotropic mechanical performance of 3D printed fiber reinforced sustainable construction material](#), *Materials Letters* 209 (2017) 146–149. doi:10.1016/j.matlet.2017.07.123. URL <https://doi.org/10.1016/j.matlet.2017.07.123>
- [89] Y. Weng, M. Li, Z. Liu, W. Lao, B. Lu, D. Zhang, M. J. Tan, [Printability and fire performance of a developed 3d printable fibre reinforced cementitious composites under elevated temperatures](#), *Virtual and Physical Prototyping* 0 (0) (2018) 1–9. arXiv:<https://doi.org/10.1080/17452759.2018.1555046>, doi:10.1080/17452759.2018.1555046. URL <https://doi.org/10.1080/17452759.2018.1555046>
- [90] F. P. Bos, Z. Y. Ahmed, R. J. M. Wolfs, T. A. M. Salet, 3d printing concrete with reinforcement, in: D. Hordijk, M. Luković (Eds.), *High Tech Concrete: Where Technology and Engineering Meet*, Springer International Publishing, Cham, 2018, pp. 2484–2493.
- [91] V. C. Li, [On engineered cementitious composites \(ECC\). A review of the material and its applications](#), *Journal of Advanced Concrete Technology* 1 (3) (2003) 215–230. doi:10.3151/jact.1.215. URL <http://jlc.jst.go.jp/JST.JSTAGE/jact/1.215?from=Google>

- [92] S. Müller, V. Mechtcherine, [Fatigue behaviour of strain-hardening cement-based composites \(SHCC\)](#), *Cement and Concrete Research* 92 (2017) 75–83. doi:10.1016/j.cemconres.2016.11.003. URL <http://dx.doi.org/10.1016/j.cemconres.2016.11.003>
- [93] F. Altmann, V. Mechtcherine, [Durability design strategies for new cementitious materials](#), *Cement and Concrete Research* 54 (2013) 114–125. doi:10.1016/j.cemconres.2013.08.008. URL <http://dx.doi.org/10.1016/j.cemconres.2013.08.008>
- [94] D. G. Soltan, V. C. Li, [A self-reinforced cementitious composite for building-scale 3d printing](#), *Cement and Concrete Composites* 90 (2018) 1 – 13. doi:<https://doi.org/10.1016/j.cemconcomp.2018.03.017>. URL <http://www.sciencedirect.com/science/article/pii/S095894651730536X>
- [95] V. N. Nerella, H. Ogura, V. Mechtcherine, [Incorporating reinforcement into digital concrete construction](#), in: *Proceedings of the IASS Symposium 2018 Creativity in Structural Design*, Boston, 2018.
- [96] M. Rubio, M. Sonebi, S. Amziane, [3D PRINTING OF FIBRE CEMENT-BASED MATERIALS: FRESH AND RHEOLOGICAL PERFORMANCES](#), in: S. AMZIANE, M. SONEBI (Eds.), *2nd International Conference On Bio-Based Building Materials*, RILEM, 119 (PRO 119), Clermont Ferrand, 2017. URL <http://www.rilem.org/gene/main.php?base=500218>
- [97] R. J. Wolfs, F. P. Bos, T. A. Salet, [Early age mechanical behaviour of 3D printed concrete: Numerical modelling and experimental testing](#), *Cement and Concrete Research* 106 (February) (2018) 103–116. doi:10.1016/j.cemconres.2018.02.001. URL <https://doi.org/10.1016/j.cemconres.2018.02.001>
- [98] M. Hambach, D. Volkmer, [Properties of 3D-printed fiber-reinforced Portland cement paste](#), *Cement and Concrete Composites* 79 (2017) 62–70. doi:10.1016/j.cemconcomp.2017.02.001. URL <http://dx.doi.org/10.1016/j.cemconcomp.2017.02.001>
- [99] X. Zhou, Z. Li, [Characterization of rheology of fresh fiber reinforced cementitious composites through ram extrusion](#), *Materials and Structures* 38 (February) (2005) 17–24. doi:10.1617/14064.
- [100] J. J. Benbow, J. Bridgwater, [The Influence of Formulation on Extrudate Structure and Strength](#), *Chemical Engineering Science* 42 (1987) 753–766.
- [101] J. J. Benbow, E. W. Oxley, [THE EXTRUSION MECHANICS OF PASTES- THE INFLUENCE OF PASTE FORMULATION EXTRUSION PARAMETERS](#), *Chemical Engineering Science* 42 (1967) (1987) 1467 – 1473.
- [102] S. Srinivasan, D. Deford, P. Shah, [The use of extrusion rheometry in the development of extrudate fibre-reinforced cement composites](#), *Concrete Science and Engineering* 1 (11) (1999) 26–36.
- [103] R. Nath Das, C. D. Madhusoodana, K. Okada, [Rheological studies on cordierite honeycomb extrusion](#), *Journal of the European Ceramic Society* 22 (16) (2002) 2893–2900. doi:10.1016/S0955-2219(02)00045-6.
- [104] X. Zhou, Z. Li, M. Fan, H. Chen, [Cement & Concrete Composites Rheology of semi-solid fresh cement pastes and mortars in orifice extrusion](#), *Cement and Concrete Composites* 37 (2013) 304–311. doi:10.1016/j.cemconcomp.2013.01.004. URL <http://dx.doi.org/10.1016/j.cemconcomp.2013.01.004>
- [105] S. F. Santos, R. Schmidt, A. E. F. S. Almeida, G. H. D. Tonoli, H. Savastano, [Supercritical carbonation treatment on extruded fibre – cement reinforced with vegetable fibres](#), *Cement & Concrete Composites* 56 (2015) 84–94. doi:10.1016/j.cemconcomp.2014.11.007.
- [106] V. da Costa Correia, S. F. Santos, R. Soares Teixeira, H. Savastano Junior, [Nanofibrillated cellulose and cellulosic pulp for reinforcement of the extruded cement based materials](#), *Construction and Building Materials* 160 (2018) 376–384. doi:10.1016/j.conbuildmat.2017.11.066. URL <https://doi.org/10.1016/j.conbuildmat.2017.11.066>

- [107] S. F. U. Ahmed, H. Mihashi, A review on durability properties of strain hardening fibre reinforced cementitious composites (SHFRCC), *Cement and Concrete Composites* 29 (5) (2007) 365–376. doi:[10.1016/j.cemconcomp.2006.12.014](https://doi.org/10.1016/j.cemconcomp.2006.12.014).
- [108] M. Şahmaran, V. C. Li, Durability properties of micro-cracked ECC containing high volumes fly ash, *Cement and Concrete Research* 39 (11) (2009) 1033–1043. doi:[10.1016/j.cemconres.2009.07.009](https://doi.org/10.1016/j.cemconres.2009.07.009).
- [109] J. Zheng, W. B. Cadson, J. S. Reed, Flow Mechanics on Extrusion through a Square-Entry Die, *Journal of the American Ceramic Society* (75) (1992) 3011–3016. doi:[10.1111/j.1151-2916.1992.tb04380.x](https://doi.org/10.1111/j.1151-2916.1992.tb04380.x).
- [110] J. J. Benbow, S. H. Jazayeri, J. Bridgwater, The flow of pastes through dies of complicated geometry, *Powder Technology* 65 (1991) 393–401.
- [111] J. Zhou, S. Qian, M. G. Sierra Beltran, G. Ye, K. Breugel, V. C. Li, Development of engineered cementitious composites with limestone powder and blast furnace slag, *Materials and Structures* 43 (6) (2010) 803–814. doi:[10.1617/s11527-009-9549-0](https://doi.org/10.1617/s11527-009-9549-0).
- [112] P. Wang, F. H. Wittmann, P. Zhang, E. Lehmann, T. Zhao, Durability and Service Life of Elements Made With Shcc Under Imposed Strain, in: SHCC3 - 3rd International RILEM Conference on Strain Hardening Cementitious Composites, 2014, pp. 33–41.
- [113] Y. J. M. Soto, Adequação de formulações para a produção de placas de fibrocimento por extrusão, Ph.D. thesis, Escola Politécnica da Universidade de São Paulo (2010). doi:[10.11606/T.3.2010.tde-04072012-180623](https://doi.org/10.11606/T.3.2010.tde-04072012-180623).
- [114] R. Wolfs, F. Bos, T. Salet, [Early age mechanical behaviour of 3d printed concrete: Numerical modelling and experimental testing](#), *Cement and Concrete Research* 106 (2018) 103 – 116. doi:<https://doi.org/10.1016/j.cemconres.2018.02.001>.
URL <http://www.sciencedirect.com/science/article/pii/S000888461730532X>
- [115] J. Blaber, B. Adair, A. Antoniou, Ncorr: Open-Source 2D Digital Image Correlation Matlab Software, *Experimental Mechanics* 55 (6) (2015) 1105–1122. doi:[10.1007/s11340-015-0009-1](https://doi.org/10.1007/s11340-015-0009-1).
- [116] N. Roussel, [Rheological requirements for printable concretes](#), *Cement and Concrete Research* (April) (2018) 1–10. doi:[10.1016/j.cemconres.2018.04.005](https://doi.org/10.1016/j.cemconres.2018.04.005).
URL <https://doi.org/10.1016/j.cemconres.2018.04.005>
- [117] X. Huang, R. Ranade, W. Ni, V. C. Li, [Development of green engineered cementitious composites using iron ore tailings as aggregates](#), *Construction and Building Materials* 44 (2013) 757–764. doi:[10.1016/j.conbuildmat.2013.03.088](https://doi.org/10.1016/j.conbuildmat.2013.03.088).
URL <http://dx.doi.org/10.1016/j.conbuildmat.2013.03.088>
- [118] G. Song, G. V. Zijl, Tailoring ECC for Commercial Application, *Proceedings of the 6th RILEM symposium on fiber* (September) (2004) 1391–1400.
- [119] S. Chaves Figueiredo, C. Romero Rodríguez, Z. Y. Ahmed, D. H. Bos, Y. Xu, T. M. Salet, O. Çopuroğlu, E. Schlangen, F. P. Bos, [Mechanical behavior of printed strain hardening cementitious composites](#), *Materials* 13 (10) (2020). doi:[10.3390/ma13102253](https://doi.org/10.3390/ma13102253).
URL <https://www.mdpi.com/1996-1944/13/10/2253>
- [120] T. Wangler, N. Roussel, F. P. Bos, T. A. Salet, R. J. Flatt, [Digital concrete: A review](#), *Cement and Concrete Research* 123 (2019) 105780. doi:<https://doi.org/10.1016/j.cemconres.2019.105780>.
URL <http://www.sciencedirect.com/science/article/pii/S0008884619303680>
- [121] T. Wangler, E. Lloret, L. Reiter, N. Hack, F. Gramazio, M. Kohler, M. Bernhard, B. Dillenburger, J. Buchli, N. Roussel, R. Flatt, [Digital concrete: Opportunities and challenges](#), *RILEM Technical Letters* 1 (2016) 67–75. doi:[10.21809/rilemtechlett.2016.16](https://doi.org/10.21809/rilemtechlett.2016.16).
URL <https://letters.rilem.net/index.php/rilem/article/view/16>

- [122] G. D. Schutter, K. Lesage, V. Mechtcherine, V. N. Nerella, G. Habert, I. Agusti-Juan, [Vision of 3d printing with concrete — technical, economic and environmental potentials](#), *Cement and Concrete Research* 112 (2018) 25 – 36, sI : Digital concrete 2018. doi:<https://doi.org/10.1016/j.cemconres.2018.06.001>.
URL <http://www.sciencedirect.com/science/article/pii/S000888461731219X>
- [123] B. Panda, M. J. Tan, [Experimental study on mix proportion and fresh properties of fly ash based geopolymer for 3d concrete printing](#), *Ceramics International* 44 (9) (2018) 10258 – 10265. doi:<https://doi.org/10.1016/j.ceramint.2018.03.031>.
URL <http://www.sciencedirect.com/science/article/pii/S0272884218305819>
- [124] Y. Chen, Z. Li, S. Chaves Figueiredo, O. Çopuroğlu, F. Veer, E. Schlangen, [Limestone and calcined clay-based sustainable cementitious materials for 3d concrete printing: A fundamental study of extrudability and early-age strength development](#), *Applied Sciences* 9 (9) (2019). doi:10.3390/app9091809.
URL <http://www.mdpi.com/2076-3417/9/9/1809>
- [125] Y. Chen, S. Chaves Figueiredo, c. Yalçinkaya, O. Çopuroğlu, F. Veer, E. Schlangen, [The effect of viscosity-modifying admixture on the extrudability of limestone and calcined clay-based cementitious material for extrusion-based 3d concrete printing](#), *Materials* 12 (9) (2019). doi:10.3390/ma12091374.
URL <http://www.mdpi.com/1996-1944/12/9/1374>
- [126] D. Asprone, C. Menna, F. P. Bos, T. A. Salet, J. Mata-Falcón, W. Kaufmann, [Rethinking reinforcement for digital fabrication with concrete](#), *Cement and Concrete Research* 112 (2018) 111 – 121, sI : Digital concrete 2018. doi:<https://doi.org/10.1016/j.cemconres.2018.05.020>.
URL <http://www.sciencedirect.com/science/article/pii/S0008884618300309>
- [127] D. Asprone, F. Auricchio, C. Menna, V. Mercuri, [3d printing of reinforced concrete elements: Technology and design approach](#), *Construction and Building Materials* 165 (2018) 218 – 231. doi:<https://doi.org/10.1016/j.conbuildmat.2018.01.018>.
URL <http://www.sciencedirect.com/science/article/pii/S0950061818300187>
- [128] G. Ma, Z. Li, L. Wang, G. Bai, [Micro-cable reinforced geopolymer composite for extrusion-based 3d printing](#), *Materials Letters* 235 (2019) 144 – 147. doi:<https://doi.org/10.1016/j.matlet.2018.09.159>.
URL <http://www.sciencedirect.com/science/article/pii/S0167577X18315490>
- [129] J. H. Lim, B. Panda, Q.-C. Pham, [Improving flexural characteristics of 3d printed geopolymer composites with in-process steel cable reinforcement](#), *Construction and Building Materials* 178 (2018) 32 – 41. doi:<https://doi.org/10.1016/j.conbuildmat.2018.05.010>.
URL <http://www.sciencedirect.com/science/article/pii/S0950061818310675>
- [130] D. Shen, X. Wang, D. Cheng, J. Zhang, G. Jiang, [Effect of internal curing with super absorbent polymers on autogenous shrinkage of concrete at early age](#), *Construction and Building Materials* 106 (2016) 512 – 522. doi:<https://doi.org/10.1016/j.conbuildmat.2015.12.115>.
URL <http://www.sciencedirect.com/science/article/pii/S0950061815307868>
- [131] S. F. Santos, R. Schmidt, A. E. Almeida, G. H. Tonoli, H. Savastano, [Supercritical carbonation treatment on extruded fibre–cement reinforced with vegetable fibres](#), *Cement and Concrete Composites* 56 (2015) 84 – 94. doi:<https://doi.org/10.1016/j.cemconcomp.2014.11.007>.
URL <http://www.sciencedirect.com/science/article/pii/S0958946514002108>
- [132] M. Hambach, M. Rutzen, D. Volkmer, [Chapter 5 - properties of 3d-printed fiber-reinforced portland cement paste](#), in: J. G. Sanjayan, A. Nazari, B. Nematollahi (Eds.), *3D Concrete Printing Technology*, Butterworth-Heinemann, 2019, pp. 73 – 113. doi:<https://doi.org/10.1016/B978-0-12-815481-6.00005-1>.
URL <http://www.sciencedirect.com/science/article/pii/B9780128154816000051>

- [133] B. Panda, S. C. Paul, M. J. Tan, [Anisotropic mechanical performance of 3d printed fiber reinforced sustainable construction material](#), *Materials Letters* 209 (2017) 146 – 149. doi:<https://doi.org/10.1016/j.matlet.2017.07.123>.
URL <http://www.sciencedirect.com/science/article/pii/S0167577X17311679>
- [134] B. Nematollahi, P. Vijay, J. Sanjayan, A. Nazari, M. Xia, V. Naidu Nerella, V. Mechtcherine, [Effect of polypropylene fibre addition on properties of geopolymers made by 3d printing for digital construction](#), *Materials* 11 (12) (2018). doi:[10.3390/ma11122352](https://doi.org/10.3390/ma11122352).
URL <https://www.mdpi.com/1996-1944/11/12/2352>
- [135] Y. Weng, M. Li, M. J. Tan, S. Qian, [Design 3D printing cementitious materials via Fuller Thompson theory and Marson-Percy model](#), *Construction and Building Materials* 163 (2018) 600–610. doi:[10.1016/j.conbuildmat.2017.12.112](https://doi.org/10.1016/j.conbuildmat.2017.12.112).
URL <https://doi.org/10.1016/j.conbuildmat.2017.12.112>
- [136] B. Zareiyan, B. Khoshnevis, [Effects of mixture ingredients on interlayer adhesion of concrete in contour crafting](#), *Rapid Prototyping Journal* 24 (3) (2018) 584–592.
URL <https://doi.org/10.1108/RPJ-02-2017-0029>
- [137] F. P. Bos, E. Bosco, T. A. M. Salet, [Ductility of 3d printed concrete reinforced with short straight steel fibers](#), *Virtual and Physical Prototyping* 14 (2) (2019) 160–174. arXiv:<https://doi.org/10.1080/17452759.2018.1548069>, doi:[10.1080/17452759.2018.1548069](https://doi.org/10.1080/17452759.2018.1548069).
URL <https://doi.org/10.1080/17452759.2018.1548069>
- [138] S. Müller, V. Mechtcherine, [Fatigue behaviour of strain-hardening cement-based composites \(shcc\)](#), *Cement and Concrete Research* 92 (2017) 75 – 83. doi:<https://doi.org/10.1016/j.cemconres.2016.11.003>.
URL <http://www.sciencedirect.com/science/article/pii/S0008884616305993>
- [139] E. Özbay, O. Karahan, M. Lachemi, K. M. A. Hossain, C. D. Atis, [Dual effectiveness of freezing-thawing and sulfate attack on high-volume slag-incorporated ECC](#), *Composites Part B: Engineering* 45 (1) (2013) 1384–1390. doi:[10.1016/j.compositesb.2012.07.038](https://doi.org/10.1016/j.compositesb.2012.07.038).
- [140] A. Kamal, M. Kunieda, N. Ueda, H. Nakamura, [Evaluation of crack opening performance of a repair material with strain hardening behavior](#), *Cement and Concrete Composites* 30 (10) (2008) 863 – 871. doi:<https://doi.org/10.1016/j.cemconcomp.2008.08.003>.
URL <http://www.sciencedirect.com/science/article/pii/S095894650800111X>
- [141] Y. Bao, M. Xu, D. Soltan, T. Xia, A. Shih, H. L. Clack, V. C. Li, [Three-dimensional printing multifunctional engineered cementitious composites \(ecc\) for structural elements](#), in: T. Wangler, R. J. Flatt (Eds.), *First RILEM International Conference on Concrete and Digital Fabrication – Digital Concrete 2018*, Springer International Publishing, Cham, 2019, pp. 115–128.
- [142] J. Yu, C. K. Y. Leung, [Impact of 3d printing direction on mechanical performance of strain-hardening cementitious composite \(shcc\)](#), in: T. Wangler, R. J. Flatt (Eds.), *First RILEM International Conference on Concrete and Digital Fabrication – Digital Concrete 2018*, Springer International Publishing, Cham, 2019, pp. 255–265.
- [143] H. Ogura, V. N. Nerella, V. Mechtcherine, [Developing and testing of strain-hardening cement-based composites \(shcc\) in the context of 3d-printing](#), *Materials* 11 (8) (2018). doi:[10.3390/ma11081375](https://doi.org/10.3390/ma11081375).
URL <http://www.mdpi.com/1996-1944/11/8/1375>
- [144] M. Moini, J. Olek, J. P. Youngblood, B. Magee, P. D. Zavattieri, [Additive manufacturing and performance of architected cement-based materials](#), *Advanced Materials* 30 (43) (2018) 1802123.
- [145] D. Jiang, R. Hoglund, D. E. Smith, [Continuous fiber angle topology optimization for polymer composite deposition additive manufacturing applications](#), *Fibers* 7 (2) (2019). doi:[10.3390/fib7020014](https://doi.org/10.3390/fib7020014).
URL <http://www.mdpi.com/2079-6439/7/2/14>

- [146] R. Wolfs, F. Bos, T. Salet, [Hardened properties of 3d printed concrete: The influence of process parameters on interlayer adhesion](#), *Cement and Concrete Research* 119 (2019) 132 – 140. doi:<https://doi.org/10.1016/j.cemconres.2019.02.017>.
URL <http://www.sciencedirect.com/science/article/pii/S0008884618310482>
- [147] D. Marshall, B. Cox, [A j-integral method for calculating steady-state matrix cracking stresses in composites](#), *Mechanics of Materials* 7 (2) (1988) 127–133. doi:[https://doi.org/10.1016/0167-6636\(88\)90011-7](https://doi.org/10.1016/0167-6636(88)90011-7).
URL <https://www.sciencedirect.com/science/article/pii/0167663688900117>
- [148] T. Kanda, V. C. Li, [Practical design criteria for saturated pseudo strain hardening behavior in ecc](#), *Journal of Advanced Concrete Technology* 4 (1) (2006) 59–72. doi:[10.3151/jact.4.59](https://doi.org/10.3151/jact.4.59).
- [149] S. Wang, V. C. Li, [Engineered cementitious composites with high-volume fly ash](#), *Materials Journal* 104 (2007) 233–241.
URL <https://www.concrete.org/publications/internationalconcreteabstractsportal.aspx?m=details&ID=18668>
- [150] B. Panda, S. C. Paul, N. A. N. Mohamed, Y. W. D. Tay, M. J. Tan, [Measurement of tensile bond strength of 3d printed geopolymers mortar](#), *Measurement* 113 (2018) 108 – 116. doi:<https://doi.org/10.1016/j.measurement.2017.08.051>.
URL <http://www.sciencedirect.com/science/article/pii/S0263224117305560>
- [151] V. N. Nerella, S. Hempel, V. Mechtcherine, [Effects of layer-interface properties on mechanical performance of concrete elements produced by extrusion-based 3d-printing](#), *Construction and Building Materials* 205 (2019) 586 – 601. doi:<https://doi.org/10.1016/j.conbuildmat.2019.01.235>.
URL <http://www.sciencedirect.com/science/article/pii/S0950061819302843>
- [152] M. Luković, H. Dong, B. Šavija, E. Schlangen, G. Ye, K. van Breugel, [Tailoring strain-hardening cementitious composite repair systems through numerical experimentation](#), *Cement and Concrete Composites* 53 (2014) 200 – 213. doi:<https://doi.org/10.1016/j.cemconcomp.2014.06.017>.
URL <http://www.sciencedirect.com/science/article/pii/S0958946514001176>
- [153] M. Luković, B. Šavija, H. Dong, E. Schlangen, G. Ye, [Micromechanical study of the interface properties in concrete repair systems](#), *Journal of Advanced Concrete Technology* 12 (9) (2014) 320–339. doi:[10.3151/jact.12.320](https://doi.org/10.3151/jact.12.320).
- [154] J. Van Der Putten, K. De Schutter, G. and Van Tittelboom, [The effect of print parameters on the \(micro\)structure of 3d printed cementitious materials](#), in: T. Wangler, R. J. Flatt (Eds.), *First RILEM International Conference on Concrete and Digital Fabrication – Digital Concrete 2018*, Springer International Publishing, Cham, 2019, pp. 234–244.
- [155] C. Schröfl, V. N. Nerella, V. Mechtcherine, [Capillary water intake by 3d-printed concrete visualised and quantified by neutron radiography](#), in: T. Wangler, R. J. Flatt (Eds.), *First RILEM International Conference on Concrete and Digital Fabrication – Digital Concrete 2018*, Springer International Publishing, Cham, 2019, pp. 217–224.
- [156] I. Arganda-carreras, V. Kaynig, C. Rueden, K. W. Eliceiri, J. Schindelin, A. Cardona, H. S. Seung, [Trainable Weka Segmentation : a machine learning tool for microscopy pixel classification](#), *Bioinformatics* 33 (March) (2017) 2424–2426. doi:[10.1093/bioinformatics/btx180](https://doi.org/10.1093/bioinformatics/btx180).
- [157] J. Schindelin, I. Arganda-carreras, E. Frise, V. Kaynig, T. Pietzsch, S. Preibisch, C. Rueden, S. Saalfeld, B. Schmid, J.-y. Tinevez, D. J. White, V. Hartenstein, P. Tomancak, A. Cardona, [Fiji - an Open Source platform for biological image analysis](#), *Nature Methods* 9 (7) (2012) 676–82. doi:[10.1038/nmeth.2019](https://doi.org/10.1038/nmeth.2019).
[Fiji](http://www.fiji.sc/).
- [158] T. Le, S. Austin, S. Lim, R. Buswell, R. Law, A. Gibb, T. Thorpe, [Hardened properties of high-performance printing concrete](#), *Cement and Concrete Research* 42 (3) (2012) 558 – 566. doi:<https://doi.org/10.1016/j.cemconres.2011.12.003>.
URL <http://www.sciencedirect.com/science/article/pii/S0008884611003255>

- [159] R. Manno, W. Gao, I. Benedetti, [Engineering the crack path in lattice cellular materials through bio-inspired micro-structural alterations](#), *Extreme Mechanics Letters* 26 (2019) 8 – 17. doi:<https://doi.org/10.1016/j.eml.2018.11.002>.
URL <http://www.sciencedirect.com/science/article/pii/S2352431618301627>
- [160] S. C. Figueiredo, O. Çopuroğlu, E. Schlangen, [Effect of viscosity modifier admixture on portland cement paste hydration and microstructure](#), *Construction and Building Materials* 212 (2019) 818 – 840. doi:<https://doi.org/10.1016/j.conbuildmat.2019.04.020>.
URL <http://www.sciencedirect.com/science/article/pii/S0950061819308645>
- [161] J. Wilkes, Y. Hagedorn, W. Meiners, K. Wissenbach, [Additive manufacturing of ZrO₂-Al₂O₃ ceramic components by selective laser melting](#), *Rapid Prototyping Journal* 19 (1) (2013) 51–57. doi:[10.1108/13552541311292736](https://doi.org/10.1108/13552541311292736).
URL <http://www.emeraldinsight.com/doi/10.1108/13552541311292736>
- [162] T. Kamada, V. C. Li, [Effects of surface preparation on the fracture behavior of ECC/concrete repair system](#), *Cement and Concrete Composites* 22 (6) (2000) 423–431. doi:[10.1016/S0958-9465\(00\)00042-1](https://doi.org/10.1016/S0958-9465(00)00042-1).
- [163] K. H. Khayat, [Viscosity-enhancing admixtures for cement-based materials — an overview](#), *Cement and Concrete Composites* 20 (2) (1998) 171 – 188. doi:[https://doi.org/10.1016/S0958-9465\(98\)80006-1](https://doi.org/10.1016/S0958-9465(98)80006-1).
URL <http://www.sciencedirect.com/science/article/pii/S0958946598800061>
- [164] L. Patural, P. Marchal, A. Govin, P. Grosseau, B. Ruot, O. Devès, [Cellulose ethers influence on water retention and consistency in cement-based mortars](#), *Cement and Concrete Research* 41 (1) (2011) 46–55. doi:[10.1016/j.cemconres.2010.09.004](https://doi.org/10.1016/j.cemconres.2010.09.004).
URL <http://dx.doi.org/10.1016/j.cemconres.2010.09.004>
- [165] D. Bülchen, J. Kainz, J. Plank, [Working mechanism of methyl hydroxyethyl cellulose \(MHEC\) as water retention agent](#), *Cement and Concrete Research* 42 (7) (2012) 953–959. doi:[10.1016/j.cemconres.2012.03.016](https://doi.org/10.1016/j.cemconres.2012.03.016).
URL <http://dx.doi.org/10.1016/j.cemconres.2012.03.016>
- [166] A. Pierre, A. Perrot, V. Picandet, Y. Guevel, [Cellulose ethers and cement paste permeability](#), *Cement and Concrete Research* 72 (2015) 117–127. doi:[10.1016/j.cemconres.2015.02.013](https://doi.org/10.1016/j.cemconres.2015.02.013).
URL <http://dx.doi.org/10.1016/j.cemconres.2015.02.013>
- [167] C. Brumaud, R. Baumann, M. Schmitz, M. Radler, N. Roussel, [Cellulose ethers and yield stress of cement pastes](#), *Cement and Concrete Research* 55 (2014) 14 – 21. doi:<https://doi.org/10.1016/j.cemconres.2013.06.013>.
URL <http://www.sciencedirect.com/science/article/pii/S0008884613001580>
- [168] D. Marchon, S. Kawashima, H. Bessaies-Bey, S. Mantellato, S. Ng, [Hydration and rheology control of concrete for digital fabrication: Potential admixtures and cement chemistry](#), *Cement and Concrete Research* 112 (2018) 96 – 110, sI: Digital concrete 2018. doi:<https://doi.org/10.1016/j.cemconres.2018.05.014>.
URL <http://www.sciencedirect.com/science/article/pii/S0008884617314011>
- [169] E. Knapen, D. Van Gemert, [Cement hydration and microstructure formation in the presence of water-soluble polymers](#), *Cement and Concrete Research* 39 (1) (2009) 6–13. doi:[10.1016/j.cemconres.2008.10.003](https://doi.org/10.1016/j.cemconres.2008.10.003).
URL <http://dx.doi.org/10.1016/j.cemconres.2008.10.003>
- [170] P. Pichniarczyk, G. Malata, [Microcalorimetric analysis of methylcellulose influence on the hydration process of tricalcium aluminate, alite and their mixture](#), *Journal of Thermal Analysis and Calorimetry* 128 (2) (2017) 771–778. doi:[10.1007/s10973-016-5960-2](https://doi.org/10.1007/s10973-016-5960-2).

- [171] J. Pourchez, A. Peschard, P. Grosseau, R. Guyonnet, B. Guilhot, F. Vallée, HPMC and HEMC influence on cement hydration, *Cement and Concrete Research* 36 (2) (2006) 288–294. doi:10.1016/j.cemconres.2005.08.003.
- [172] J. Pourchez, P. Grosseau, B. Ruot, [Current understanding of cellulose ethers impact on the hydration of C3A and C3A-sulphate systems](#), *Cement and Concrete Research* 39 (8) (2009) 664–669. doi:10.1016/j.cemconres.2009.05.009.
URL <http://dx.doi.org/10.1016/j.cemconres.2009.05.009>
- [173] J. Pourchez, P. Grosseau, B. Ruot, [Changes in C3S hydration in the presence of cellulose ethers](#), *Cement and Concrete Research* 40 (2) (2010) 179–188. doi:10.1016/j.cemconres.2009.10.008.
URL <http://dx.doi.org/10.1016/j.cemconres.2009.10.008>
- [174] Z. H. Ou, B. G. Ma, S. W. Jian, [Influence of cellulose ethers molecular parameters on hydration kinetics of Portland cement at early ages](#), *Construction and Building Materials* 33 (2012) 78–83. doi:10.1016/j.conbuildmat.2012.01.007.
URL <http://dx.doi.org/10.1016/j.conbuildmat.2012.01.007>
- [175] B. Ma, Y. Peng, H. Tan, S. Jian, Z. Zhi, Y. Guo, H. Qi, T. Zhang, X. He, [Effect of hydroxypropyl-methyl cellulose ether on rheology of cement paste plasticized by polycarboxylate superplasticizer](#), *Construction and Building Materials* 160 (2018) 341–350. doi:10.1016/j.conbuildmat.2017.11.010.
URL <https://doi.org/10.1016/j.conbuildmat.2017.11.010>
- [176] B. Wu, G. Ye, [Development of porosity of cement paste blended with supplementary cementitious materials after carbonation](#), *Construction and Building Materials* 145 (2017) 52 – 61. doi:<https://doi.org/10.1016/j.conbuildmat.2017.03.176>.
URL <http://www.sciencedirect.com/science/article/pii/S0950061817305627>
- [177] P. Lura, [Autogenous Deformation and Internal Curing of Concrete](#), Ph.D. thesis, Delft University of Technology (2003).
URL <http://resolver.tudelft.nl/uuid:1a1efc2d-a638-4787-b543-5bd643a39a4b>
- [178] J. Zhang, G. W. Scherer, [Comparison of methods for arresting hydration of cement](#), *Cement and Concrete Research* 41 (10) (2011) 1024–1036. doi:10.1016/j.cemconres.2011.06.003.
URL <http://dx.doi.org/10.1016/j.cemconres.2011.06.003>
- [179] O. Çopuroğlu, [Revealing the dark side of portlandite clusters in cement paste by circular polarization microscopy](#), *Materials* 9 (3) (2016). doi:10.3390/ma9030176.
- [180] M. S. Konsta-Gdoutos, Z. S. Metaxa, S. P. Shah, [Highly dispersed carbon nanotube reinforced cement based materials](#), *Cement and Concrete Research* 40 (7) (2010) 1052–1059. doi:10.1016/j.cemconres.2010.02.015.
URL <http://dx.doi.org/10.1016/j.cemconres.2010.02.015>
- [181] A. K. Suryavanshi, J. D. Scantlebury, S. B. Lyon, [Mechanism of Friedel’s salt formation in cements rich in tri-calcium aluminate](#), *Cement and Concrete Research* 26 (5) (1996) 717–727. doi:10.1016/S0008-8846(96)85009-5.
- [182] F. R. Lago, J. Dweck, T. Analysis, [Evaluation of Influence of Salt in the Cement Hydration to Oil Wells](#), *Materials Research* 20 (2017) 743–747. doi:<http://dx.doi.org/10.1590/1980-5373-MR-2017-0049>.
- [183] B. Šavija, E. Schlangen, [Chloride ingress in cracked concrete- a literature review](#), in: C. Andrade, J. Gulikers (Eds.), *Advances in Modeling Concrete Service Life*, Springer Netherlands, Dordrecht, 2012, pp. 133–142.
- [184] B. Šavija, J. Pacheco, E. Schlangen, [Lattice modeling of chloride diffusion in sound and cracked concrete](#), *Cement and Concrete Composites* 42 (2013) 30–40. doi:10.1016/j.cemconcomp.2013.05.003.
- [185] H. F. W. Taylor, [Cement Chemistry](#), Academic Press, 1990.
URL <https://books.google.nl/books?id=kICPQgAACAAJ>

- [186] A. Mezeencevova, V. Garas, H. Nanko, K. E. Kurtis, Influence of Thermomechanical Pulp Fiber Compositions on Internal Curing of Cementitious Materials, *Journal of Materials in Civil Engineering* 24 (8) (2012) 970–975. doi:10.1061/(ASCE)MT.1943-5533.0000446.
- [187] P. Jongvisuttisun, C. Negrello, K. E. Kurtis, Effect of processing variables on efficiency of eucalyptus pulps for internal curing, *Cement and Concrete Composites* 37 (2013) 126–135. doi:https://doi.org/10.1016/j.cemconcomp.2012.11.006.
URL <http://www.sciencedirect.com/science/article/pii/S0958946512002326>
- [188] D. Zou, H. Zhang, Y. Wang, J. Zhu, X. Guan, Internal curing of mortar with low water to cementitious materials ratio using a normal weight porous aggregate, *Construction and Building Materials* 96 (2015) 209–216. doi:https://doi.org/10.1016/j.conbuildmat.2015.08.025.
URL <http://www.sciencedirect.com/science/article/pii/S0950061815302427>
- [189] A. Bentur, S. ichi Igarashi, K. Kovler, Prevention of autogenous shrinkage in high-strength concrete by internal curing using wet lightweight aggregates, *Cement and Concrete Research* 31 (11) (2001) 1587–1591. doi:https://doi.org/10.1016/S0008-8846(01)00608-1.
URL <http://www.sciencedirect.com/science/article/pii/S0008884601006081>
- [190] E. Namsone, G. Šahmenko, A. Korjakins, Durability Properties of High Performance Foamed Concrete, *Procedia Engineering* 172 (2017) 760–767. doi:10.1016/j.proeng.2017.02.120.
URL <http://dx.doi.org/10.1016/j.proeng.2017.02.120>
- [191] N. K. Singh, P. C. Mishra, V. K. Singh, K. K. Narang, Effects of hydroxyethyl cellulose and oxalic acid on the properties of cement, *Cement and Concrete Research* 33 (9) (2003) 1319–1329. doi:10.1016/S0008-8846(03)00060-7.
- [192] Y. Chen, S. Chaves Figueiredo, Yalçınkaya, O. Çopuroğlu, F. Veer, E. Schlangen, The effect of viscosity-modifying admixture on the extrudability of limestone and calcined clay-based cementitious material for extrusion-based 3d concrete printing, *Materials* 12 (9) (2019). doi:10.3390/ma12091374.
URL <https://www.mdpi.com/1996-1944/12/9/1374>
- [193] Y. Chen, Z. Li, S. Chaves Figueiredo, O. Çopuroğlu, F. Veer, E. Schlangen, Limestone and calcined clay-based sustainable cementitious materials for 3d concrete printing: A fundamental study of extrudability and early-age strength development, *Applied Sciences* 9 (9) (2019). doi:10.3390/app9091809.
URL <https://www.mdpi.com/2076-3417/9/9/1809>
- [194] M. Şahmaran, S. B. Keskin, G. Ozerkan, I. O. Yaman, Self-healing of mechanically-loaded self consolidating concretes with high volumes of fly ash, *Cement and Concrete Composites* 30 (10) (2008) 872–879. doi:https://doi.org/10.1016/j.cemconcomp.2008.07.001.
URL <http://www.sciencedirect.com/science/article/pii/S0958946508000838>
- [195] J. G. Calvo, G. Pérez, P. Carballosa, E. Erkizia, J. Gaitero, A. Guerrero, Development of ultra-high performance concretes with self-healing micro/nano-additions, *Construction and Building Materials* 138 (2017) 306–315. doi:https://doi.org/10.1016/j.conbuildmat.2017.02.015.
URL <http://www.sciencedirect.com/science/article/pii/S0950061817301873>
- [196] D. J. Kim, S. H. Kang, T.-H. Ahn, Mechanical characterization of high-performance steel-fiber reinforced cement composites with self-healing effect, *Materials* 7 (1) (2014) 508–526. doi:10.3390/ma7010508.
URL <https://www.mdpi.com/1996-1944/7/1/508>
- [197] D. Homma, H. Mihashi, T. Nishiwaki, Self-Healing Capability of Fibre Reinforced Cementitious Composites, *Journal of Advanced Concrete Technology* 7 (2) (2009) 217–228. doi:10.3151/jact.7.217.
- [198] Y. Yang, M. D. Lepech, E. H. Yang, V. C. Li, Autogenous healing of engineered cementitious composites under wet-dry cycles, *Cement and Concrete Research* 39 (5) (2009) 382–390. doi:10.1016/j.cemconres.2009.01.013.
URL <http://dx.doi.org/10.1016/j.cemconres.2009.01.013>

- [199] S. Qian, J. Zhou, E. Schlangen, [Influence of curing condition and precracking time on the self-healing behavior of engineered cementitious composites](#), *Cement and Concrete Composites* 32 (9) (2010) 686–693. doi:<https://doi.org/10.1016/j.cemconcomp.2010.07.015>. URL <http://www.sciencedirect.com/science/article/pii/S0958946510001010>
- [200] Z. Zhang, Q. Zhang, V. C. Li, [Multiple-scale investigations on self-healing induced mechanical property recovery of ecc](#), *Cement and Concrete Composites* 103 (2019) 293–302. doi:<https://doi.org/10.1016/j.cemconcomp.2019.05.014>. URL <http://www.sciencedirect.com/science/article/pii/S0958946518312848>
- [201] K. Van Tittelboom, N. De Belie, [Self-healing in cementitious materials—a review](#), *Materials* 6 (6) (2013) 2182–2217. doi:[10.3390/ma6062182](https://doi.org/10.3390/ma6062182). URL <https://www.mdpi.com/1996-1944/6/6/2182>
- [202] M. Sahmaran, G. Yildirim, E. Ozbay, K. Ahmed, M. Lachemi, [Self-healing ability of cementitious composites: effect of addition of pre-soaked expanded perlite](#), *Magazine of Concrete Research* 66 (8) (2014) 409–419. arXiv:<https://doi.org/10.1680/macrc.13.00250>, doi:[10.1680/macrc.13.00250](https://doi.org/10.1680/macrc.13.00250). URL <https://doi.org/10.1680/macrc.13.00250>
- [203] K. Sisomphon, O. Copuroglu, A. Fraaij, [Application of encapsulated lightweight aggregate impregnated with sodium monofluorophosphate as a self-healing agent in blast furnace slag mortar](#), *Heron* 56 (1/2) (2011). URL <http://resolver.tudelft.nl/uuid:989836d6-dd5c-4bb0-8d9f-925390dddbae>
- [204] H. X. Lee, H. S. Wong, N. R. Buenfeld, [Self-sealing of cracks in concrete using superabsorbent polymers](#), *Cement and Concrete Research* 79 (2016) 194–208. doi:[10.1016/j.cemconres.2015.09.008](https://doi.org/10.1016/j.cemconres.2015.09.008). URL <http://dx.doi.org/10.1016/j.cemconres.2015.09.008>
- [205] A. Mignon, D. Snoeck, D. Schaubroeck, N. Luicx, P. Dubruel, S. Van Vlierberghe, N. De Belie, [pH-responsive superabsorbent polymers: A pathway to self-healing of mortar](#), *Reactive and Functional Polymers* 93 (2015) 68–76. doi:[10.1016/j.reactfunctpolym.2015.06.003](https://doi.org/10.1016/j.reactfunctpolym.2015.06.003). URL <http://dx.doi.org/10.1016/j.reactfunctpolym.2015.06.003>
- [206] E. Gruyaert, B. Debbaut, D. Snoeck, P. Díaz, A. Arizo, E. Tziviloglou, E. Schlangen, N. D. Belie, [Self-healing mortar with pH-sensitive superabsorbent polymers: testing of the sealing efficiency by water flow tests](#), *Smart Materials and Structures* 25 (8) (2016) 084007. doi:[10.1088/0964-1726/25/8/084007](https://doi.org/10.1088/0964-1726/25/8/084007). URL <https://doi.org/10.1088/0964-1726/25/8/084007>
- [207] G. Hong, S. Choi, [Rapid self-sealing of cracks in cementitious materials incorporating superabsorbent polymers](#), *Construction and Building Materials* 143 (2017) 1–9. doi:[10.1016/j.conbuildmat.2017.03.133](https://doi.org/10.1016/j.conbuildmat.2017.03.133). URL <http://dx.doi.org/10.1016/j.conbuildmat.2017.03.133>
- [208] V. Wiktor, H. M. Jonkers, [Quantification of crack-healing in novel bacteria-based self-healing concrete](#), *Cement and Concrete Composites* 33 (7) (2011) 763–770. doi:[10.1016/j.cemconcomp.2011.03.012](https://doi.org/10.1016/j.cemconcomp.2011.03.012). URL <http://dx.doi.org/10.1016/j.cemconcomp.2011.03.012>
- [209] B. Dong, Y. Wang, W. Ding, S. Li, N. Han, F. Xing, Y. Lu, [Electrochemical impedance study on steel corrosion in the simulated concrete system with a novel self-healing microcapsule](#), *Construction and Building Materials* 56 (2014) 1–6. doi:<https://doi.org/10.1016/j.conbuildmat.2014.01.070>. URL <http://www.sciencedirect.com/science/article/pii/S0950061814001044>
- [210] C. R. Rodríguez, S. C. Figueiredo, M. Deprez, D. Snoeck, E. Schlangen, B. Šavija, [Numerical investigation of crack self-sealing in cement-based composites with superabsorbent polymers](#), *Cement and Concrete Composites* 104 (2019) 103395. doi:<https://doi.org/10.1016/j.cemconcomp.2019.103395>. URL <http://www.sciencedirect.com/science/article/pii/S0958946519303762>
- [211] E. Quagliarini, S. Lenci, [The influence of natural stabilizers and natural fibres on the mechanical properties of ancient roman adobe bricks](#), *Journal of Cultural Heritage* 11 (3) (2010) 309–314. doi:<https://doi.org/10.1016/j.culher.2009.11.012>. URL <http://www.sciencedirect.com/science/article/pii/S1296207410000312>

- [212] H. Binici, O. Aksogan, T. Shah, [Investigation of fibre reinforced mud brick as a building material](#), *Construction and Building Materials* 19 (4) (2005) 313 – 318. doi:<https://doi.org/10.1016/j.conbuildmat.2004.07.013>.
URL <http://www.sciencedirect.com/science/article/pii/S0950061804001631>
- [213] L. Yan, B. Kasal, L. Huang, [A review of recent research on the use of cellulosic fibres, their fibre fabric reinforced cementitious, geo-polymer and polymer composites in civil engineering](#), *Composites Part B: Engineering* 92 (2016) 94 – 132. doi:<https://doi.org/10.1016/j.compositesb.2016.02.002>.
URL <http://www.sciencedirect.com/science/article/pii/S1359836816001025>
- [214] R. S. Coutts, [A review of australian research into natural fibre cement composites](#), *Cement and Concrete Composites* 27 (5) (2005) 518 – 526, natural fibre reinforced cement composites. doi:<https://doi.org/10.1016/j.cemconcomp.2004.09.003>.
URL <http://www.sciencedirect.com/science/article/pii/S0958946504001428>
- [215] H. Savastano, P. Warden, R. Coutts, [Microstructure and mechanical properties of waste fibre–cement composites](#), *Cement and Concrete Composites* 27 (5) (2005) 583 – 592, natural fibre reinforced cement composites. doi:<https://doi.org/10.1016/j.cemconcomp.2004.09.009>.
URL <http://www.sciencedirect.com/science/article/pii/S0958946504001490>
- [216] C. Rodrigues, M. Pereira, S. Figueiredo, K. Ghavami, P. Stroeven, [Durability of cellulose-cement composites assessed by accelerated testing under temperature and moisture variations - Effects of blending by rice husk ash](#), in: *Brittle Matrix Composites 10*, BMC 2010, 2012.
- [217] J. E. M. Ballesteros, V. dos Santos, G. Mármol, M. Frías, J. Fiorelli, [Potential of the hornification treatment on eucalyptus and pine fibers for fiber-cement applications](#), *Cellulose* 24 (5) (2017) 2275–2286. doi: [10.1007/s10570-017-1253-6](https://doi.org/10.1007/s10570-017-1253-6).
URL <https://doi.org/10.1007/s10570-017-1253-6>
- [218] J. Claramunt, M. Ardanuy, J. A. García-Hortal, R. D. T. Filho, [The hornification of vegetable fibers to improve the durability of cement mortar composites](#), *Cement and Concrete Composites* 33 (5) (2011) 586 – 595. doi:<https://doi.org/10.1016/j.cemconcomp.2011.03.003>.
URL <http://www.sciencedirect.com/science/article/pii/S0958946511000394>
- [219] J. E. M. Ballesteros, G. Mármol, R. Filomeno, L. Rodier, H. Savastano, J. Fiorelli, [Synergic effect of fiber and matrix treatments for vegetable fiber reinforced cement of improved performance](#), *Construction and Building Materials* 205 (2019) 52 – 60. doi:<https://doi.org/10.1016/j.conbuildmat.2019.02.007>.
URL <http://www.sciencedirect.com/science/article/pii/S0950061819302922>
- [220] F. de Andrade Silva, N. Chawla, R. D. de Toledo Filho, [An experimental investigation of the fatigue behavior of sisal fibers](#), *Materials Science and Engineering: A* 516 (1) (2009) 90 – 95. doi:<https://doi.org/10.1016/j.msea.2009.03.026>.
URL <http://www.sciencedirect.com/science/article/pii/S0921509309003505>
- [221] R. Coutts, [Autoclaved beaten wood fibre-reinforced cement composites](#), *Composites* 15 (2) (1984) 139 – 143. doi:[https://doi.org/10.1016/0010-4361\(84\)90726-2](https://doi.org/10.1016/0010-4361(84)90726-2).
URL <http://www.sciencedirect.com/science/article/pii/0010436184907262>
- [222] R. S. P. Coutts, P. Kightly, [Microstructure of autoclaved refined wood-fibre cement mortars](#), *Journal of Materials Science* 17 (6) (1982) 1801–1806. doi:[10.1007/BF00540809](https://doi.org/10.1007/BF00540809).
URL <https://doi.org/10.1007/BF00540809>
- [223] H. Savastano, V. Agopyan, A. M. Nolasco, L. Pimentel, [Plant fibre reinforced cement components for roofing](#), *Construction and Building Materials* 13 (8) (1999) 433 – 438. doi:[https://doi.org/10.1016/S0950-0618\(99\)00046-X](https://doi.org/10.1016/S0950-0618(99)00046-X).
URL <http://www.sciencedirect.com/science/article/pii/S095006189900046X>

- [224] B. J. Mohr, J. J. Biernacki, K. E. Kurtis, Supplementary cementitious materials for mitigating degradation of kraft pulp fiber-cement composites, *Cement and Concrete Research* 37 (11) (2007) 1531–1543. doi:[10.1016/j.cemconres.2007.08.001](https://doi.org/10.1016/j.cemconres.2007.08.001).
- [225] R. D. T. Filho, K. Ghavami, G. L. England, K. Scrivener, [Development of vegetable fibre–mortar composites of improved durability](#), *Cement and Concrete Composites* 25 (2) (2003) 185 – 196. doi:[https://doi.org/10.1016/S0958-9465\(02\)00018-5](https://doi.org/10.1016/S0958-9465(02)00018-5).
URL <http://www.sciencedirect.com/science/article/pii/S0958946502000185>
- [226] C. de Souza Rodrigues, M. A. Pereira, S. C. Figueiredo, K. Ghavami, P. Stroeven, [Durability of cellulose-cement composites assessed by accelerated testing under temperature and moisture variations - effects of blending by rice husk ash](#), in: A. Brandt, J. Olek, M. Glinicki, C. Leung (Eds.), *Brittle Matrix Composites* 10, Woodhead Publishing, 2012, pp. 387 – 396. doi:<https://doi.org/10.1533/9780857099891.387>.
URL <http://www.sciencedirect.com/science/article/pii/B9780857099884500372>
- [227] M. S. Rodrigues, A. L. Beraldo, H. Savastano Júnior, S. F. Santos, [Cinza de palha de cana-de-açúcar como adição mineral em fibrocimento](#), *Revista Brasileira de Engenharia Agrícola e Ambiental* 17 (2013) 1347 – 1354.
URL http://www.scielo.br/scielo.php?script=sci_arttext&pid=S1415-43662013001200014&nrm=iso
- [228] M. Sierra-Beltran, [Ductile Cement-Based Composites with Wood Fibres - material design and experimental approach](#), Ph.D. thesis, Delft University of Technology (2011).
URL <http://resolver.tudelft.nl/uuid:fd452dae-f48a-40e1-b48b-6fe528ecd7e3>
- [229] M. Benzerzour, N. Sebaibi, N. E. Abriak, C. Binetruy, [Waste fibre–cement matrix bond characteristics improved by using silane-treated fibres](#), *Construction and Building Materials* 37 (2012) 1 – 6, non Destructive Techniques for Assessment of Concrete. doi:<https://doi.org/10.1016/j.conbuildmat.2012.07.024>.
URL <http://www.sciencedirect.com/science/article/pii/S095006181200493X>
- [230] S. R. Ferreira, F. de Andrade Silva, P. R. L. Lima, R. D. Toledo Filho, [Effect of natural fiber hornification on the fiber matrix interface in cement based composite systems](#), in: *Non-Conventional Materials and Technologies for Sustainable Development*, Vol. 668 of *Key Engineering Materials*, Trans Tech Publications Ltd, 2016, pp. 118–125. doi:[10.4028/www.scientific.net/KEM.668.118](https://doi.org/10.4028/www.scientific.net/KEM.668.118).
- [231] S. R. Ferreira, F. de Andrade Silva, P. R. L. Lima, R. D. T. Filho, [Effect of hornification on the structure, tensile behavior and fiber matrix bond of sisal, jute and curauá fiber cement based composite systems](#), *Construction and Building Materials* 139 (2017) 551 – 561. doi:<https://doi.org/10.1016/j.conbuildmat.2016.10.004>.
URL <http://www.sciencedirect.com/science/article/pii/S0950061816316087>
- [232] C. M. M. [Effect of cellulose fibers on the crystallinity and mechanical properties of starch-based films at different relative humidity values](#), *Carbohydrate Polymers* 77 (2) (2009) 293 – 299. doi:<https://doi.org/10.1016/j.carbpol.2008.12.030>.
URL <http://www.sciencedirect.com/science/article/pii/S0144861709000228>
- [233] D. Snoeck, J. Dewanckele, V. Cnudde, N. De Belie, [X-ray computed microtomography to study autogenous healing of cementitious materials promoted by superabsorbent polymers](#), *Cement and Concrete Composites* 65 (2016) 83–93. doi:[10.1016/j.cemconcomp.2015.10.016](https://doi.org/10.1016/j.cemconcomp.2015.10.016).
URL <http://dx.doi.org/10.1016/j.cemconcomp.2015.10.016>
- [234] D. Palin, H. Jonkers, V. Wiktor, [Autogenous healing of sea-water exposed mortar: Quantification through a simple and rapid permeability test](#), *Cement and Concrete Research* 84 (2016) 1–7. doi:<https://doi.org/10.1016/j.cemconres.2016.02.011>.
URL <https://www.sciencedirect.com/science/article/pii/S0008884616301600>

- [235] S. C. Figueiredo, O. Çopuroğlu, B. Šavija, E. Schlangen, Piezoresistive properties of cementitious composites reinforced by pva fibres, in: V. Mechtcherine, V. Slowik, P. Kabele (Eds.), *Strain-Hardening Cement-Based Composites*, Springer Netherlands, Dordrecht, 2018, pp. 709–717.
- [236] American Society of Civil Engineers, 2013 Report Card for America's Infrastructure Findings :Roads (2013).
- [237] INEA-RJ, Relatório Gerencial 1 (2014) 74.
- [238] V. C. Li, D. K. Mishra, H. C. Wu, Matrix design for pseudo-strain-hardening fibre reinforced cementitious composites, *Materials and Structures* 28 (10) (1995) 586–595. doi:10.1007/BF02473191.
- [239] V. C. Li, H. Obla, Effect of Fiber Length Variation Properties of Carbon-Fiber Cement on Tensile, *Composites Engineering* 4 (9) (1994) 947–964.
- [240] R. Zhang, K. Matsumoto, T. Hirata, Y. Ishizeki, J. Niwa, *Application of PP-ECC in beam-column joint connections of rigid-framed railway bridges to reduce transverse reinforcements*, *Engineering Structures* 86 (2015) 146–156. doi:10.1016/j.engstruct.2015.01.005.
URL <http://dx.doi.org/10.1016/j.engstruct.2015.01.005>
- [241] S. H. Park, D. J. Kim, G. S. Ryu, K. T. Koh, *Tensile behavior of ultra high performance hybrid fiber reinforced concrete*, *Cement and Concrete Composites* 34 (2) (2012) 172–184. doi:10.1016/j.cemconcomp.2011.09.009.
URL <http://dx.doi.org/10.1016/j.cemconcomp.2011.09.009>
- [242] F. d. A. Silva, B. Mobasher, R. D. T. Filho, *Cracking mechanisms in durable sisal fiber reinforced cement composites*, *Cement and Concrete Composites* 31 (10) (2009) 721–730. doi:10.1016/j.cemconcomp.2009.07.004.
URL <http://dx.doi.org/10.1016/j.cemconcomp.2009.07.004>
- [243] H. Pakravan, M. Jamshidi, M. Latifi, *The effect of hybridization and geometry of polypropylene fibers on engineered cementitious composites reinforced by polyvinyl alcohol fibers*, *Journal of Composite Materials* 50 (8) (2016) 1007–1020. doi:10.1177/0021998315586078.
URL <http://jcm.sagepub.com/cgi/doi/10.1177/0021998315586078>
- [244] S. Kwon, T. Nishiwaki, H. Choi, H. Mihashi, *Effect of Wollastonite Microfiber on Ultra-High-Performance Fiber-Reinforced Cement-Based Composites Based on Application of Multi-Scale Fiber-Reinforcement System*, *Journal of Advanced Concrete Technology* 13 (7) (2015) 332–344. doi:10.3151/jact.13.332.
URL https://www.jstage.jst.go.jp/article/jact/13/7/13_{ }332/{ }article
- [245] C. Song, S. Choi, *Moisture-dependent Piezoresistive Responses of CNT-embedded Cementitious Composites*, *Composite Structures* 170 (2017) 103–110. doi:10.1016/j.compstruct.2017.03.009.
URL <http://linkinghub.elsevier.com/retrieve/pii/S0263822317302015>

LIST OF PUBLICATIONS

1. van Overmeir, Anne Linde; **Chaves Figueiredo, Stefan**; Šavija, Branko; Bos, Freek P; Schlangen, Erik. *Design and analyses of printable strain hardening cementitious composites with optimized particle size distribution*. Construction and Building Materials. 324. 126411. Elsevier. 2022.
2. Matos, Ana Mafalda; **Chaves Figueiredo, Stefan**; Nunes, Sandra; Schlangen, Erik; Barroso-Aguiar, José L. *Durability of an UHPFRC under mechanical and chloride loads*. Construction and Building Materials. 311. 125223. Elsevier. 2021.
3. Chen, Yu; **Chaves Figueiredo, Stefan**; Li, Zhenming; Chang, Ze; Jansen, Koen; Çopuroğlu, Oğuzhan; Schlangen, Erik. *Improving printability of limestone-calcined clay-based cementitious materials by using viscosity-modifying admixture*. Cement and Concrete Research. 132. 106040. Pergamon. 2020.
4. Li, Victor C; Bos, Freek P; Yu, Kequan; McGee, Wes; Ng, Tsz Yan; **Chaves Figueiredo, Stefan**; Nefs, Karsten; Mechtcherine, Viktor; Nerella, Venkatesh Naidu; Pan, Jinlong. *On the emergence of 3D printable engineered, strain hardening cementitious composites (ECC/SHCC)*. Cement and Concrete Research. 132. 106038. Pergamon. 2020.
5. **Chaves Figueiredo, Stefan**; Romero Rodríguez, Claudia; Y Ahmed, Zeeshan; Bos, Derk H; Xu, Yading; Salet, Theo M; Çopuroğlu, Oğuzhan; Schlangen, Erik; Bos, Freek P. *Mechanical behavior of printed strain hardening cementitious composites*. Materials. 13. 10. 2253. Multidisciplinary Digital Publishing Institute. 2020.
6. Rodríguez, C Romero; de Mendonça Filho, F França; **Chaves Figueiredo, Stefan**; Schlangen, E; Šavija, B. *Fundamental investigation on the frost resistance of mortar with microencapsulated phase change materials*. Cement and Concrete Composites. 113. 103705. Elsevier. 2020.
7. **Chaves Figueiredo, Stefan**; Overmeir, Anne L van; Nefs, Karsten; Schlangen, Erik; Salet, Theo AM; Šavija, Branko; Suiker, Akke SJ; Bos, Freek P. *Quality assessment of printable strain hardening cementitious composites manufactured in two different printing facilities*. RILEM International Conference on Concrete and Digital Fabrication. 824-838. Springer, Cham. 2020.
8. Krstic, Marija; Davalos, Julio F; Rossi, Emanuele; **Chaves Figueiredo, Stefan**; Çopuroğlu, Oğuzhan. *Freeze–Thaw Resistance and Air-Void Analysis of Concrete with Recycled Glass–Pozzolan Using X-ray Micro-Tomography*. Materials. 14. 1. 154. MDPI. 2020.
9. Matos, Ana Mafalda; Nunes, Sandra; **Chaves Figueiredo, Stefan**; Schlangen, Erik; Aguiar, José L Barroso. *Chloride Ion Penetration into Cracked UHPFRC During Wetting-drying Cycles*. RILEM Spring Convention and Conference. 227-238. Springer, Cham. 2020.
10. Xu, Yading; Zhang, Hongzhi; Šavija, Branko; **Chaves Figueiredo, Stefan**; Schlangen, Erik. *Deformation and fracture of 3D printed disordered lattice materials: Experiments and modeling*. Materials Design. 162. 143-153. Elsevier. 2019.

11. **Chaves Figueiredo, Stefan**; Rodríguez, Claudia Romero; Ahmed, Zeeshan Y; Bos, Derk H; Xu, Yading; Salet, Theo M; Çopuroğlu, Oğuzhan; Schlangen, Erik; Bos, Freek P. *An approach to develop printable strain hardening cementitious composites*. Materials Design. 169. 107651. Elsevier. 2019.
12. **Chaves Figueiredo, Stefan**; Çopuroğlu, Oğuzhan; Schlangen, Erik. *Effect of viscosity modifier admixture on Portland cement paste hydration and microstructure*. Construction and Building Materials. 212. 818-840. Elsevier. 2019.
13. Chen, Yu; **Chaves Figueiredo, Stefan**; Yalçinkaya, Çağlar; Çopuroğlu, Oğuzhan; Veer, Fred; Schlangen, Erik; The effect of viscosity-modifying admixture on the extrudability of limestone and calcined clay-based cementitious material for extrusion-based 3D concrete printing. Materials. 12. 9. 1374. MDPI. 2019.
14. Chen, Yu; Li, Zhenming; **Chaves Figueiredo, Stefan**; Çopuroğlu, Oğuzhan; Veer, Fred; Schlangen, Erik. *Limestone and calcined clay-based sustainable cementitious materials for 3D concrete printing: a fundamental study of extrudability and early-age strength development*. Applied Sciences. 9. 9. 1809. MDPI. 2019.
15. Rodríguez, Claudia Romero; **Chaves Figueiredo, Stefan**; de Mendonça Filho, Fernando França; SCHLANGEN, ERIK; Šavija, Branko. *Frost Damage Progression Studied Through X-Ray tomography In Mortar With Phase Change Materials*. 10th International Conference on Fracture Mechanics of Concrete and Concrete Structures: FraMCoS-X. 2019.
16. Mercuri, L; Rodríguez, C Romero; Xu, Yading; Figueiredo, **Chaves Figueiredo, Stefan**; Mors, Renee; Rossi, Emanuele; Anglani, G; Antonaci, P; Šavija, Branko; Schlangen, E. *On the role of soft inclusions on the fracture behaviour of cement paste*. Proceedings of the 10th International Conference on Fracture Mechanics of Concrete and Concrete Structures. 2019.
17. Romero Rodríguez, C; **Chaves Figueiredo, Stefan**; França de Mendonça Filho, F; Schlangen, E; Šavija, B. *Frost damage progression studied through X-Ray tomography in mortar with Phase Change Materials*. . . 2019.
18. Rodríguez, C Romero; Figueiredo, **Chaves Figueiredo, Stefan**; Deprez, Maxim; Snoeck, Didier; Schlangen, Erik; Šavija, B. *Numerical investigation of crack self-sealing in cement-based composites with superabsorbent polymers*. Cement and Concrete Composites. 104. 103395. Elsevier. 2019.
19. Bos, Freek; Ahmed, Zeeshan; Rodríguez, Claudia Romero; **Chaves Figueiredo, Stefan**. *3D concrete printing for structural applications*. Spool. 6. 2. 05-Oct. 2019.
20. Rodríguez, C Romero; **Chaves Figueiredo, Stefan**; Schlangen, Erik; Snoeck, Didier. *Modeling water absorption in cement-based composites with SAP additions*. Computational Modelling of Concrete Structures. 295-304. CRC Press. 2018.
21. **Chaves Figueiredo, Stefan**; Çopuroğlu, Oğuzhan; Schlangen, Erik. *Effect Of Viscosity Modifier Admixture On Portland Cement Hydration*. 4th Brazilian Conference on Composite Materials. Rio de Janeiro. 2018.
22. Mafalda Matos, Ana; **Chaves Figueiredo, Stefan**; Nunes, Sandra; Schlangen, E. *Durability of fibre reinforced cementitious composites: Coupling mechanical and chloride environment loads*. Rilem. 2018.

23. Romero Rodríguez, Claudia; **Chaves Figueiredo, Stefan**; Snoeck, Didier; Savija, Branko; Schlangen, Erik. *Modelling strategies for the study of crack self-sealing in mortar with superabsorbent polymers*. Symposium on Concrete Modelling (CONMOD2018). 127. 333-341. Rilem. 2018.
24. Matos, Ana Mafalda; **Chaves Figueiredo, Stefan**; Nunes, Sandra; Schlangen, Erik. *Durability of fibre reinforced cementitious composites: Coupling mechanical and chloride environment loads*. 4th International Conference on ServiceLife Design for Infrastructures. 721-732. Rilem. 2018.
25. Nunes, Sandra; Matos, Ana Mafalda; **Chaves Figueiredo, Stefan**; Schlangen, Erik. *Durability of fibre reinforced cementitious composites: coupling mechanical and chloride environment loads*. CONMOD2018 International Symposium on Concrete Modelling. 2018.
26. **Chaves Figueiredo, Stefan**; Çopuroğlu, Oğuzhan; Šavija, Branko; Schlangen, Erik. *Piezoresistive properties of cementitious composites reinforced by PVA fibres*. International Conference on Strain-Hardening Cement-Based Composites. 709-717. Springer, Dordrecht. 2017.
27. Schlangen, Erik; Šavija, Branko; **Chaves Figueiredo, Stefan**; Mendoça Filho, Fernando França de; Luković, Mladena. *Mechanical Properties of Ductile Cementitious Composites Incorporating Microencapsulated Phase Change Materials*. International Conference on Strain-Hardening Cement-Based Composites. 115-122. Springer, Dordrecht. 2017.
28. Zhang, Hongzhi; Šavija, Branko; **Chaves Figueiredo, Stefan**; Schlangen, Erik. *Experimentally validated multi-scale modelling scheme of deformation and fracture of cement paste*. Cement and Concrete Research. 102. 175-186. Elsevier. 2017.
29. Zhang, Hongzhi; Šavija, Branko; **Chaves Figueiredo, Stefan**; Lukovic, Mladena; Schlangen, Erik. *Microscale testing and modelling of cement paste as basis for multi-scale modelling*. Materials. 9. 11. 907. MDPI. 2016.
30. Rodríguez, Claudia Romero; **Chaves Figueiredo, Stefan**; Chiaia, Bernardino; Schlangen, Erik. *Induction healing of concrete reinforced by bitumen-coated steel fibres*. 9th International Conference on Fracture Mechanics of Concrete and Concrete Structures. 2016.
31. Rodrigues, Conrado; Figueiredo, Stefan; Santos, Jefferson; Santos, Luciana; Zucowski, Bartosz. *Co-generation biomass wastes in low Co 2 cement composites and concretes: Combining energy efficiency and technical performance in sustainable building materials*. 2015 International Conference on Solar Energy and Building (ICSoEB). 01-Jun. IEEE. 2015.
32. **Chaves Figueiredo, Stefan**; de Souza Rodrigues, Conrado; F. Vasconcelos, Maria Clara. *Durability of autoclaved cellulose cements composites with different ratios of cement replacement by quartz and rice husk ash on the matrix*. D-P131. Brazilian MRS Meeting (12.: 2013 : Campos do Jordão – SP). XII Brazilian MRS Meeting Program book (SBPMat) / Sociedade Brasileira de Materiais – Rio de Janeiro: SBPMat. 2013.
33. de Souza Rodrigues, Conrado; Pereira, Mariana Arruda; **Chaves Figueiredo, Stefan**; Ghavami, Khosrow; Stroeven, Piet. *Durability of cellulose-cement composites assessed by accelerated testing under temperature and moisture variations-effects of blending by rice husk ash*. Brittle Matrix Composites 10. 387-396. Woodhead Publishing. 2012.

34. de Souza Rodrigues, Conrado; Pereira, Mariana Arruda; **Chaves Figueiredo, Stefan**; Ghavami, Khosrow; Stroeven, Piet. *Brittle Matrix Composites: Durability of cellulose-cement composites assessed by accelerated testing under temperature and moisture variations-effects of blending by rice husk ash*. Elsevier Inc. Chapters. 2012.